THE UNIVERSITY
of EDINBURGH

Identification of Novel IFITM1/IFITM3 Signalling Pathways Implicated in the Interferon Response

Maria Gómez Herranz

Doctor of Philosophy
University of Edinburgh

October 8, 2019

“Nothing in life is to be feared, it is only to be understood. Now is time to understand more, so that we may fear less.”

Marie Curie

Dedicated to...

“… those who would rather die of passion than of boredom.”

Vincent van Gogh

Declaration

I declare that this thesis was composed by myself, that the work contained herein is my own except where explicitly stated otherwise in the text, and that this work has not been submitted for any other degree or processional qualification except as specified.

Parts of this work have been published in Appendix B (Gomez Herranz *et al.*, 2019).

Maria Gómez Herranz

October 8, 2019

Acknowledgements

First and foremost, I offer my sincerest gratitude to each and every one who has contributed to this thesis, both during the project and even before I started. While I cannot mention everyone involved, I am well aware that many people contributed greatly and in many different ways, without your help this thesis would not have been possible.

To my supervisor, Prof. Ted Hupp, who has supported me with his useful comments, remarks and engagement throughout these years. I am thankful to Prof. Kathryn Ball, Prof. Jurgen Haas, Prof. Mark Arends and Dr. Rob O'Neil for their helpful comments and advice. I also acknowledge the contributions of our collaborators in RECAMO, Brno (Czech Republic) and in the University of Gdansk (Poland). I gratefully acknowledge the funding and support received from Medical Research Scotland PhD fellowship.

To the lab, I feel extremely fortunate to be surrounded by colleagues that with time became friends and who are highly enthusiastic, engaged, and eager to collaborate. They inspire me to give my best. I honestly hope I expressed my gratitude in person. My humble appreciation goes to the technical services and microscopy teams who have offered their support and kind words.

To the reader who is taking time to go through my work and to Ainhoa and Ashita who have read this thesis and made great comments, and to Borja who has helped with the formatting of this thesis.

To my family, who have always supported me, and to my friends; Marta, Agustina, Serra, Jèssica, Julia, Pau, Anne, Carolin, Suzannah, Irene, and Lilia -for showing me there is life out there, for caring, and for bringing joy.

To my beloved city of Edinburgh which has brought me endless wonderful memories and remarkable people. It started as a short stay and became a long thrilling journey. I am thankful for all the challenges and setbacks that I have had along the way, and for the valuable lessons learned both personally and professionally. As the Edinburgh airport banner says: "welcome home", to a place where I feel homesick every time I land, and every time I take off. I hope my next stop will be as enjoyable as Edinburgh has been.

Lay summary

Interferon induced transmembrane proteins (IFITM) 1 and 3 are molecules implicated in cancer. They are found in several cancer types. In particular, they are manifested in those patients that do not improve with chemotherapy treatments. Thus far, there is insufficient knowledge about how IFITM1 and IFITM3 function. Therefore, the main aim of this project is to better understand how IFITM1 and IFITM3 are able to facilitate cancer progression.

This study proposes a new function for IFITM1 and IFITM3 in which they are implicated in the production of some molecules and thereby increasing their amount inside the cell. This process is known as protein synthesis. Moreover, this project has identified new IFITM1 and IFITM3 associated molecules. The results show that IFITM1 and IFITM3 bind to ISG15 and HLA-B: two molecules also highly implicated in cancer by different mechanisms.

In conclusion, this work provides new cellular mechanisms for how IFITM1 and IFITM3 molecules function. These findings may contribute to better understand IFITM1 and IFITM3 cellular functions.

Abstract

Interferon induced transmembrane protein 1 (IFITM1) is an interferon (IFN) stimulated protein upregulated during development of radiation resistance in cancer. It is present in resistant tumours, generating a multi-drug resistant phenotype and escaping from pro-apoptotic effects (Weichselbaum *et al.*, 2008a; Yang *et al.*, 2007). The signal transduction events that are orchestrated by IFITM1/IFITM3 are not well defined. As IFITM1 is the main isoform described as a pro-oncogene, we started studying its interactome.

To begin to elucidate its molecular mechanism of action, isogenic *IFITM1* null and *IFITM1/IFITM3* double null cervical cancer cells, engineered by CRISPR/Cas9 system, were used to define dominant pathways mediated by IFITM1/IFITM3 proteins. The results suggested a specific role for IFITM1/IFITM3 in regulating ribosomal integrity. In this study, therefore, we explored whether IFITM1/IFITM3 were capable of facilitating protein synthesis. The localization of IFITM/IFITM3 to ribosomal translation protein factors prompted an analysis of IFNγ-dependent protein synthesis using pulse SILAC-mass spectrometry. The IFITM1/IFITM3–IFNγ complex mediates signal transduction through ISG15, IRF1, and HLA-B molecules. Additional experimental work consolidated the association between IFITM1/IFITM3 and HLA-B or ISG15. Moreover, the implications of IFITM1/IFITM3 loss of expression on RNA regulation were further investigated by RNA-Seq and RT-qPCR.

In conclusion, the present study characterises a novel function for IFITM1/IFITM3 proteins. They are implicated in protein synthesis in IFNγ-stimulated cells, providing a new insight into how these proteins are relevant in cancer. These data have implications for the function of IFITM1/IFITM3 in mediating appropriate antigen presentation recognition and protein modification by ISGylation.

Abbreviations

μg	Microgram
μl	Microliter
μm	Micrometer
2-5A synthetase	2-5oligoadenylate synthetase
4EBP1	4E (eI4E)-binding protein 1
IFITM1/IFITM3 double null	Isogenic SiHa *IFITM1/IFITM3* knock out cell line
IFITM1 null	Isogenic SiHa *IFITM1* knock out cell line
IFITM3 null	Isogenic SiHa *IFITM3* knock out cell line
APC	Antigen presenting cell
B2M	β-2-microglobulin
bp	Base pair
BSA	Bovine serum albumin
Cas9	CRISPR associated protein 9
CIN/SIL	Cervical intraepithelial neoplasia/Squamous intraepithelial lesion
CRISPR	Clustered Regularly Interspaced Short Palindromic Repeats
CTL	Cytotoxic T lymphocytes
DAPI	4',6-diamidino-2-phenylindole
DDA	Data dependent acquisition method
DMEM	Dulbeccos Modified Eagle Media
DNA	Deoxyribonucleic acid
DRiPs	Defective ribosomal products

DSB	Double strand break
dsRAD	dsRNA specific adenosine deaminase
DTT	Dithiothreitol
ECL	Enhanced chemiluminescence
EDTA	Ethylenediaminetetraacetic acid
eIF2	Eukaryotic initiation factor 2
ER	Endoplasmic reticulum
EV	Empty vector
FASP	Filter-aided sample preparation
FDA	Food and drug administration
GAS	Gamma-interferon activation site
gRNA	Guide RNA
HDR	Homology directed repair
HLA-A	Human leukocyte antigen A
HLA-B	Human leukocyte antigen B
HLA-C	Human leukocyte antigen C
HLA-E	Human leukocyte antigen E
HLA-G	Human leukocyte antigen G
HPV	Human papillomavirus
HRP	Heat shock protein
IF	Immunofluorescence
IFIT	Interferon-induced protein with tetratricopeptide repeats 1
IFITM1	Interferon induced transmembrane protein 1
IFITM2	Interferon induced transmembrane protein 2
IFITM3	Interferon induced transmembrane protein 3
IFNα	Interferon alpha

IFNβ	Interferon beta
IFNγ	Interferon gamma
IFNGR1	Interferon gamma receptor 1
IFNGR2	Interferon gamma receptor 2
IRF1	Interferon regulatory factor 1
ISG15	Interferon-stimulated gene 15
ISGF3	IFN-stimulated gene factor 3
ISRE	IFN-stimulated regulatory element
JAK	Janus kinase
kDa	Kilo Dalton
LB	Luria-Bertani
LC-MS/MS	Liquid-chromatography coupled with tandem mass spectrometry
m/z	mass to charge ratio
MHC class I	Major histocompatibility complex class I
MHC class II	Major histocompatibility complex class II
min	Minute
ml	Millilitre
mM	Millimolar
mRNA	Messenger RNA
MS	Mass spectrometry
ng	Nanogram
NGS	Next generation sequencing
NHEJ	Non-homologous end joining
NK cell	Natural killer cell
NMD	Nonsense-mediated mRNA decay
nt	Nucleotide

OAC	Oesophageal adenocarcinoma
PAM	Protospacer adjacent motive
PBS	Phosphate-buffered saline
PBS-T	Phosphate-buffered saline Tween-20
PCNA	Proliferating cell nuclear antigen
PCR	Polymerase chain reaction
pH	Potential of hydrogen
PI3K	Phosphoinositide 3-kinase
PIAS1	Protein inhibitor of activated STAT 1
PKR	Protein kinase R
PLA	Proximity ligation assay
pRb	Ritinoblastoma protein
RNA	Ribonucleic acid
RPMI	Roswell Park Memorial Institute
RT	Room temperature
RT-PCR	Real time polymerase chain reaction
SBP-IFITM1 SiHa	Isogenic SiHa-SBP tagged-IFITM1 knock in cell line
SDS-PAGE	Sodium dodecyl sulphate polyacrylamide gel electrophoresis
SH2	Src Homology 2
SILAC	Stable Isotope Labelling with Amino acids in Cell Culture
siRNA	Small interfering RNA
SOCS3	Suppressor of cytokine signalling 3
ssRNA	Single stranded RNA
STAT1	Signal transducer and activator of transcription 1
STAT2	Signal transducer and activator of transcription 2
SWATH	Sequential window acquisition of all theoretical fragment ion mass spectra

TALEN	Transcription activator-like effector nucleases
TAM	Tumour associated macrophages
TAP	Transporter associated with antigen processing
TCR	T cell receptor
TEMED	Tetramethylethylenediamine
TIL	Tumour-infiltrating lymphocytes
TMA	Tissue microarray
TNF-α	Tumour necrosis factor-alpha
TP53	Tumour protein 53
tracrRNA	Trans-activating crRNA
Tris	Tris(hydroxymethyl)aminomethane
Ubl domain	Ubiquitin like domains
v/v	volume/volume
VEGF	Vascular endothelial growth factor
wt	Wild type
XIC	Extracted ion chromatogram
ZFN	Zinc finger nuclease

Contents

List of Figures

List of Tables

Chapter 1

Introduction

1.1 Present perspectives and future directions

Cancer cells are able to hijack physiological pathways in their interest to achieve an advantageous state over normal cells and, consequently, to increase their survival. Many mechanisms have been proposed to explain the genesis of the cancer. Among these, genomic instability is common to all types of cancer. Despite this, the ideal of understanding cancer as a mere genomic disease is completely outdated (Negrini *et al.*, 2010). In fact, tumours are much more than just cancer cells; they are complicated structures composed of a wide variety of cell types, including normal cells. These normal cells form what is known as tumour-associated stroma and play an active role in tumourigenesis and cancer development. In 2000, Hanahan and Weinberg combined the main cancer capabilities into six hallmarks: sustaining proliferative signalling, evading growth suppressors, activating invasion and metastasis, enabling replicative immortality, inducing angiogenesis, and resisting cell death (Figure 1.1) (Hanahan & Weinberg, 2000).

Cancer biology is constantly under revision and continuous research contributes to a better framework of cancer events. A more profound understanding of cancer led to reporting of four new complementary hallmarks that are also implicated in cancer development. These added hallmarks are: deregulating cellular energetics, genome instability and mutation, tumour-promoting inflammation, and avoiding immune destruction (Figure 1.2) (Hanahan & Weinberg, 2011). This thesis particularly focuses on the last hallmark, avoiding immune destruction. Tumour cells are able to manipulate the immune system and consequently escape from the immune response. A large body of research has documented a strong relationship between cancer cell survival and inhibition of immune system, and however, the first observations were made long ago. The next section will highlight the main discoveries that allowed this field to progress.

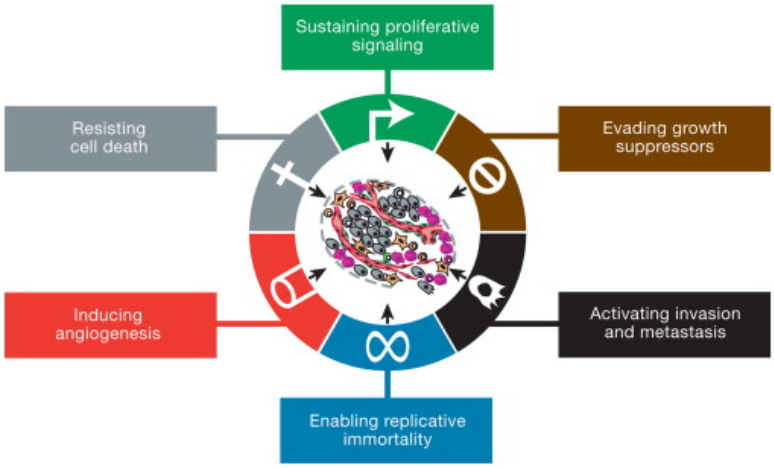

Figure 1.1: The original Hallmarks of Cancer (Hanahan & Weinberg, 2000). Representation of fundamental acquired capabilities in cancer. All characteristics are thought to be shared across all types of cancer and allow the disease to originate and progress. Sustaining proliferation signalling promotes continuous cell growth (i.e. Ras oncoprotein) (in green). In parallel, cancer evades growth suppressors activating different mechanisms (e.g. alterations in pRb and TP53 activities) (in brown). Overactivation of these pathways can lead cell senescence as intrinsic cellular self-defence to inhibit uncontrolled growth. Resting cell death is characterised by inhibiting apoptosis programs (in grey). Enabling replicative immortality is acquired by unrestricted replicative potential (in blue). Inducing angiogenesis is essential to maintain a sustained source of nutrients and oxygen (in red). Finally, activating invasion and metastasis allow the tumour to spread in other tissues to acquire the final and most aggressive state leading to the death of the host (in black).

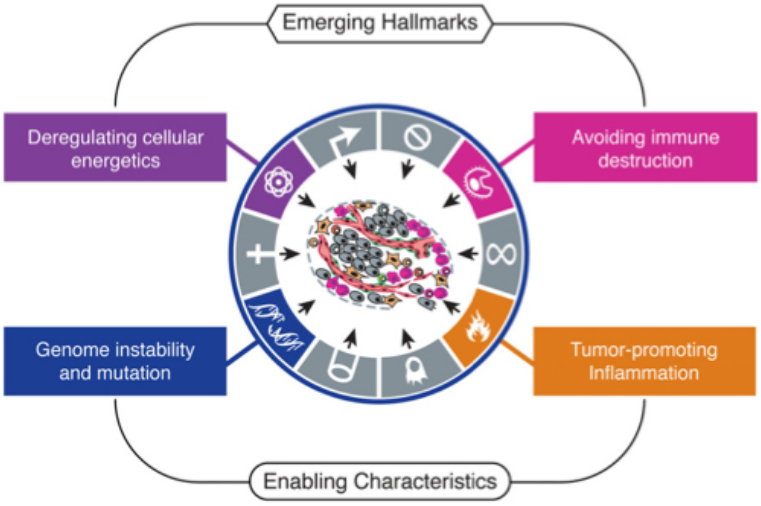

Figure 1.2: The Next Generation Hallmarks of Cancer (Hanahan & Weinberg, 2011). Four new hallmarks are believed to be involved in pathogenesis in most cancers. They are subdivided into two pairs of characteristics. The first, emerging hallmarks comprises two blocks: avoiding immune destruction (cancer capability of scape immunological recognition) and deregulating cellular energetics (alteration of cellular metabolism to facilitate cancer proliferation). The second, enabling characteristics comprised two further blocks: tumour-promoting inflammation (benefitting from the inflammation characteristics to progress, thus inflammation will positively influence other hallmarks), and genomic instability (accumulation of genetic mutations that allow cancer to acquire its tumourigenic phenotype).

1.2 Cancer Immunosurveillance and Immunoediting

There are many examples in scientific history where it has been shown that the immune system is implicated in tumour recognition and elimination. For instance, in the late 19th century Bradley Coley observed that immune responses activated by streptococcal bacteria provoked tumour remission after patients with inoperable bone sarcoma were inoculated with the "Coley vaccine" (Coley, 1893; McCarthy, 2006). The results achieved great success and it was routinely used as one of the earliest immunotherapies for decades. However, Coleys toxins were strongly criticized by the scientific community, gradually fell into disuse, and finally were disapproved by the Food and Drug Administration (FDA). This therapy was replaced with novel radiation and chemotherapy treatments developed at that time.

It was back in 1909 that Paul Ehrlich formally proposed, for the first time, that the immune system plays an active role in tumour elimination (Ehrlich, 1909). He postulated that there was a higher risk of developing cancer if the immune system was compromised. Some studies in murine models supported this hypothesis finding that tumour-specific neoantigens were able to alert the immune system (Gross, 1943; Klein & Klein, 1956).

For a long time, this revolutionary concept was discarded and even forgotten due to the lack of experimental evidence that supported the idea. In the late 1950s, the concept was revived with the immune surveillance hypothesis proposed by Burnet and Thomas (Burnet, 1955; Thomas, 1959). Intensive studies on immune responses conducted in mice revealed rejection of tumour allografts induced by carcinogens (Klein, 1966; Old & Boyse, 1964). It was suggested that the immune system can recognize and eliminate spontaneously generated malignant cells. They proposed that this feature arose from the natural necessity of protecting the host from malignant cell transformation. The hypothesis was seriously debated and again abandoned in the mid 1970s due to contradictory results; several different types of immunocompromised mouse models showed no significant differences in tumour formation compared to wild type (Rygaard & Povlsen, 1974; Stutman, 1979a). Further experiments of Stutman were those that disproved the hypothesis (Stutman, 1979b). Thus, the limited immunological knowledge at the time led to the dismissal of the immune surveillance hypothesis.

During the following 20 years there were several advances in the field. The discovery that self-produced interferon gamma (IFNγ) repressed formation of transplanted, induced or spontaneous tumours was particularly groundbreaking. Extensive work on depleting a wide range of IFNγ-signal molecules such as INFγ receptor and STAT1 made murine models more prone to develop tumours. Indeed, absence of perforin also increased spontaneous tumour formation. Perforin is known to be essential for cytotoxic T cells, and at the time the recently-discovered NK cells to mediate tumour eradication (Russell & Ley, 2002; Smyth *et al.*, 2000; Van den Broek *et al.*, 1996). These experiments, in concordance with others, gave some insights into tumour recognition, where many immune cell types

and molecules are implicated in the process. Another example is the revolutionary work of Ciampricotti *et al.* in which they generated a RAG2-/-MMTV-NeuT transgenic mice model of breast carcinoma that supported the theory. Their experiments found that spontaneous malignant cell transformations can escape from the immune system in implanted or chemically induced tumours (Ciampricotti *et al.*, 2011).

However, how cancer originated in humans and, more importantly, how it happened in immunocompetent individuals were still open questions. In consequence, the immune surveillance hypothesis was re-evaluated and finally resurrected at the end of the 20th century with the cancer immunoediting theory of Robert Schreiber and colleagues (Dunn *et al.*, 2002). After compiling results from several studies, they proposed a new model comprising a multi-step process to fit the tumour immune recognition events in which innate and adaptive immune systems participate. What follows is named "the three Es" phases: elimination, equilibrium, and escape (Figure 1.3). Immune surveillance only covers the first phase: elimination. The immune system can actively detect and enhance inflammatory cascades, antiproliferative and apoptotic programs, repress angiogenesis and activate other mechanisms that can mediate tumour elimination. On this matter, there is supporting evidence from a large-scale study on patients with breast, bladder, colon, prostate, ovarian and neuroblastoma tumours, indicating that the presence of tumour infiltrated lymphocytes, specifically $CD8^+$ T cells, correlates with a favourable prognosis (Deligdisch *et al.*, 1982; Epstein & Fatti, 1976; Jass, 1986; Lipponen *et al.*, 1992; Nacopoulou *et al.*, 1981; Naito *et al.*, 1998; Palma *et al.*, 1978; Rilke *et al.*, 1991). But certain tumour cells adapt to evade immune recognition, surviving and growing in a positive selection process to achieve the equilibrium phase. This phase can extend for several years until this lethargy transitions into the last step: escape. In this phase, tumour cells are no longer immunogenic and remain non-responsive to any immune attack. By these means, they can proliferate without control, metastasize and manifest as a relapse of the disease.

In this context it is mandatory to emphasize the tight relationship between IFNs as part of the host immune response and tumour recognition. Both type I and type II IFNs, play active roles as immunomodulators and suppress tumourigenesis. It has also been described that IFNγ has independent roles in this process. A singular feature of IFNγ is that it promotes tumour rejection by stimulating $CD4^+$ and $CD8^+$ T cells and consequently activating the MHC pathway associated to tumour–antigen recognition (Figure 1.4) (Dunn *et al.*, 2006). This characteristic will be relevant to the development of this thesis. In contrast, emerging studies suggest that sustained IFNγ signalling is closely related to chronic inflammation and elevates the risk of developing cancer (Cheon & Stark, 2009). Such contradictory outcomes require deeper understanding of the IFNγ physiology and its crosstalk with tumour structures and microenvironments. Nonetheless, description of IFNγ pathway and immune-effects will be reviewed in detail in upcoming sections.

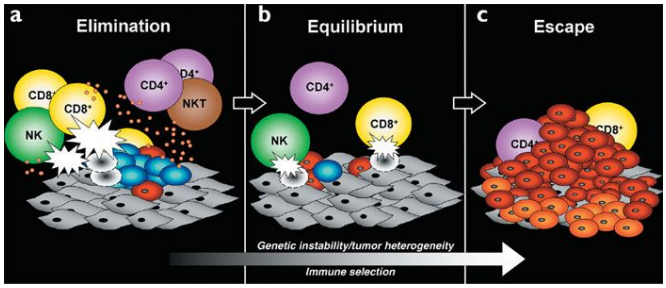

Figure 1.3: The Three Es of cancer immunoediting (Dunn *et al.*, 2002). Cancer immunoediting is described in a 3-step process that explains tumour progression in relation to tumour immunogenicity events. This new concept opens new insights into the cancer immunosurveillance hypothesis, a less refined and elaborated hypothesis. The three immunoediting phases are: elimination, equilibrium, and escape. (a) Elimination is explained by the immunosurveillance hypothesis. (b) Equilibrium refers to those tumour cells (blue) and tumour variants (red) that have adapted and survived the elimination phase. (c) Escape is when adapted tumour cells (red) including new tumour variants (orange) grow unrestricted, evading the immune system (yellow, green, and purple).

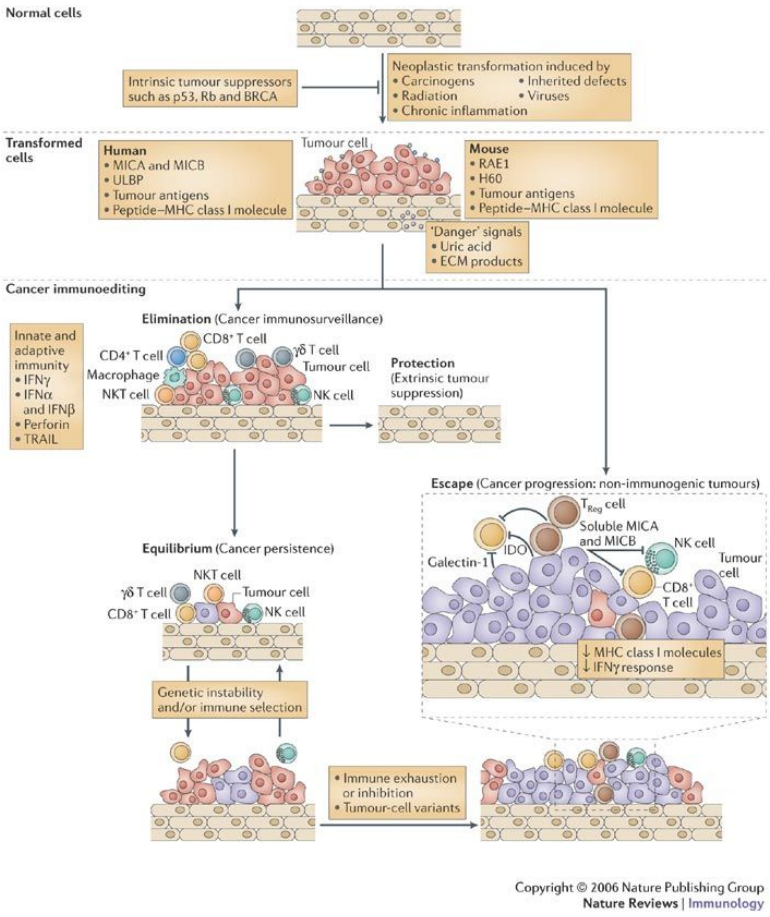

Figure 1.4: Cancer immunogenicity activates IFNγ and MHC molecules as downstream effectors (Dunn *et al.*, 2006). Schematic representation of the cancer immunoediting hypothesis. During the first stages of tumour development, MHC class I and II molecules are able to recognize and eliminate malignant cells by selectively recognizing tumour-specific peptides (transformed cell and elimination section). At advanced stages, surviving tumours develop mechanisms to decrease MHC-polypeptide-related sequences (depicted as MICA and MICB), enhancing tumour evasion and prompting adverse outcomes (escape box).

1.3 Genesis of cancer by viral infection

It remains an open question which cancer variants will be more immune-reactive. High tumour heterogeneity displays a wide landscape of interactions between the immune system and malignant cells. Indeed, tumour cells will spontaneously generate a complex variety of mutations to tolerate the continuous immune-scanning of their surroundings. However, it seems a reasonable observation that immunosuppressed patients, either after transplantation or with an immune abnormality, are more prone to grow tumours (Penn, 1978). This correlation reinforces the idea of the equilibrium phase in cancer immunoediting theory, where unstable tumour cells find ways to bypass immune system recognition and remain undetected in the host until relapse of the disease. Nonetheless, it is not known why some tumour types, such as cervical carcinoma or Kaposi's sarcoma, tend to be of viral nature while others like breast or colon cancers seem to have completely different origins (Lunn *et al.*, 2017).

In fact, the idea that tumour malignancies can be originated by viruses goes back a long time. In 1909, Peyton Rous studied the spreading of avian tumours by injecting small "filtrates" (then considered virus) of chicken donor sarcoma into healthy chickens, these developing tumours in weeks. His revolutionary work inspired others and he was awarded the Nobel Prize for Medicine and Physiology in 1966. Decades later, Howard Temin continued working with Rous sarcoma virus, finding that continued infection caused normal cells to transform into tumour-like cells (Weiss & Vogt, 2011). This observation had great consequences, changing the perspective on cancer from being abnormal tissue to a disease of the cell. In the mid-1950s, some scientists still considered that cancer was a parasitic disease (Burnet, 1955). This lack of understanding generated misleading assumptions and wrong conclusions.

Nowadays, the view that all cancers are virus-initiated has been discarded. Nevertheless, there still exists a high association between viral infections and the manifestation of particular cancer types. Actually, it is believed that around 12–15% of cancer cases are caused by viruses; Epstein-Barr, hepatitis B, and papillomavirus being most well-known. Viral infection is not sufficient to trigger cancer but there is evidence to suggest that some viruses establish the perfect conditions for development of a specific cancer. The process normally requires a long period of time in which cumulative changes in host cells and tumour environment result in carcinogenesis (Hausen, 1991; Liao, 2006; Lunn *et al.*, 2017). A proof of this is an exhaustive epidemiological study in Uganda of individuals infected with HIV, conducted over four decades. Individuals with AIDS suffered from a wide range of infection-related illnesses, and also had increased likelihood of having Kaposis sarcoma but not other cancer types such as cervical or Hodgkins disease (Parkin *et al.*, 1999). AIDS dysregulates natural killer and dendritic cells, and decreases the activation of $CD4^+$ and $CD8^+$ T cell response (Boasso *et al.*, 2009). This acquired immunodeficiency may create a suitable environment to carcinogenesis (Mortaz *et al.*, 2016).It remains unclear why some

cancers are associated with viruses and others are not. Moreover, it is very difficult to conclude that HIV is the main reason why the incidence of Kaposis sarcoma has increased drastically, but it definitely indicates that cancer and virus infection are closely related.

HPV infection is a risk factor for cervical cancer, and persistent infection leads to random integration of the viral particles to the host genome promoting cell immortalization. The E6 and E7 viral oncoproteins facilitate tumour malignancy. E6 inactivates p53-MDM2 pathway, targets P53 to proteosomal degradations, and prevents shortening of the telomerase promoting DNA replication. E7 is critical in tumour transformation as it represses the G1 to S phase transition by targeting pRB for degradation (Tomaic, 2016).

Interferon induced transmembrane protein 1 (IFITM1), the protein of study for this thesis, is an example of a protein with a pivotal role in viral restriction and cancer disease. However, its mechanisms of actions remain poorly understood. As such, this thesis is entirely dedicated to dissecting IFITM1 cellular functions. But first, some relevant IFITM1 features will be disclosed to frame this protein in its cellular and biochemical context.

1.4 Interferon signalling

IFN signalling is a very sophisticated and complex system. Great work has been done in recent years to better comprehend the conditions in which IFN pathways are activated, how cells respond to IFN and which elements are mediated by the IFN response. Nonetheless, more research is needed to fully understand the IFN signalling landscape.

IFNs are pleiotropic cytokines produced by the innate immune system as a defensive response (Takaoka & Yanai, 2006). Many biological functions have been described for the IFN pathway. Among them, the best characterized are anti-tumour activity, immunomodulatory effects, anti-pathogen, and anti-viral activities (Platanias, 2005).

IFN effects rely on the interaction with three different types of receptors: type I (IFNα, IFNβ and IFNω), type II (IFNγ) and type III (IFNλ) (Bekisz *et al.*, 2004; Borden *et al.*, 2007). All types accomplish redundant cellular effects. Some evidence shows that type I influences IFNγ responses by modulating STAT1, a key mediator shared by both IFN types (Gough *et al.*, 2010). Moreover, supressing type I receptors attenuates IFNγ effects (Hamilton *et al.*, 1996; Takaoka *et al.*, 2000) and, conversely, activating type I pathway enhances IFNγ responses (Hamilton *et al.*, 1996; Marie *et al.*, 1998; Vogel & Fertsch, 1984)

Nonetheless, there is a biological reason why different IFN types exist and that is so that specific IFN ligands can bind to specific receptor types and can activate unique pathways. IFNγ responds to immune and inflammatory stimuli, whereas IFNα and β are known to be secreted by virus-infected cells. As such, type I and type II IFNs have different protein structures, chromosomal location and bind to different receptor types (Staeheli, 1990).

Once the ligand binds to its receptor, the signalling cascade begins by phosphorylation of Janus Kinases (JAK) at a tyrosine residue. Sequentially, phosphotyrosine will facilitate interactions between two elements of the signal transducer and activator of tran-

scription signal transducer (STAT), forming a heterodimer for type I IFN or homodimer for type II IFN. STAT dimerization involves interactions at the SH2 domains. Then, STAT homodimers bind to a gamma-interferon activation site (GAS) that facilitates specificity on genes expressed on the first IFN-stimulated gene (ISG) factor synthesis wave, where rapidly-induced genes will be transcribed. STAT also binds to an interferon regulatory factor (IRF) member forming the IFN-stimulated gene factor 3 (ISGF3) trimer in type I and this will bind to genes containing IFN-stimulated regulatory element (ISRE). Consequently, gene regulation by IFN type I will differ from that regulated by type II. However, the system is promiscuous in that both STAT1–STAT2 heterodimers and STAT1–STAT1 homodimers form in response to IFN type I. Moreover, genes containing ISRE elements are mostly regulated by IFN type I but some of them are also induced by IFN type II (Stark *et al.*, 1998) (Figure 1.5).

It is been shown that interferon induced transmembrane proteins (IFITMs) are a family of proteins induced by IFN. Work done in rat neonatal cardiomyocytes, at the mRNA level, shows that *IFITM3* is mainly inducible by IFN type I whereas *IFITM1* greatly responds to IFN type II. *IFITM2* does not respond to either type of IFN (Lau *et al.*, 2012). Nonetheless, it is been shown that *IFITM1* gene induction can also be regulated through the IFN–STAT2 pathway by BRG1, a chromatin-remodelling factor (Huang *et al.*, 2002). Even so, both isoforms may contribute to the same cellular processes; this project has a particular interest in how IFITM1 contributes to cancer events. For this reason, IFNγ signalling will be described with special emphasis.

1.4.1 Interferon gamma

Immunomodulatory effects of IFNs have been widely studied. Here we will focus on those immune responses orchestrated by IFNγ. Previously, it is been described that IFNs are the first defence in response to pathogens. If the IFNγ-pathway is inactivated, by being IFNγ, IFNGR1 or STAT1 deficient, but the IFNα/β pathway is otherwise intact, this results in catastrophic disruption of the innate immunity, exposing the host to higher risk of infection in front of Influenza A virus, Listeria monocytogenes, Tuberculosis, and Mycobacteria, among others. This finding is relatable to studies conducted with mice as translatable to humans (Dalton *et al.*, 1993; Durbin *et al.*, 2016; Huang *et al.*, 1993; Jouanguy *et al.*, 1997; Marc & Moulin, 2003; Newport *et al.*, 2017; Price *et al.*, 2000). Thus, physiological role of IFNγ in immune surveillance is undeniable.

IFNγ is selectively produced by Natural Killer (NK) cells (Perussia, 1991), type 1 T helper cells (Th1) (Mosmann & Coffman, 1989), and $CD8^+$ T cells (Subash Sad & Tim, 1995). But IFNγ receptors are present in practically all cell types (Bach *et al.*, 1997). IFN pathway activation requires the participation of Interferon Gamma Receptor 1 (IFNGR1) (90 kDa receptor α-chain) and Interferon Gamma Receptor 2 (IFNGR2) (62 kDa receptor β-chain) receptor subunits; IFNGR1 is implicated in ligand binding, ligand trafficking through the

cell and signal transduction, while IFNGR2 is mostly implicated in signalling. In these regards, IFNGR1 is moderately but constitutively expressed on the cell membrane, whereas IFNGR2 is expressed at low levels and is inducible under certain stimuli. IFNγ receptor subunits remain unphosphorylated until the binding of the ligand to the receptor. Ligand binding promotes oligomerization between two IFNGR1 subunits that creates two binding sites for two IFNGR2 subunits. Intracellular JAK1 and JAK2 tyrosine kinases bind reciprocally to the IFNGR1 and IFNGR2 (C. Schindler, 1995; Darnell *et al.*, 1994). Signal transduction occurs when JAK 1 and JAK2 are auto- and trans-phosphorylated providing a unique phosphotyrosine binding site on the receptor for STAT1, the key element of the pathway (Bach *et al.*, 1997). STAT1 undergoes to Tyr701 phosphorylation, liberating it from the receptor to form a homodimer which will translocate to the nucleus. Transcriptional activity of STAT1 is increased by Ser727 phosphorylation. Interestingly, emergent studies have identified alternative functions for IFNγ through STAT1-independent pathways. Depletion of STAT1 alters the canonical gene expression profile of IFNγ (Ramana *et al.*, 2002), for example it decreases the generation of pro-apoptotic molecules but increases the generation of other molecules such SOCS3. Nonetheless, the STAT1-independent pathway remains unexplored (Figure 1.5).

IFITM1, initially known as 9-27 gene, was firstly identified as an IFN-inducible gene in the early 90s. *IFITM1* contains a 13 bp IFN-stimulated response element (ISRE). This motif (GGAAATAGAAACT) is located in the 5' flanking sequence and is thought to be necessary and sufficient to induce response. Importantly, not only the ISRE motif itself but also the position in which it is found will determine how inducible it will be by each IFN type (Lewin *et al.*, 1991; Reid *et al.*, 1989). Moreover, additional elements apart from the transcription factor may affect the affinity of DNA-binding (i.e. STAT homodimer along with p48 complex binds to ISRE rather than to the GAS element in IFITM1–IFNγ induction) and impact on gene inducibility (Bluyssen *et al.*, 1995; Muller *et al.*, 1993).

It is been known for a long time that IFNs have different mechanisms of regulating the transcriptional process of target genes. A given gene may be IFNγ as well as IFNα inducible but its response may differ; *IFITM1* is IFNγ and IFNα inducible but mature mRNA accumulates in a sustained and more rapid manner with IFNα compared to a more transient and slower accumulation with IFNγ (Friedman *et al.*, 1984; Kelly *et al.*, 1985). However, no differences in *IFITM1* mRNA stability are found after IFNγ stimulation. That implies that IFN may also operate at a post-transcriptional level (Ackrill *et al.*, 1991).

IFNγ has a tumour cell immunogenicity function. It is involved in tumour rejection by enhancing tumour-specific T cells that will detect and eliminate tumour primary cells (Dighe *et al.*, 1994). In addition, experimental procedures probed that mice deficient in the IFNγ pathway developed more spontaneous tumours after being exposed to a carcinogen, in comparison to wild type mice. Inactivated IFNγ signalling in conjugation with p53-/- tumours were developed even more rapidly (Kaplan *et al.*, 1998).

IFNγ exhibits a dose-dependent apoptotic effect on normal endothelial cells. Further-

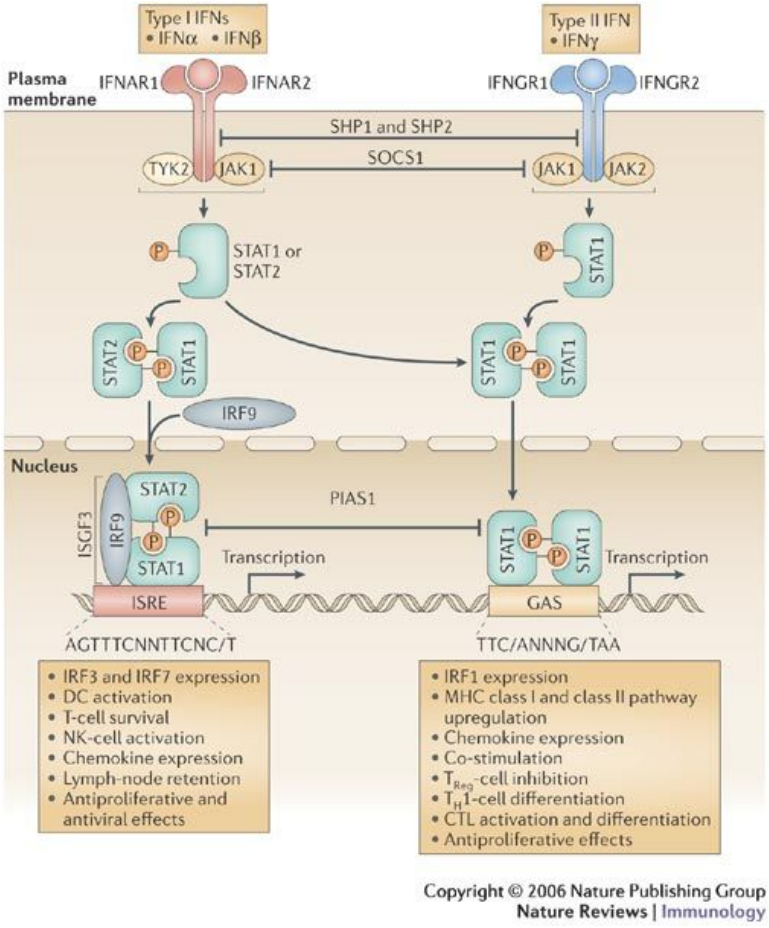

Figure 1.5: IFNγ signal transduction (Dunn *et al.*, 2006). IFNγ facilitates the rearrangement of IFNGR1 and IFNGR2 (IFNγ-receptor subunits) and trigger the signal cascade by activating JAK1 and JAK2 associated kinases. Phosphorylation of JAK kinases leads to homodimerization of the key signal transducer STAT1. IFN type I can also enhance IFN type II signalling by enhancing STAT1 activation. Once phosphorylated, STAT1 will translocate to the nucleus and bind to promoters at IFNγ-activated sites (GAS), such as IRF1 and HLAs (codify for MHC proteins) promoters. The signal cascade will be inactivated by receptor dephosphorylation, suppression of JAKs (mediated by SOCS1), proteosomal degradation of JAKs, or suppression of STAT1 (mediated by PIAS1).

more, IFNγ shows a dual effect on transformed endothelial cell growth; low concentrations stimulate cell proliferation while high doses have the opposite effect. Indeed, IFNγ receptor increases in coordination with IFNγ stimulus. IFNγ effects switch from proliferation to apoptosis according to the number of receptor units displayed in the cell membrane; high receptor expression triggers IFNγ-signal transduction activating apoptosis while constitutive low levels induce cell growth (Bernabei *et al.*, 2001). Related to this, normal cells tend to have high levels, dictating apoptosis, and tumour cells exhibit low levels promoting proliferation (Maier *et al.*, 1995). This may be explained by the dynamic expression of IFNγR2 receptor in T cells, B cells, and myeloid cells. Unresponsiveness to IFNγ may be a key event in malignant transformation, although doses of exogenous IFNγ (i.e. immunotherapy) may reverse the effect.

The first function described for IFNγ was as a molecule with anti-viral activity (Wheelock, 1965). As such, IFNγ has physiological relevance in immunomodulation and proinflammatory activities. A wide variety of functions have been described for IFNγ, among which it is implicated in antigen presentation, leukocyte-endothelium interactions, cell proliferation, apoptosis, and controlling gene expression.

One of the key functions of IFN is that it enhances major histocompatibility complex (MHC) class I as well as β-2-microglobulin (B2M) transcription, promoting the activation of $CD8^+$ T cell response (Boehm *et al.*, 1997; Schroder *et al.*, 2004), mainly by IRF1 (Chang *et al.*, 1992; Reis *et al.*, 1992). Absence of STAT1 or IRF1 attenuates MHC class I proteins on the cellular membrane in response to IFN stimulus. IFNγ is also responsible for MHC class II expression and, in consequence, enhancement of $CD4^+$ T cell responses (Mach *et al.*, 1996). Additionally, IFNγ regulates antigen processing by regulating some proteasomal subunits such as increasing expression of enzymatic subunits LMP2, LMP7 and MECL1 or decreasing the non-enzymatic subunit PA28 (Boes *et al.*, 1994; Groettrup *et al.*, 1996). IFNγ also stimulates overexpression of transporter associated with antigen presentation 1 and 2 (TAP1 and TAP2), proteins that are responsible for guiding peptides from the proteasomal complex to the endoplasmic reticulum, where they will interact with the MHC class I (Epperson *et al.*, 2018; Trowsdale *et al.*, 1990). Taking all together, IFNγ impacts on the production of peptides; tailoring which types of peptides will be generated and recognized by the MHC class I complex.

IFNγ acts as a tumour suppressor by promoting recognition of the transformed cells by the immune system. Certain types of naturally arising human tumours become unresponsive to IFNγ (i.e. IFNγR-/-), bypassing the tumour-suppressor mechanisms of the host. This phenotype will confer tumour selectivity as it will be advantageous for survival. IFNγ has a pivotal role between innate and adaptive immunity; it can enhance innate immunity by recruiting NK cells, macrophages and neutrophils to eliminate tumour cells but it can also promote adaptive immunity by tumour-antigen processing and presentation activating MHC class I and II pathway.

Gene regulation is a fundamental and yet complicated activity of IFNγ. In 1990, Stae-

heli identified several IFNγ-stimulated genes (Staeheli, 1990), but the list currently extends to hundreds. To begin with, many transcription factors are IFNγ inducible, generating a sequential cascade of induced expressed genes. For example, IFNγ attenuates viral infection by controlling transcription of double-stranded RNA activated protein kinase (PKR), 2–5oligoadenylate synthetase (2–5A synthetase), and dsRNA-specific adenosine deaminase (dsRAD). Viral RNA and DNA interacts with PKR producing autophosphorylation and phosphorylation of the α- subunit of eukaryotic initiation factor (eIF2) blocking the generation of eIF-2-GTP (active form) and resulting in inhibition of translation (Hovavessian, 1993). Type I and II IFNs control the induction of PKR. The 2–5A synthetase degrades viral and host ssRNAs, preventing viral protein expression (Greenlund *et al.*, 1993). The dsRAD edits mRNA producing aberrant viral proteins (Bass *et al.*, 1989). Nonetheless, it is still unclear which are the functional implications for many of the induced genes. IFNγ is also involved in further cellular programs such macrophage activation.

Physiological properties of IFNγ involving activation of innate and adaptive immune system have led to this versatile leukokine becoming exploited as immunotherapeutic agent. Manguso *et al.* showed that negative response to immunotherapy is connected to malfunctions in the IFNγ pathway (Manguso *et al.*, 2018). IFNγ suppresses development of transplanted tumours via anti-proliferative and pro-apoptotic cellular programs, but also by inhibiting angiogenesis and boosting the antigen presentation pathway (Ikeda *et al.*, 2002).

Some of the key reasons why IFNγ is a potent molecule capable of achieving tumour rejection will be described below. IFNγ is responsible for inhibiting angiogenesis by decreasing levels of vascular endothelial growth factor (VEGF). Also, it blocks differentiation into tumour-associated macrophages (TMAs), one of the main sources of VEGF in a cancer microenvironment (Allavena *et al.*, 2008), increasing infiltrating monocytes and macrophages as well as anti-tumour chemokine and cytokine secretion (Briesemeister *et al.*, 2011; Sun *et al.*, 2014). As such, it has exhibited great potential as an anti-tumour drug. Positive responses to IFNγ therapy have been found in bladder and ovarian cancers (Giannopoulos *et al.*, 2003; Marth *et al.*, 2004; Stavropoulos *et al.*, 1998; Wall *et al.*, 2003; Windbichler *et al.*, 2000).

Conversely, some studies have noted that IFNγ also has pro-tumourigenic effects, so it has to be carefully administered. For instance, a study found that a physiological dose of IFNγ confers cell growth arrest but also enhances cell invasiveness of lung metastasis in a melanoma mouse model (Taniguchi *et al.*, 1987). Additionally, an independent small-scale clinical trial conducted on patients with cutaneous malignant melanoma, treated with recombinant IFNγ, did not show a favourable outcome (Meyskens *et al.*, 1990). Adverse effects have also been found in metastatic renal-cell carcinoma, colon cancer, and small-cell lung cancer (Gleave *et al.*, 1998; Jett *et al.*, 1994; Wiesenfeld *et al.*, 1995).

Why does IFNγ show these antagonistic effects? The reality is that uncontrolled immunological pathways may put host survival at risk; unrestrained IFNγ will activate cellu-

lar programs to terminate "non-self" structures, also leading to indiscriminate attacking of healthy cells. This leads to the Mellor and Munn hypothesis in which focalised persistent inflammation induces immunosuppression (Mellor & Munn, 2008) (Figure 1.6). Paradoxically, inflammatory events can confer favourable conditions to the tumour microenvironment. Tumours tend to promote a moderate local inflammation so they can benefit from growth but without alerting the immune system (Balkwill F., 2001). As an example, tumour-associated macrophages (TAM), attracted by secreted tumour chemokines, are notoriously present in the tumour surroundings. Under appropriate conditions, TAM can facilitate angiogenesis, proliferation, invasion and metastasis. Also, tumour-associated dendritic cells are often immature and not capable of fully activating antigen-specific recognition. Other inhibitory mechanisms comprise T cell stimulation by APC impairment and suppression of effector activity of tumour infiltrating T cells. As proposed in Dvarak's review tumours behave, in many ways, as wounds that do not heal (Dvorak, 2016).

Due to antagonistic responses in different cancer types, IFNγ effects in tumourigenic events need to be evaluated. At this point many efforts have driven to the very powerful approach of using the host immune system to cure cancer malignancies, despite the scientific debate about how successful it may be. Thus far, we are still in the early days of fully understanding the whole system and any possible adverse effects that may arise while boosting the immune system. But what it is even more important, we still need to comprehend the biology of the cancer in each patient to deliver the appropriate immunotherapy.

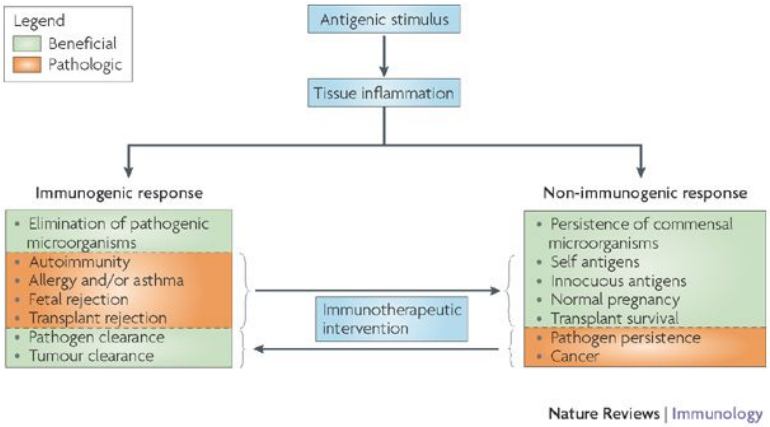

Figure 1.6: Immunogenic and non-immunogenic responses to antigenic stimuli (Mellor & Munn, 2008). Optimal fitness of the immune system is essential to differentiate between self- and non-self antigen. Dysregulation of the immune response may lead it to consider chronic pathogens or malignant cells as non-immunogenic. Alternatively, hyper-activation of the immune response may lead to recognition of self-antigens (i.e. auto-immune disease or allergy) as well as transplant rejection. Immunotherapeutic intervention aims to correct these undesirable effects.

1.5 Interferon resistance DNA-damage signature

For the last century, radiotherapy and chemotherapy have been the traditional anti-cancer therapies. A conventional point of view considers that IFNs activate pro-apoptotic and anti-proliferative programs. As such, elevated doses of IFNs are routinely administrated for anti-cancer therapy. Interestingly, Gerber *et al.* proposed that radiation not only promotes DNA damage but also boosts the $CD8^+$ T cells and the antigen presentation pathway. Their study found significantly less tumour regression in murine colon adenocarcinoma deficient in IFNγ compared to control mouse (Gerber *et al.*, 2013).

Unfortunately, IFN signalling is more complicated in that it also activates immunosuppressive and tumour-survival pathways. In consequence, tumour resistance in response to IFNs as chemotherapeutic agents have given rise to great concern (Minn, 2015). Notoriously, many cancer therapies are not successful in eliminating all malignant cells; a few cancer cells manage to survive, by positive selection, often giving more aggressive features. Intrigued by these poor outcomes, continuous scientific effort is attempting to identify alternative IFN pathways. Weichselbaum *et al.* found an IFN-dependent protein signature in a variety of cancer types after chemotherapy failure. As described previously, IFNs are responsible for expressing a wide range of ISGs, usually associated with anti-cancer effects. By studying consistent gene overexpression across several cancer cell types, they were able to define a subset of ISG genes they called the IRDS signature (Table 1.1). Intrigued by this observation, further investigation of clinical data on breast cancer revealed positive responses to chemotherapy associated with low expression of IRDS signature. This was additionally corroborated with other breast cancer data sets (Weichselbaum *et al.*, 2008a). Another pioneer study also reported poor prognosis correlated with IRDS signature in glioblastoma (Duarte *et al.*, 2012), and an independent study also found upregulation of the IRDS gene profile after radiation in breast, prostate and glioma cancer cells (Tsai *et al.*, 2007).

Underlying molecular mechanism by which IFNs confer cancer protective effects through IRDS genes are being explored (Figure 1.7). In a healthy cellular state, one could expect that the STAT1/IFN pathway will be activated in response to cellular DNA damage. In fact, sensitivity to DNA damage is closely related to responsiveness to IFNs (Khodarev *et al.*, 2007). In normal conditions, no free DNA or RNA is expected to be in the cytosol. Therefore, under pathogen attack host cells will activate immune-related pathways (i.e. IFN-signalling) that recognize non-self genetic material (Takeuchi & Akira, 2010). Paradoxically, in pathological conditions (i.e. cancer and chronic inflammation) there is a sustained infusion of low levels of IFN and, in cancer, this leads to tumour resistance. In fact, studies are emerging that suggest that resistance to DNA damage is caused by chronic IFN stimulation (Cheon *et al.*, 2014; Weichselbaum *et al.*, 2008a)). In brief, it is hypothesized that ssDNA fragments originating in the nucleus, caused by the DNA-damaging effect of cancer therapy, will accumulate in the cytosol. As a consequence, immune responses will

be continuously activated (Erdal *et al.*, 2017).

IRDS genes enhance pro-tumour phenotypes such as resistance to DNA damage, suppression of T cell toxicity, metastasis, and facilitation of epithelial–mesenchymal transition (Wallace *et al.*, 2011). Thus, the IRDS gene signature is proposed as a therapy-predictive marker for anticipating negative responses prior to chemotherapy and radiation (Weichselbaum *et al.*, 2008b). In summary, IRDS are thought to be oncogenic genes modulated by STAT1. However, how the IRDS signature confers a protective effect against radiotherapy and chemotherapy has not been investigated in detail. A better understanding of the complexity of this genetic signature needs to be addressed to improve cancer therapy. Therefore, in this study we explore the oncogenic implications of IFITM1, one component of the IRDS signature. By extension, we will also investigate other IRDS genes that we suspect are also implicated with IFITM1 cellular roles. The next section will be dedicated to describing essential features of IFITM1 and other interesting members of the IRDS signature featuring in this research.

Table 1.1: IRDS protein list (Weichselbaum *et al.*, 2008a).

Gene symbol	Alternative symbols	Gene Name
BST2	Tetherin	Bone marrow stromal cell antigen 2
CCNA1		Cyclin A1
CXCL1	GRO1; GROA; SCYB1	Chemokine (C-X-C motif) ligand 1
CXCL10	IP10; SCYB10; INP10	Chemokine (C-X-C motif) ligand 10
EIF2AK2	PRKR; PKR; p68 Kinase	Eukaryotic translation initiation factor 2-alpha kinase 2
HERC6	FLJ206371	Hect domain and RLD 6
HLA-B	SPDA1	Major Histocompatibility complex class I, B
HLA-G	TCA; HLA6.0; HLA60	Major Histocompatibility complex class I, G
IFI27	ISG12	Interferon, alpha-inducible protein 27
IFI35	IFP35	Interferon-induced protein 35
IFI44	p44	Interferon-induced protein 44
IFI44L	C1orf29	Interferon-induced protein 44 like
IFI6	G1P3	Interferon, alpha-inducible protein 6
IFIH1	MDA5	Interferon induced with helicase C domain 1
IFIT1	IFI56; G10P1; ISG56	Interferon-induced protein with tetratricopeptide repeats 1
IFIT3	RIGG; IFI60	Interferon-induced protein with tetratricopeptide repeats 3
IFITM1	**IFI17; leu13; fragilis; 9-27**	**Interferon induced transmembrane protein 1**
IRF7	IRF7A	Interferon regulatory factor 7
ISG15	G1P2; IFI15	ISG15 ubiquitin-like modifier
LAMP3	DCLAMP	Lysosomal-associated membrane protein 3
LGALS3BP	MAC2BP; L3 ANTIGEN	Lectin galactoside-binding soluble binding protein
LY6E	RIGE; TSA1	Lymphocyte antigen 6 complex, locus E
MCL1	BCL2L3	Myeloid cell leukemia sequence 1 (BCL2-related)
MX1	IFI78, MxA	Myxovirus (influenza virus) resistence 1
MX2	MxB	Myxovirus (incluenze virus) resistence 2
OAS1	OIAS	2-5'-oligodenylate synthetase 1, 40/46 kDa
OAS3	p100	2-5'-oligodenylate synthetase 3, 100 kDa
OASL	TRIP14; p59 OASL	2-5'-oligodenylate synthetase-like
PLSCR1	MMTRA1B	Phospholipid scramblase 1
STAT1	STAT91	Signal transducer and activator of transcription 1, 91 KDa
USP18	USP43	Ubiquitin specific peptidase 1

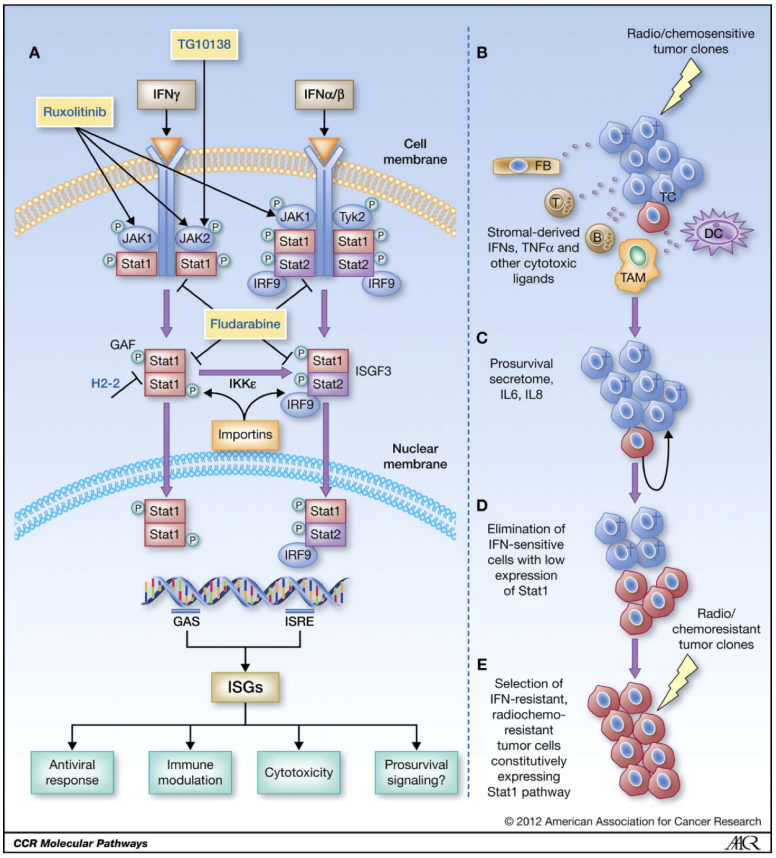

Figure 1.7: Role of the IRDS signature in the tumour resistance (Khodarev *et al.*, 2012). Anti-tumour treatments confer a positive selection to radio- and/or chemoresistant tumour clones. (A) IFN/STAT1 pathway highlighting most common anti-cancer drug targets. (B) Majority of tumour cells will be eliminated after cancer treatment in cooperation with immune-system activity. (C) A discrete subset of tumour cells is insensitive to genotoxic therapy and progresses. (D) Clonal expansion of those tumour clones resistant to cytotoxic stress. (E) Resistant tumour variants populate tumour microenvironment.

1.5.1 IFITM1

This section will serve as a brief description of IFITM1 implications in relation to chemotherapeutic drug resistance. Additional IFITM1 features will be discussed in more detail in upcoming sections. IFNs are widely administrated as anti-cancer drugs and it is reported that IFNs are able to induce IFITM1 expression. Nonetheless, the role of IFITM1 in this respect is controversial. On one hand, low level expression of IFITM1 is found in high-risk leukemia patients who are less responsive to IFNγ therapy (Akyerli *et al.*, 2005), and an independent study of cisplatin treatment in oesophageal squamous cell carcinoma identified an inverse correlation between IFITM1 levels and tumour resistance after treatment with cisplatin (Fumoto *et al.*, 2008). On the other hand, cisplatin treatment also identified IFITM1 as a candidate for tumour resistance in lung cancer cells (Whiteside *et al.*, 2004). Another study argued that continuous treatment of type I IFN promotes cell resistance to X-rays and correlates with induction of IFITM1 expression (Kita *et al.*, 2003). As previously stated, Khodarev *et al.* identified overexpressed STAT1 in tumour-radioresistant human tumour xenografts (Khodarev *et al.*, 2004). Notoriously, IFITM1 as well as other IRDS genes were highly induced in this subset. This observation indicated that IFITM contributes to cancer cell survival and leads to tumour relapse. Taking in consideration the antiproliferative role of IFITM1 associated with constitutively activated IFN, it may be possible that IFITM1 confers advantages to tumour cells in the presence of anticancer treatments (i.e. radiotherapy) that select for proliferative cells. However, no convincing proof has been revealed about which specific mechanism(s) is activated by IFITM1 in cancer therapy. Interestingly, another study suggested that absence of IFITM2/IFITM3 could be used as a predictor for poor response to chemotherapy in osteosarcoma (Salas *et al.*, 2009).

In conclusion, it is difficult to identify biomarkers responsible of drug resistance. It may be possible that cancer cell survival in the presence of chemotherapeutic agents is conferred by accumulative effects prompted by several molecules. Despite this, IFITM1 gene expression is enhanced after administration of different chemotherapeutics. Even so, there is no consensus on how this protein functions at the molecular level. In fact, it may have a pleiotropic effect depending on cancer type and/or tumour stage, where overexpression as well as depletion may have an impact on cancer relapse. Consequently, there is a need to elucidate both alternative cellular functions of IFITM1.

1.5.2 ISG15

Interferon-stimulated gene of 15 kDa (ISG15) is another molecule upregulated by IFNs (Farrel *et al.*, 1979), particularly by type I IFN (Haas *et al.*, 1987; Korants *et al.*, 1984). In fact, it is considered to be one of the most highly expressed genes in response to IFN treatment (Der *et al.*, 1998), and it contains two ISRE sequences responsible for activation of its transcription by IFNs (Zhang & Zhang, 2011). In addition, transcription and expression of

ISG15 are induced by other stress stimuli such as DNA damage, radiation and chemotherapeutic drugs (Gentile *et al.*, 2003; Liu *et al.*, 2004; Park *et al.*, 2016). Nonetheless, it remains uncertain whether ISG15 confers a protective effect or enhances cancer malignancies in drug therapy. For example, ISGylation of proliferating cell nuclear antigen (PCNA) enhances the DNA repair mechanism promoting a chemoresistant phenotype (Park *et al.*, 2014). Alternatively, it is suggested that ISGylation of a splice variant of the transcription factor p63 confers a chemosensitive phenotype by promoting cell arrest and apoptosis (Jeon *et al.*, 2012).

There are many ways to regulate the fate and function of proteins after their synthesis. ISG15 is a great example of covalent conjugation to proteins by ISGylation: a process very similar to ubiquitination (Liu *et al.*, 2013), one of the most well-studied type of posttranslational modification (PTM) (Weston *et al.*, 2014). Ubiquitin was discovered in the late 1970s (Ciehanover *et al.*, 1978; Hershko *et al.*, 1980), and since then many other homologs have been classified as ubiquitin-like proteins (Ubls), the first identified being ISG15 (Farrel *et al.*, 1979). In contrast to other ubiquitin-like proteins, ISG15 is exclusively found in vertebrates but is not well conserved across species (Zhang & Zhang, 2011).

ISG15 is composed of two Ubl domains linked by a proline residue. It has the same C-terminal motif (LRLRGG) as mature ubiquitin, and the last glycine of the motif binds to a lysine located in the target protein. This motif is essential to form ISG15, as well as ubiquitin, conjugates (Haas *et al.*, 1987). The mature ISG15 form undergoes an N-terminal methionine cleavage (Blomstrom *et al.*, 1986) and the last C-terminal eight amino acids (GTEPGGRS) are also removed from the precursor polypeptide (Knigth *et al.*, 1988). As in ubiquitination, ISGylation is a multistep process that also requires a series of specific enzymes; ISG15-activation enzyme (E1-UbE1L) (Yuan & Krug, 2001), ISG15-conjugating enzyme (E2-UbcH8) (Zhao *et al.*, 2004), ISG15-protein ligases (such as E3-Herc5) (Dastur *et al.*, 2006), and ISG15-specific protease (USP18/UBP43, enzyme that liberates ISG15 from the target protein) (Malakhov *et al.*, 2002).

A substantial amount of work remains to be done before the molecular implications of ISG15 are fully understood i.e. which proteins are ISGylated, and what are their functions. Despite this, continuous scientific efforts aim to identify new ISG15-target proteins (Giannakopoulos *et al.*, 2005; Takeuchi *et al.*, 2006), and several hundreds of protein candidates have been identified (Durfee *et al.*, 2010). Some of these protein targets are defined as IFN-related proteins such as STAT1 or JAK1 (Zhao *et al.*, 2005). Based on the broad biological roles of these proteins, it presents a real challenge to determine fundamental cellular implication(s) for ISG15.

There are two forms described for ISG15: free, and in conjugation. Cellular functions of free and conjugated ISG15 differ and free ISG15 is found both intra- and extracellularly. Interestingly, IFN induction of ISG15 in its free form does not necessarily lead to an increase of ISGylation. ISG15 stimulation or depletion of UBP43 protease sustains type I IFN signalling (Malakhova *et al.*, 2003). Moreover, the free ISG15 form is able to induce

production and secretion of IFNγ from CD3+ cells to activate the cytotoxic effect of NK cells (Recht *et al.*, 2018) . In addition, ISG15 associates with target proteins (Loeb & Haas, 1994; Loeb & Haas, 1992) while in its free form is generally related to cytokine generation and enhancing the immune system (Cunha *et al.*, 1996; Recht *et al.*, 2018).

Similar to IFITM1, ISG15 also has roles in both antiviral activity and cancer. Initially, ISG15 was described as anti-viral molecule and is upregulated with bacterial and viral infection (Mossman *et al.*, 2001; Nicholl *et al.*, 2000). ISG15 deficiencies increase susceptibility to infection; for example *Isg15* $^{-/-}$ mice are more prone to influenza, herpes, and Sindbis infections. In fact, lack of LRLRGG motif in ISG15 (responsible of intracellular ISG15 conjugation) abrogates protection from Sindbis virus (Hsiang *et al.*, 2009; Lenschow *et al.*, 2007; Lenschow *et al.*, 2005). In addition, free ISG15 inhibits ubiquitylation of Ebola virus VP40 protein by intercepting Nedd4 (ubiquitin E3). Mechanistically, ISG15 (even in its free form) inhibits the interaction of Nedd4-like E3 ligase with viral PPXY motifs by preventing its interaction with the E2 and the substrate protein complex. Consequently, VP40 protein is not ubiquitinated and the viral particles are not released extracellularly (Malakhova & Zhang, 2008). Likewise, ISG15 restricts the release of HIV-1 virions by inhibiting the ubiquitination of Gag and Tsg101 viral particles, consequently impeding their interaction (Okumura *et al.*, 2006). In response, viruses engineer new mechanisms to inhibit the anti-viral effect of ISG15. For example, influenza B virus NS1 protein inactivates ISG15 conjugation (Yuan & Krug, 2001). Other viruses also inactivate the protective effect of conjugated ISG15 by having a de-ISGylated activity (Clementz *et al.*, 2010; Lindner *et al.*, 2007).

From the cancer perspective, emerging studies have related ISG15 to tumourigenicity. ISG15 overexpression has been reported in several cancer types (Andersen *et al.*, 2006; Darb-Esfahani *et al.*, 2014; Vincent-Chong *et al.*, 2012; Wood *et al.*, 2012). In this regard, high-grade serous carcinoma, the most recurrent type of ovarian carcinoma, is responsive to chemotherapy, but the incidence of tumour relapse is also high and this usually leads to a low survival rate (Thigpen *et al.*, 2011). There is an increase in ISG15 expression in patients with relapsed ovarian carcinomas and this significantly correlates with a favourable prognosis, possibly by mediation of the NF-kB factor (Darb-Esfahani *et al.*, 2014). In contrast, ISG15 is related to carcinogenesis; ISG15 expression and global protein ISGylation are elevated in distinct types of cancer cells compared to normal cells (Desai *et al.*, 2006; Kiessling *et al.*, 2009). Moreover, ISG15 shows an inhibitory effect on protein polyubiquitination, altering protein degradation in the ubiquitin/26S proteasome pathway (Desai *et al.*, 2006; Desai *et al.*, 2012). Immunochemistry analysis of breast cancer tissue shows elevated ISG15 in comparison to normal tissue and, in addition, ISG15 has poor response to chemotherapy or radiation. In fact, it is proposed as tumour-associated antigen suitable for cancer immunotherapy (Wood *et al.*, 2012).

1.5.3 HLA-B

HLA-B is a gene member of the human leucocyte antigen (HLA) complex. This gene complex is located on human chromosome 6 and it encodes the major histocompatibility complex (MHC). The MHC is divided into three groups: class I (HLA-A, HLA-B, HLA-C); class II (HLA-DR, HLA-DQ, HLA-DP); and class III (genes that complement the MHC signalling cascade). Additional allelic variants have been described, but they are less well characterized (Dendrou *et al.*, 2018). Because HLA-B (in conjugation with HLA-G) is identified as a component in the IRDS signature and is a member of the MHC class I molecules, this section will concentrate on describing the main features of the MHC class I pathway (Figure 1.8). Furthermore, the principal focus of this thesis is to investigate those proteins related to IFITM1, and HLA-B is relevant to this study.

The MHC is one of the most hypervariable loci in the human genome, and this makes it extremely difficult to study. Each allelic variant has specific affinity for a subset of peptides, and each differs in expression as well as complex assembly. As a consequence, the physiological functions of these molecules are essential for cell survival; these complexes are critical factors in the immune response to viruses and other intracellular aberrations. If dysregulated, the MHC is associated with most autoimmune diseases, but also with tumour–antigen recognition and transplant rejection.

Both MHC class I and MHC class II molecules, effectively present peptides (typically 8–10 amino acids in length) (Rammensee *et al.*, 1993) at the cell surface, and theses are recognized by $CD8^+$ and $CD4^+$ T cells respectively. From a mechanistic point of view, they are implicated in the cell-defence mechanism that distinguishes self-proteins from proteins produced by foreign invaders (i.e. viruses or bacteria). In particular, $CD8^+$ T cells (also known as cytotoxic T lymphocytes or CTL) are responsible of eliminating the infected or tumour cell by releasing cytotoxic granules that contain perforin and granzymes. Perforin attacks the cell membrane, making pores, and granzymes cleave intracellular proteins; all together result in cell death by activating the apoptosis program. Additional Fas/FasL interactions between CTL and infected cells also enhances apoptosis by activation of the caspase cascade. CTL also secrete TNF-α and IFNγ which have anti-microbial and anti-tumour effects (Halle *et al.*, 2017). In addition, IFNγ induces HLA genes, as well as other components of the cascade, consequently enhancing the antigen-presentation pathway (Früh & Yang, 1999; Rosa & Fellous, 1988).

MHC class I molecules are comprised of two subunits synthesized in the ER: a variable heavy α-chain (the most well-known haplotypes are: HLA-A, HLA-B, and HLA-C) and an invariable light β-chain (B2M). HLAs are highly polymorphic and this feature impacts on protein structure. Each variant has a different peptide-binding groove and consequently, this increases the repertoire of peptides displayed in association with MHC class I (Trowsdale, 2005). HLA-B is loaded with peptide and guided to the cell membrane more rapidly than the other two counterparts, HLA-A and HLA-C (Peh *et al.*, 1998). In addition, HLA-B

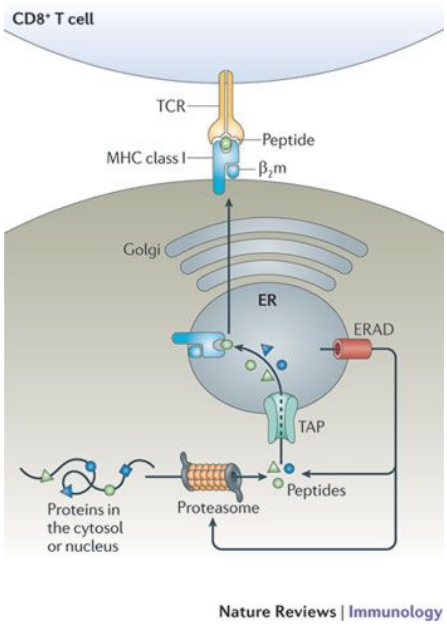

Figure 1.8: MHC class I antigen presentation pathway (Neefjes *et al.*, 2011). The initial step involves protein degradation in the proteasome to obtain antigenic peptides. Peptides will then be incorporated to the endoplasmic reticulum (ER) via transporter associated with antigen processing (TAP). Once inside the ER, peptides will be loaded onto the MCH class I complex, sent to the Golgi apparatus and finally guided to the plasma membrane. Optimal assembly on the cell surface is required for it to be recognized by T cell receptor (TCR) on the $CD8^+$ T cell.

(in most of its polymorphic variants) tends to be successfully loaded with peptide more frequently than HLA-A and HLA-C (Neefjes & Ploegh, 1988). Once at the cell membrane, MHC class I molecules loaded with peptide are highly stable. In contrast, the dissociated heavy chain has a very short life (Neefjes *et al.*, 1992). The complex is normally recycled by the endocytic pathway (Adiko *et al.*, 2015).

MHC class I molecules are ubiquitous and present peptides of an intracellular nature. Peptides are cell-associated antigens of different types: tumour-, viral- or self-antigens. An alternative and non-canonical presentation pathway has been described, in which there is cross-presentation of exogenous peptides via MHC class I found in dendritic cells (Vyas *et al.*, 2008). Antigen presentation requires the proteolysis of the protein to produce the antigenic peptide. Theoretically, the half-life is highly variable between proteins and it will determine the frequency with which the MHC class I presentation machinery will be able to expose the antigenic peptide for $CD8^+$ T cell recognition (Figure 1.9). Nonetheless, empirical observation shows that viral proteins are presented more rapidly than expected. In fact, many proteins are degraded before being functional as a result of synthesis defects. These products known as defective ribosomal products (DRiPs) are degraded and used as a substrate for the MHC class I-peptide loading (Reits *et al.*, 2000). In addition to DRiPs, age-associated damage or incorrectly folded proteins are another source of peptide formation (Yewdell, 2001).

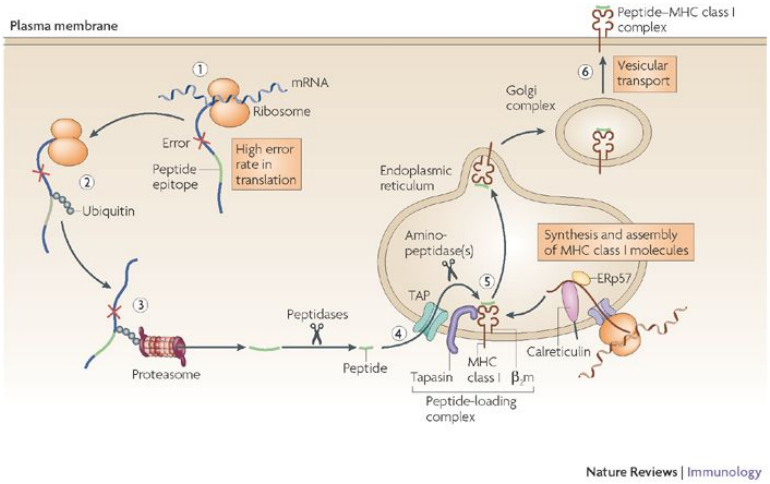

Figure 1.9: Trafficking of MHC class I molecules to the cell surface (Vyas *et al.*, 2008). (1) The first event involves the production of an aberrant protein. Oncoproteins could also be interpreted as aberrant by the cell. (2) Protein is targeted with ubiquitin for degradation. (3) Proteasome is responsible of degrading the protein to produce peptides. (4) Peptides are translocated into the ER by TAP and tapasin; TAP channels cytosolic peptides into the ER and tapasin, also known as TAPBP, is a chaperone that promotes peptide folding and correct binding to the MHC class I. (5) Nascent MCH class I becomes accessible in the ER to load the peptide. This process will be facilitated by tapasin and other ER proteins such as calreticulin and ERp57. (6) Once the MCH class I is loaded with the peptide it guided to the cell membrane through the Golgi apparatus.

A large amount of MHC class I molecules are unable to correctly bind to peptides and so they are eliminated by the ER-associated protein degradation system (Hughes *et al.*, 1997). As such, antigen presentation is limited by rate of protein synthesis but also by the pool of completely functional MHC class I molecules. If peptide binding to the MHC class I complex fails, peptides are trimmed, recycled back to the ER lumen and subjected to another round of recognition. Alternately, they are eliminated by peptidases after being released into the cytosol (Koopmann *et al.*, 2000; Roelse *et al.*, 1994). Strikingly, the proteasome produces 10^4–10^6 fold more peptides than MHC class I molecules are able to bind. This is compensated by the rapid rate of the antigen presentation cycle and additional massive degradation of those peptides that are unbound (Figure 1.10) (Princiotta *et al.*, 2003; Yewdell *et al.*, 2003).

From a clinical perspective, Ferrara *et al.* revealed that radiation in combination with immunotherapy leads to a better outcome than each alone. Radiation has negative collateral effects producing a suboptimal immunological response. To overcome this, anticancer immunotherapies have been designed to enhance CTL–tumour cell recognition to specifically target cancer neoantigens (Ferrara *et al.*, 2009). Paradoxically, radiation also upregulates expression rates of immune-related mediators in surviving radiated tumours, making them more susceptible to immuno-recognition. Among these, MHC class I-peptide presentation is enhanced (Garnett *et al.*, 2004; Reits *et al.*, 2006). Interestingly, the MHC class I antigenic peptide repertoire changes after irradiation. This effect is in accordance with the fact that HLA-B is a component of the IRDS genes and

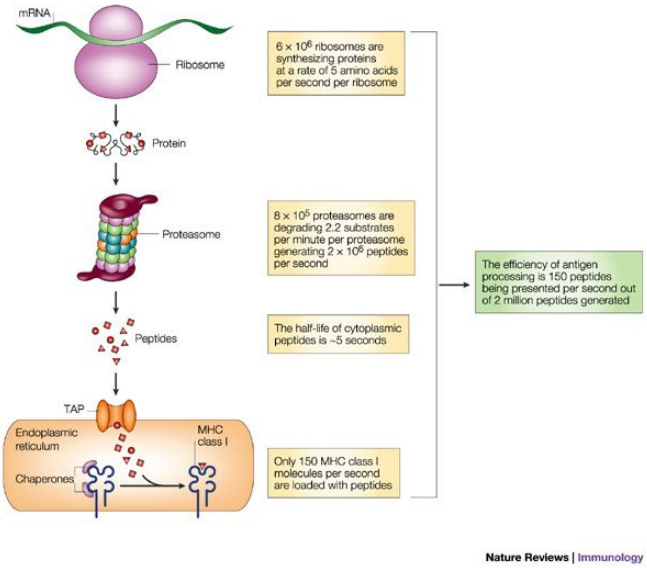

Figure 1.10: Cellular efficiency of MHC class I antigen processing (Yewdell *et al.*, 2003). Representation of the estimated efficiency of antigen processing by the MCH class I complex. These results are based on empirical work, and results should be considered as average; physiological and pathological conditions will alter the outcome. This work is based on measurements taken on L929 cells where it is predicted that only 1 or 2 in 10,000 peptides will bind to the MHC class I complex. DRiPs correspond to approximately 30% of the total protein amount synthetized by ribosomes. The number of MHC class I molecules loaded with peptide per second was measured considering their half-life and the number of molecules assembled at the cell surface.

these have been found upregulated after chemo- and radiotherapy. In contrast, tumours evolve rapidly and activate immune escape mechanisms such depletion of MCH class I and tumour-antigens to attenuate the immune attack. Changes in HLA function inhibits the HLA–oncopeptide–TCR interactions decreasing tumour recognition by immune system (Dendrou *et al.*, 2018). In this respect, loss of MHC is a widespread mechanism identified in multiple cancer types. Several MHC alterations have been described in cancer; HLA defects are found at gene level with loss of heterozygosity, hypermethylation, and mutations of the *HLA* and $\beta 2M$ genes; and at transcript level by decreasing HLA and β2M mRNA (Garrido *et al.*, 2010). MHC class I molecules have been found recurrently mutated across several human cancer types, thus producing differences in the functional nature of these proteins. Systematic patterns in somatic mutations are identified for specific cancers such as HLA single mutations found in glioblastoma and lack of mutations in liver cancer (Shukla *et al.*, 2015). In addition, somatic HLA mutations are highly prevalent in head and neck, lung squamous and stomach cancer (Shukla *et al.*, 2015).

1.5.4 Description of additional IRDS components of interest: STAT1, Mx1, and IFIT1

STAT1 is the putative downstream effector of INFγ signalling. Gene expression profiling of multiple cancer types consistently identified induced *STAT1* and *IFITM1* in breast,

prostate, and gliosarcoma cells exposed to radiation (Tsai *et al.*, 2007). Interestingly, it is believed that tumours with persistent IFN exposure will overexpress STAT1, but in contrast cells will fail in activating a cytotoxic response when irradiated or externally stimulated with IFN (Khodarev *et al.*, 2007). In fact, an IFN non-canonical pathway leads to induction of IRDS genes through unphosphorylated STATs. As a result, the expression of immune-related genes, IRDS, is sustained for a longer time in comparison to phosphorylated STATs (Cheon & Stark, 2009; Cheon *et al.*, 2011). In addition, unphosphorylated STATs were found to promote a gene expression profile related to anti-viral and DNA damage resistance by binding to alternative ISRE sites (Cheon *et al.*, 2013). Increased STAT1 correlates with a radiation-resistance phenotype in injected head and neck cancer xenografts in a murine model (Khodarev *et al.*, 2004). Moreover, STAT1 protein amount is elevated after ionizing radiation but IFNγ remain unchanged (Sreekumar *et al.*, 2001). An independent study also argues that constitutive expression of STAT1, mediating the expression of other IRDS, is responsible for the protective effect in radiation (Khodarev *et al.*, 2004). These findings were also demonstrated in a murine model of melanoma where sustained activation of STAT1 has been correlated with metastasis and resistance to chemotherapy (Khodarev *et al.*, 2009).

Mx1 is repeatedly identified as a component of the IRDS signature in several independent studies (Duarte *et al.*, 2012; Erdal *et al.*, 2017; Weichselbaum *et al.*, 2008a). Mx1 are IFN-inducible proteins belonging to the GTPases-dynamin superfamily. They attenuate a wide diversity of RNA viruses by detecting viral nucleocapsid structures and blocking viral replication. For example, an Mx1 murine model restricts influenza by inhibiting the interaction of virus polymerase subunit PB2 and nucleoprotein (Strandem *et al.*, 1993; Verhelst *et al.*, 2012). Human Mx proteins are accumulated in the cytoplasm and distributed in granules. In fact, Mx1 has been found in the smooth endoplasmic reticulum (Haller & Kochs, 2002).

Interferon-induced protein with tetratricopeptide repeats 1 (IFIT1) is one of the first described ISG genes. IFIT1 is clustered with IFIT3, another gene from the same family that is also identified as IRDS. Both genes are induced by IFN, virus attack, dsRNA or LPS structures. IFIT1 suppresses translation by interacting with eIF3 and inhibiting the formation of eIF3–GTP–Met-tRNA ternary complex (Fensterl & Sen, 2011). Additionally IFIT1 is associated with IFIT2 which has an apoptotic role (Stawowczyk *et al.*, 2011). Association of IFIT1 in translational complexes in the ribosome affect the replication of viruses, such as Hepatitis C or West Nile (Wacher *et al.*, 2007; Wang *et al.*, 2003). Moreover, IFIT1 interacts with E1 protein in HPV virus, impeding the viral DNA replication (Terenzi *et al.*, 2008).

1.6 IFITM phylogenetic features and study of IFITM topology

The interferon-induced transmembrane (*IFITM*) gene family is comprised of the following members: *IFITM1, IFITM2, IFITM3, IFITM5, IFITM6, IFITM7, IFITM10* and addi-

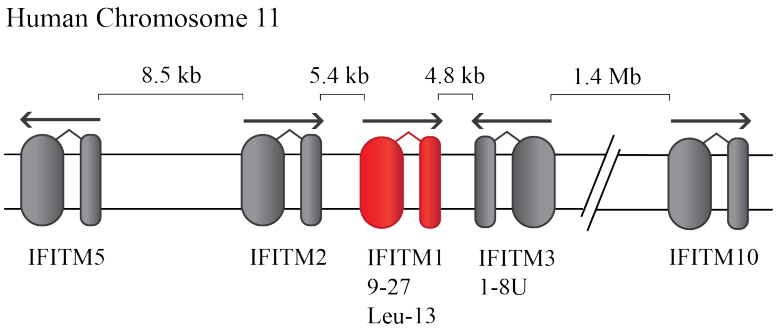

Figure 1.11: Chromosome location of the human *IFITM* genes (adapted from (Zhang *et al.*, 2012)). Order and orientation of *IFITM* genes in the gene-cluster. Two connected boxes represent two exons of each *IFITM* gene and the arrow indicates the orientation of transcription. Only chromosomes containing genes from the *IFITM* gene-cluster and *IFITM10* are shown in the panel.

tional IFITM-like genes. All of them, except *IFITM5* and *IFITM10*, are IFN inducible. They are present in a wide range of cell types and their expression levels vary during development and in malignancies. IFITM6 and IFITM7 are only identified in rats and mice (Zhang *et al.*, 2012) whereas IFITM5 is associated exclusively with bone formation (Hanahan & Weinberg, 2011; Moffatt *et al.*, 2008).

IFITMs were first discovered in IFN stimulated T98G neuroblastoma cells by Friedman *et al.* (Friedman *et al.*, 1984). Some years later, further work conducted by Reid *et al.* and Lewin *et al.* established IFITMs as a protein family and corroborated their inducibility by IFN (Reid *et al.*, 1989; Lewin *et al.*, 1991). Other family members, like IFITM5, were reported after searching for genetic homology.

An extensive phylogenetic analysis in 27 vertebrate genomes stratified *IFITM* genes in three clades: IFN-related, *IFITM5* and *IFITM10*. The IFN-related IFITMs are clustered in the same group in different mammalian species suggesting that they are conserved through evolution. Interestingly, mammals contain more IFN-related IFITMs compared to other vertebrates. Analysis showed that *IFITM2* and *IFITM3* originated in a common ancestor between humans and other hominids. Moreover, it is suggested that during evolution the *IFITM1* gene was duplicated, producing *IFITM2* and *IFITM3* (Zhang *et al.*, 2012). IFITM1, IFITM2 and IFITM3 have been described as restriction factors, providing antiviral activity in the presence of a wide range of pathogens. Their role in viral inhibition will be discuss in detail in later sections.

Homologues of IFITMs have been identified in several species, although their specific chromosomal arrangement differs even between hominids. The focus of this study is human IFITM1 and, by extension, IFITM2 and IFITM3. Human IFITM1 is encoded by the *IFITM1* gene located on chromosome 11p15.5 and is flanked by the *IFITM2* and *IFITM3* genes. *IFITM5* is located 8.5 kb upstream and *IFITM10* 1.4 Mb downstream (Figure 1.11).

It remains unclear if absence of IFITM1 promotes cancer development by increasing aggressiveness and invasiveness or, on the contrary, it has a protective effect. What seems

```
sp|P13164|IFITM1_HUMAN      ----------------------MHKEEHEVAVLGPPPSTILPRSTVINIHSETSVPDHVVW
sp|Q01629|IFITM2_HUMAN       MNHIVQT-FSPVNSGQPPNYEMLKEEQEVAMLGVPHNPAPPMSTVIHIRSETSVPDHVVW
sp|Q01628|IFITM3_HUMAN       MNHTVQTFFSPVNSGQPPNYEMLKEEHEVAVLGAPHNPAPPTSTVIHIRSETSVPDHVVW
                                          * ***:***:** * ..  * ****:*.***********

sp|P13164|IFITM1_HUMAN       SLFNTLFLNWCCLGFIAFAYSVKSRDRKMVGDVTGAQAYASTAKCLNIWALILGILMTIG
sp|Q01629|IFITM2_HUMAN       SLFNTLFMNTCCLGFIAFAYSVKSRDRKMVGDVTGAQAYASTAKCLNIWALILGIFMTIL
sp|Q01628|IFITM3_HUMAN       SLFNTLFMNPCCLGFIAFAYSVKSRDRKMVGDVTGAQAYASTAKCLNIWALILGILMTIL
                             *******:* ********************************************:***

sp|P13164|IFITM1_HUMAN       FILLLVFGSVTVYHIMLQIIQEKRGY
sp|Q01629|IFITM2_HUMAN       LIIIPVL-----------VVQAQR--
sp|Q01628|IFITM3_HUMAN       LIVIPVL-----------IFQAYG--
                             :*:: *:           :.*
```

Figure 1.12: Alignment of IFITM1, IFITM2, and IFITM3 amino acid sequences. Isoform sequences were taken from Uniprot; IFITM1 (accession number: P12164), IFITM2 (accession number: Q01629), and IFITM3 (accession number: Q01628) and aligned using CLUSTAL2.1 multiple sequence alignment by MUSCLE (3.8) online tool. Predicted transmembrane residues are highlighted in bold.

consistent is that IFITM1 is the main isoform found dysregulated in many types of cancer. Understanding the peculiarities of this isoform and how it differs from other family members may help in elucidating this issue.

A close look at IFITM topology may give some clues as to how these isoforms may have redundant roles and yet small differences in sequence may give rise to unique cellular functions (Figure 1.12). All three family members share high sequence identity (68% IFITM1:IFITM2, 71% IFITM1:IFITM3, and 87% IFITM2:IFITM3). Additionally, all three IFITM proteins share a large CD225 domain in which two transmembrane domains are predicted. However, terminal regions are not conserved between isoforms; IFITM1 contains an additional 13 amino acids at the C-terminus whereas IFITM2 and IFITM3 have a larger N-terminus with an extra 20 (IFITM2) and 21 (IFITM3) amino acids (Siegrist *et al.*, 2011). Nonetheless, all three have a very similar molecular weight; 13.9 KDa IFITM1, and 14.6 KDa IFITM2/IFITM3.

The IFITM immunity-related protein family are composed of short amino-terminal and carboxy-terminal domains, two transmembrane domains, and a cytoplasmic domain. IFITM1 is slightly different from IFITM2 and IFITM3, with some studies demonstrating that IFITM1 is widely expressed at the cell surface (Weston *et al.*, 2014; Jia *et al.*, 2015).

Several posttranslational modifications have been described for IFITM3. To begin with, IFITM3 is been mapped with S-palmitoylation sites at Cys71, Cys72, and Cys105, closely related to maintaining its cell membrane localization (Yount *et al.*, 2010). Conversely, palmitoylation modifications on murine IFITM1 enhances its anti-viral effect (Hach *et al.*, 2013). In addition, IFITM3 is ubiquitylated at Lys24, Lys83, Lys88 and Lys104. If IFITM3 is not ubiquitylated at these residues it is transported to the late endosomes increasing its antiviral activity (John *et al.*, 2013; Yount *et al.*, 2010). Finally, phosphorylation at Tyr20 affects its endocytic process (Bonifacino & Traub, 2003; Jia *et al.*, 2012). Almost all these residues are shared between these proteins suggesting that these isoforms may also be subjected to these modifications.

Indeed, these modifications have an impact on IFITM molecular functions. It is been reported that particular posttranslation modifications on IFITM3 are implicated in viral resistance mechanisms (Yount *et al.*, 2010). For example, specific S-palmitoylation and ubiquitination decrease antiviral activity. Alternatively, it can also modulate protein traffic to other subcellular compartments. A non-canonical C-terminus signal sequence is responsible for internalizing IFITM1 protein to the early endosomes (Li *et al.*, 2015).

A variety of models have been proposed to explain the dynamic topology of IFITMs, but their topology remains controversial; studies have predicted different arrangements in the cellular membrane. It is clear that they contain an intracellular domain, but it remains under discussion which is the orientation of N-terminus and C-terminus. A study on leukaemia proposed that N-terminus sequence of IFITM1 could be exposed extracellularly (Chen *et al.*, 1984). This hypothesis was also supported by an independent study where IFITM1 was immunoprecipitated from the cell surface (Takahashi *et al.*, 1990). Flow cytometry experiments suggested that the N-terminus and C-terminus can be exposed in the cell membrane (Brass *et al.*, 2009; Li *et al.*, 2013). On the contrary, others concluded that the N-terminus is orientated towards the cytosol by studying residue modifications catalysed by cytoplasmic enzymes (Jia *et al.*, 2012).

In summary, cell type may have an active influence on IFITM1 topology. But regardless of cell type, IFITM1 continues to be remodelled in response to particular stimuli, some of them having potentially the same effect across all IFN-related proteins. That is why there is a need to characterise the different protein conformations and the conditions under which they occur, so as to better understand their functional implications.

1.6.1 IFITMs in cancer malignancy

IFITM1 is a pro-oncogenic receptor and a component of the IRDS pathway. Basal expression of IFITM proteins is observed in some cells and expression can also be induced by type I and type II IFN (Yang *et al.*, 2005). IFITM1 is upregulated during development of radiation resistance, as cells escape from pro-apoptotic and anti-proliferative effects. Therefore, it is present in chemoresistant tumours, with forced expression generating a multi-drug resistant phenotype (Weichselbaum *et al.*, 2008a; Yang *et al.*, 2007).

The functions of IFITM1 in carcinogenesis are poorly understood. Nonetheless, IFITM1 expression has been extensively reported to be dysregulated in many types of cancer (i.e. breast, cervix, colon, ovary, brain and oesophagus) and its high degree of overexpression correlates well with tumour progression and poor prognosis (Borg *et al.*, 2016; Györffy *et al.*, 2008; Novita Sari *et al.*, 2016; Seyfried *et al.*, 2008a; Weichselbaum *et al.*, 2008a; Ogony *et al.*, 2016; Yu *et al.*, 2015). Extensive research has been conducted on this topic. For example, proteomic analysis of purified membrane fraction of mouse astrocytoma cells by LC-MS/MS followed by RT-PCR validation found upregulated IFITM1 and IFITM3, but not IFITM2, in comparison with mouse astrocyte cells (Seyfried *et al.*, 2008b).

In addition, a large-scale study of gene expression in murine colorectal tumours identified IFITMs as highly expressed in adenomas from a murine familial adenomatous polyposis model; expression increased rapidly in response to β-catenin activation. Interestingly, aberrant adenomatous polyposis coli (APC) causes β-catenin accumulation and Wnt signalling impairment, thought to be a key event in development of sporadic cancer in familial adenomatous polyposis (Radtke & Clevers, 2005). Importantly, Radtke & Clevers could not differentiate IFITM2 and IFITM3 isoforms, so it is open to speculation whether both are involved in colorectal carcinogenesis. Moreover, IFITMs are highly expressed at different tumour stages and expression closely correlates with adenoma formation. Thus, it is proposed as a potential biomarker in colorectal cancer diagnosis (Andreu *et al.*, 2006). Another study found upregulated IFITM1 in colorectal cancer where the levels of expression closely correlate with lymph-node and distant metastasis, both being independent prognosticators for poor survival (Liu *et al.*, 2008). In addition, IFITM3, also upregulated, is proposed as a tumour-associated antigenic candidate suitable for developing a cancer vaccine to treat colon carcinoma (Tirosh *et al.*, 2007).

A meta-analysis of ovarian carcinoma gene expression revealed dysregulation of *IFITM1* in a variety of the studies analysed (Györffy *et al.*, 2008). Moreover, alteration of *IFITM1* and *Isg15* mRNA levels are seen in nude mice with human ovarian carcinoma xenografts treated with paclitaxel, also known as Taxol (Bani *et al.*, 2004). The drug destabilizes microtubule assembly causing cell division inhibition at the mitotic phase (Jordan & Wilson, 1998). Paclitaxel is regularly administrated in ovarian carcinomas, but there is risk of development of chemotherapy-resistant tumours (Rowinky & Donehower, 1995).

Another study screened the molecular profiling of oesophageal cancer tissue extracted from patients with familial oesophageal cancer antecedents and IFITM1 was identified in the cluster of upregulated genes. However, after RT-qPCR and TMA validation it was concluded that there was no difference between individuals with familial and non-familial related oesophageal tumours. This indicates that, for the identified group of genes tested, oesophageal cancer development is due to environmental effects (Chattopadhyay *et al.*, 2009).

Proliferative and antiproliferative effects of IFITM proteins prove to be quite cell type-specific. *IFITM1* gene transcripts directly correlate with favourable prognosis in chronic myeloid leukaemia patients (Akyerli *et al.*, 2005). On the contrary, IFITM3 was greatly expressed in glioma patients and loss of IFITM3 on glioma cells decreased proliferation and promoted cell arrest in G0/G1 (Zhao *et al.*, 2013). A study of colorectal cancer gene expression found overexpression of IFITM proteins in early and late stage of intestinal neoplasm in mice as well as in humans (Andreu *et al.*, 2006). In addition, depletion of IFITM1 performed in five different human glioma cell lines decreased proliferation, migration and invasion (Yu *et al.*, 2011). Similarly, IFITM1 is implicated in invasion and migration in head and neck cancer types (Hatano *et al.*, 2008).

It remains unknown which IFN-dependent genes affect the cell cycle but IFITMs may

be participating in this function. A study conducted by Yang *et al.* correlated IFITM1 to the antiproliferative effect of IFNγ (Yang *et al.*, 2007). It was found that IFITM1 plays a fundamental role in inhibiting cell growth and tumourigenesis. Additionally, IFITM1 arrests cell cycle progression in G1 phase in a p53-dependent manner, promoting p53 transcription and stabilization through inhibiting Thr55 phosphorylation. Several studies have found evidence that the IFN-dependent antiproliferative effect extends the cell cycle by inhibiting G0/G1 and prolonging S phase (Murphy *et al.*, 2001; Sangfelt *et al.*, 1999; Vannucchi *et al.*, 2005).

IFITM1 mRNA is overexpressed in gastric tumour tissue as well as in cell lines. Remarkably, it was induced by IFNγ but not by TNFα or TGFβ1 stimulation. IFITM1 induced by IFNγ for 24 hours confers a cell phenotype more prone to migrate, invade and is resistant to NK cell neutralization. Using a gastric cell model, IFITM1 was proposed as a cell surface receptor that inhibits NK cytotoxicity, conferring immune-evasion (Yang *et al.*, 2005).

Given the highly heterogeneous nature of cancer, it is difficult to conclude at which stage of the disease IFITM1 may have an impact, or if IFITM1 has different effects depending on the cancer type and stage. All-in-all, it is essential to better understand the type of cancer under study. High heterogeneous tumour formation and environment can completely change the status of the cancer and, therefore, the proteome expressed as well as the pathways activated.

1.7 IFITMs in viral pathology

Organisms are constantly threatened by the invasion of viral pathogens. Mammalian cells have developed self-defence mechanisms involving the activation of restriction factors that mediate viral suppression. Viral invasion, in RNA or DNA form, triggers almost immediately the production of type I IFN (Stetson & Medzhitov, 2006). However, immunomodulatory effects of type II IFN are essential in the longer term. Secreted IFN will alert neighbouring cells of the pathogenic presence and consequently ISG expression will be induced to neutralize the virus. Both IFN types are extremely versatile and are involved in the activation of several cellular pathways in health and disease. Thus, viral inhibition is the result of cooperative effects of several ISGs (Schoggins *et al.*, 2011). In combination, they confer one of the first described and more fundamental immune responses.

Viruses are considered to be the most abundant biological entities. Their molecular diversity and high predisposition to continuous mutations challenge mammalian cells to develop cellular systems to attenuate infection. Moreover, it is complicated to identify molecules capable of broadly targeting several virus types. Nonetheless, IFITM family members are one of the most dominant anti-viral ISGs, capable of attenuating the pathogenic effect of many human and animal viruses. Interferon stimulated-IFITM1/2/3 proteins repress viral replication of influenza A and flaviviruses, including dengue virus and West Nile, among others. Interestingly, each IFITM family member exhibits specific

viral preferences; in the case of IFITM1, it is particularly known for its attenuation of HCV, influenza A and SARS coronavirus (Bailey *et al.*, n.d.; Brass *et al.*, 2009; Huang *et al.*, 2011; Wilkins *et al.*, 2013).

IFITM family proteins inhibit cytosolic entry of viruses by preventing fusion of viral and host membranes. The protein–protein interaction networks by which IFITM proteins inhibit membrane fusion still remain unclear. Interestingly, all these viruses contain viral envelope proteins. One study proposed IFITM2/3 as one of the most dominant ISG-stimulated genes involved in suppressing viral entry in Nile virus and dengue virus (Jiang *et al.*, 2010). Similarly, the N-terminal sequence of IFITM2/3 is capable of inhibiting entry of HIV-1 virus, possibly by interfering in HIV-1 endocytosis and dynamin-dependent cell fusion (Miyauchi *et al.*, 2009). Additionally, IFITM1/2/3 depletes virus production by interfering with the viral Gag expression (Lu *et al.*, 2011). It is suggested that IFITM3 resides in endosomes where it is able to interfere with influenza A endosomal trafficking. High levels of IFITM3 prevent incorporation of the viral genome in the host cell nucleus and promote formation of late endosomes and lysosomes that will potentially degrade viral particles (Feeley *et al.*, 2011). Mice with *Ifitm3* gene deleted are more susceptible to influenza A. Indeed, people who have certain IFITM3 polymorphisms are more susceptible to infection and more risk to be hospitalized. For instance, SNP rs12252 C allele induces an alternative splicing variant that lacks the first 21 amino acids (Everitt *et al.*, 2012).

Consistently, IFITMs are described as restriction factors. Several studies have hypothesized that IFITM are able to block viral entry by inhibiting fusion between host plasma membrane and virus, and by suppressing viral traffic in early endosomes. However, the exact mechanism by which IFITM1 inhibits viral endocytosis remains unclear. Comparing IFITM isoforms, IFITM1 lacks the first 20 N-terminal amino acids and it compensates with a larger C-terminal sequence. These structural differences between IFITM1 and IFITM3 may indicate why they are prone to restrict different (or with different intensity) types of virus. For instance, a study described the 20-YEML-23 motif in IFITM3, which is absent in IFITM1, promotes endocytic influence on pH-dependent viral restriction (Jia *et al.*, 2014). This sorting signal, however, is not associated with attenuation of HIV, as wild type IFITM3 and the 21-amino acid deletion mutant show equal inhibition. Thus, IFITM3 should have alternative mechanisms to repress viruses (Jia *et al.*, 2012). In addition, S-palmitoylation posttranslational modification of IFITM3 increases attenuation of influenza (H1N1 and PR8 strain) virus (Yount *et al.*, 2010). IFITM1 represses HCV entry by interacting and redistributing CD81 (HCV coreceptor) in hepatic tight junctions (Narayana *et al.*, 2015; Wilkins *et al.*, 2013). Moreover, truncation of C-terminal 117-QIIQEKRGY-125 of IFITM1 diminishes HIV-1 replication but not that of VSV virus. This mutant is able to trap IFITM1 in the cell membrane as it perturbs the natural subcellular distribution (Jia *et al.*, 2015). Supporting research shows that mutation of two residues in the C-terminal (KR/AA) diminishes IFITM1 ubiquitination and alters IFITM1 endocytic trafficking (Li *et al.*, 2015).

Continuous scientific effort has begun to elucidate the molecular mechanism(s) of

IFITMs as a restriction factor, however there is still a lot to be investigated. This thesis focuses on understanding IFITM1 from a cancer perspective but ideally, we aim to translate our findings to a viral point of view.

1.8 Aims of the project

The initial goal of the present study was to better understand the molecular function(s) of IFITM1 and IFITM3 proteins. The IFN pathway is very complex and is able to mediate the expression of hundreds of genes. As such, the greatest challenge of this thesis was to be able to dissect IFITM1/IFITM3–IFNγ dependencies. The ultimate aim was to understand the fundamental roles of IFITM1/IFITM3 after IFNγ stimulation in the cancer context. To answer these questions:

- An isogenic *IFITM1* null and *IFITM1/IFITM3* double null cervical cancer model was depeloved employing CRISPR/Cas9 system to define dependent pathways of IFITM1/3 signalling (chapter 3).
- We aimed to define new IFITM1 interacting partners by mass spectrometry methodologies to start characterizing new pathways involved in cancer progression (chapter 4).
- Moreover, we studied the RNA loading on the ribosome and the emerging polypeptides by polysome profiling, subcellular SWATH-MS, and pulse SILAC (chapter 5).
- RNA-seq analysis was performed to investigate possible differences in the transcript expression associated with IFITM1/IFITM3 loss (chapter 6).

All-in-all, the final goal was to propose an IFNγ-responsive biochemical model for the IFITM1/IFITM3 proteins as a mechanism to explain why loss of IFITM1/IFITM3 might stimulate cancer metastasis.

Chapter 2

Materials and Methods

2.1 Plasmids

The plasmids used throughout this thesis are: pEXPR-IBA105-SBP-tagged (IBA Lifesciences); pMA-T-15ADAZQP wild type IFITM1 (Invitrogen); pEXPR-IBA105-SBP-tagged wild type IFITM1 (IBA Lifesciences); pcDNA3.1 (Addgene), pcDNA3.1 wild type IFITM1 (Addgene); pSF-CMV-FLuc-CMV-Zep-BgH-sbf1 (Oxford Genetics); pCMV-myc-hIFITM3 (Clontech); pSF-CMV-FLuc-CMV-Zep-BgH-sbf1-IFITM3 (Oxford Genetics); pCG T7-SF2/ASF (Addgene); pT-Rex-DEST30TM SBP-tagged (Thermo Fisher); pT-Rex-DEST30TM SBP-tagged wild type ISG15 (Thermo Fisher) and pT-Rex-DEST30TM SBP-tagged mutated ISG15AA (Thermo Fisher).

2.2 Cell culture

2.2.1 Cell lines and maintenance

Wt-SiHa cells, *IFITM1* null cells, *IFITM1/IFITM3* double null cells, *IFITM3* null cells, and SBP-IFITM1 SiHa cells were grown in RPMI 1640 media (Invitrogen) (Table 2.1). Cells were supplemented with 10% (v/v) foetal bovine serum (FBS) (Labtech) and 1% (v/v) 0.5 U/ml penicillin/ 500 ng/ml streptomycin (P/S) (Invitrogen) and incubated at 37°C with 5% CO_2. Cell culture work was carried in a category 1 tissue culture room.

Cells were routinely sub-cultured in 10 cm tissue culture dishes (Greiner CELLSTAR, Sigma), according to cell growth, 1 to 3 times per week. Cells were washed with 10 ml of sterile 1x phosphate buffered saline (PBS) and trypsinised with 2 ml of warmed 1x Trypsin–EDTA 0.5% (Gibco, Life Technologies). Cells were kept in the incubator for 10 min to detach and then 8 ml of fresh warm media was added. Cells were seeded in a new 10 cm tissue culture dish at the required dilution, typically 1:5.

Cells were counted by mixing 10 μl of trypsinised cells in fresh media 1:1 with trypan blue stain 0.4% (Labtech) and 10 μl were added to Luna counting slides (Labtech) and

counted in a Luna Automated BF cell counter (Labtech). An appropriate number of cells was seeded, according to each experimental design.

Table 2.1: Cell lines used.

Cell line	Description
wt-SiHa	Human cervical carcinoma cells, wild type
IFITM1 null	Human cervical carcinoma cells, *IFITM1* knock out
IFITM1/IFITM3 double null	Human cervical carcinoma cells, *IFITM1/IFITM3* knock out
IFITM3 null	Human cervical carcinoma cells, *IFITM3* knock out
SBP-IFITM1 SiHa	Human cervical carcinoma cells, SBP tagged-IFITM1 knock in

2.2.2 Cell storage

Around 1 x10^6 to 5 x10^6 viable cells per vial were resuspended in 1 ml of freezing media; 50% FBS, 20% DMSO, and 30% RPMI media (not supplemented with FBS or P/S). Cells were in 1 ml aliquots in cryotubes. Vials were placed in a freezing container (Nalgene Cryo) and kept at -80 ^{o}C for progressive cooling down to -80 ^{o}C. Finally, frozen cells were transferred to liquid nitrogen for long-term storage.

2.2.3 Cell recovery

Cell vials were warmed up at 37^{o}C then transferred to a Falcon tube and centrifugated at 1,000 rpm for 5 min to remove toxic DMSO. The cell pellet was transferred into a new 10 cm dish with appropriate fresh media supplemented with FBS and P/S antibiotics.

2.2.4 IFNγ treatment

SiHa cells were stimulated with a final concentration of 100 ng/ml recombinant human interferon-gamma (Gibco, PHC4031) (henceforth IFNγ) for 24 hours, except otherwise stated.

2.2.5 SILAC labelling

Fully labelled cells by SILAC media

For performing SILAC experiment, wt-SiHa cells, *IFITM1* null cells, and *IFITM1/IFITM3* double null cells were grown in SILAC media as biological triplicates over 5 generations to fully incorporate (if grown in heavy media) the heavy isotopic amino acids from the media. Before harvesting, cells were stimulated for 24 or 48 hours with or without 100 ng/ml IFNγ before harvesting. Cells were isotopically labelled using SILAC RPMI-heavy media (Dundee Cell Products, UK); L-[^{13}C6^{14}N4] arginine (R6) and

L-[^{13}C6^{14}N2] lysine (K6). Cells were harvested in a buffer containing 8 M urea, 0.1 M Tris pH 8.5. Total protein in extracts was measured by Bradford assay (section 2.6.3).

Partially labelled cells by pulse SILAC

For performing pulse SILAC experiment, wt-SiHa cells, *IFITM1* null cells, and *IFITM1/IFITM3* double null cells were grown as biological triplicates and incubated with SILAC heavy media for 6 and 24 hours with or without 100 ng/ml IFNγ before harvesting. Cells were isotopically pulse-labelled using SILAC RPMI heavy media (Dundee Cell Products, UK); L-[^{13}C6^{14}N4] arginine (R6) and L-[^{13}C6^{14}N2] lysine (K6). Cells were harvested in a buffer containing 8 M urea, 0.1 M Tris pH 8.5. Total protein extracts were measured by Bradford assay (section 2.6.3).

2.2.6 Transient transfection of plasmid DNA

For transfection, cells were grown to approximately 80% confluency. SiHa cells showed a good transfection efficiency using Attractene transfection reagent (Qiagen, 301007). Manufacturers recommendations were followed; preliminary titrations of DNA (μg) as well as Attractene volume was performed to determine optimal conditions (data not shown). A 6-well plate transfection mixture was : 1.2 μg of DNA, 4.5 μl of Attractene, and 100 μl serum-free media without antibiotics; A 10 cm dish transfection mixture was: 4 μg of DNA and 15 μl of Attractene, 300 μl serum free media without antibiotics; A 15 cm dish transfection mixture was: 6 μg of DNA and 24 μl of Attractene, 500 μl serum free media without antibiotics . In the case of co-transfection, smaller amounts of each vector was transfected to maintain the same total amount of DNA. All the reagents were mixed and incubated at RT for 15 min. Finally, the transfection mixture was added dropwise to the plate and cells were transfected for 24 or 48 hours, depending on experimental requirements.

2.2.7 Harvesting cells and cell lysis

Cells were harvested on ice to avoid proteolysis. Cells were washed twice in ice-cold PBS, then scraped from the surface and collected for centrifugation at 2,600 rpm at 4 ^{o}C for 10 min. The cell pellet was snap-frozen and kept at -80^{o}C for future use or lysed with denaturing urea lysis buffer (unless stated otherwise) (Table 2.2). Then, the cell pellets were lysed in four times their volume by adding urea lysis buffer and mixed by pipetting up and down. Lysis was performed for 30 min on ice followed by a 20 min centrifugation at 13,000 rpm at 4 ^{o}C. Supernatants were transferred to a new Eppendorf tube.

Table 2.2: 8 M urea lysis buffer.

8 M urea lysis buffer
8 M urea
0.1 M DTT
0.1% (v/v) Triton X-100
25 mM NaCl
20 mM HEPES pH 8
1x Protease inhibitor mix (20 μg/μl leupeptin, 1 μg/μl aprotinin, 2 μg/μl pepstatin, 1 mM benzamidine, 10 μg/μl soybean trypsin inhibitor, 2 mM pefabloc, and 1 mM EDTA- final concentrations).

2.3 Microbiological Techniques

Bacterial cultures were grown in Luria–Bertani (LB) broth in an incubator-shaker at 200 rpm at 37°C. They were grown in Erlenmeyer flasks or Falcon tubes, always four times bigger than the culture volume, to provide enough oxygen.

2.3.1 Glycerol stocks

Glycerol stocks were prepared using 800 μl of the bacterial culture grown overnight an mixed with 200 μl of 80% (v/v) sterile glycerol in a sterile microcentrifuge tube. The tube was snap-frozen using liquid nitrogen and stored at -80°C.

2.4 Preparation of DH5α competent cells

DH5α competent cells from a glycerol stock were incubated in a mini-culture with 5 ml of LB at 200 rpm at 37°C overnight. An aliquot of this culture was transferred into 100 ml LB at 200 rpm at 37 °C and grown until OD_{600nm} reached 0.4. The culture was centrifuged at 4,000 rpm at 4°C for 15 min. The following steps were carried out on ice in the cold room: The pellet was resuspended with 32 ml ice-cold competent buffer I (Table 2.3). After 10 min incubation on ice, cells were centrifuged at 4,000 rpm at 4 °C for 15 min. The pellet was resuspended in 4 ml of ice-cold competent buffer II (Table 2.3). After 10 min incubation on ice, 30 μl of competent cells were aliquoted into pre-chilled sterile Eppendorf tubes, immediately snap-frozen in liquid nitrogen, and stored at -80°C.

Table 2.3: Buffers for making competent cells.

Competent cells buffer I	**Competent cells buffer II**
100 mM RbCl	10 mM RbCl
40 mM $MgCl_2 \cdot 6\ H_2O$	10 mM MOPS
60 mM CH_3COOK	
100 mM $CaCl_2 \cdot 2\ H_2O$	75 mM $CaCl_2 \cdot 2\ H_2O$
15% (v/v) glycerol	15%(v/v) glycerol
pH 5.8 (adjusted with CH_3COOH)	pH 6.5 (adjusted with NaOH)
Sterilised with 0.22 μm filter	Sterilised with 0.22 μm filter

2.4.1 Bacterial transformation using heat shock

Competent cells were stored at -80°C. First, 50 μL of DH5α *E. Coli* competent cells were thawed on ice. Then, 1 to 10 μl of ligation reaction or vector (1–100 ng of plasmid DNA) was added, and tubes were incubated on ice for 30 min. In the meantime, 250 μL of autoclaved LB without antibiotics was warmed at 37°C. Competent cells with the ligation reaction or vector were heat shocked at 42°C for 90 sec and immediately replaced on ice for 2 min. Finally, 250 μL of pre-warmed LB was added and the bacterial cells were incubated with shaking at 250 rpm at 37°C for 1 h and 30 min.

LB agar (Table 2.4) was melted by heating and cooled down before being supplemented with appropriate antibiotic, typically ampicillin at 100 μg/ml final concentration (Sigma, A9518). The media was poured into sterile 90 mm petri dishes (Sterilin) solidified and then plates were dried at 37°C before use.

Between 20–200 μl of transformation product was spread onto LB agar plates with appropriate antibiotic. The pipetting was done under aseptic conditions next to a Bunsen burner, using sterile tips and a sterile spreader. Plates were incubated, inverted, at 37°C overnight for bacterial growth.

Table 2.4: LB broth and LB agar composition.

Luria–Bertani (LB) broth	**LB Agar**
25 g LB in 1 L dH_20	40 g LB agar in 1 L dH_20
1% (w/v) Tryptone	1% (w/v) Tryptone
0.5% (w/v) Yeast extract	0.5% (w/v) Yeast extract
1% (w/v) NaCl	1% (w/v) NaCl
	1.5% (w/v) Agar

2.5 Molecular Biology Techniques

2.5.1 Plasmid DNA purification and quantification

The day after bacterial transformation (subsection 2.4.1), a single colony was picked and inoculated into a tube of LB containing 1:1,000 ampicillin (100 μg/ml) and grown shaking at 220 rpm overnight, then, 3 mL or 150 mL of the culture was used for mini-preps and maxi-preps of DNA, respectively. Bacterial cells were centrifuged at 4,000 rpm from the overnight culture and Plasmid DNA extracted using a QIAprep Spin Miniprep Kit (Qiagen, 27104) and GeneJET Plasmid Maxi Prep Kit (Thermo Scientific, K0492) respectively. DNA obtained was quantified using a NanoDrop ND-1000 Spectrophotometer.

2.5.2 DNA extraction

Chromosomal DNA was extracted from frozen cell pellets following the Gentra Puregene Cell kit instruction manual (Qiagen).

2.5.3 Total RNA isolation and cDNA synthesis

Non-stimulated or IFNγ-stimulated for 24 hours wt-SiHa cells, *IFITM1* null cells and *IFITM1/IFITM3* double null cells were grown in triplicate on 6-well plates. Cells were grown in parallel until 90% cell confluency and then were harvested at the same time and frozen prior to RNA extraction. Total RNA was extracted from frozen cell pellets of 6-well plates following the RNeasy Mini kit instruction manual (Qiagen). RNA samples were pretreated with RNase-free DNase I (Qiagen) to remove DNA contaminant. The quality and purity of the total RNA were analysed using a NanoDrop 2000c Spectophotomer (Thermo Scientific). The cDNA was used for RNA-Seq and RT-qPCR. Equal amounts of three RNA biological replicates were combined in a single sample and 1 μg RNA (at 50 ng/μl) was analysed for RNA-Sequencing by Otogenetics (Atlanta, USA). The remaining RNA (for individual biological replicates) was reverse transcribed into cDNA using qScript cDNA SuperMix in a total volume of 20 μl following the manufacturer's instructions (Quantabio) (Table 2.5).

Table 2.5: PCR conditions for cDNA synthesis.

PCR conditions
5 min at 25^{o}C
30 min at 42^{o}C
5 min at 85^{o}C
Hold at 4^{o}C

2.5.4 Real-time quantitative PCR analysis

The PCR reaction was carried out using cDNA as template. The reaction mixture contained 2 μl of synthesized cDNA mixed with 7.5 μl SYBR green (Sybr Select Master mix, Applied Biosystems), 0.3 μl of mixed specific forward and reverse primers (Sigma, 5 μM stock) (Table 2.6) in a final volume of 20 μl. The PCR was carried out under the cycling conditions described in Table 2.7. Melting curve analysis was performed under the conditions described in Table 2.8.

Table 2.6: Genes and primer pairs used for RT–qPCR.

Gene	Primer	Amplicon
IFITM1	Forward 5' ACTGGTATTCGGCTCTGTGAC 3'	172 bp
	Reverse 5' GCTGTATCTAGGGGCAGGAC 3'	
IFITM3	Forward 5' CAAACCTTCTTCTCTCCTGTCAA 3'	129 bp
	Reverse 5' GATGTGGATCACGGTGGAC 3'	
IRF1	Forward 5' CTCTGAAGCTACAACAGATGAG 3'	218 bp
	Reverse 5' GTAGACTCAGCCCAATATCCC 3'	
ISG15	Forward 5' CTGCTGGTGGTGGACAAATG 3'	162 bp
	Reverse 5' TCAGCCAGAACAGGTCGTC 3'	
B2M	Forward 5' CTCGCTCCGTGGCCTTAG 3'	153 bp
	Reverse 5' GGATGAAACCCAGACACATAGC 3'	
HLA-B	Forward 5' CACTGAGCTTGTGGAGACCA 3'	219 bp
	Reverse 5' ATGACCACAACTGCTAGGACA 3'	
STAT1	Forward 5' GAGCTTCACTCCCTTAGTTTTGA 3'	84 bp
	Reverse 5' CACAACGGGCAGAGAGGT 3'	
β *-ACTIN*	Forward 5 CATGTACGTTGCTATCCAGGC 3	250 bp
	Reverse 5' CTCCTTAATGTCACGCACGAT 3'	

Table 2.7: PCR cycling conditions used for RT–qPCR.

PCR cycling conditions		
Holding Stage	95^{o}C	10 min
Cycling Stage (40 times)	95^{o}C	15 sec
	60^{o}C	30 sec
	72^{o}C	15 sec

Table 2.8: Melting curve parameters.

Melting curve parameters	
95°C	15 sec
60°C	1 min (increasing temperature 0.3°C)
95°C	15 sec

2.5.5 Cloning by PCR

pSF-CMV-IFITM3 primer design

The IFITM3 cDNA was cloned by PCR amplification into untagged pSF-CMV-FLuc-CMV-Zep-BgH-sbf1 (henceforth EV, standing for empty vector) expression vector. Primers were designed to amplify IFITM3 cDNA in the pCMV-myc-hIFITM3 donor vector; forward primer was 5'-GATTGGTACCATGAATCACACTGTCCAAACC-3' and reverse primer was 5'-CGTAGGATCCCTATCCATAGGCCTGGAAGAT-3'. Primers contain recognition sites for KpnI and BamHI restriction enzymes respectively.

SBP-IFITM1 primer design

The IFITM1 cDNA was cloned by PCR into pEXPR-IBA105 (henceforth EV, standing for empty vector) expression vector containing the SBP tag at the N-terminus of the coding region. Primers were designed to amplify IFITM1 cDNA in the pcDNA3.1 donor vector; forward primer was 5'-GGGGGGTACCGATGCACAAGGAGGAA-3' and reverse primer was 5'-CCCCGATATCCTAGTAACCCCGTTT-3'. Primers contain recognition sites for KpnI and EcoRV restriction enzymes respectively.

PCR mix

PCR reaction (20 μl) was performed using the following reagents:

Table 2.9: PCR reagent mix.

PCR reagent mix	
x2 Pfu Mastermix (Rovalab)	10 μl
Forward primer (10 μM)	1 μl
Reverse primer (10 μM)	1 μl
Template vector	5-50 ng dsDNA
Nuclease free H_2O	to up to final volume 20 μl

PCR conditions

PCR amplifications were performed using the following conditions:

Table 2.10: PCR cycling conditions.

PCR cycling conditions		
Hot start	95°C	2 min
Denature DNA*	95°C	45 sec
Annealing*	62°C	45 sec
Elongation*	72°C	1 min
		*Cycle repeated 35 times
Last elongation	72°C	3 min

2.5.6 CRISPR/Cas9 clone validations by Sanger sequencing

Primer design

A PCR technique was used to successfully validate knock out clones generated by CRISPR/Cas9 system. The genomic DNA region of interest was amplified by PCR using the primers in Table 2.11. Note that in some constructs, recognition sites for restriction enzymes were included in the designed primer sequence for further cloning.

Table 2.11: Primers used to sequence the CRISPR/Cas9 clones.

1st set of primers: 475 bp amplicon
2nd set of primers: 1102 bp amplicon
3rd set of primers: 443 bp amplicon
4th set of primers: 976 bp amplicon

1st set of primers:
Forward primer *IFITM1*: 5'-TACAAACAGCAGGAAATAGAAACTT-3'
Reverse primer *IFITM1*: 5'-ACTCACAGTCACAGGGACAC-3'

2nd set of primers:
Forward primer *IFITM1*: 5'-GGGGGGTACCGATGCACAAGGAGGAA-3'
Reverse primer *IFITM1*: 5'-CCCCGATATCCTAGTAACCCCGTTT-3'

3rd set of primers:
Forward primer *IFITM3*: 5'-AGCCCCTCTTTCCTCCCT-3'
Reverse primer *IFITM3*: 5'-TCACGGAGTAGGCGAATG-3'

4th set of primers:
Forward primer *IFITM3*: 5'-GATTGGTACCATGAATCACACTGTCCAAACC-3
Forward primer *IFITM3*: 5'-CGATGAATTCCTACTATCCATAGGCCTGGAAGAT-3'

PCR conditions

PCR amplifications were performed using the following conditions:

Table 2.12: PCR cycling conditions for the 1st set of primers.

PCR cycling conditions		
Hot start	95°C	2 min
Denature DNA*	95°C	45 sec
Annealing*	48°C	30 sec
Elongation*	72°C	1 min
		*Cycle repeated 35 times
Last elongation	72°C	3 min

Table 2.13: PCR cycling conditions for the 2nd set of primers.

PCR cycling conditions		
Hot start	95°C	2 min
Denature DNA*	95°C	20 sec
Annealing*	58°C	45 sec
Elongation*	72°C	1 min
		*Cycle repeated 35 times
Last elongation	72°C	5 min

Table 2.14: PCR cycling conditions for the 3rd set of primers.

PCR cycling conditions		
Hot start	95°C	2 min
Denature DNA*	95°C	45 sec
Annealing*	51 °C	30 sec
Elongation*	72°C	1 min
		*Cycle repeated 35 times
Last elongation	72°C	3 min

Table 2.15: PCR cycling conditions for the 4th set of primers.

PCR cycling conditions		
Hot start	95°C	2 min
Denature DNA*	95°C	20 sec
Annealing*	62 °C	45 sec
Elongation*	72°C	1 min
		*Cycle repeated 35 times
Last elongation	72°C	5 min

2.5.7 Agarose gel electrophoresis

Once the amplicon was amplified (subsection 2.5.5 and subsection 2.5.6), a 1.5–2% (w/v) agarose gel was prepared by heating ultrapure agarose (Electrophoresis-grade, Invitrogen) dissolved in 1x TAE (Table 2.16) and DNA gel stain 1:10,000 SYBR safe (Invitrogen) was added. Then, it was poured immediately into a gel chamber. The sample was mixed with 6x DNA loading dye (New England Biolabs) before loading. Gel was run at 100 V.

Table 2.16: 1x TAE buffer.

1x TAE
40 mM Tris-HCl
1 mM EDTA
pH 8.0 (adjusted with glacial acetic acid)

2.5.8 Gel extraction

If the amplified band had the desired molecular weight, the gel band was cut and purified following the protocol of the GenJet Gel Extraction Kit (Thermo Fisher, K0691) or QIAquick Gel extraction kit (Qiagen, 28714).

2.5.9 Digestion

Then, if required, vector and amplicon were digested with the appropriate restriction enzymes typically at 37°C for 2 hours (Table 2.17).

Table 2.17: Digestion reaction.

Digestion reaction	
Vector, amplicon	0.5 to 2 μg
Smart Cut Buffer (NEB)	2 μl
Restriction enzyme 1 (NEB)	1 μl (10 units)
Restriction enzyme 2 (NEB)	1 μl (10 units)
H_2O_{MQ}	top up to final volume 20 μl

2.5.10 Ligation

After digestion, the vector product was run on a 1–2% agarose gel and purified following subsection 2.5.7 and subsection 2.5.8. Then vector and insert were ligated at RT for 15 min or 16°C overnight (Table 2.18).

Table 2.18: Ligation reaction.

Ligation reaction	
T4 DNA Ligase Buffer 10x (NEB)	2 μl
Vector	50 ng for 3 Kb
Insert	50 ng for 1 Kb
T4 DNA ligase (NEB)	1 μl
H_2O_{MQ}	top up to final volume 20 μl

2.5.11 Validation by DNA sequencing

Validation of cloning as well as edited DNA sequences were confirmed by Sanger sequencing at Source BioScience Service (Scotland or Nottingham). Sample and primers conditions were sent following their requirements. Chromas v1.45 version was used to visualise the sequence chromatogram, SnapGene v3.0 version and Clustwl Omega were used to perform alignment of the DNA sequence.

2.6 Biochemical Techniques

2.6.1 Affinity purification in label-free cells

Wt-SiHa cells were grown in heavy RPMI media in duplicate. Cells were transfected with pEXPR-IBA105-SBP-tagged or pEXPR-IBA105-SBP-tagged full length IFITM1 for 24 and 48 hours. Then, cells were stimulated with 100 ng/ml IFNγ (Invitrogen) for 24 hours for one replicate in order to "stabilize" potential IFNγ-activated SBP-IFITM1 interacting proteins. Cells were washed twice in ice cold PBS and scraped into Triton X-100 buffer containing: 100 mM KCl, 20 mM HEPES pH 7.5, 1 mM EDTA, 1 mM EGTA, 0.5 mM Na3VO4, 10 mM NaF, 10% (v/v) glycerol, protease inhibitor mix, and 0.1% Triton X-100, then incubated for 30 min on ice and centrifuged at 13,000 rpm at 4 °C for 15 min. Equal amounts of protein (at least 250 ng of protein) were used to perform the affinity capture. Streptavidin agarose-conjugated beads (Millipore) were pre-washed with PBS, then cell lysate was added and incubated at RT for 2 hours with gentle rotation. Binding proteins were eluted by heating at 85°C for 5 min with a buffer containing 20 mM HEPES pH 8, 2 mM DTT, and 8 M urea buffer.

2.6.2 Subcellular protein fractionation

A subcellular protein fractionation kit for cultured cells (Thermo Fisher) was used to obtain cytoplasmic, membrane, nuclear soluble, chromatin-bound and cytoskeletal fractions, following protocol instructions.

2.6.3 Protein quantification, SDS-PAGE, and Western blotting

Protein quantification

Protein from lysed samples was quantified using Protein Assay Dye Reagent (Bio-Rad, based on the Bradford protein assay). Bovine serum albumin (BSA) (Sigma) was used as protein standards at concentration rage 0–10 mg/ml was used to determine protein concentration. Bradford reagent was diluted five times in ultrapure water (Milli-Q). The assay consisted of 200 μl of Bradford reagent plus 1 μl of protein standard or lysate mixed in a 96-well plate. After gentle shaking for 10 min, the samples were measured at OD_{595nm} using Bio-rad, iMark microplate reader coupled to MPM 6-microplater Manager software. Protein concentration was determined from the linear standard curve obtained from the BSA standards.

For SDS polyacrylamide gel electrophoresis (SDS–PAGE) protein lysate (normally 20 μg) was mixed 1:1 with 2x SDS sample buffer (Table 2.19) and heated at 85 ^{o}C for 5 min.

Table 2.19: 2x SDS sample buffer.

2x SDS sample buffer
125 mM (5% (w/v)) SDS
25% (v/v) glycerol
0.3 M Tris pH 6.8
200 mM DTT
Bromophenol blue (to desired colour)

SDS-PAGE

Polyacrylamide gels (typically 1.5 mm thick) were prepared in a Mini-PROTEAN 3 Cell apparatus (Bio-Rad) (Table 2.20). Pre-stained protein standard (PageRuler Plus prestained protein ladder; Thermo Fisher) was loaded as a marker and proteins were separated at 100–180 V in 1x SDS running buffer (Table 2.21).

Table 2.20: Resolving and stacking reagents to prepare gels for SDS-PAGE.

Resolving Gel	**Stacking Gel**
15% Acrylamide mix (Protogel, 30% (v/v))	5% Acrylamide mix (Protogel, 30% (v/v))
39 M Tris-HCl pH 8.8	0.13 M Tris-HCl pH 6.8
0.1% (w/v) SDS	0.1% (w/v) SDS
0.1% (w/v) Ammonium persulphate (APS)	0.1% (w/v) Ammonium persulphate (APS)
0.04% (v/v) TEMED	0.04% (v/v) TEMED
top up to final volume with dH_2O	op up to final volume with dH_2O

Western blotting

After resolution by SDS-PAGE (often using 15% resolving gels), proteins were transferred onto nitrocellulose membranes (Amersham Protran, GE Healthcare) in a Mini Trans-Blot wet electroblotting systems (Bio-Rad) in transfer buffer (Table 2.21) at 100 V for 60–90 min. Membranes were stained with ink (Pelican Black), washed with 0.1% PBS-Tween 20 (PBS-T), and blocked with 5% dried skimmed milk (Marvel) in PBS-T at RT for 1 hour (Table 2.22). Appropriate primary antibody diluted in blocking solution was incubated at 4°C for 1 hour or overnight. The next day, the blot was washed three times with PBS-T and incubated with appropriate secondary antibody at RT for 1 hour. The blot was washed three more times for 5 min in PBS-T and then processed using enhanced chemiluminescence (ECL) reagents 1:1 for 1 min (Table 2.23). Blot was sequentially exposed to X-ray film (SLS) or Amersham hyperfilm ECL (GE Healthcare) increasing exposure time and finally developed (SRX-101A film processor, Konica Minolta).

Table 2.21: Running and transfer buffers.

Running Buffer	**Transfer Buffer**
192 mM glycine	192 mM glycine
25 mM Tris-HCl pH 6.8	25 mM Tris-HCl pH 6.8
0.1% (w/v) SDS	20% (v/v) methanol
top up to final volume with dH_2O	top up to final volume with dH_2O

Table 2.22: Washing and blocking buffers.

PBS	**PBS-T**	**5% dried skimmed milk in PBS-T**
1.37 M NaCl	1x PBS	1x PBS-T
0.1 M Na_2HPO_4	0.1% (v/v) Tween 20	5% w/v dried skimmed milk
27 mM KCl		
18 mM KH_2PO_4		

Table 2.23: ECL reagents.

ECL Solution 1	**ECL Solution 2**
100 mM Tris-HCl pH 8.5	100 mM Tris-HCl pH 8.5
2.5 mM luminol stock	0.02% (v/v) H_2O_2
0.4 mM p-coumaric acid	
top up to final volume with dH_2O	top up to final volume with dH_2O

2.6.4 Coomassie staining of SDS-PAGE gels

Coomassie brilliant blue staining was used to visualize proteins; SDS-PAGE gels were fixed at RT for 10 min, and then stained with Coomassie blue stain for 1 hour (Table 2.24). Stained gels were then de-stained overnight, washed in water and visualised with a LI-COR Odyssey, using Odyssey Sa Version 1.1.4 software.

Table 2.24: Fixation, staining and de-staining buffer.

Fixation buffer	**Staining buffer**
50% (v/v) methanol	50% (v/v) methanol
10% (v/v) glacial acetic acid	10% (v/v) glacial acetic acid
	0.2% (w/v) Coomassie brilliant blue R-250
top up to final volume with dH_2O	top up to final volume with dH_2O
De–staining buffer	
7.5% (v/v) methanol	
10% (v/v) glacial acetic acid	

2.6.5 Antibodies

Proteins were detected using the primary antibodies described in Table 2.25. Mouse monoclonal antibodies were generated against a peptide that is identical in IFITM1 and IFITM3 (MHK4.1 or MHK2.1) (Moravian Biotechnologies). This antibody cannot distinguish between IFITM1 and IFITM3 and it is specifically stated that IFITM1/IFITM3 were measured. Detection of primary antibody was performed using the following secondary antibodies: Swine anti-rabbit 1:1,000 (Dako, PO217) and rabbit anti-mouse 1:1,000 (Dako, PO260).

Table 2.25: List of primary antibodies.

Antibody	Company	Dilution
Mouse monoclonal anti-β-ACTIN	Sigma (a5441)	1:4,000
Rabbit monoclonal anti-BIOTIN	Cell Sigaling (5597S)	1:200
Mouse monoclonal anti-GAPDH	Abcam (a5441)	1:1,000
Rabbit polyclonal anti-HLA-B	Thermo Scientific (PA5-29911)	1:1,000
Mouse monoclonal anti-HSP-90	Stressgen (SPA-830)	1:1,000
Rabbit polyclonal anti-H3 HISTONE	Cell Signaling (9717S)	1:1,000
Mouse monoclonal anti-IFITM1/IFITM3 (MHK2.1 or 4.1)	Moravian Biotechnologies	1:4,000
Mouse monoclonal anti-IFITM1	Proteintech (60074IG)	1:1,000
Rabbit monoclonal anti-IFITM1 (CVY)	Moravian Biotechnologies	1:500
Mouse monoclonal anti-IFITM2	Proteintech (66137IG)	1:1,000
Rabbit polyclonal anti-IFITM3	Cell Signaling (59212)	1:1,000
Mouse monoclonal anti-IRF1	BD transduction Laboratories (612047)	1:1,000
Rabbit polyclonal anti-ISG15	Cell Signaling (2743S)	1:500
Rabbit polyclonal anti-RPL7a	Cell Signaling (2415S)	1:1,000
Mouse monoclonal anti-SBP-tag	EMD Millipore (MAB10764)	1:1,000
Rabbit polyclonal anti-SRSF1	Thermo Scientific (PA5-30220)	1:1,000
Rabbit monoclonal anti-STAT1	Cell Signaling (9172S)	1:1,000
Rabbit polyclonal anti-T7-tag	EMD Millipore (AB3790)	1:1,000

2.7 Cell biology techniques

2.7.1 Immunofluorescence

Wt-SiHa and *IFITM1/IFITM3* double null cells were grown on 16 mm diameter glass coverslips. Cells were stimulated with 100 ng/ml IFNγ for 24 hours, then fixed with 4% (v/v) paraformaldehyde in PBS at RT for 15 min, washed with PBS three times, and permeabilised using 0.25% Triton X-100 in PBS at RT for 10 min. Cells were again washed three times with PBS and blocked with 3% BSA in PBS for 1 hour. The primary antibody was incubated at the appropriate dilution (typically 1:1,000) overnight. In colocalization assays, two primary antibodies from different species (mouse monoclonal anti-IFITM1/IFITM3 and rabbit polyclonal anti-T7-tag) were incubated simultaneously. The next day, Alexa Fluor (Invitrogen) secondary antibody (Table 2.26) was incubated for 1 hour at RT. Coverslips were washed three times with PBS between each step. Cells were incubated in DAPI (Invitrogen) diluted at 1:10,000 with dH_2O for 5 min to stain the cell nucleus. After an additional 3 washes with dH_2O, a single drop of Fluorescence Mounting Medium (Dako, S3023) was used to mount the cells onto the slide. Images were observed using a Zeiss Axioplan 2 microscope (63x or 100x oil immersion objective). Images were acquired by Micro-Manager 1.4 software, and processed in ImageJ 2.0.

Table 2.26: Secondary antibodies for immunofluorescence.

Secondary antibody	Dilution
Alexa Fluor 488 goat anti-mouse IgG (H+L) (Invitrogen, A11029)	1:2,000
Alexa Fluor 488 donkey anti-rabbit IgG (H+L) (Invitrogen, A11034)	1:2,000
Alexa Fluor 594 goat anti-mouse IgG (H+L) (Invitrogen, A11032)	1:2,000
Alexa Flor 594 donkey anti-rabbit IgG (H+L) (Invitrogen, A21207)	1:2,000

2.7.2 Proximity ligation assay (PLA)

Wt-SiHa and *IFITM1/IFITM3* double null cells were grown and processed as described in the Immunofluorescence method (subsection 2.7.1). Primary antibody pairs from different species were incubated overnight on the fixed, permeabilised, and blocked cells (subsection 2.7.1): mouse monoclonal IFITM1/IFITM3 (1:500 dilution) with rabbit polyclonal SRSF1 (1:250 dilution), or mouse monoclonal IFITM1/IFITM3 (1:500 dilution) with rabbit polyclonal HLA-B (1:250 dilution), or mouse monoclonal IFITM1/IFITM3 (1:500 dilution) with rabbit polyclonal RPL7a (1:250 dilution). The next day, samples were incubated with the PLA probes (4 μl probe-mouse MINUS (Sigma, DUO92004) , 4 μl probe anti- rabbit PLUS (Sigma, DUO92002), 32 μl blocking solution) at 37^{o}C for 1 hour. Samples were washed three times with buffer A for 5 min and then incubated with ligation buffer (8 μl 5x ligation stock, 1 μl ligase and 31 μl of ultrapure water on each coverslip) at 37^{o}C for 30 min. Samples were again washed three times with buffer A for 5 min and incubated with amplification buffer (8 μl 5x amplification stock, 0.5 μl polymerase and 31.5 μl of ultrapure water on each coverslip) at 37^{o}C for 2 hours. Reagents were from Duolink in Situ Detection Reagents Green assays (Sigma, DUO92014). Samples were then washed twice with buffer A, three times with buffer B, and once with 0.01x buffer B (Table 2.27). Cells were incubated in DAPI (Invitrogen) diluted at 1:10,000 with 0.01x buffer B for 5 min to stain the cell nucleus. An additional 2 washes with 0.01x buffer B for 5 min were performed and cells were mounted as described in immunofluorescence method (subsection 2.7.1). The fluorescent signal was detected using a Zeiss Axioplan 2 microscope (63x or 100x oil immersion objective). Images were acquired by Micro-Manager 1.4 software, and processed in ImageJ 2.0.

Table 2.27: Buffer A and buffer B.

Buffer A	Buffer B
150 mM NaCl	100 mM NaCl
10 mM Tris base	50 mM Tris base
0.05% (v/v) Tween 20	
Adjust pH to 7.4	Adjust pH 7.5
Filter sterilize (0.22 μm)	Filter sterilize (0.22 μm)

2.7.3 RNA In Situ Hybridization-PLA (rISH-PLA)

Wt-SiHa cells and *IFITM1/IFITM3* double null cells were plated on 12 mm-diameter coverslips in 24-well plates and duplicates were IFNγ-stimulated for 24 hours. Cells were fixed with 4% paraformaldehyde in PBS at RT for 20 min and washed with PBS for 10 min, then incubated in 70% (v/v) ethanol at 4^{o}C overnight. The next day, samples were washed in PBS for 30 min and permeabilised with 0.05% CHAPS and 0.4% Triton X-100 for 10 min at RT. Next, samples were incubated with hybridization buffer (Table 2.28) for 30 min at RT then incubated for hybridization with 40 μl of hybridization buffer containing 50 ng of heat-denatured (80^{o}C for 5 min) HLA-B-biotin DNA probe (5'-TGTCCTAGCAGTTGTGGTCATCGGAGCTGTGGTCGCTGCTGTGAT-biotin-3') (Sigma) in a humidified chamber overnight. Then, samples were washed for 20 min each with 2x SSC and 10% formamide at RT, twice with hybridization buffer at 37^{o}C, 2x SSC at RT, and finally with PBS at RT. Next, samples were blocked with 3% BSA and 0.1% saponin in PBS at RT for 30 min. After that, they were incubated with mouse monoclonal IFITM1/IFITM3 (1:500 dilution) and with rabbit monoclonal anti-biotin (1:200 dilution) antibodies at RT for 2 hours.

Table 2.28: Hybridization buffer.

Hybridization buffer
10% (v/v) formamide
2x SSC
0.2 mg/ml *E. coli* 522 tRNAs
0.2 mg/ml sheared salmon sperm DNA
2 mg/ml BSA

Samples were incubated with the PLA probes(4 μl probe-mouse MINUS (Sigma, DUO92004) , 4 μl probe anti- rabbit PLUS (Sigma, DUO92002), 32 μl blocking solution) at 37^{o}C for 1 hour. Samples were washed three times with buffer PBS for 5 min and then incubated with ligation buffer (8 μl 5x ligation stock, 1 μl ligase and 31 μl of ultrapure water on each coverslip) at 37^{o}C for 30 min. Samples were again washed twice times with PBS for 5 min and incubated with amplification buffer (8 μl 5x amplification stock, 0.5 μl polymerase and 31.5 μl of ultrapure water on each coverslip) at 37^{o}C for 1 hour 40 min. Reagents are from Duolink in Situ Detection Reagents Green assays (DUO92014, Sigma). Finally, samples were washed twice with PBS and incubated in DAPI (Invitrogen) diluted at 1:10,000 with PBS for 5 min to stain the cell nucleus and an additional 2 washes of PBS for 5 min were performed before mounting (subsection 2.7.1).

2.7.4 Sucrose gradient sedimentation

Wt-SiHa and *IFITM1/IFITM3* double null cells grown in 15-cm dish. Depending on the experiment, cells were transfected with IFITM1 and IFITM3 (or the respective empty vectors) for 48 hours and cells were stimulated with 100 ng/ml IFNγ for 24 hours. If transfected, cells were split between two plates prior to IFNγ stimulation to reach an 80% cell confluence before collection. Cells were treated with 50 μg/ml cycloheximide (Merck Chemicals) for 30 min before collection, to inhibit translation elongation and preserve mRNA on the ribosome. Cells were washed in PBS containing 1x RSB and harvested. Cell pellets were collected after centrifugation at 7,000 rpm for 1 min at 4 ^{o}C, then lysed by resuspending the cell pellets in 250 μl of 1x RSB/RNasin buffer and 250 μl PEB buffer (Table 2.29). Mechanical disruption of the cell lysate was carried out by passing the lysate though a needle (25G) five times. Lysates were incubated on ice for 10 min and centrifuged at 10,000 g for 10 min at 4^{o}C. Supernatant was transferred into a new tube and RNA concentration was measured by NanoDrop 2000c spectophotometer (Thermo Scientific). Lysates were processed as described by Sanford *et al.* (Sanford *et al.*, 2004). Sucrose gradients (10–45%) containing 1x RSB were generated in centrifuge tubes (Beckman Coulter, 344059) using a BioComp gradient master (SW41, 10–45% w/v 1st program). Preparation of the linear sucrose gradient was a critical step and perturbation of the gradient by air bubbles can interfere with successful ribosomal subunit separation. For the same reason, ultra-centrifugation was carried out at maximum speed for acceleration and at minimum speed for deceleration. Samples were kept at 4^{o}C at all times and immediately processed to fractionation to maintain RNA integrity. Lysates were applied onto the gradient and centrifuged at 41,000 rpm for 2 hours 30 min at 4^{o}C using a SW41 rotor. The IFNγ-stimulated wt-SiHa cells and IFNγ-stimulated *IFITM1/IFITM3* double null cell lysates were subjected to sucrose density gradient sedimentation. The aim was to extract the free mRNA, 40S, 60S, 80S, and polysomes in different fractions. Fractions, each containing 500 μl of the elute, were collected in 18 x 1.5 ml sterile screw tubes (SSIbio, 2231-S0), using a BioComp gradient station model 153 (BioComp Instruments, New Brunswick, Canada). While eluting, samples were measured at OD254; elutes corresponding to the same subpolysomal and polysomal fractions were pooled together for further analysis by SWATH-MS to define changes in ribosomal protein profile in the wt-SiHa and *IFITM1/IFITM3* double null cells. Samples were processed for SWATH-MS in technical triplicates.

Table 2.29: 10x RSB stock buffer, 1xRSB/RNasin buffer, and PEB buffer.

10x RSB stock buffer	**1xRSB/RNasin (2 ml)**
200 mM Tris pH 7.5 1 M KCl 100 mM $MgCl_2$	200 μl 1x RSB 50 μl RNasin (Promega, N2511)
Polysome extraction buffer (PEB) (10 ml)	
1 ml 1x RSB 50 μl NP-40 1 pill cOmplete Tablets, Mini EDTA-free, EASYpack (Roche-Sigma, 04693159001)	

2.7.5 Trichloroacetic acid (TCA) precipitation

Protein fractions, as collected, were in a very dilute 500 μl sucrose buffer solution. In order to concentrate them, they were precipitated using TCA; 1 μg/μl of BSA was added to each prechilled fraction, then, 90 μl of ice-cold TCA was mixed and incubated on ice for 60 min. Eluates were centrifuged at maximum speed at 4°C for 10 min, the supernatant was carefully saved and the pellet was again centrifuged to remove the remaining supernatant. The pellet was not visible at this stage. The pellet was washed with 250 μl of ice-cold acetone and centrifuged for 5 min at 4°C. Finally, the supernatant was discarded, and a visible small white precipitate was air dried. If the recovery is very low, the saved supernatant was incubated with TCA on ice for 4 hours and centrifugation and wash steps were repeated. Protein was then resuspended in 2x sample buffer to proceed with a Western blot.

2.8 Mass spectrometry; free-labelled SWATH and SILAC Orbitrap methodology

2.8.1 Sample preparation for mass spectrometry (MS)

Peptide generation using FASP

Cell lysates, immunoprecipitates, or gradient fractions were processed using a filter-aided sample preparation protocol (FASP)(Wiśniewski *et al.*, 2009). Urea buffer (8 M urea in 0.1 M Tris pH 8.5) was added to a 30 kDa cut-off spin-filter column (MRCPRT010, Microcon). Protein concentration was determined using the RC-DC method (Bio-rad). Normalized samples (20-100 μg of protein) were added to the spin filter column and centrifuged at 12,200 rpm for 15 min at 20°C. Urea buffer was added again with 100 mM Tris (2-carboxyethyl) phosphine hydrochloride (Aldrich) and mixed. The column was incubated for 30 min at 37°C on a shaking thermo-block at 600 rpm and then centrifuged at 12,200 rpm for 15 min at 20°C. Urea buffer and 300 mM of iodoacetamide (Sigma) were mixed

using a thermo-mixer at 600 rpm in the dark for 1 min, then was maintained statically at RT for a further 20 min in the dark. The sample was centrifuged at 12,200 rpm for 15 min at 20°C and the supernatant was discarded. A solution containing 100 μM ammonium bicarbonate were added to the column and then it was centrifuged at 12,200 rpm for 20 min at 20°C . This step was repeated once more. The column was placed in a new collecting tube (low binding affinity) and 50 mM ammonium bicarbonate was added, along with trypsin diluted in trypsin buffer (Promega) at a 1:100 ratio. The column was incubated at 37°C overnight. The following day the column was centrifuged at 12,200 rpm for 15 min at 20°C. Determination of the peptide concentration was performed using the Quantitative Colorimetric Peptide Assay (Pierce, ThermoScientific).

Desalting peptides using C18 column

Peptides were desalted on micro-spin columns C-18 (Harvard Apparatus, USA). The columns were conditioned 3 times with 100% acetonitrile (AcN) and 0.1% formic acid (FA) and centrifuged at 1,200 rpm for 2 min at RT. The column was washed with 0.1% FA and centrifuged at 1,200 rpm for 2 min at RT then hydrated in 0.1% FA for 15 min following centrifugation at 1,800 rpm for 3 min at RT. The sample was loaded into the column and centrifuged at 2,300 rpm for 3 min. After washing the column 3 times with 0.1% FA, the peptides were eluted in 3 consecutive centrifugations at 2,300 rpm for 3 min using 50%–80% and 100% AcN with 0.1% FA. Subsequently, peptide eluates were evaporated and dissolved in 5% AcN with 0.05% FA.

LC-MS/MS analysis

Enzymatically digested samples were processed using isotopically-labelled amino acids and were separated using UltiMate 3000 RSLCnano chromatograph. Peptides were loaded on a pre-column (μ-precolumn, 30 mm i.d., 5 mm length, C18 PepMap 100, 5 μm particle size, 100 Å pore size) and further separated on an Acclaim PepMap RSLC column (75 mm i.d., length 500 mm, C18, particle size 2 mm, pore size 100 Å) with a 300 nl/min flow rate using a linear gradient: 2% B over 4 min, 2 – 40% B over 64 min, 40–98% B over 2 min, with A = 0.1% aq. formic acid and B = 80% ACN in 0.08% aq. formic acid. Peptides eluting from the column were introduced into an Orbitrap Elite operating in Top20 data dependent acquisition mode. A survey scan of 400–2000 m/z was performed in the Orbitrap at 120 000 resolution with an AGC target of 1 x 106 and 200 ms injection time followed by twenty data-dependent MS2 scans performed in the LTQ linear ion trap with 1 microscan, 10 ms injection time and 10 000 AGC.

2.8.2 Database searching and analysis

Orbitrap-MS

The data from the mass spectrometer were processed using either Proteome Discoverer 1.4 or Proteome Discoverer 2.2 that is equipped with statistical tools. Proteome Discoverer 1.4 processed the data using Mascot search engine with the following search settings: database Swiss-Prot human (April 2016); enzyme trypsin; 2 missed cleavage sites; precursor mass tolerance 10 ppm; fragment mass tolerance 0.6 Da; dynamic modifications: carbamidomethyl [C], oxidation [M], acetyl [protein N-terminus]. The results of the search were further submitted to generate the final report considering 1% FDR on both PSM and peptide group levels. For the protein quantification we used only unique peptides. SILAC labels of R6 and K6 were chosen for heavy and R0 and K0 for light. The relative quantification value was represented as heavy/light ratio (Table B.2). The higher version of Proteome Discoverer 2.2 was used for processing of the same raw files, but different settings for the data evaluation were used according to the requirements of this program. The processing and consensus workflows used subsequent nodes: the Minora feature detector, the Precursor ion quantifier, and the Feature mapper. The data were processed using Sequest HT engine with the following search settings: database Swiss-Prot 2017-10-25, # sequences 42252, taxonomy: Homo sapiens (updated February 2018); enzyme trypsin; 2 missed cleavage sites; precursor mass tolerance 10 ppm; fragment mass tolerance 0.6 Da; static modification carbamidomethyl [+57.021 Da, (C)], label 13C(6) [+6.020 Da (K, R)]; dynamic modifications oxidation [peptide terminus, +15.995 Da (M)], Met-loss+Acetyl[protein terminus, -89.030 Da (M)]. The results of the search were further submitted to generate the final report with a 1% FDR using Percolator. For the protein quantification and statistical assessment of the biological triplicates, only unique peptides and razor peptides were used. The relative quantification value is represented as the relative peak area of the peptides with the heavy isotope labels with IFNγ-stimulated cells/IFNγ non-stimulated cells ratios (Table B.5). This work was conducted by Prof. Ing. Lenka Hernychova, in Regional Centre for Applied Molecular Oncology, Masaryk Memorial Cancer Institute, Brno.

SWATH-MS

Label free quantitation was performed using FASP-processed tryptic digests with liquid chromatography coupled to tandem MS on an Eksigent Ekspert nanoLC 400 (SCIEX, Dublin, Caliorwaornia), inline connected to a TripleTOF 5600+ (SCIEX, Toronto, Canada) mass spectrometer. Cell lysates were processed in technical triplicates. Prior to separation the peptides were concentrated and desalted on a cartridge trap column (300 μm i.d. $\times$ 5 mm) packed with C18 PepMap100 sorbent with 5 μm particle size (Thermo Fisher Scientific, Waltham, MA, USA). After a 10-min washing using 0.05% trifluoroacetic acid in 5%

acetonitrile and 95% water, the peptides were eluted using a gradient of acetonitrile/water (300nL/min) using a capillary emitter column PicoFrit® nanospray columns 75 μm × 210 mm (New Objective, Woburn, USA) self-packed with ProntoSIL 120-3-C18 AQ sorbent with 3 µm particles (Bischoff, Leonberg, Germany). Mobile phase A was composed of 0.1% (v/v) formic acid in water, and mobile phase B was composed of 0.1% (v/v) formic acid in acetonitrile. Gradient elution started at 5% mobile phase B for the first 30 min, then the proportion of mobile phase B increased linearly up to 40% B for the following 120 min. Output from the separation column was directly coupled to an ion source (nano-electrospray). Nitrogen was used as a drying and nebulizing gas. Temperature and flow of the drying gas was set to 150°C and 12. Voltage at the capillary was 2.65 kV. Pooled sample for the spectral library was measured in data-dependent positive mode. The MS precursor mass range was set from m/z 400 up to m/z 1250 and from m/z 200 up to m/z 1600 in MS/MS. Cycle time was 2.3 seconds and in each cycle 20 most intensive precursor ions were fragmented. Subsequently, their corresponding MS/MS spectra were measured. Precursor exclusion time was set to 12s. Precursor ions with intensity below 50cps were suspended from the IDA experiment. The extraction of mass spectra from chromatograms, their annotation and deconvolution were performed using Protein Pilot 4.5 (SCIEX, Toronto, Canada). MS and MS/MS data were searched using the Uniprot+swissprot database (02. 2016) non-redundant restricted to H. sapiens taxonomy. Fixed modification – alkylation on cysteine using iodoacetamide and digestion using trypsin was set for all searches. The resulting group file was imported into Peakview 1.2.0.3 (SCIEX, Toronto, Canada), where only proteins with FDR below 1% were imported into the spectral library (465 proteins for SBP-IFITM1 pull down SWATH and 1320 proteins in polysomal SWATH). In SWATH mode, the mass spectrometer operated in high sensitivity positive mode. Precursor range was set from m/z 400 up to m/z 1200. It was divided into 67 precursor ion windows with the width of 12 Da and 1 Da overlap. Accumulation time was 50 ms per SWATH window and the duty cycle was 3.0 seconds, which enabled acquisition of at least 10 data points across a chromatographic peak. Product ions were scanned from m/z 400 up to m/z 1600. Data extraction was performed in Peakview 1.2.0.3 (SCIEX, Toronto, Canada) with the spectral library. The retention time window for extraction was manually set to 4 min for SBP-IFITM1 pull down SWATH (Table B.3) and 10 min in polysomal SWATH (Table B.4). SWATH protein quantification was performed using up to 4 peptides and 6 transitions per protein. Scope of peptides used for quantification was narrowed to only those with peptide confidence higher than 99% and without any variable modification. Protein summed peak areas were normalized using total area sums option in MarkerView 1.2.1.1 (SCIEX, Toronto, Canada). Samples were compared pairwise using a paired t-test. Statistics was done on 3 technical replicates from each polysomal fraction. Resulting protein fold-changes were considered as statistically significant at p-value<0.05. This work was conducted by Dr. Jakub Factor, in Regional Centre for Applied Molecular Oncology, Masaryk Memorial Cancer Institute, Brno.

2.9 Bioinformatic analysis of the RNA-sequencing

RNA samples of IFNγ-stimulated and non-stimulated wt-SiHa cells, *IFITM*1 null cells and *IFITM1/IFITM3* double null cells were processed by Otogenetics for paired end RNA-sequencing analysis, using an Illumina HiSeq 2500 and designated 20 million reads. The pair of fastq files obtained from the sequencer were checked for quality control, merged and processed using CLC Genomic Workbench 12.0 to obtain the total RNA expression levels. GRCh38 was taken as the human reference genome with the following settings: mismatch cost: 2, insertion cost: 3, deletion cost: 3 (Table B.6). The results were compared using RNA gene expression for each condition, creating seven different scatter plots that compared IFNγ stimulated to non-stimulated conditions, and wt-SiHa cells to *IFITM1* null cells or *IFITM1/IFITM3* double null cells (Figure 6.6). Comparisons were performed taking the TPM values as reporting abundances and log2 (TPM condition 1 versus log2 (TPM condition 2) as comparison values. An additional heat map was generated with the list of IRDS genes to compare the gene expression of these genes of interest across samples (Figure 6.7 A). Following the same parameters, another heat map was created to compare isoform switches using sum of RNA transcript expression levels (Figure 6.7 B) or the RNA transcript expression level of particular transcripts (Figure 6.7 C). This work was conducted by Marcos Yébenes Mayordomo, in ECRC–IGMM, University of Edinburgh.

Chapter 3

Generating isogenic IFITM knock out cervical carcinoma cell models

3.1 Introduction

Cervical cancer is the most common cancer among females in developing countries and the second most common cancer type manifested in women across all countries (Callahan & Caughey, 2013). It is been postulated that the disease arises from continuous infection by human papilloma virus (HPV) (Burd, 2003). In this regard, a study performed in the late 90s reported that 99.7% of women with cervical cancer were infected with HPV, and 75% of them were carrying HPV-16 and HPV-18 virus strands (Walboomers *et al.*, 1999). Sadly, the most economically deprived areas do not have access to routine screening programs and preventive vaccine. Therefore, current efforts are focused on developing affordable diagnostic assays and therapeutic tools for the less developed countries.

3.1.1 Clinical relevance of IFITM1 in cervical cancer

IFITM1 is dysregulated in cervical cancer. Pan *et al.* conducted a RNA screening and identified IFITM1 related to cervical carcinogenesis (Pan *et al.*, 2010). Tumour and normal cervix tissue were extracted from 16 women who did not receive chemotherapy or radiotherapy prior to biopsy resection. This study showed 46 genes dysregulated in tumour tissue compared to normal cervix tissue, and IFITM1 was found to be one of the 22 downregulated genes in cervical tumours.

Using immunohistochemistry (IHC) on tissue microarrays (TMA) of cores from squamous cervix carcinoma we have shown a direct correlation between IFITM1/IFITM3 staining and advanced cervical cancer stage (Gomez Herranz *et al.*, 2019). The microarray panel contained samples of both normal tissue and cancer tissue at different stages. This work was conducted by Dr. Rudolf Nenutil and Dr. Marta Nekulová, in the Regional Centre for

Applied Molecular Oncology, Masaryk Memorial Cancer Institute, Brno. Biopsies for sample preparation were extracted from women who did not have preoperative treatment. The results presented a dynamic range of staining in 74 cervical cancer tissues, where some samples had a high presence of IFITM1/IFITM3 staining and others were completely negative (Figure 3.1 A and C). Squamous cervical carcinoma exhibited differential expression (Figure 3.1 A-C) while high expression was observed for cervical adenocarcinoma (Figure 3.1 D). Remarkably, 10 out of 74 specimens showed no staining (Figure 3.1 F). After stratifying samples by manifestation of metastases, there was a statistically significant inverse correlation between IFITM1/IFITM3 staining and presence of nodal metastases (Figure 3.1 F II). This result suggested that IFITM1/IFITM3 proteins may be playing a dual role where overexpression, but also loss of expression, facilitates cervical cancer development. Interestingly, a gene expression study also revealed inverse correlation between IFNγ and lymph node metastases in women with cervical cancer and this association was confirmed by immunochemistry analyses (Kim *et al.*, 2007).

3.1.2 Study of IFITM1-dependent signalling pathways in a cervical cancer cell model

The immunohistochemistry study presented in the previous section led to continued exploration of the molecular role of IFITM1. As such, additional work performed in our group explored pathways by which IFITM1 is implicated in cervical cancer. An assay to define IFITM1 dependence on the steady-state protein levels was developed using IFITM1-targeted small interfering RNA (siRNA) in wt-SiHa cells coupled to mass spectrometry (MS) analysis.

The use of siRNA is a powerful tool to determine gene dependencies in cell models. In this assay was asked whether transient reduction in IFITM1 protein might affect steady-state levels of the related cluster of IFN responsive proteins. Wt-SiHa cells were treated for 48 and 72 hours with either control siRNA or IFITM1-targeted siRNA (Figure 3.2 A, lanes 4 and 2 vs lanes 3 and 1) to identify IFITM1 dependent proteins. This work was performed by Dr. Elisabeth Sinclair, in ECRC–IGMM, University of Edinburgh.

However, similar to plasmid transfection, siRNA itself can activate an IFN response and that may impact on IFITM1 signalling (Huerfano *et al.*, 2013). In fact, previous work from our group found that siRNA can also induce an IRF-1 dependent IFN response (data not shown). IRF-1 is a key transcription factor that coordinates the expression of multiple IFN-related genes. That is why an alternative methodology is developed in this thesis, in which an isogenic gene-edited null cell model is generated to interrogate which are the IFITM1-IFNγ dependent signalling responses.

Nevertheless, a close look at the above effects of IFITM1-targeted siRNA revealed that there was a striking and selective reduction in IFN-responsive proteins, 8 of which are components of the IRDS (Figure 3.2 B, highlighted in orange)(Weichselbaum *et al.*, 2008a),

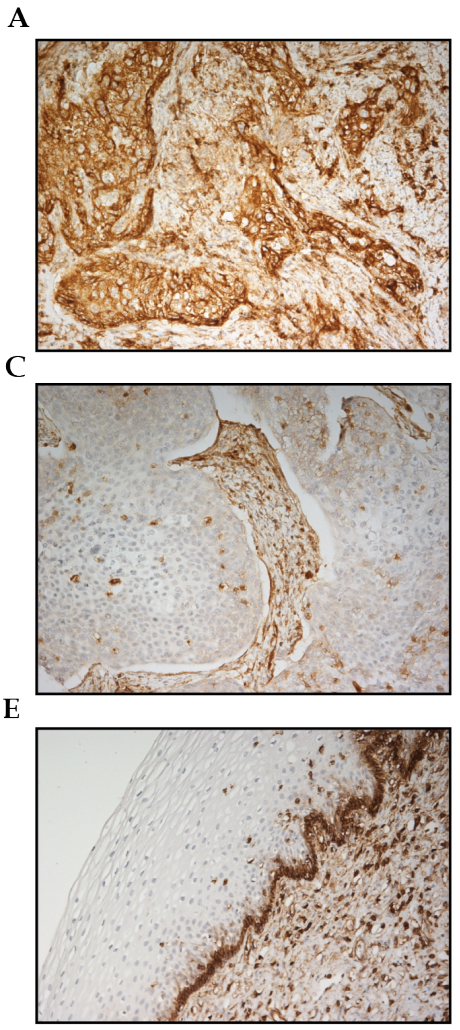

F Quantitation of IFITM1/3 expression in cervical cancer

Expression of IFITM1/3 as a function of histology

	Squamous	Adenocarcinoma	Neuroendocrine
IFITM1/3 -ve	8	1	1
IFITM1/3 focally +ve	23	4	0
IFITM1/3 strongly +ve	29	7	1

Expression of IFITM1/3 as a function of metastasis

	Negative nodes	Positive nodes
IFITM1/3 -ve	4	6
IFITM1/3 focally +	18	9
IFITM1/3 strongly +	29	7

p value=0.042 (chi square)

Figure 3.1: Tissue microarray suggests inverse correlation between IFITM1/IFITM3 presence and nodal metastasis (Gomez Herranz *et al.*, 2019). TMA was performed on formalin-fixed, paraffin-embedded cervical carcinoma tissues. Representative slides showing grades of IFITM1/IFITM3 staining; high expression in squamous cell carcinoma (A), discrete expression in squamous cell carcinoma (B), absence of expression in squamous cell carcinoma (C), high expression in adenocarcinoma (D), and expression in basal stem cell layer in normal tissue (E) Quantification of IFITM1/IFITM3 expression in cervical cancer in relation to histology type (I) and metastasis (II) (F).

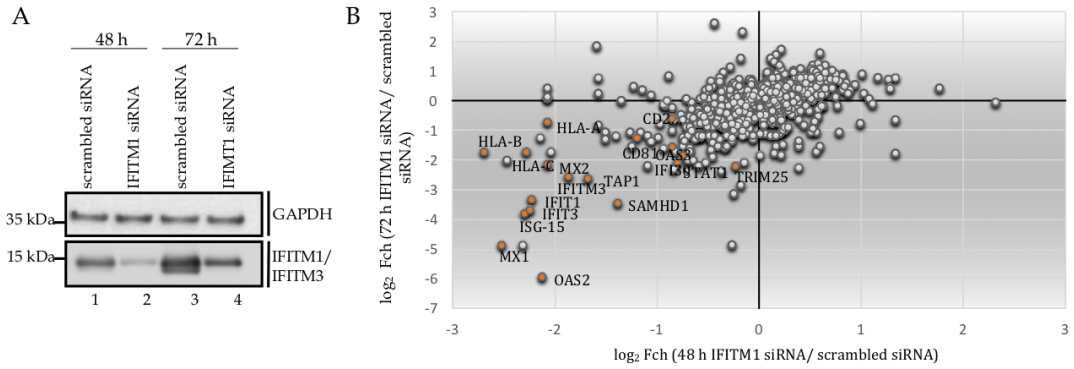

Figure 3.2: The impact of IFITM1 targeted siRNA on the steady-state proteome (Gomez Herranz *et al.*, 2019). (A) IFITM1-targeted siRNA can attenuate IFITM1and IFITM3 protein levels. Cells were treated with control siRNA (lanes 1 and 3) or IFITM1 siRNA (lanes 2 and 4) for 48 and 72 hours to study the overlapping dynamic in the IFITM1 signalling pathway. Lysates were immunoblotted with the IFITM1/IFITM3 antibody and GAPDH was used as loading control. (B) Representation of the proteome in response to siRNA targeting of IFITM1 in two time points (48 and 72 hours) in wt-SiHa cells using SWATH-MS. These data are plotted as log2 fold change (Fch) in protein levels (IFITM1 siRNA vs control siRNA) as a function of either the 48 hour time point (x-axis) and 72 hour time point (y-axis). The proteins of interest whose levels were decreased after IFITM1-targeted siRNA treatment are highlighted in orange (bottom left quadrant). Data extracted from Table B.1.

specifically ISG15 and HLA family members as well as other proteins of the MHC class I pathway. This finding is consistent with further results presented in this thesis (chapter 4 and chapter 5). In addition, this assay shows decreased CD81 expression with IFITM1 depletion, which is particularly interesting as interaction of CD81:IFITM1 has been reported in homotypic cell adhesion in leukocytes and growth arrest (Matsumoto *et al.*, 1993; Takahashi *et al.*, 1990).

All-in-all, this was the first evidence that IFITM1 may be a dominant receptor that mediates induction of other IRDS members. Collectively, the described experiments above set the foundations for this thesis.

3.2 Developing new strategy for understanding the role of IFITM1/IFITM3

The first goal of this thesis was to generate and validate cell models to study the role of IFITM1, using CRISPR/Cas9 methodology. As previously described, IFITM1 and IFITM3 play different roles in the cell. However, both isoforms are highly homologous suggesting that IFITM1 and IFITM3 may have overlapping functions or orchestrate cellular processes together. Thus, we decided to generate *IFITM1*, *IFITM3* and *IFITM1/IFITM3* knock out cell models (henceforth *IFITM1*, *IFITM3* and *IFITM1/IFITM3* null cell models)

SiHa cells, which originated from squamous cell carcinoma of cervix, were chosen as a model because they express IFITM1/IFITM3 at detectable endogenous levels with higher

protein expression after IFNγ stimulation (Figure 3.11). Interestingly, SiHa cells (representative of the majority of cervical cancer cells) are infected by human papillomavirus 16 (HPV 16) and IFITMs were initially considered to be a restriction factor. Despite the fact that HPV virus was not the main theme of this study, it is interesting to highlight that infection with HPV 16 and 18 strains are considered to be one of the main causes of tumourigenesis in the precursor cervical intraepithelial neoplasia/squamous intraepithelial lesions (CIN/SIL) for this cancer type. IFITM1 may have unknown implications in the very early events of HPV-driven cervical cancer but the current studies suggest that HPV inhibits IFITMs effects by downregulating their expression (Warren *et al.*, 2014; Ma *et al.*, 2016). However, the central goal was to understand the cellular functions of IFITM1 in relation to the IFNγ signalling landscape. The study of IFNγ effects on IFITM1 signalling is a significant challenge. Clinical data as well as studies *in vitro* showed inconsistent results and it has been suggested that IFN will reduce the activation of HPV virus, particularly expression of E6 and E7 oncogenes (Kim *et al.*, 2000). Nonetheless, this effect can be only observed in some cervical cancer cell lines or in certain patients with cervical carcinoma tested with IFN type I and II (Chang & Laimonis, 2000). Additionally, it has been reported that late passage cells are less responsive to IFNγ, suggesting that accumulation of mutations may impact on IFNγ regulatory effects, which has also been observed in patients with advanced cancer disease (Kim *et al.*, 2000).

IFITM1 plays a dual role in metastatic cell growth and spread, and also in restriction of RNA viruses. Consequently, we aim to use these functional IFITM null cell models as a tools to compare the cellular consequences of IFITM1, IFITM3 or IFITM1/IFITM3 loss in comparison with IFITM wild-type cells. As such, isogenic *IFITM1* null, *IFITM3* null, and *IFITM1/IFITM3* double null cell models of SiHa cervical carcinoma cells were generated through genome editing using CRIPSR/Cas9 technology (Ran *et al.*, 2013).

The Clustered Regulatory Interspaced Short Palindromic Repeats (CRISPR)/Cas9 system is a sophisticated genome-editing tool based on the microbial adaptive immune system, consisting of RNA-guided/Cas9 nuclease that can precisely target specific genomic loci for cleavage. The system was originally discovered in bacteria and archaea as an evolutionary mechanism in response to viral phages and plasmid threats (Wiedenheft *et al.*, 2012). This defence mechanism is activated after repetitive pathogen attack and relies on genomic incorporation of short palindromic spaced repeats or protospacers that have been excised from the pathogenic intruder and integrated into a CRISPR array in the microbial host genome. This way, the bacterial or archaeal host keeps on producing a library of CRISPR sequences for future identifications of pathogens. This repertoire is transcribed and assembled into CRISPR-derived RNAs (crRNAs) containing short complementary genomic sequences of the pathogenic intruders. CrRNA are associated with trans-activating CRISPR RNA (tracrRNA), responsible for its maturation (Deltcheva *et al.*, 2011). This mechanism was first observed in *Escherichia coli* (Ishino *et al.*, 1987) but the system was not completely understood until *in silico* analysis identified four CRISPR-associated

(Cas) genes that encode nucleases. Remarkably, the study showed that Cas genes were uniquely present in prokaryotes containing CRISPR loci (Jansen *et al.*, 2002). Cas genes are responsible for generating the Cas enzymes that are able to precisely cleave the foreign genome in a site-specific manner by recognition of the protospacer adjacent motif (PAM), a flanking sequence present in the foreign genome. Then, base complementary pairing between crRNA and the specific locus in the foreign genome enhances the interaction and facilitates the targeted double strand (DBS) cleavage by the Cas enzyme. Different CRISPR/Cas system types have been described, but all of them contain the same core components and fundamentally function in the same manner (Jinek *et al.*, 2012).

The CRISPR/Cas system discovery has revolutionized many fields in academia as well as in industry and the applications are very broad. Previous genome-editing technologies such as zinc fingers (ZFN) and transcription activator-like effector nucleases (TALEN) are not as fast and easy to apply as CRISPR/Cas9. This targeted genome-editing machinery is notable not only for its sophistication but also for being highly precise and effective for manipulating genetic material. As a result, this tool has been engineered for use in eukaryotic systems to successfully target and modify particular genes of interest (Cong *et al.*, 2013; Jinek *et al.*, 2013). In this work, we used the CRISPR/Cas9 system to generate isogenic cell models to study the cellular roles of IFITM1 and IFITM3.

There are different types of CRISPR/Cas systems, but the most widely used is CRISPR/Cas9. As in the prokaryotic system, the underlying principle of CRISPR/Cas9 is also based on two elements; crRNA and tracrRNA. Both components together are also referred to as single guide RNA (sgRNA) (Figure 3.3 A). The crRNA contains a cluster of Cas genes, noncoding RNAs and an array of repetitive elements interspaced by protospacers. The tracrRNA acts as an auxiliary scaffold for processing the crRNA. The system has fused together the crRNA and tracrRNA sequences to generate a sgRNA sequence that precisely cleaves the DNA at the intended location producing a double strand break (DSB). The crRNA sequence consists of a 20-nucleotide sequence that target gene sequence to be modified. In the host genome this 20-nucleotide sequence is flanked by a 5'-NGG, which is the protospacer adjacent motive (PAM) (Figure 3.3 B) (Gaj *et al.*, 2013; Ran *et al.*, 2013). The Cas9 nuclease binds to the sgRNA and the host gene target sequence to produce a DSB in the desired genomic locus (Figure 3.3 C). The DSB can be repaired by either non-homologous end joining (NHEJ), or homology directed repair (HDR) pathways (Figure 3.4). NHEJ repair machinery does not use a template and so is prone to introducing errors, such as insertion or deletions, while repairing the DSB. In contrast, HDR is of high fidelity and it repairs a DSB by homologous recombination directed by a double-stranded DNA donor (template sequence) in dividing cells. The NHEJ repair is a less sophisticated system that is activated throughout the cell cycle, so it is more frequently used by the cell (Figure 3.4). As a result, it is more likely that some indels (insertions and/or deletions) will be introduced into the gene of interest, resulting in gene knock out (Figure 3.3 D).

Genes for *IFITM1*, *IFITM2* and *IFITM3* are located on chromosome 11p15.5, around 5

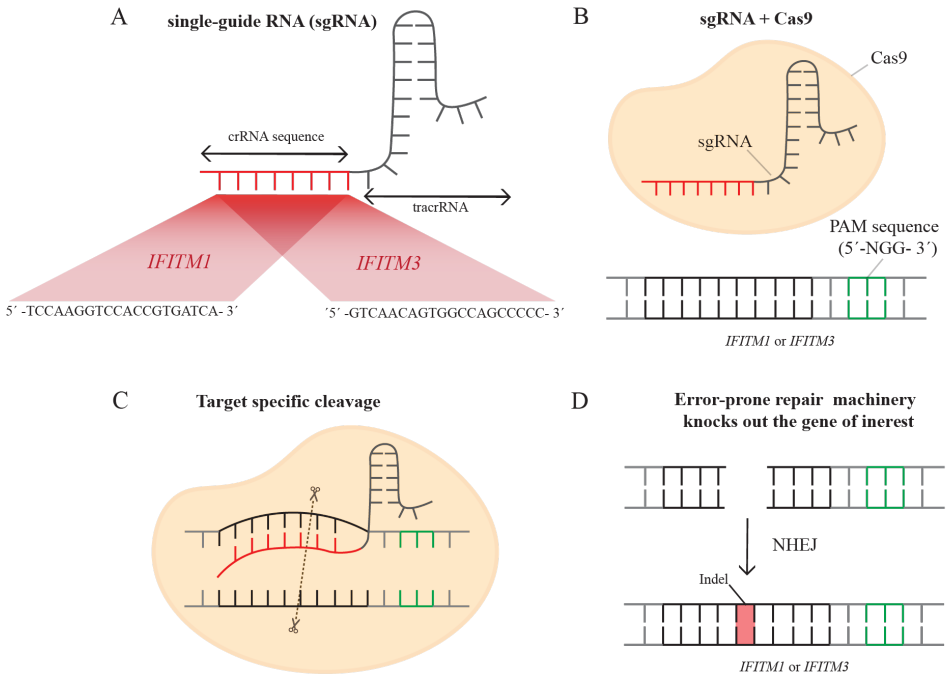

Figure 3.3: Schematic of CRISPR/Cas9 system. The sgRNA is composed of crRNA and tracrRNA. crRNA sequence is specifically designed to target the gene of interest, in this case *IFITM1* (5' -TCCAAGGTCCACCGTGATCA- 3') and *IFITM3* (5' -GTCAACAGTGGCCAGCCCCC- 3'). (B) sgRNA binds to the recombinant form of Cas9 nuclease from *S. pyogenes*. Together they target the genomic DNA by base pair-complementary binding between sgRNA and the specific locus of interest which is flanked with a 5-NGG protospacer adjacent motif (PAM) in the host genome. (C) After sequence recognition, Cas9 will produce a DSB approximately 3 bp upstream of the PAM motif. (D) The cleavage site can be repaired by NHEJ (an error-prone repairing mechanism), resulting in indels that will prematurely terminate either *IFITM1* and/or *IFITM3* genes and thus resulting in loss of funcitons.

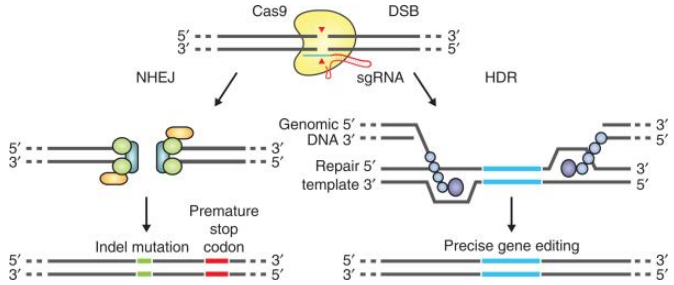

Figure 3.4: CRISPR/Cas9 system to generate targeted gene editing (Ran *et al.*, 2013). DSB can be repaired by either error-prone NHEJ (promoting random indel mutations) or HDR (precise editing). Indel mutations are susceptible to production of aberrant forms of the genomic sequence, such as introducing a premature stop codon or creating a frameshift in the nucleotide sequence.

kb apart Figure 1.11. According to the the American type culture collection (ATCC) source, SiHa is an hypertriploid cancer cell line that originated from a human squamous cell carcinoma of the cervix. Aneuploidy events could have complicated the genetic editing of these clones, but chromosome 11 is not affected. The *IFITM1* gene has 855 bp that are translated into a 13.9 kDa protein. It contains a single intron, that divides exon 1 from exon 2, 186 and 189 base pairs long, respectively (Figure 3.5 A). The *IFITM3* gene has 0.97 kb that encodes a 14.6 kDa protein and it is also divided into two exons of 249 bp and 150 bp, respectively (Figure 3.5 B). The rationale behind the sgRNA design was to target exon 1 in both the *IFITM1* and *IFITM3* genes in order to introduce an indel. This random indels will either encode a premature stop codon or generate a sequence frameshift at an early stage of protein translation.

The methodology used to produce the null cell lines required the design of sgRNAs followed by cloning into pLentiV2 plasmid. sgRNA sequences were designed for *IFITM1* (5' -TCCAAGGTCCACCGTGATCA- 3') and for *IFITM3* (5' -GTCAACAGTGGCCAGCCCCC- 3'). The guide RNA was cloned into the lentiCRISPRv2 expression vector (Sanjana *et al.*, 2014). SiHa cells were transduced with gRNA in pLentiV2 plasmid along with viral coat protein. After transduction, cells were selected with puromycin and single cells were sorted into a 96-well plate using FACS. Then, cells were further selected for resistance to puromycin to allow stable integration of the *IFITM1*, *IFITM3*, or *IFITM1* in combination with *IFITM3* targeting single guide RNA cassette. After a few weeks, individual clones were screened for absence of IFITM1, IFITM3 or IFITM1/IFITM3 protein expression by Western blot (Figure A.1). This work was kindly performed by Dr. Marta Nekulová in RECAMO, Masaryk Memorial Cancer Institute, Brno. Validation of isogenic clones by Western blot is included in Appendix A 1. Gene editing was confirmed by Sanger sequencing.

Because IFITM1 (and not IFITM3) was the receptor oncogene and IFITM1/IFITM3 absence was found in TMA cervical staining, we started with generating isogenic cell lines for these combinations; *IFITM1* null and *IFITM1/IFITM3* double null cells. During this research, there was a need to validate our results with an *IFITM3* null cell model to inves-

tigate whether this isoform by itself also contributes to the phonotype seen (described in upcoming chapters). Unfortunately, it took several attempts to successfully obtain *IFITM3* null clones. For this reason, the *IFITM3* null cells were not further analysed in this thesis. Nonetheless, an *IFITM3* null SiHa clone has been engineered and validated (data shown in this chapter), so it is ready to be used in future projects.

3.3 Aims of the chapter

The aim of this chapter is to successfully validate an isogenic SiHa cell model panel generated using the CRISPR/Cas9 system. Validation was performed at the genomic level by DNA sequencing of the produced CRISPR/Cas9 indels, and at the protein expression level by Western blotting and by immunofluorescence assays using a set of specific antibodies. The cervical cancer cell panel is composed by wt-SiHa and the isogenic *IFITM1* null, *IFITM3* null, and *IFITM1/IFITM3* double null cells. This will allow determination of the inducibility of IFITM1 and IFITM3 by IFNγ stimulation. The panel will serve as a tool in future chapters to validate possible protein–protein interactions between IFITM1 and its interacting partners. In addition, this panel will allow investigation of the cellular roles of IFITM1 and IFITM3, including their roles in cancer development, by studying the absence of IFITM1/IFITM3 protein production in the cell. Overall, this chapter will set the foundations of IFITM1/IFITM3 signalling in relation to the IFNγ landscape in the SiHa cancer cell model.

3.4 Results

3.4.1 Genetic screening of engineered clones obtained by CRISPR/Cas9 technology in the SiHa cancer cell model panel

The production of potential cell models of gene knock outs using the CRISPR/Cas9 system ultimately relies on the capacity of the cell to repair a DSB in the genomic DNA introducing sequence errors. Hence, the sgRNA were designed to introduce indels into the target IFITM sequences that had an adjacent PAM sequence. First, primers were designed to amplify 475 bp of *IFITM1* leaving the recognition site for the sgRNA (upstream to the PAM sequence) in the middle of the amplicon. The designed forward primer was 5' -TACAAACAGCAGGAAATAGAAACTT- 3' and reverse primer was 5'-ACTCACAGTCACAGGGACAC- 3' (Figure 3.5 A I). It was also confirmed that no other IFITM isoform shared these particular sequences. After chromosomal DNA extraction from potential *IFITM1* null cells, the DNA was amplified by PCR, and analysed by 2% agarose gel electrophoresis. A single band was observed for the potential *IFITM1* null cells and this was subsequently sequenced (Figure 3.7 A, lane 2). The DNA sequence chromatogram revealed an increased signal noise with overlapping nucleotide peaks (indicating an indel

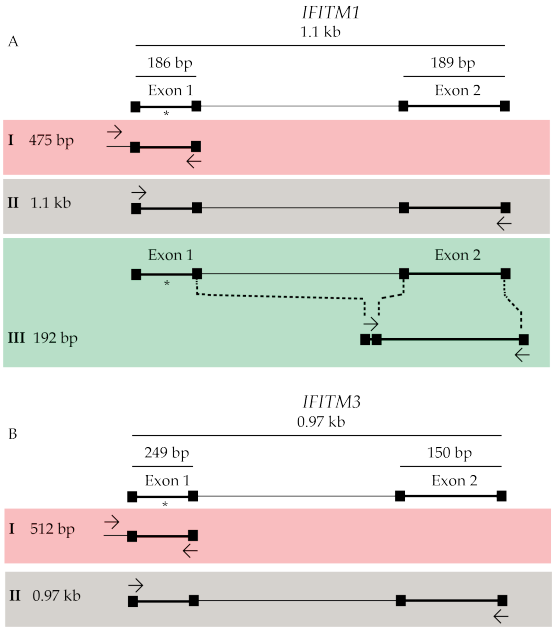

Figure 3.5: Designing primers to identify CRISPR/Cas9-generated indels in *IFITM1* and *IFITM3* genes. (A) Genomic *IFITM1* sequence organization shown at the top of the panel. Primers designed for *IFITM1*. (I) Primers designed to amplify 475 bp amplicon surrounding the sgRNA recognition site (asterisk). (II) Primers designed to amplify 1.1 kb amplicon of the whole *IFITM1* gene. (III) Primers designed to amplify 192 bp amplicon with the forward primer covering a combination of the last few nucleotides of exon 1 and the first nucleotides of exon 2. (B) Genomic *IFITM3* sequence organization shown at the top of the panel. Primers designed for *IFITM3*. (I) Primers designed to amplify 512 bp amplicon surrounding the sgRNA recognition site (asterisk). (II) Primers designed to amplify 0.97 kb amplicon of the whole *IFITM3* gene.

event), starting just after the PAM sequence (Figure 3.6 B, indicated with a black arrowhead chevron).

This pattern of increased signal noise with overlapping nucleotide peaks (Figure 3.6 B) was an indication of a heterozygote indel where each allele had a different mutation. To elucidate that possibility, the next approach was to carefully amplify the whole *IFITM1* gene, including the single intron, and clone it into a plasmid backbone. The designed forward primer was 5' -GGGGGGTACCGATGCACAAGGAGGAA- 3' and the reverse primer was 5' -CCCCGATATCCTAGTAACCCCGTTT- 3' (Figure 3.5 A II). Recognition sequences for restriction enzymes were included as part of the primer sequences in order to facilitate the cloning. A single band was seen at the same size as wt-SiHa and this was cut and cloned into a vector to be able to sequence the whole *IFITM1* (Figure 3.7 A, lane 1 vs 2). Out of 12 clones sequenced, 7 of them had a single point insertion and the rest a single point deletion at the target site. Following cloning, the DNA sequence chromatograms were free of signal noise with overlapping peaks. Both *IFITM1* alleles were gene edited in representative *IFITM1* null clone that created frameshifts by a single nucleotide deletion or insertion, resulting in transcripts with premature stop codon and frameshift mutation, respectively, and consequently being eliminated by nonsense-mediated mRNA decay (NMD) pathway

or producing a truncated protein (Figure 3.6 C and D).

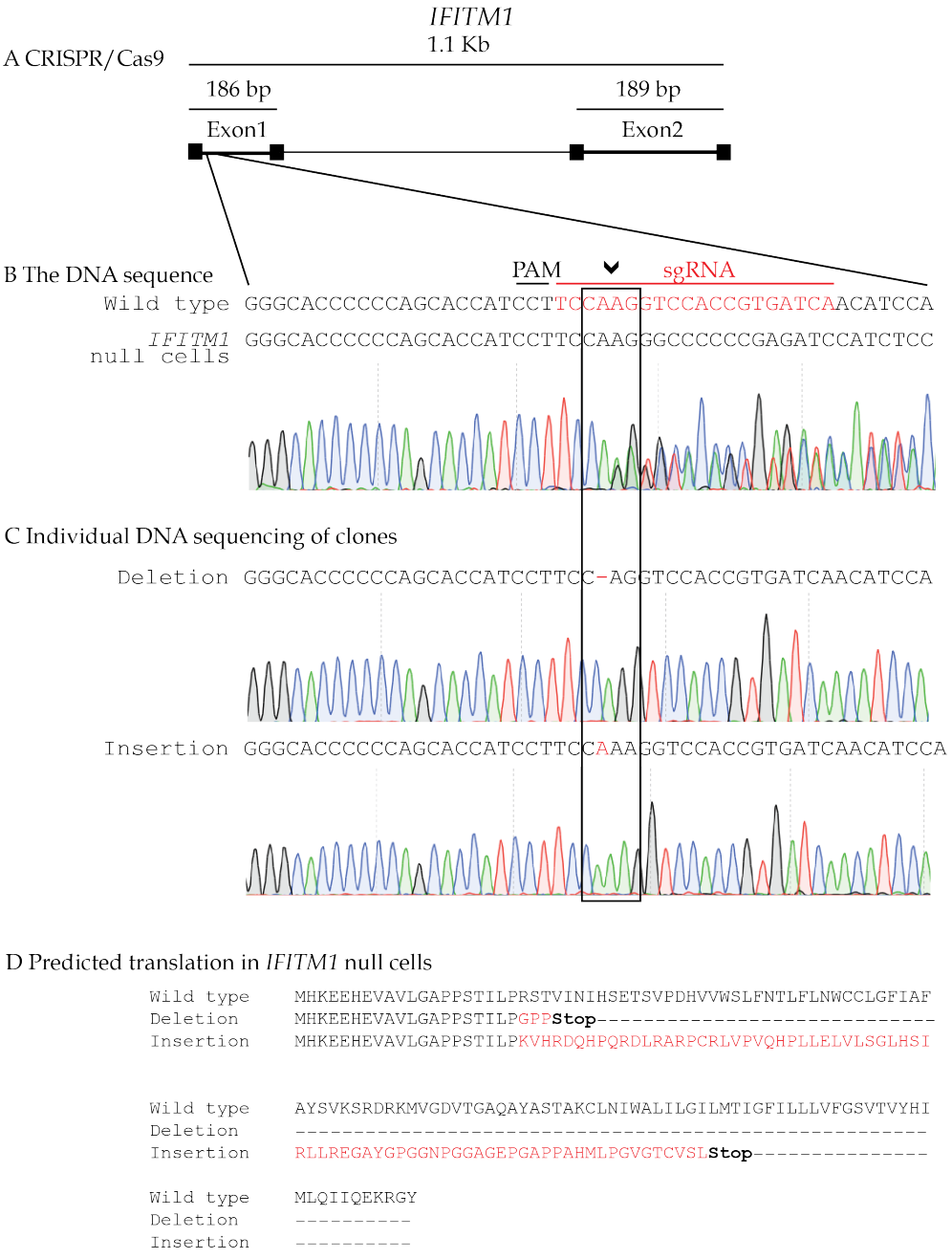

Figure 3.6: Validation of *IFITM1* knock out in engineered *IFITM1* null cells by sequencing. (A) Gene structure of the *IFITM1* gene highlighting its two coding exons and one intron. (B) Amplification of genomic *IFITM1* that targets exon 1 on 475 bp amplicon surrounding the sgRNA recognition site (indicated in Figure 3.5 A I). Representation of the wt-SiHa and *IFITM1* null alignment, sgRNA is indicated in red font with the wild-type sequence in black font. There is an increase of the signal noise with overlapping peaks starting just after the PAM sequence (black arrowhead chevron) suggesting heterozygosity of the alleles. (C) Identification of heterozygote *IFITM1* showing different indels after cloning the PCR amplified *IFITM1* gene into a vector and then sequencing individual clones for the type of gene edit. One allele of *IFITM1* gene has one bp insertion and the other has one bp deletion (in red) (D) Predicted amino acid sequence obtained from the ExPAsy translate tool shows a frameshift and premature stop codon with both genes edits.

A similar approach was followed for validation of the *IFITM1/IFITM3* double null cells. After chromosomal DNA extraction from potential *IFITM1/IFITM3* double null cells, whole *IFITM1* gene was amplified (Figure 3.5 A II), and a single gel electrophoretic band was observed below 500 bp in size, instead of an expected 1.1 kb band (Figure 3.7 A, compare lane 1 to lane 3). The DNA in this band was cloned and sequenced following the same protocol as for *IFITM1* null cells. Surprisingly, sequencing showed it resulted in a precise intron deletion in *IFITM1* null cells (Figure 3.8). To rule out possible technical problems with the sample it was corroborated, in parallel, that control wt-SiHa cells had the intron present (data not shown).

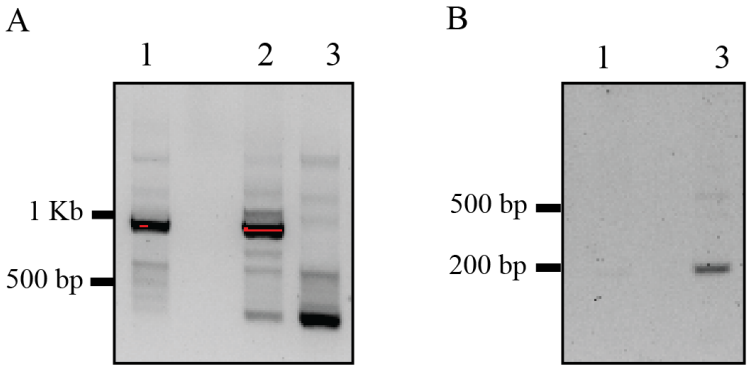

Figure 3.7: Validating of IFITM1 knock out following CRISPR/Cas9 editing in engineered *IFITM1/IFITM3* double null cells. Amplification of *IFITM1* in wt-SiHa cells (lane 1), potential *IFITM1* null cells (lane 2) and *IFITM1/IFITM3* double null cells (lane 3). (A) Primers to amplify full length gene were used, it was notied that *IFITM1/IFITM3* double null cells had a smaller band indicating a large deletion. After sequencing, intron deletion was identified. (B) Forward primer was designed comprising the last few nucleotides of exon 1 and first nucleotides of exon 2 in order to further validate the results in (A). This single band was exclusively found in *IFITM1/IFITM3* double null cells (lane 3). DNA from the single band in the *IFITM1/IFITM3* double null clone was extracted and sequenced from lane 3 in (A).

For further validation we designed a forward primer that flanked the end of exon 1 with the beginning of exon 2 (Figure 3.5 A III). The designed forward primer was 5' -ACTCCGTGAAGTCTAGGGACA- 3' and the reverse primer was 5' -CCCCGATATCCTAGTAACCCCGTTT- 3'. PCR amplification of DNA from wt-SiHa cells was used as a negative control, it was observed that there was a single band of 192 bp in size found only for *IFITM1/IFITM3* double null cells (Figure 3.7 B, lane 1 vs 3). These two alternative approaches give supporting evidence that *IFITM1/IFITM3* double null cells have an intron deletion in the *IFITM1* gene (Figure 3.7 C).

Figure 3.8: Investigation of the *IFITM1* intron loss following engineering by CRISPR/Cas9 in potential *IFITM1/IFITM3* double null cells. Gene structure of the *IFITM1* gene highlighting its two coding exons and single intron is shown at the top of the panel. This figure shows the amplicon sequence obtained using primers that target the whole *IFITM1* gene (Figure 3.5 A II). Identification of intron loss after cloning the PCR amplified *IFITM1* DNA into a vector and then sequencing individual plasmids for the type of gene edit. Highlighted in red is the absent region corresponding to the single intron present in *IFITM1* gene. Not a single mismatch was identified for the rest of the sequence analysed. (*) indicates sgRNA recognition site.

To test for abnormalities of the *IFITM3* gene, the designed forward primer was 5' -AGCCCCTCTTTCCTCCCT- 3' and the reverse primer was 5' -TCACGGAGTAGGCGAATG- 3' (Figure 3.5 B-I). After PCR amplification, 2% agarose gel electrophoretic separation, excision of the band, extraction of its DNA, and sequencing, some indels surrounding the PAM sequence in *IFITM3* gene were identified (Figure 3.9 B). Interestingly, the sequenced amplicon was free of signal noise due to overlapping peaks, suggesting that both alleles had the same indel pattern. Predicted amino acid sequence from the DNA sequence obtained indicates ablation of IFITM3 protein expression (Figure 3.9 C).

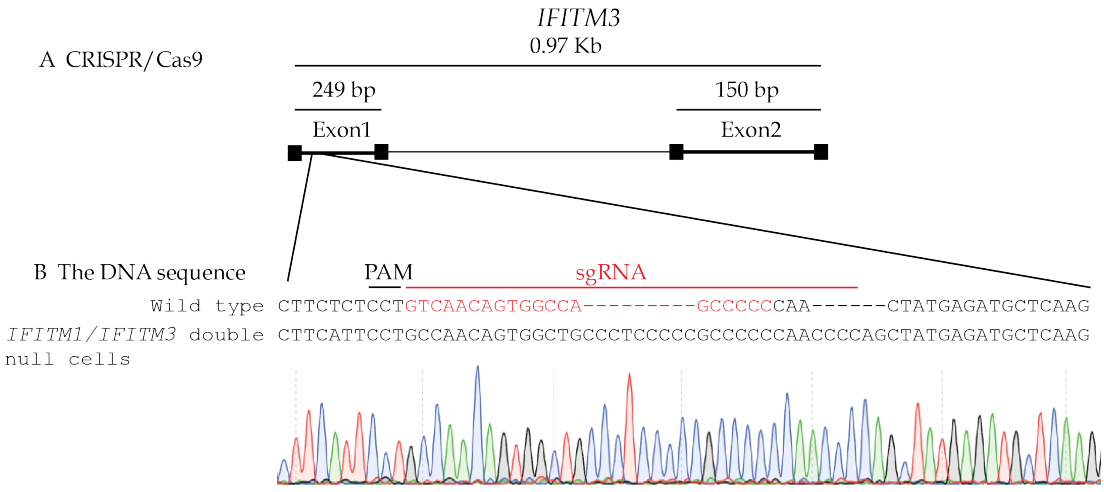

C Predicted translation in *IFITM1/IFITM3* double null cells

```
Wild type      MNHTVQTFFSPVNSGQP-----PNYEMLKEEHEVAVLGAPHNPAPPTSTVIHIRSETSVP
Insertion      MNHTVQTFFIPANSGCPPPPPNPSYEMLKEEHEVAVLGAPHNPAPSMSTMIHICSETSCV

Wild type      DHVVWSLFNTLFMNPCCLGFIAFAYSVKS-----------RDRKMVGDVTGAQAYASTAK
Insertion      Stop----------------------------------------------------------

Wild type      CLNIWALILGILMTILLIVIPVLIFQAYG
Insertion      -----------------------------
```

Figure 3.9: Validation of *IFITM3* knock out following CRISPR/Cas9 engineering of potential *IFITM1/IFITM3* double null cells by sequencing. (A) Gene structure of the *IFITM3* gene highlighting its two coding exons and one intron. (B) PCR amplification and DNA sequencing of wild type *IFITM3* gene following CRISPR/Cas9 engineering that targets exon 1 sequence of 512 bp surrounding the sgRNA target sequence. Representation of the wt-SiHa cell sequence and the *IFITM1/IFITM3* double null sequence alignment, with the sgRNA sequence indicated in red and wild type sequence in black font. Identification of the homozygous *IFITM3* indels after cloning the PCR amplified *IFITM3* DNA into a vector and then sequencing individual plasmids for the identification of gene edit. The *IFITM3* gene has two insertions that result in a poly-proline frame-shift introducing a premature stop codon (bottom strand in red font). (C) Predicted amino acid sequence obtained from the ExPAsy translate tool shows a truncated protein with insertion of prolines and alternative amino acid residues changes; as a result, full-lenght IFITM3 protein is not predicted to be expressed.

During the course of this research, *IFITM3* null cells were generated using CRISPR/Cas9 genome editing in a similar way. *IFITM3* null cells were generated for

the purpose of resolving any findings obtained with *IFITM1/IFITM3* double null cells. We wished to identify which effects are seen for *IFITM1* and *IFITM3* knock out alone or due to a combination of *IFITM1/IFITM3* knock out. Generation of *IFITM3* null by CRIPSR/Cas9 technology took several attempts. Finally, we obtained clones that were tested by amplifying and sequencing the *IFITM3* gene. The designed forward primer was 5' -GATTGGTACCATGAATCACACTGTCCAAACC- 3' and the reverse primer 5' -CGATGAATTCCTACTATCCATAGGCCTGGAAGAT- 3' (Figure 3.5 B II). Recognitions sites for KpnI and EcoRI restriction enzymes were included in the primers to facilitate cloning. As previously mentioned, PCR amplicons were run in 2% agarose gel electrophoresis, excised, and cloned into a vector (subsection 2.5.5 and subsection 2.5.7). In this case, the *IFITM3* gene has a single 7 bp deletion (Figure 3.10 B) that leads to a premature stop codon and consequent loss of expression of the full-length IFITM3 protein (Figure 3.10 C).

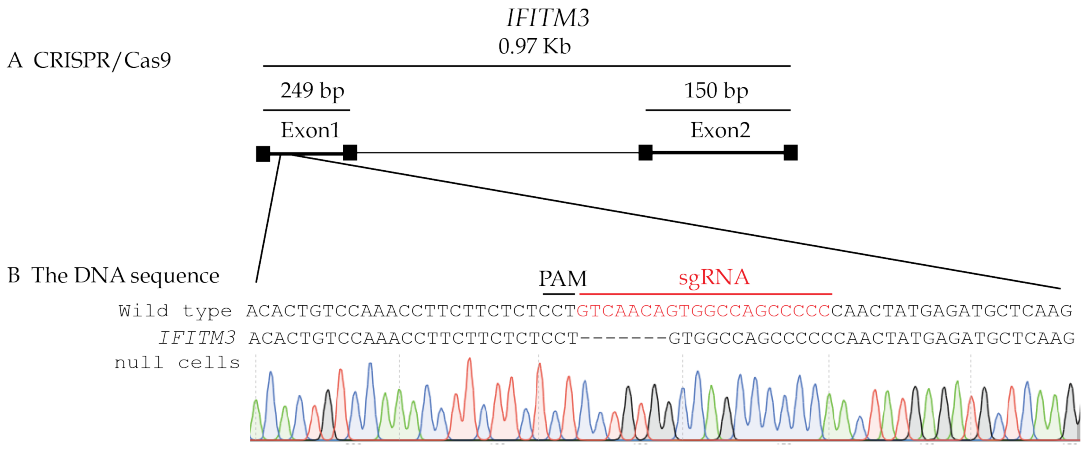

Figure 3.10: Validation of knock out of *IFITM3* in potential engineered *IFITM3* null cells by DNA sequencing. (A) Gene structure of the *IFITM3* gene highlighting its two coding exons and one intron. (B) PCR amplification of genomic *IFITM3* that targets exon 1 sequence of 0.97 kb surrounding sgRNA recognition site (indicated in the wild type strand in red font). Identification of a 7 bp deletion (indicated with a black arrowhead chevron) in *IFITM3* after cloning the PCR amplified *IFITM3* gene into a vector and then sequencing individual plasmids for the type of gene edit. The *IFITM3* gene has a single deletion that results in a frame-shift creating a premature stop codon (bottom strand in red font). (C) Predicted amino acid sequence obtained from the ExPAsy translate tool shows a truncated protein with a single deletion and alternative amino acid changes. As a result, expression of normal IFITM3 protein is predicted to be ablated.

3.4.2 Validation of *IFITM1* null cells, *IFITM3* null cells, and *IFITM1/IFITM3* double null cells by Western blot analysis

The gene edits were confirmed by DNA sequencing, however it had to be determined whether they were functionally null or expressed as truncated protein. A panel of commercial antibodies produced to specifically bind to IFITM1 or IFITM3 were tested. However, robust antibodies that distinguish between IFITM1, IFITM2 and IFITM3 were not available at the time. For that reason, monoclonal antibodies were generated in-house against IFITM1 protein (Moravian Biotechnologies). A previous alanine scanning performed by Dr. Elisabeth Sinclair revealed that the VLGxP motif at the N-terminus of IFITM1 showed high binding towards one representative monoclonal antibody (data not shown). Nonetheless, the amino acidic motif is shared between IFITM1 and IFITM3, but not with IFITM2 (Gomez Herranz *et al.*, 2019). For accuracy, as a result of this cross-reaction between IFITM1 and IFITM3, it is stated throughout this thesis that this monoclonal antibody recognizes IFITM1/IFITM3 proteins.

To confirm total absence of IFITM1, IFITM3 or IFITM1/IFITM3 protein expression, cells were stimulated with IFNγ to induce their expression. Previous studies performed *in vitro* have used variable concentration of IFNγ to stimulate cells; 100 U/ml IFNγ are used in some studies (Bernabei *et al.*, 2001; Croitoru-Lamoury *et al.*, 2011), but other studies have used a higher dose (Costa-Pereira *et al.*, 2002; Garbe *et al.*, 1990; Gorbacheva *et al.*, 2002; Ha *et al.*, 2008). To determine the appropriate dose an IFNγ dose titration (from 0–100 ng/ml) corresponding to an upper range dosage was evaluated (Appendix A, Figure A.3 A). A concentration of 100 ng/ml of IFNγ was selected for further experiments. In addition, a time course (0, 4, 6, 24, 48, and 72 hours) with 100 ng/ml of IFNγ was performed, and 24 hours was selected as the optimal time point to use in these experiments. Higher levels of IFITM1/IFITM3 protein induction are observed at 24 hours. (Appendix A,Figure A.3 B). It was decided to stimulate SiHa cells with a higher dose of IFNγ to ensure that any cellular dysfunctions would be more obvious in the absence of IFITM1 (*IFITM1* null cells), IFITM3 (*IFITM3* null cells), and IFITM1/IFITM3 (*IFITM1/IFITM3* double null cells) as a result of a dominant effect of these proteins and that IFNγ signalling will not be able to mask their effects (Cheon & Stark, 2009; Khodarev *et al.*, 2007).

The CRISPR guide RNA was designed to target unique regions in *IFITM1* or *IFITM3* genes. As such, there is no reason to expect additional knock out of the *IFITM3* in *IFITM1* null cells or of *IFITM1* in *IFITM3* null cells. Comparing signal produced by IFITM1/IFITM3-specific monoclonal antibody, endogenous IFITM1 (in *IFITM3* null) and IFITM3 (in *IFITM1* null) proteins can be observed in Western blots from gene edited cells (Figure 3.11 A, lanes 3 and 4, and Figure 3.11 E, lanes 11 and 12). However, neither IFITM1 nor IFITM3 was detected in *IFITM1/IFITM3* double null cells (Figure 3.11 A, lanes 5 and 6). While performing this study, commercial antibodies that specifically bind to IFITM1, IFITM2 and IFITM3 were found (Figure 3.11 B-D and Figure 3.11 E, lanes 1-9). Nonethe-

less, the suppliers did not specify to which epitopes these antibodies bind. It is of relevance to highlight that all three protein isoforms are highly homologous and so production of isoform-specific antibodies is complicated.

As expected, IFITM1/IFITM3 antibody was able to detect both IFITM1 and IFITM3 (Figure 3.11 A, lane 1-4). The wt-SiHa cell line exhibits a diffused band around the predicted molecular weight (15 KDa) that is intensified after IFNγ stimulation. Both IFITM1 (Figure 3.11 B, lanes 1-2) and IFITM3 (Figure 3.11 D, lanes 1-4) may have posttranslational modifications or may form dimers, they are manifested by the upper band running at a higher position than its theoretical molecular weight. Comparing IFITM1/IFITM3 antibody detection with IFITM1- and IFITM3-specific antibodies (Figure 3.11 A and E, lanes 10-12 vs B-D and E, lanes 1-9), it is clear that IFITM1 has increased posttranslational modification after IFNγ stimulation, whereas IFITM3 does not. This suggests that IFITM1 is the main isoform that is IFNγ inducible.

Additionally, we determined the IFITM2 status in this SiHa cell model panel. Importantly, IFITM2 is highly homologous with IFITM3, sharing 87% of its amino acid sequence, suggesting that they could have redundant cellular roles. IFITM2 was found not expressed, or was below the limit of detection, in the SiHa cell panel, both endogenously and after IFNγ induction (Figure 3.11 C). It was considered the possibility that the IFITM2-specific antibody may not be sufficiently sensitive, or had other technical problems, as an IFITM2 band was detected when used in other assays (data not shown).

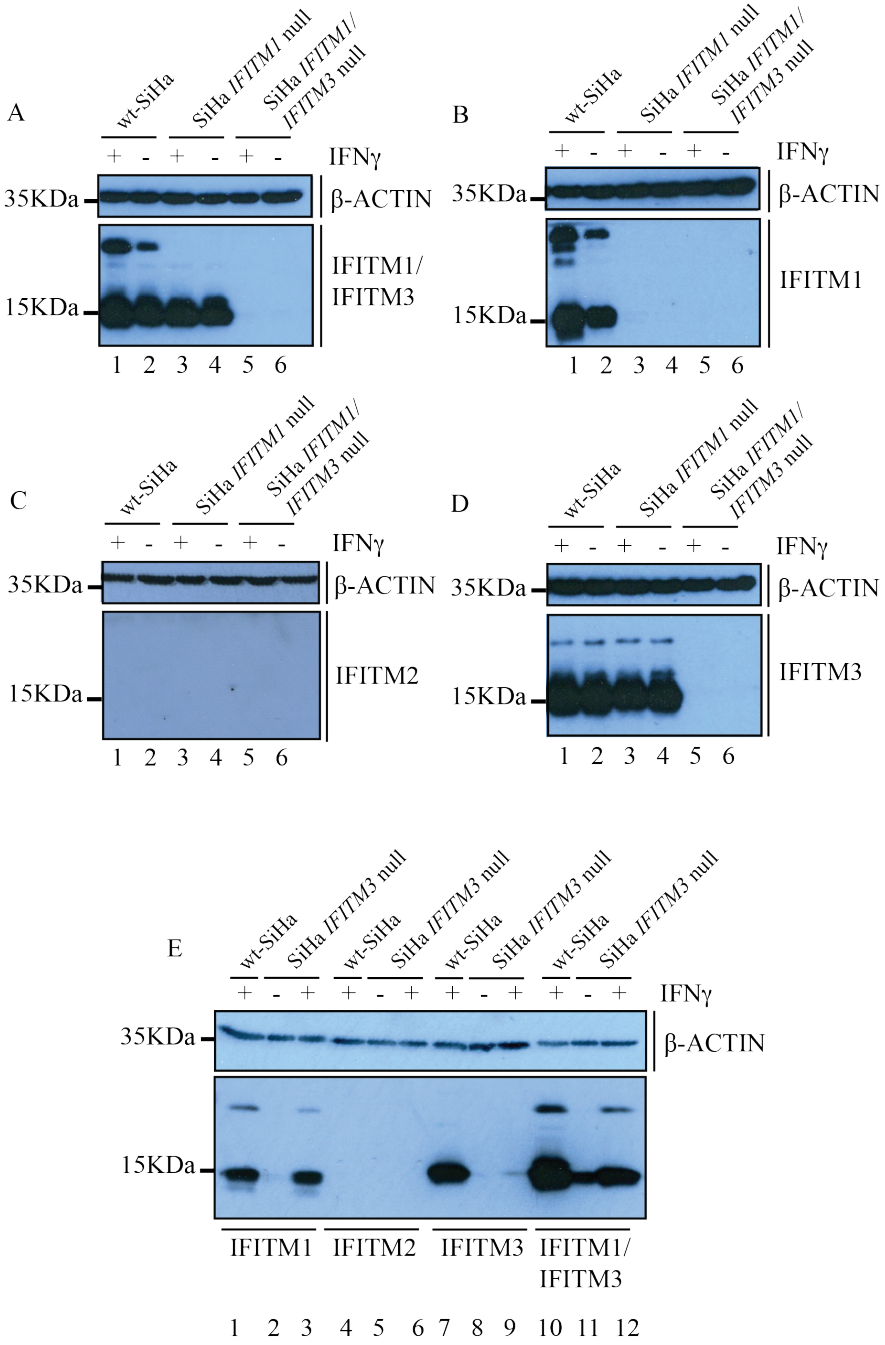

Figure 3.11: IFITM1, IFITM2 and IFITM3 induction by IFNγ in the SiHa cervical cancer cell model panel. IFITM family proteins (approximately 15 KDa) were detected in wt-SiHa cells, *IFITM1* null cells, *IFITM*3 null cells, and *IFITM1/IFITM3* double null cells using antibodies against; IFITM1/IFITM3 (A), IFITM1 (B), IFITM2 (C), and IFITM3 (D). SiHa cell model panel was composed of; wt-SiHa cells stimulated with IFNγ (lane 1), wt-SiHa cells non-stimulated (lane 2), *IFITM1* null cells stimulated with IFNγ (lane 3), *IFITM1* null cells non-stimulated (lane 4), *IFITM1/IFITM3* double null cells stimulated with IFNγ (lane 5) and *IFITM1/IFITM3* double null cells non-stimulated (lane 6). (E) IFITM family proteins were detected in *IFITM3* null using antibodies against; IFITM1 (lane 1-3), IFITM2 (lane 4-6), IFITM3 (lane 7-9), and IFITM1/IFITM3 (lane 10-12). Cells were non-stimulated (lanes 2, 5, 8, and 11) or stimulated with IFNγ (lanes 3, 6, 9, and 12). Wt-SiHa stimulated with IFNγ was used as positive control (lanes 1, 4, 7, and 10). Protein induction was tested by comparing endogenous levels with 100 ng/ml IFNγ stimulation for 24 hours. β-ACTIN (approximately 35 KDa) was used as a loading control.

3.4.3 Testing specificity of anti-IFITM1/IFITM3, IFITM1, and IFITM3 antibodies by immunofluorescence and characterization of cellular localization of IFITM1, and IFITM3 proteins in the SiHa cell model panel

After validating ablation of *IFITM1*, *IFITM3*, and *IFITM1/IFITM3* genes in the respective isogenic SiHa cells by Sanger sequencing and Western blotting, protein expression was additionally assayed using immunofluorescence (Figure 3.12, Figure 3.13, Figure 3.14, and Figure 3.15). As stated previously, there are not many suitable IFITM antibodies available commercially. For that reason, antibodies used in Western blotting (IFITM1/IFITM3, IFITM1, and IFITM3) were also tested by immunofluorescence as they were proven to be IFITM isoform specific. The IFITM2 antibody was not included as SiHa cells do not express this isoform (Figure 3.11 C and E, lanes 4-6) and it is beyond the focus of this study. Control conditions consisting of staining with secondary antibody only (in absence of primary antibody) were included to determine the background fluorescence signal (Figure 3.12, Figure 3.13, Figure 3.14, Figure 3.14; A and F).

This immunofluorescence assay is used to evaluate the endogenous production of IFITM1 and IFITM3 proteins (independently by anti-IFITM1 or IFITM3 specific antibodies or in combination with anti-IFITM1/IFITM3 antibody). IFITM1 and IFITM3 are detected in wt-SiHa cells, with an increase in their expression after IFNγ stimulation (Figure 3.12 B vs C). Both IFITM1 and IFITM3 are present in a perinuclear location after IFNγ stimulation (Figure 3.12 C). This feature is also observed in *IFITM1* null cells (Figure 3.13 C) and *IFITM3* null cells (Figure 3.15 C), but the intensity is attenuated in these cells as *IFITM1* or *IFITM3*, respectively, has been knocked out.

IFITM3 protein is also induced after IFNγ stimulation in wt-SiHa (Figure 3.12 H vs I) and, in an attenuated pattern in *IFITM1* null cells (Figure 3.13 H vs I). Interestingly, IFITM3 shows a more punctate pattern across the cytosol, that may correlate with vesicles as described by Amini-Bavil-Olyaee *et al.* (Amini-Bavil-Olyaee *et al.*, 2013). Moreover, it is negative in *IFITM3* null cells (Figure 3.15 H and I).

IFITM1 antibody shows a low staining by immunofluorescence, slightly intensified after stimulating the cells with IFNγ in wt-SiHa and *IFITM3* null cells (Figure 3.12 and Figure 3.15, E and F). The intensity observed in non-stimulated *IFITM3* null cells is similar to the background in *IFITM1* null and *IFITM1/IFITM3* double null cells (Figure 3.15 E vs Figure 3.13 E and Figure 3.14 E). Moreover, *IFITM1/IFITM3* double null cells are negative for both proteins using all three antibodies. This provides additional evidence that this cell line is unable to produce either IFITM1 or IFITM3 proteins even after IFNγ stimulation (Figure 3.14).

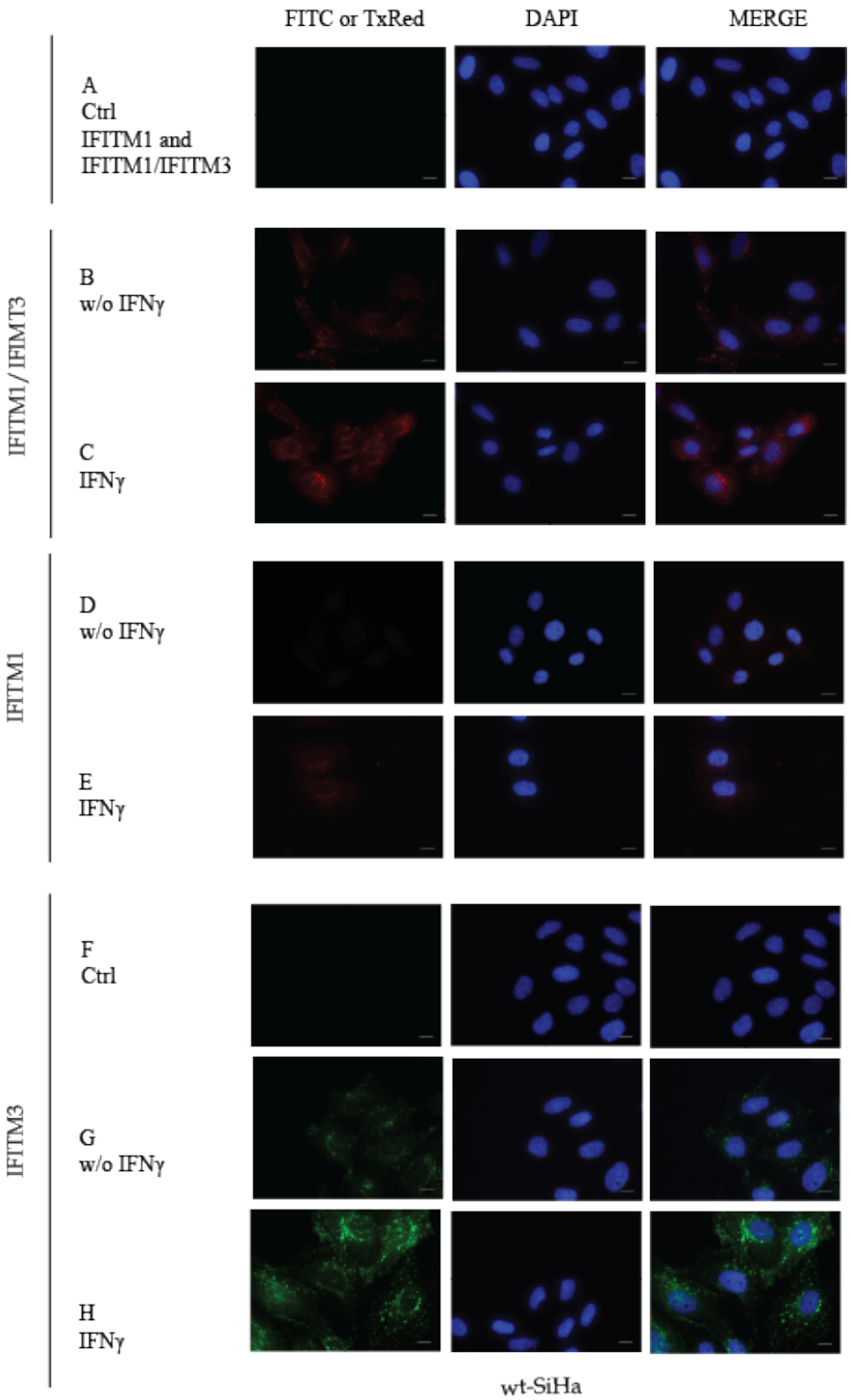

Figure 3.12: Study of IFITM1 and IFITM3 cellular distribution in wt-SiHa cells. Wt-SiHa cells were grown to 80% confluency and fixed with 4% (w/v) paraformaldehyde, permeabilised using 0.25% Triton X-100 and blocked with 3% (w/v) BSA. (A) Control immunofluorescence staining with anti-mouse Alexa Fluor 594 secondary antibody (Invitrogen). Immunofluorescence detecting IFITM1/IFITM3 protein (1:4000 dilution of IFITM1/IFITM3 antibody) in non-stimulated cells (B) or IFNγ-stimulated cells for 24 hours (C). Immunofluorescence detecting IFITM1 protein (1:1000 dilution of IFITM1 antibody) in non-stimulated cells (D) or IFNγ-stimulated cells for 24 hours (E). (F) Control immunofluorescence staining with anti-rabbit Alexa Fluor 488 secondary antibody (Invitrogen). Immunofluorescence detecting IFITM3 protein (1:1000 dilution of IFITM3 antibody) in non-stimulated cells (G) or IFNγ-stimulated cells for 24 hours (H). Scale bar= 10 μm.

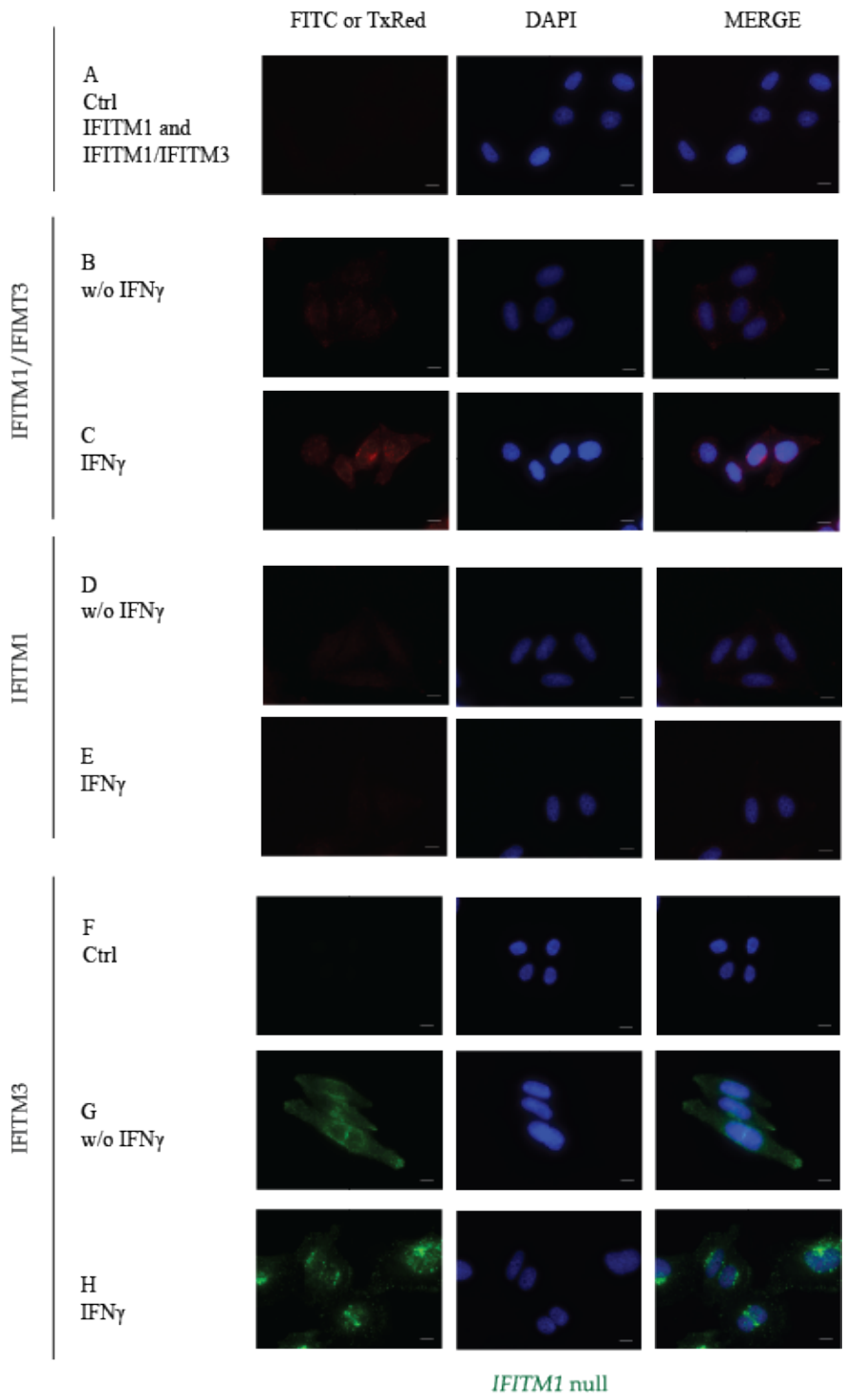

Figure 3.13: Study of IFITM1 and IFITM3 cellular distribution in *IFITM1* null cells. *IFITM1* null cells were grown to 80% confluency and fixed with 4% (w/v) paraformaldehyde, permeabilised using 0.25% Triton X-100 and blocked with 3% (w/v) BSA. (A) Control immunofluorescence staining with anti-mouse Alexa Fluor 594 secondary antibody (Invitrogen). Immunofluorescence detecting IFITM1/IFITM3 protein (1:4000 dilution of IFITM1/IFITM3 antibody) in non-stimulated cells (B) or IFNγ-stimulated cells for 24 hours (C). Immunofluorescence detecting IFITM1 protein (1:1000 dilution of IFITM1 antibody) in non-stimulated cells (D) or IFNγ-stimulated cells for 24 hours (E). (F) Control immunofluorescene staining with anti-rabbit Alexa Fluor 488 secondary antibody (Invitrogen). Immunofluorescence detecting IFITM3 protein (1:1000 dilution of IFITM3 antibody) in non-stimulated cells (G) or IFNγ-stimulated cells for 24 hours (H). Scale bar= 10 μm.

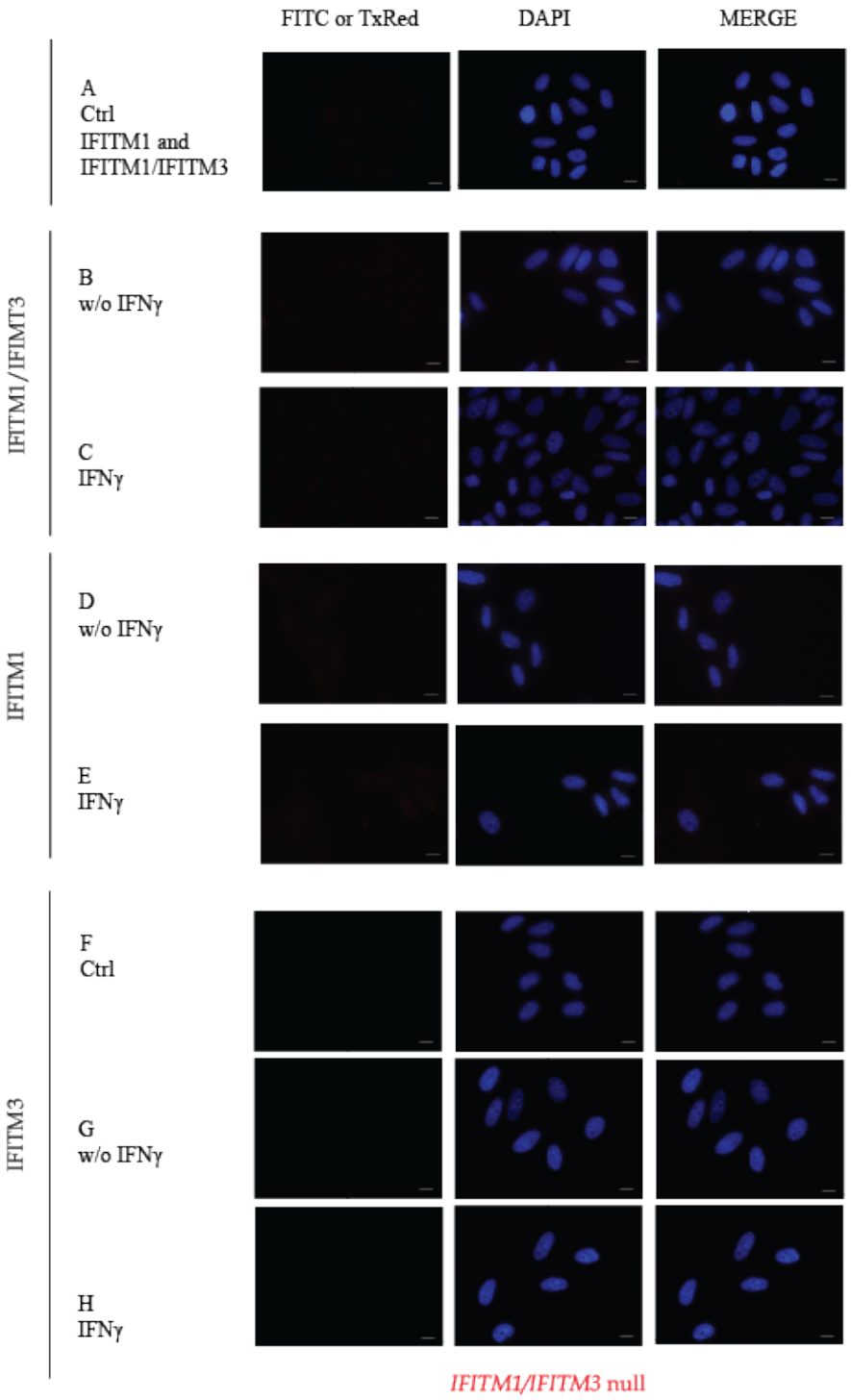

Figure 3.14: Study of IFITM1 and IFITM3 cellular distribution in *IFITM1/IFITM3* double null cells. *IFITM1/IFITM3* null cells were grown to 80% confluency and fixed with 4% (w/v) paraformaldehyde, permeabilised using 0.25% Triton X-100 and blocked with 3% (w/v) BSA. (A) Control immunofluorescence staining with anti-mouse Alexa Fluor 594 secondary antibody (Invitrogen). Immunofluorescence detecting IFITM1/IFITM3 protein (1:4000 dilution of IFITM1/IFITM3 antibody) in non-stimulated cells (B) or IFNγ-stimulated cells for 24 hours (C). Immunofluorescence detecting IFITM1 protein (1:1000 dilution of IFITM1 antibody) in non-stimulated cells (D) or IFNγ-stimulated cells for 24 hours (E). (F) Control immunofluorescence staining with anti-rabbit Alexa Fluor 488 secondary antibody (Invitrogen). Immunofluorescence detecting IFITM3 protein (1:1000 dilution of IFITM3 antibody) in non-stimulated cells (G) or IFNγ-stimulated cells for 24 hours (H). Scale bar= 10 μm.

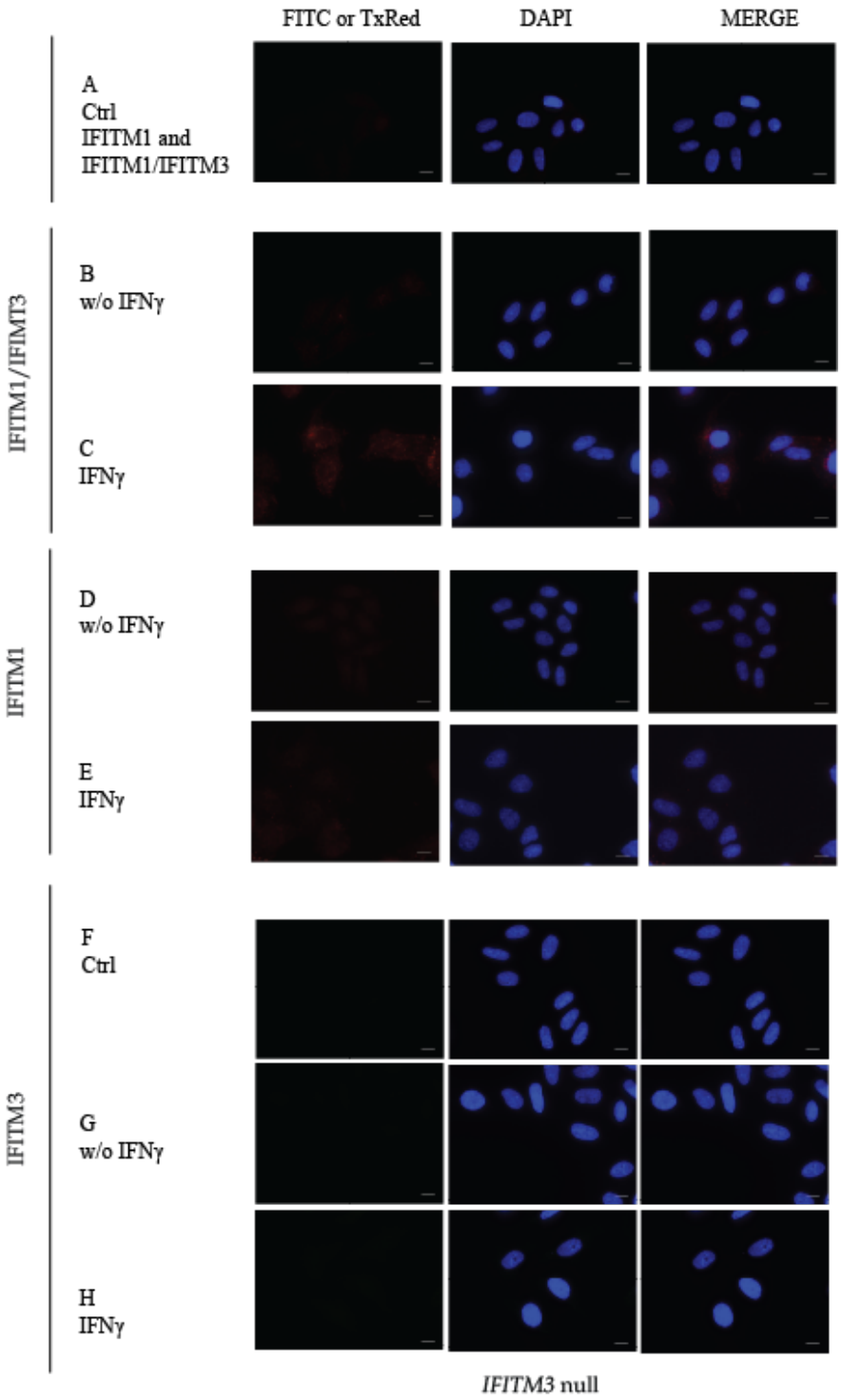

Figure 3.15: Study of IFITM1 and IFITM3 cellular distribution in *IFITM3* null cells. *IFITM3* null cells were grown to 80% confluency and fixed with 4% (w/v) paraformaldehyde, permeabilised using 0.25% Triton X-100 and blocked with 3% (w/v) BSA. (A) Control immunofluorescence staining with anti-mouse Alexa Fluor 594 secondary antibody (Invitrogen). Immunofluorescence detecting IFITM1/IFITM3 protein (1:4000 dilution of IFITM1/IFITM3 antibody) in non-stimulated cells (B) or IFNγ-stimulated cells for 24 hours (C). Immunofluorescence detecting IFITM1 protein (1:1000 dilution of IFITM1 antibody) in non-stimulated cells (D) or IFNγ-stimulated cells for 24 hours (E). (F) Control immunofluorescence staining with anti-rabbit Alexa Fluor 488 secondary antibody (Invitrogen). Immunofluorescence detecting IFITM3 protein (1:1000 dilution of IFITM3 antibody) in non-stimulated cells (G) or IFNγ-stimulated cells for 24 hours (H). Scale bar= 10 μm.

3.5 Discussion

Initially, work published by Bouchal *et al.* inspired the present study on the cellular role of IFITM1 and its implications in cancer (Bouchal *et al.*, 2009). Bouchal *et al.* study aimed to discover novel biomarkers for breast cancer. Tissue biopsies from low-grade breast primary tumours in the presence and absence of metastases, along with lymph node metastasis samples, were compared to non-metastatic tumour. MS was employed to identify potential protein candidates related to the metastatic process. Among the short-listed proteins presented, IFITM1 was the only cell membrane receptor. Its druggable potential and its potential for developing other tools for diagnosis made IFITM1 an exceptional protein candidate to study (Andreu *et al.*, 2006; Bouchal *et al.*, 2009; Fumoto *et al.*, 2008). Additional work performed in our group supported the idea that IFITM1 could be a potential biomarker for cancer.

We expanded the knowledge on IFITM1 by genetically modifying SiHa cells to ablate *IFITM1* and/or *IFITM3* genes to successfully produce *IFITM1* null cells, *IFITM1/IFITM3* double null cells, and *IFITM3* null cells. The *IFITM1/IFITM3* double null cells created a cell model that removed any redundancy of IFITM3 in the IFITM1–IFNγ interaction landscape. Apart from removing possible synergy between IFITM1 and IFITM3, this is of particular importance as IFITM3 is highly homologous to IFITM1 and this also eliminates antibody cross-reactivity between IFITM1 and IFITM3.

The key approach used to evaluate the role of IFITM1 in IFNγ-dependent protein production was the utilization of RNA-guided CRISPR/Cas9 system to create isogenic null cells. We relied less on the use of siRNA since this would only give a transient (and often incomplete) reduction of a target protein, but also siRNA itself can induce IFN response (Huerfano *et al.*, 2013). This would have complicated the analysis of the IFN-responsive nature of any IFITM1 protein interactions to be visualized and measured. In turn, the limitation of using gene knock out tools to reduce or eliminate expression of a protein requires that loss of the protein(s) is not lethal. In this regard, lethality is related to those protein(s) that play a central role in many cellular networks and thus their knock out compromises cell survival (Jeong *et al.*, 2001). *Ifitm1* and *Ifitm3* knock out mice are reported to be viable, and mice with the entire IFITM chromosomal locus deleted are also viable (Bailey *et al.*, 2012). Thus, it was not unexpected to be able to generate a panel of *IFITM1* null, *IFITM1/IFITM3* double null, and *IFITM3* null -SiHa cells. We confirmed the loss of IFITM1 and IFITM3 at the protein level by Western blot analysis (subsection 3.4.2) and immunofluorescence (subsection 3.4.3). Additionally, genetic ablation of IFITM1 and/or IFITM3 was assessed by sequencing the genetic region where the CRISPR/Cas9 system produced the indel mutations (subsection 3.4.1).

IFITM1 null cells produced a heterozygotic IFITM1 mutation after the DSB repair: one single nucleotide insertion for one allele and one single nucleotide deletion in the other (Figure 3.6). The first amino acids in the N-terminal region of IFITM1 (in *IFITM1* null cells)

are not mutated and no premature stop codon has been found in this region. However, the IFITM1-antibody is not able to recognize this fragment by Western blotting. This suggests that IFITM1, if induced, is being degraded as there is no protein production found on the immunoblot (Figure 3.11 A and B). Likewise, two major insertions and minor mutations were identified for the *IFITM3* gene (Figure 3.9) in *IFITM1/IFITM3* double null cells that depleted IFITM3 protein expression (Figure 3.11 A and D). After several attempts, *IFITM3* null cells were validated with a single 7 bp deletion that produced *IFITM3* ablation (Figure 3.10).

Albeit far less frequently, CRISPR/Cas9 system can induce large genomic deletions implicated in large cassette-unit skipping. A representative example is intron deletion in *IFITM1* of *IFITM1/IFITM3* double null cells (Figure 3.8 and Figure 3.7 B). Moreover, it has been reported that CRISPR/Cas9 can mediate genetic aberrations associated with alternative splicing. Thus, this type of genomic lesion may generate modifications in the recognition site for splicing, creating alternative transcripts as a collateral effect (Mou *et al.*, 2017). This may relate to whether repair machinery is associated with splicing regulation. In fact, alternative functions of splicing factors include protecting the integrity of the genome by actively cooperating with DNA repair proteins to correct genetic lesions (Naro *et al.*, 2015; Shin *et al.*, 2007). In return, RNA splicing machinery is also influenced by deleterious genotoxic stress and when this is severe it may lead to aberrant transcript production (Wickramasinghe & Venkitaraman, 2016).

In addition, it remains unexplored how NHEJ repair machinery fixes DSB. The premise is that NHEJ functions randomly and so DNA repair does not follow any specific pattern. Nonetheless, emerging studies suggest the opposite where NHEJ mediates DNA repair in a non-arbitrary way (Van Overbeek *et al.*, 2016). To support this evidence, we identified the exact same intron deletion in *IFITM1* null-OE33 cells, another CRISPR/Cas9 engineered cell line using the same sgRNA (data not shown). Both cell lines, SiHa and OE33, have different origins and so it suggests that the repairing pattern is something fundamental and not cell-type specific. Furthermore, there was a different indel produced for *IFITM1* null cells and, it implies that there is not a unique indel produced for each sgRNA. In fact, even though observed in few events, our results fit with Van Overbeek *et al.* investigation where there is a consistent group of indels found across different cell lines tested (Van Overbeek *et al.*, 2016). As in OE33-*IFITM1* isogenic null cells (data not shown), disruption of the intron causes total inactivation of *IFITM1* in *IFITM1/IFITM3* double null-SiHa cells and consequently there is a complete depletion of protein expression. Seeing depletion of protein production by intron deletion, even only twice, made the finding more plausible. Moreover, the relevance of intronic sequences linked to transcription regulation has been reported previously. Loss of intron may interfere with mRNA production and processing and it will ultimately impact on protein expression levels (Buchman & Berg, 1988; Chung & Perry, 1989). Splicing is also modulated by the transcription machinery. For example, RNA Polymerase II and promotor structure associate and regulate spliceosomes (Cramer

et al., 1999; Hicks *et al.*, 2006; Mortillaro *et al.*, 1996). All three processes, including DNA repair, are interplay almost simultaneously (Cramer *et al.*, 1999; Muñoz *et al.*, 2009).

In summary, based on this empirical work we provide evidence in relation to intron-dependencies coupled to transcription of *IFITM1*. Even though this issue is not one of the key focus of this study, these results suggest that IFITM1 expression is influenced by its intronic region.

After validation of CRISPR/Cas9 gene edited SiHa cell model panel, IFITM1 and/or IFITM3 protein expression in null isogenic cell models was characterized. Initially, our interest was to study the cellular role of the oncogenic receptor IFITM1, but we also wanted to investigate the synergetic effects between IFITM1 and IFITM3. For this purpose, the anti-IFITM1/IFITM3 in-house antibody (Moravian Biotechnology), capable of recognizing both isoforms, was developed. Its binding domain binds to IFITM1 and IFITM3 but not to IFITM2 (Figure 3.11 A and E). Additionally, specific anti-IFITM1/2/3 antibodies were also used for clone validation (Figure 3.11 B-E). As seen in Figure 3.1, clinical data derived from women with cervical cancer have a wide range of IFITM1/IFITM3 expression levels, from totally absent signal to strong immunostaining. SiHa cells were chosen as a cervical cancer model for this study as they present high IFITM1 and IFITM3 endogenous levels compared with other cell lines, and they are induced upon IFNγ stimulation. Our results show endogenous detection of IFITM1 and elevated posttranslational modification or possible dimerazation in the presence of IFNγ (Figure 3.11 A and B, upper bands in lanes 1 and 2). Besides, IFITM1 is induced by IFNγ (Figure 3.11 B, lane 1 vs 2). By contrast, IFITM3 is not as responsive to IFNγ stimulation (Figure 3.11 D, lane 1 vs 2) (Lau *et al.*, 2012).

Immunofluorescence assays validated total loss of IFITM1/IFITM3 expression in *IFITM1/IFITM3* double null cells, and absence of IFITM1 or IFITM3 in *IFITM*1 null cells and *IFITM3* null cells, respectively. The subcellular localization of IFITMs is still under debate. Initially, IFITM1 was described at the cell surface, promoting aggregation of T-cells (Chen *et al.*, 1984). Nevertheless, 4% paraformaldehyde fixation for immunofluorescence was not able to show much cell membrane staining. Cell membrane staining was more clear when fixed by the methanol:acetone method (data not shown). However, other studies have found evidence of subcellular distribution of IFITM proteins in cytoplasmic endolysosomal vesicles (Amini-Bavil-Olyaee *et al.*, 2013; Feeley *et al.*, 2011; Huang *et al.*, 2011). This could correlate with the punctuate distribution pattern seen for IFITM3, and substantial perinuclear distribution of IFITM1/IFITM3 after IFNγ stimulation (Figure 3.12 and Figure 3.13; C and I).

Several clones for each null cell type were tested for validation. A single representative clone was selected for *IFITM1* null cells, *IFITM3* null cells, and *IFITM1/IFITM3* double null cells. We are aware that some features could be produced due to clonal effects and so we performed preliminary assays to confirm that our chosen clones behave similarly to the parental cells. Here, some evidence is provided suggesting that isogenic SiHa cell models have the expected phenotype and do not exhibit off-target effects. Firstly, *IFITM1* null

clones were subjected to chemotherapy by cisplatin and X-ray treatment and the selected clone showed chemosensitivity, along with other clones (data not shown). The chemosensitivity experiments were kindly performed by Dr. Marta Nekulova and Miss Erisa Nita, respectively. This outcome resembles the results obtained with cellular sensitivity studies upon 5-fluorouracil and cis-platinum treatment in depletion of IFITIM1 or in patients diagnosed with oesophageal squamous cancer cell carcinoma (Fumoto *et al.*, 2008).

Moreover, we compared our experiments (described in upcoming chapters) with the signature of proteins found downregulated after depletion of IFITM1 using an siRNA approach (Figure 3.2) where several IRDS protein levels decreased. Additionally, we looked for internal controls such as STAT1 (upstream effector of IFITM1 and IFITM3 in the IFNγ signalling pathway) that were independent of the IFITM1 effect while some downstream effectors, such as MHC class I and ISG15 among others, were altered (Figure 5.9). Additionally, *IFITM1/IFITM3* double null cells presented a much deeper dysregulation of the target proteins suggesting that IFITM3 is implicated and its absence produces a more aberrant IFNγ signature. Finally, another knock out panel of *IFITM1* null, *IFITM3* null and *IFITM1/IFITM3* double null cells was generated by CRIPR/Cas9 technology using A549 cells, a human lung carcinoma cell model. Preliminary results using these null cell lines resembled those obtained with the SiHa cell model (data not shown).

Besides these, several efforts were made to rescue the wild type phenotype by complementation, creating stable cell lines by integration of transfected IFITM1 and/or IFITM3 expressing constructs in the null cells. Firstly, untagged IFITM1 and/or IFITM3 were transfected and selected by drug resistance, using neomycin and zeocin markers, respectively. As *IFITM1/IFITM3* double null cells had to be complemented with two different constructs it was important to use vectors with different antibiotic resistance. Unfortunately, untransfected cells were also resistant to both drugs, even at high concentration (much higher than the manufacturer's recommendation). Consequently, it was not possible to select potential candidate clones. As a second approach, IFITM1-GFP tagged was transfected. In this case, cells were FACS sorted after being transfected for 10 days to increase number of cells expressing GFP by stable integration. Single cells were sorted in 96-well plates and grown in sequentially bigger plates. In the end, only 4 clones grew but none of them had integrated IFITM1 construct. It is difficult to provide direct evidence to support the idea that CRISPR/Cas9 epigenetic change does not allow addition back of deleted genes, but by this experimental approach it has not been possible to integrate either IFITM1 or IFITM3 vectors. Nonetheless, alternative methods will be engineered to validate the cellular effects of IFITM1/IFITM3 proteins.

Taking everything together, this chapter describes the construction and validation of cervical cancer cell models that are suitable for study of IFITM1/IFITM3 signalling in IFNγ landscape. This SiHa cell model panel will be used as a tool to study IFITM1/IFITM3 oncogenic roles in the rest of this thesis, in particular in *IFITM1/IFITM3* double null cells.

Chapter 4

Defining IFITM1-IFNγ dependent signalling pathways

4.1 Introduction

4.1.1 Interacting partners identified for IFITM1

The IFITM family of proteins have roles in oncogenic cell homeostasis. IFTM1, in particular, has pro-metastatic as well as pro-oncogenic implications. It is the only IFITM family member with a potential extracellular role due to its partial residence outside of the plasma membrane (Weston *et al.*, 2014). The molecular functions of IFITM1 are largely undefined and not many interacting partners have been identified so far. In this chapter, we begin to set up assays that identify IFITM1 binding proteins in a cervical cancer cell model in order to understand possible dominant protein–protein interactions that might be involved in IFITM1 signalling, and to identify how it can impact on signal transduction in cancer cells.

The IFITM protein family was identified in whole genome siRNA screens as having a dominant role as RNA virus restriction factors (Brass *et al.*, 2009). Additionally, a yeast two-hybrid screen, with IFITM3 as a bait, identified new protein–protein interactions within the IFITM family. IFITM3 was found identified to interact with the vesicle membrane protein associated protein A (VAPA). It was not possible to distinguish between IFITM3 to IFITM1 or to IFITM2 isoforms in this assay. Despite this, the study focused on defining how VAPA interaction with IFITM3 results in reduction of VAPA binding to oxysterol-binding protein (OSBP), disrupting cholesterol homeostasis and preventing viral maturation. As IFITM1 and IFITM2 are also reported to bind to VAPA, it is not yet clear whether they play minor and/or redundant roles in controlling cholesterol-mediated viral maturation (Amini-Bavil-Olyaee *et al.*, 2013).

Prior to that discovery, IFITM1, known at the time as leukocyte antigen Leu-13 (Deblandre *et al.*, 1995), was characterized as a component of a cell surface complex. Another

component identified was TAPA-1, also known as CD81, which closely relates to ME491 and CD37 proteins. Collectively, these are involved in homotypic cell adhesion in leukocytes and growth arrest (Takahashi *et al.*, 1990). In this respect, an independent study found CD19, TAPA-1, CD21, and IFITM1 forming a complex in B cells (Matsumoto *et al.*, 1993).

Another study described in B lymphocytes involves IFITM1 in cell-to-cell homotypic adhesion (Evans *et al.*, 1993; Evans *et al.*, 1990). This role is dependent on IFNα stimulation and not significantly related to IFNγ. As a result, it causes aggregation of B lymphocytes in Daudi B lymphoid cells as well as in peripheral blood. IFNα significantly increases IFITM1 expression but does not induce other adhesion-related molecules such as LFA-1, ICAM-1, VLA-4 and CD44. It was also tested whether other cytokines are involved in this process, but IL-2, IL-6, and TNF-α showed no effect on stimulating IFITM1 production (Evans *et al.*, 1993; Evans *et al.*, 1990). This finding is also supported by Bradbury *et al.* (Bradbury *et al.*, 1992).

Moreover, IFITM1 has been associated with caveolin 1 (CAV1) which is implicated in cell proliferation and migration processes. A study of 229 colorectal cancer tissues from human patients identified an inverse correlation between IFITM1 and CAV1 (Novita Sari *et al.*, 2016). This was further supported by another study that found IFITM1 suppresses CAV1 to facilitate metastasis in colorectal cancer and this event is also a key components in the epithelial mesenchymal transition. Additionally, depletion of IFITM1 rescues CAV1 levels, inhibiting the migration process (Yu *et al.*, 2015).

To the best of our knowledge, these are the major interacting partners described on IFITM1 but we suspect that other proteins are implicated in IFITM1 cellular functions. MS methodologies were used to discover novel protein binders.

4.1.2 Mass spectrometry

Proteins govern most cellular events. They do not tend to function in isolation, instead they form complexes, making cellular processes even more complicated to analyse. In addition, the proteome is very dynamic; it varies between spatial (i.e. cell type) and temporal (i.e. time point or stimulus response) conditions. The described proteins above are the most well characterized IFITM1 interacting partners, but considering the few proteins identified, one can suspect that most of IFITM1 interactome is still to be discovered. Trying to define a novel protein interaction presents a great challenge. To simplify our system, our focus was to characterize IFITM1 protein–protein dominant interactions after IFNγ stimulation to enrich IFITM1 expression in a cervical cancer cell model.

Sample preparation is essential to obtain a desirable MS analysis and consequent protein identification. After lysis, analytes are subjected to filter aided sample preparation (FASP). This step removes any contaminants (i.e. sodium dodecyl sulphate, other detergents), denaturant or incompatible species (i.e. salts and lipids, among others). The pur-

pose is to purify proteins to obtain high peptide quality. In brief, the process followed includes reduction, alkylation and tryptic digestion of proteins and was performed in a spin filter column (Manza *et al.*, 2005). FASP method has been considerably improved but it still has a relatively poor peptide recovery, implying the loss of proteins during the process (Hernandez-Valladares *et al.*, 2016). This presents a substantial limitation as consequently not all the proteins contained in the mixture will be subjected to the MS analysis. In that sense, the non-identification of a specific protein does not necessarily mean that the protein was not in the protein mixture.

Prior to MS analysis, the protein mixture was incubated with trypsin to generate peptides. We relied on the capacity of trypsin to produce similar amounts of tryptic peptides in relation to protein abundance. Breaking down proteins facilitates the study of insoluble membrane proteins, such as IFITM1, as it increases protein solubility. Therefore, peptides are easily ionized to produce precursor ions. Many peptide species from the same protein will be produced and they will be discriminated according to their mass-to-charge ratios (m/z). They will be sorted depending on their mass into separated ion peaks. It is assumed that trypsin will equally dissociate proteins by proteolysis throughout the protein mixture but, nevertheless, intrinsic characteristics of certain peptides could make some proteins less disposed to be trypsinized and, consequently, poorly detected by MS.

MS is a technique widely used for the study of the proteome and it allows the identification and quantification of proteins in a complex analyte. MS instruments consist of three different parts: an ionization chamber, a mass analyser and an ion detector. After peptides are produced and separated by liquid chromatography, they are coupled to tandem mass spectrometry (MS/MS) which is a combination of two mass spectrometers. Firstly, a set of ions of interest, called precursor ions (MS1), are specifically chosen and further fragmentated into product ions (MS2). As such, MS2 is a selection of a particular peak (each corresponding to a peptide) from MS1. It is a multistep process comprised of selection, fragmentation and detection of the ion (Niessen, 1999). Several types of MS analysers have been developed, those used in the present study are the Orbitrap and SWATH, which will be described in more detail in the upcoming sections.

The assignment of MS/MS spectra is obtained by the optimal match between a theoretical peptide spectrum and the empirical peptide spectrum. A theoretical spectrum is obtained from online available data sets that use algorithms to predict the peptide spectrum. The empirical peptide spectrum is obtained after in the MS/MS analysis. Therefore, peptide identification is limited by finding an exactly-matching empirical peptide in one of the theoretical peptide libraries and matching this peptide to a unique protein. In this circumstance, an additional limitation is presented: not only it is extremely complicated to determine the sequence of the peptide but also to assign that sequence to a unique protein. Even though MS technology has profoundly evolved in the last years, the average protein coverage remains low. This aspect greatly impacts on the protein identification confidence and on the overall reliability of the analysis (Huang *et al.*, 2012; Meyer *et al.*,

2011). Even so, MS is a powerful tool with tremendous potential to identify new IFITM1 interacting proteins. To overcome the limitations described above, candidate binding proteins will be further validated by alternative biological assays.

4.1.3 Orbitrap-MS

Orbitrap is a modification of Kingdom trap, an ion trap analyser from 1923 (Kingdom, 1923). Traditional ion trap mass analysers had limited mass accuracy and reduced charge capacity. The Orbitrap mass analyser can deal with analysis of heavy and multiply-charged molecules (Figure 4.1). It consists of an outer barrel-like electrode and a central spindle-like electrode. Injected ions cycle in the space between electrodes, around the central electrode and at the same time oscillate along the horizontal axis (Perry *et al.*, 2008). The principle of the orbital mass analyser is based on the orbital trapping of ions. A positively charged ion of a particular mass (m) and charge (z) is introduced inside the analyser with an initial velocity perpendicular to the orbital trapping. The difference of potential between the central electrode and the outer electrode will promote an ion rotation around the central electrode. The ion will achieve an axial frequency independent of inherited properties used to calculate the m/z ratio, producing more accurate mass measurement and giving higher resolution. In order to be able to measure a wider mass range, ions are subjected to an electrodynamic squeezing produced by a monotonic electric field increased when ions enter the orbitrap chamber. Once ions rotate in harmonic oscillation, the voltage is kept constant to avoid possible mass changes during detection (Makarov, 2000).

To ionize the peptides in our experiments, the MS is equipped with an electrospray ionization source (ESI). Ions are then transferred to quadrupole chamber where the pressure allows ion accumulation until they are released to the Orbitrap analyser. In order to obtain high resolution, ions with mass/charge ratio must have similar movement. To achieve this, they are injected almost simultaneously. The continuous ion movement inside the Orbitrap is achieved by the modification of the electric field. To proceed to MS2 in the Orbitrap, precursor ions are selected and fragmented in an external ion trap. Mass/charge values are measured from the frequency of harmonic ion oscillations after hitting the detector by fast Fourier transform algorithm (Guan & Marshall, 1993).

MS is not a quantitative method; detector, trypsinization, ionization and other factors may produce some variability between sample populations. Nonetheless, some experimental approaches have been developed to allow protein quantification between samples. Among all the possible quantitative methods developed, stable isotope labelling with amino acids in cell culture (SILAC) was selected for this study. It was firstly described by Ong *et al.* (Ong *et al.*, 2002), and shortly after used for protein quantification (Ong & Mann, 2005). It is a metabolic labelling technique that allows quantification of protein mixtures by incorporating specific stable isotope amino acid residues in live cells. One of the main

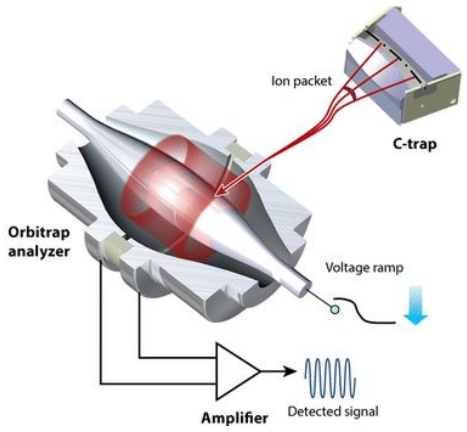

Figure 4.1: Schematic representation of ion trajectory in Orbitrap mass analyser (from Thermo Fisher Scientific). A continuous voltage increase is applied upon ion packet entry into the Orbitrap. Once ions move in harmonic circular rotation around the central electrode (ring-like trajectory) the voltage is kept constant.

advantages is that different cell populations can be labelled, and then can be mixed at very early stage in the experiment and the analysis can be carried out in a single mixture, minimizing the experimental error between samples and producing a more reliable protein quantification (Mann, 2006).

Being a data dependent acquisition method (DDA), Orbitrap has some limitations. This approach implies that only a group of the whole mixture of compounds will be selected for ion fractionation. It is usually based on the most abundant set of ions, but other criteria can be applied. It means that a limited amount of ion precursors will be processed, and the rest will not be considered for analysis. In consequence, this not only means that some compounds will never be identified, but also that reproducibility between replicates will be affected as ion selection will be determined by the abundance of peptides in the sample mixture (Gillet *et al.*, 2012).

4.1.4 SWATH-MS

In contrast to DDA, data independent acquisition (DIA) allows complete identification of all the analytes in a sample mixture. The best example of the DDA method is the sequential window acquisition of all theoretical mass spectra (SWATH-MS). To achieve this, sequential data acquisition of specific mass window of ion precursors is selected. Here, the mass window can be modified to cover the entire precursor mass range and will compile all the MS/MS data from every single ion (Figure 4.2). As a result, all the fragmented ions will be considered for analysis. In that sense, reproducibility between replicates will be more consistent. By applying highly complex algorithms SWATH is able not only to identify, but also quantify, label-free samples (Gillet *et al.*, 2012). This approach allows the analysis of all the peptides present in the analyte by separating the peptides in groups. But, reducing the level of complexity of the data acquisition requires prior knowledge of the sample.

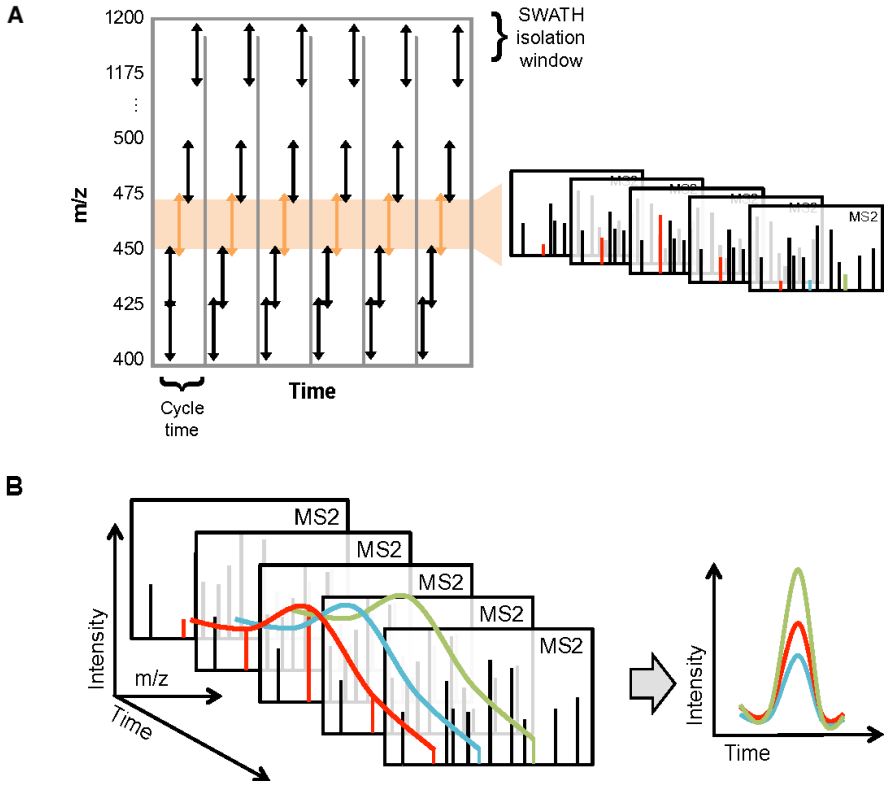

Figure 4.2: Representation of SWATH-MS cycles (Comai & Katz, 2017). (A) In each cycle, eluted peptides from LC are sequentially scanned in MS1 spectrum and a selection of peptides of similar m/z will be recruited over time for fractionation to produce the MS2 spectrum, shown in isolation windows (not included). As a result, each window will represent a group of high-resolution peptides in a particular m/z range. All together these will form a combination of high resolution MS2 spectrum covering the whole m/z range. (B) Intensities of individual fragment ions are extracted for each window and combined to generate ion chromatogram peak groups as a function of retention time and intensity. Importantly, m/z range and time of scanning are meticulously chosen so it is quick enough to cover all the m/z range and to fragment the peptides without losing resolution. Intensities of fragmented ions of interest are generated from the MS2 spectrum and presented as an extracted ion chromatogram (XIC)

It is of great importance to have a high-resolution instrument; as many precursor ions will be fragmented at the same time, it has to be capable to produce well-resolved ion peaks to obtain an error-free identification. A good analyser for this task is the TripleTOF. This is a powerful analyser that allows high speed scanning of the ion-mass dynamic range without compromising resolution.

TripleTOF configuration is comprised of three quadrupoles, the last being the TOF analyser (Chernushevich *et al.*, 2001) which measures the 'time of flight' of a given ion before hitting the detector placed at the end of the analyser. Ions are generated by an ESI source as in the Orbitrap. To achieve MS2 in SWATH, precursor ions are selected in the quadrupole and then sent to the collision cell for fragmentation. A high voltage pulse creates an electric field that initiates the ion travel through the quadrupole. The acceleration of the ion depends on the energy applied, the distance it has to travel and its mass-to-charge ratio (inherent feature of each ion). Following kinetic laws, smaller masses will achieve high speed and, on the contrary, larger masses will move at a slower velocity. Based on this principle, the detector positioned at the end of the quadrupole will deconvolute the mass-to-charge ratio of each ion, measuring arrival times (Figure 4.3) (AgilentTechnologies, 2011).

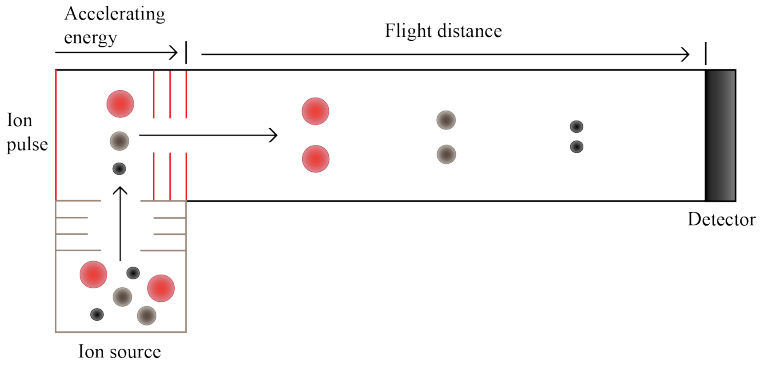

Figure 4.3: Schematic representation of 'time of flight' analysis mass sorting (adapted from (AgilentTechnologies, 2011)). According to its mass-to-charge ratio, ions will be sorted; small ions will be more accelerated than larger ions. As a result, they will travel at different velocities through the quadrupole, striking the detector at different time points.

4.2 Aims of the chapter

In this chapter we aim to identify dominant IFITM1 interacting partners after INFγ stimulation. Firstly, ectopically transfected IFITM1, with a streptavidin binding protein (SBP) tag at the N-terminus, will be pulled down by affinity enrichment. The mixture of proteins will then be determined to identify novel protein binders. To accomplish this, MS technology will be applied i.e. Orbitrap-MS and SWATH-MS. Subsequently, we will focus on validating a few candidate proteins of interest; SRSF1, ISG15, and HLA-B.

4.3 Results

4.3.1 Cloning IFITM1 into pEXPR-IBA105

The initial goal was to characterize the IFITM1 interactome. The first approach was to pull down IFITM1, along with its binding protein partners, by affinity enrichment coupled with LC-MS/MS analysis of the eluate. Isolation of IFITM1 interacting partners by immunoprecipitation would be ideal so we could work on an endogenous cellular system. But, as stated in chapter 3, IFITM proteins are highly homologous which complicates specific binding of the protein to the antibody. For this reason, an assay was developed using ectopically-tagged IFITM1.

The system consisted of tagging IFITM1 at its N-terminus with SPB that binds by affinity to streptavidin agarose conjugated beads. The first step was cloning to incorporate the SBP tag at the N-terminus of IFITM1 (Figure 4.4). Codon optimized IFITM1 was inserted into a pMA-T-15ADAZQP backbone and then cloned into pEXPR-IBA105, a vector containing two SPB tags in tandem (henceforth EV, standing for empty vector). Cloning by enzymatic digestion was not possible as the position of restriction enzyme recognition sites were not compatible. Instead, IFITM1 from pMA-T-15ADAZQP vector was amplified by PCR (section 2.5.5). Restriction enzyme recognition sites were included in the design of the primers to facilitate cloning in later steps: KpnI for the forward primer and EcoRV for the reverse primer. These restriction sites were not present in the IFITM1 sequence. To maintain the reading frame between the SBP tag and the IFITM1, a single nucleotide was added between the KpnI recognition site and the IFITM1 start codon (Figure 4.4 I).

The PCR product was run on a 1.5% agarose gel, which showed a single band at around 1 kb. This band was excised, purified and digested, along with the EV, with KpnI and EcoRV restriction enzymes (Figure 4.4 II). The purified IFITM1 amplicon along with EV were ligated (Figure 4.4 A III). The ligation mixture was transformed into DH5α competent cells which were plated in LB agar plates containing ampicillin antibiotic for selection (section 2.4) (Figure 4.4 A IV). The growing colonies were selected and the plasmid DNA was isolated by miniprep. Successful cloning of pEXPR-IBA105-SBP-IFITM1 (henceforth SBP-IFITM1) was confirmed by Sanger sequencing (subsection 2.5.11).

The SBP-IFITM1 sequence was aligned using SnapGene software to validate successful cloning. Appropriate expression in mammalian cells was tested by transfecting SBP-IFITM1 into wt-SiHa for 24 hours. Immunoblotting revealed a single band detected by mouse monoclonal anti-SBP-tag antibody and a double band with mouse monoclonal anti-IFITM1/IFITM3 antibody. As expected, the lower band (around 15 kDa) corresponded to the endogenous IFITM1/IFITM3 and the upper band, around 5 kDa higher, was SBP-IFITM1 (Figure 4.4 B, lane 2). After validation, a maxiprep (subsection 2.5.1) was performed to obtain enough product for further transfection assays.

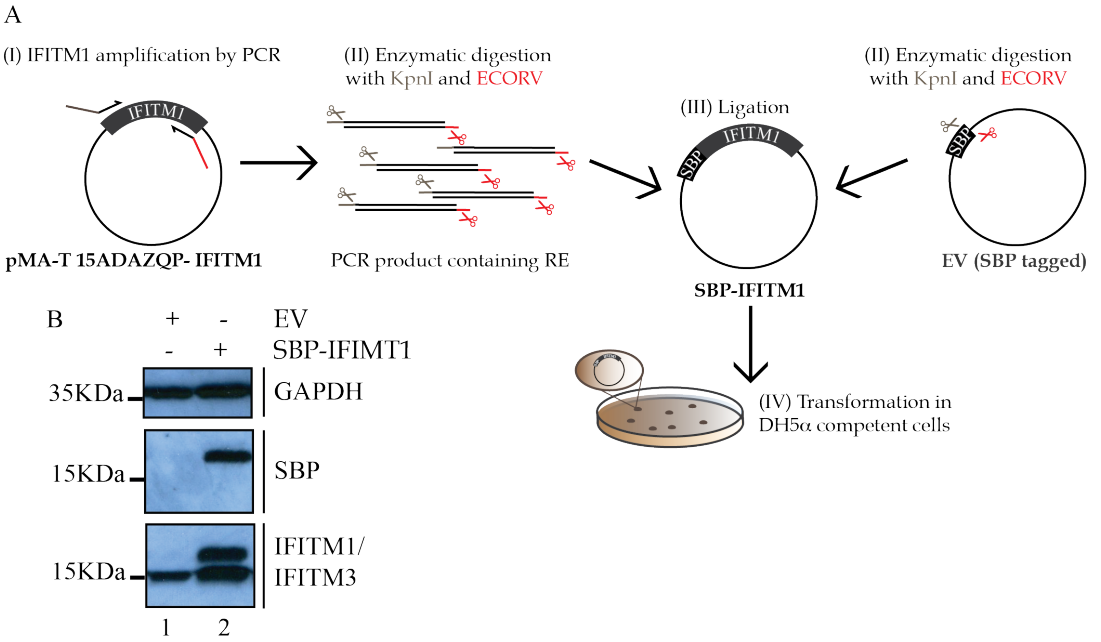

Figure 4.4: Cloning of IFITM1 into EV. (A) Workflow describing the steps followed to clone IFITM1 into EV; (I) PCR amplification of IFITM1 cDNA, (II) enzymatic digestion using KpnI and EcoRV, (III) ligation, and (IV) transformation in DH5α competent cells. (B) Immunoblot testing protein expression of the ectopically transfected SBP-IFITM1 in wt-SiHa cells. SBP panel shows no band for EV (lane 1) and a single band corresponding to tagged SBP-IFITM1 (lane 2). The IFITM1/IFITM3 panel shows a single band for the endogenous IFITM1/IFITM3 in EV (lane 1) as well as SBP-IFITM1 (lane 2). There is an additional band (around 5 kDa higher) corresponding to SBP-IFITM1, only seen in the SBP-IFITM1 transfected cells (lane 2).

4.3.2 Isolation of IFITM1 interacting proteins employing isotopically-labelled peptides

We focused on identifying the IFITM1 interactome to define pathways that function over the IFNγ signal landscape. At first, SILAC pull down methodologies were applied. Wt-SiHa cells were grown in either heavy or light SILAC media supplemented with 10% dialyzed FBS. The media used were RPMI-K6R6 (heavy media) and RPMI-R0K0 (light media) from Dundee Cell Products. The heavy media contained a metabolic labelling of L-Arginine and L-Lysine with six carbon-13 atoms (^{13}C) instead of normal carbon-12 atoms (^{12}C). These isotopic amino acids were fully incorporated into the cells after growth in the media over five generations to allow complete isotopic labelling of proteins at lysine and arginine residues. Light media does not have heavy isotopic amino acids and has the same, or similar, composition as standard RPMI media. Nonetheless, it was bought from the same supplier to avoid small differences in batches. Dialyzed FBS does not contain detectable free amino acids thus the cells cannot use the serum as an amino acid source. Standard FBS is not compatible with this assay as it contains free arginine and lysine that could interfere with the protein quantification; incorporation of these amino acids would have had a negative impact on the MS analysis (Ong *et al.*, 2002).

Wt-SiHa cells were transfected with EV (used as negative control) and SBP-IFITM1 vector for 24 and 48 hours before harvesting (subsection 2.2.6). Initially, the reciprocal combination was included in the experimental design; both transfections were tried in heavy and light SILAC media to determine optimal conditions. The affinity purification protocol using streptavidin agarose beads was designed to capture SBP-IFITM1 and associated proteins. Immunoblotting showed that less SBP-IFITM1 was pulled down from cells grown in light media, compared to those grown in heavy media (Figure 4.5 B, lanes 3-4 vs 11-12). This poorer affinity purification resulted in unsatisfactory protein identification by MS (data not shown). For this reason, the MS analysis was performed using cells with the SBP-IFITM1 (and associated proteins) grown in heavy media, whilst the transfected EV was expressed in cells grown in light media (Figure 4.5 A). Before proceeding to MS preparation, the pull down samples from cells in both heavy and light media were combined: cells transfected with EV grown in light media and cells transfected with SBP-IFITM1 in heavy media. Consequently, technical variability was decreased as both samples, EV and SBP-IFITM1, were combined prior to MS analysis. After mixing, there were two analytes: one transfected for 24 hours and the other for 48 hours.

MS can distinguish heavy-labelled proteins as they will have two amino acid types isotopically labelled; L-[13C614N4]-Arginine (R6) and L-[13C614N2]-Lysine (K6), giving a higher mass compared to proteins from cells grown in the light media. Heavy labelled peptides will be shifted slightly to the right in the MS chromatogram at the m/z axis in comparison to light labelled peptides. Thus the MS detector can distinguish the incorporation of the heavy carbon (^{13}C), due to the molecular mass difference (Mann, 2006).

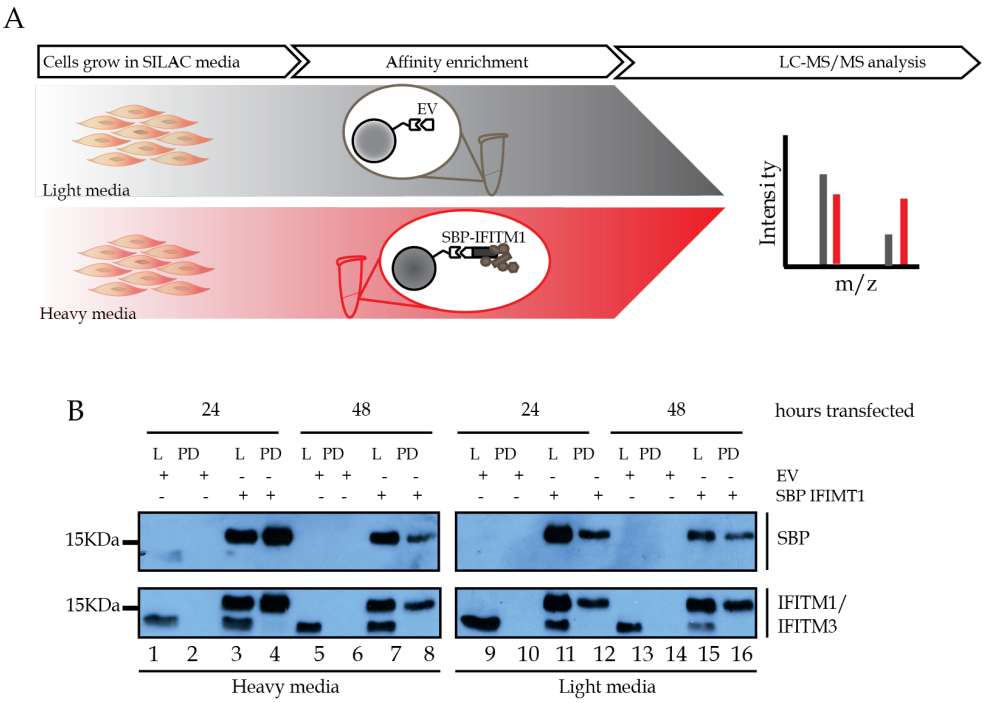

Figure 4.5: SBP-IFITM1 protein enrichment after affinity purification in isotopically labelled wt-SiHa cells. (A) Workflow describing the steps followed to perform isolation of IFITM1 interacting partners in SILAC-labelled wt-SiHa cells. Cells were grown in SILAC media to fully isotopically label all proteins. Cells were transfected with SBP-tagged IFITM1 or EV for 24 and 48 hours and lysates were subjected to pull down by affinity enrichment using streptavidin agarose beads. Eluates were processed and analysed by LC-MS/MS analysis. (B) Immunoblot showing cells transfected with SBP-tagged IFITM1 or EV. Wt-SiHa cells were harvested after 24 and 48 hours following SBP-IFITM1 or EV transfection. Lanes were loaded with lysate (20 μg of protein) [L] and pull down (10% v/v of total elute) [affinity enrichment; PD]. Transfections were performed in cells grown with heavy and light SILAC media with dialyzed serum. Both combinations were used to optimize the pull down of SBP-tagged IFITM1 and to enrich for co-associating proteins.

After elution and sample mixing, preparation was followed by FASP to produce a high-quality peptide, and a C18 column step for desalting and sample concentration was performed to produce MS compatible probes (see section 2.8.2). The high-resolution LC-MS/MS Orbitrap analyser was employed to process the samples thanks to Prof. Lenka Hernychova in the Regional Centre for Applied Molecular Oncology, Masaryk Memorial Cancer Institute, Brno. Samples were analysed by the Orbitrap Elite ETD (Thermo Fisher Scientific) and the data obtained were processed with a Proteome Discoverer 1.4 for protein identification.

Approximately three times more proteins were identified in the 48 hour transfection (1342 proteins) compared to in 24 hour transfection (478 proteins). The output of identified proteins gave a fold change ratio of heavy/light. Interpretation rationale was as follows: in transfected SBP-IFITM1 samples there were proteins at high intensity that were either absent, or at very low intensity, in the transfected EV samples. This is the principle for distinguishing specific SBP-IFITM1 interacting partners from non-specific interacting

proteins. The higher the ratio, the more specific the interaction.

IFITM was dominantly enriched in both 24 and 48 hour time points following processing in the SILAC workflow; this formed an internal positive control, providing confidence that the method was able to enrich the bait protein. The same single peptide (MVGDVTGAQAYASTAK) was identified for IFITM in both conditions; it was enriched in samples transfected with the bait (heavy) in comparison to the control (light). This peptide corresponds to an amino acid region shared with IFITM1 and other two isoforms, IFITM2 and IFITM3, however, we speculate that it belongs to the ectopically transfected SBP-IFITM1. Fold-change ratio was measured, comparing ion intensities from heavy and light inputs (Figure 4.6).

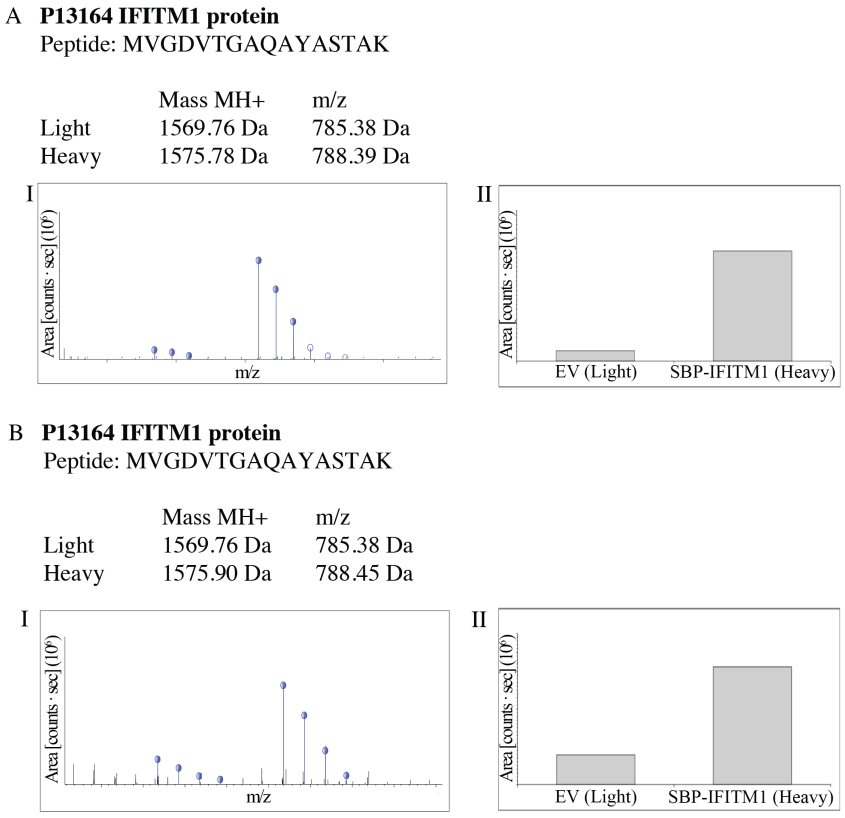

Figure 4.6: IFITM1 annotated ion product for the MVGDVTGAQAYASTAK peptide identified in the two replicates. (I) IFITM1 MS/MS spectrum from the spectral library. There is a Δ6 Da shift to the right for heavy peptides. (II) The quantification channel values plot for precursor ion quantification displays the relative peak area for EV in light isotope and SBP-IFITM1 in heavy isotope labels. The x-axis displays the quantification channel and the y-axis displays the detected area of the selected protein for the given quantification channel defined by counts x seconds. (A) Corresponds to 24 hours after transfection and there is 10.586 times increase in heavy vs light peptide. (B) Corresponds to 48 hours after transfection and there is 3.970 times increase in heavy vs light peptide.

The overall protein enrichment was reduced 48 hours post-transfection, including the SPB-IFITM1 used as a bait. Therefore, we focused on interacting proteins identified 24

hours post-transfection. Taking the top 5% of proteins that had the largest fold change (heavy/light), the most common targets identified were the splicing regulatory factors within the SRSF superfamily of serine–arginine-rich splicing factors (Table 4.1) (Das & Krainer, 2014). As with IFITM, SRSF1 peptides were also enriched in heavy over light samples; which was also the case for other SRSF family members (Figure 4.7). By contrast, taking tubulin as an internal control for normalization there was a very similar intensity for the tubulin peptide peaks between both, heavy and light samples (data not shown). SRSF peptides identified were manually checked to determine if they were unique for the specific isoform (Figure 4.7).

Other proteins detected in SBP-IFITM1 complexes commonly identified in 24 or 48 hour time points might be important in IFITM1 signalling. Nevertheless, we focused on validating SRSF interactions with IFITM1 to define the intracellular location of this protein–protein interaction and to evolve models of how IFITM1 might affect signal transduction.

Table 4.1: Main proteins identified using SILAC media coupled to Orbitrap. Table with selected binding proteins and fold change (Fch) ratios SBP-IFITM1/EV detected by MS for SBP-IFITM1 enrichment 24 and 48 hours post-transfection (from Table B.2)

Accession number	Protein name	Fch 24 h	Fch 48 h
Q01130	Serine/arginine-rich splicing factor 2	12.056	0.428
P13164	**Interferon-induced transmembrane protein**	**10.586**	**3.970**
P53999	Activated RNA polymerase II transcriptional coactivator p15	8.211	0.294
P19338	Nucleolin	5.599	0.370
Q01105	Protein SET	4.228	0.170
Q13247	Serine/arginine-rich splicing factor 6	3.752	0.435
Q96EP5	DAZ-associated protein 1	3.466	0.278
Q9P035	Very-long-chain (3R)-3-hydroxyacyl-[acyl-carrier protein] dehydratase 3	2.789	1.206
Q92945	Far upstream element-binding protein 2	2.710	0.183
P06748	Nucleophosmin	2.127	0.222
Q9BVC6	Transmembrane protein 109	2.022	0.112
Q07955	Serine/arginine-rich splicing factor 1	1.977	0.568
Q9Y2W1	Thyroid hormone receptor-associated protein 3	1.950	0.452
P84103	Serine/arginine-rich splicing factor 3	1.860	0.380
Q9BUJ2	Heterogeneous nuclear ribonucleoprotein U-like protein 1	1.500	0.193
Q01081	Splicing factor U2AF 35 kDa subunit	1.024	0.172
P57088	Transmembrane protein 33	0.978	0.157

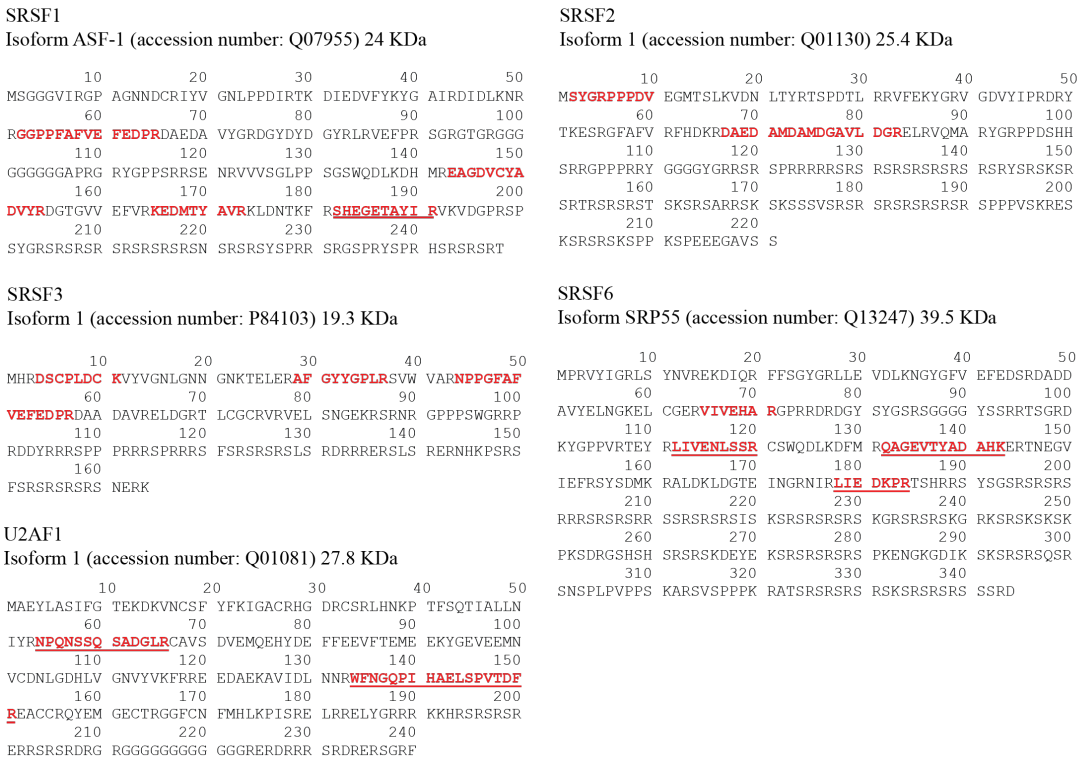

Figure 4.7: Identified SRSF proteins using SILAC media coupled to Orbitrap. Heavy isotopically labelled tryptic peptides identified from the SBP-IFITM1 affinity enrichment are highlighted in red for the SRSF family of proteins (SRSF1, SRSF2, SRSF3, SRSF6 and U2AF1). Underlined unique peptides confirm that these proteins are SRSF isoforms that shuttle between the cytoplasm and nucleus. SRSF2 is not considered a nuclear to cytoplasmic shuttled protein, however it has its C-terminal enriched in arginine and serine

4.3.3 Study of IFITM1/IFITM3 implications on SRSF1

Considering all the candidate proteins identified by SILAC-MS, we focused on the SRSF family. Out of the five SRSF proteins identified by MS analysis, SRSF1 was selected for validation as this is the best-studied isoform. First, we interrogate whether there was a direct interaction, or very close association, between IFITM1/IFITM3 and SRSF1 proteins. Even though the IFITM1 is the isoform related to cancer, it is possible that IFITM1/IFITM3 cooperate together and so focusing on one isoform only will not give the full picture of what is occurring at cellular level. For this reason, we began studying both isoforms simultaneously. Must be borne in mind that the IFITM1/IFITM3 antibody is not able to recognize IFITM2 isoform (Figure 3.11 C). Moreover, the specific antibody against IFITM2 did not identify IFITM2 expression, not even after IFNγ stimulation (Figure 3.11 C, lane 1 and 2). In that sense, IFITM2:SRSF1 interaction will not be evaluated.

To assess the interactions, *in situ* proximity ligation assays (PLA) were performed (Figure 4.8). This is an emerging methodology that assesses the interaction between two endogenously expressed proteins in fixed cells. It can recognize a protein–protein association with less than 30–40 nm separation and can detect endogenous proteins

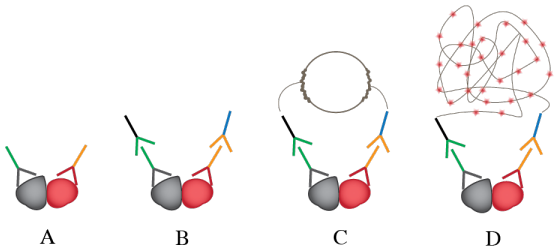

Figure 4.8: Principle of proximity ligation assay. (A) Binding of the specific primary antibodies (of different species) to the proteins of interest (i.e. mouse anti-IFITM1/IFITM3 and rabbit anti-SRSF1). (B) Binding of the secondary antibody, named as probe MINUS (mouse) and PLUS (rabbit). (C) Proteins closer than 30–40 nm will allow oligos to hybridize and amplify by rolling circular amplification. (D) Further amplification and increase of the signal by adding a fluorophore labelled probe.

in situ without relying on transfected or artificially tagged protein vectors (Koos *et al.*, 2014). Taking advantage of this method, we identified endogenous interaction between IFITM1/IFITM3:SRSF1.

In brief, PLA principle relies on the addition of two secondary antibodies with species-specific binding to the primary antibodies (Figure 4.8 A and B); in this case a mouse anti-IFITM1/IFITM3 antibody and rabbit anti-SRSF1 antibody. The secondary antibodies have unique DNA strands that will be used for hybridization in further steps when complementary oligonucleotides are added. Only when the two proteins of interest are in close proximity is sufficient to create a circular ssDNA molecule in the presence of a ligase, forming a template for the DNA polymerase (Figure 4.8 C). In the final steps, a fluorescently labelled probe is added to bind to the circular ssDNA to produce the signal that is visualised as a distinct spot under the microscope (Figure 4.8 D). This is a quantitative technique where the fluorescent signal is proportional to the protein–protein association.

Wt-SiHa cells and *IFITM1/IFITM3* double null cells were used to validate IFITM1/IFITM3:SRSF1 interaction. Four different conditions were set up: single antibody (IFITM1/IFITM3 or SRSF1 antibodies) was used to determine the background of non-specific signal, and cells without IFNγ stimulation to see the baseline signal in comparison with IFNγ-stimulated cells. Cells were stimulated with IFNγ for 24 hours. A 0–72 hour time course experiment showed major induction of IFITM1/IFITM3 protein expression after 24 hours with IFNγ (Figure A.3 B, lane 10). This time point was consistent over replicates, thus 24 hours of IFNγ stimulation was chosen.

The results show a very low autofluorescence signal in the controls (Figure 4.9 A and B), when using a single antibody only, suggesting that the signal is only produced in combination of both antibodies. A similar signal intensity is found in the absence of IFNγ stimulation (Figure 4.9 C), whereas wt-SiHa cells stimulated with IFNγ revealed a substantial signal increase (Figure 4.9 D). This outcome was confirmed by quantification of number of foci per cell in at least 50 cells, in three independent experiments (Figure 4.9 I). Each experiment had two biological replicates. To assess primary antibody specificity, the ex-

periment was also performed in parallel with *IFITM1/IFITM3* double null cells. In this case, there was only background signal for all the conditions, including IFNγ stimulated cells (Figure 4.9 E-H). Quantification of foci per cell signal confirmed the result (Figure 4.9 J).

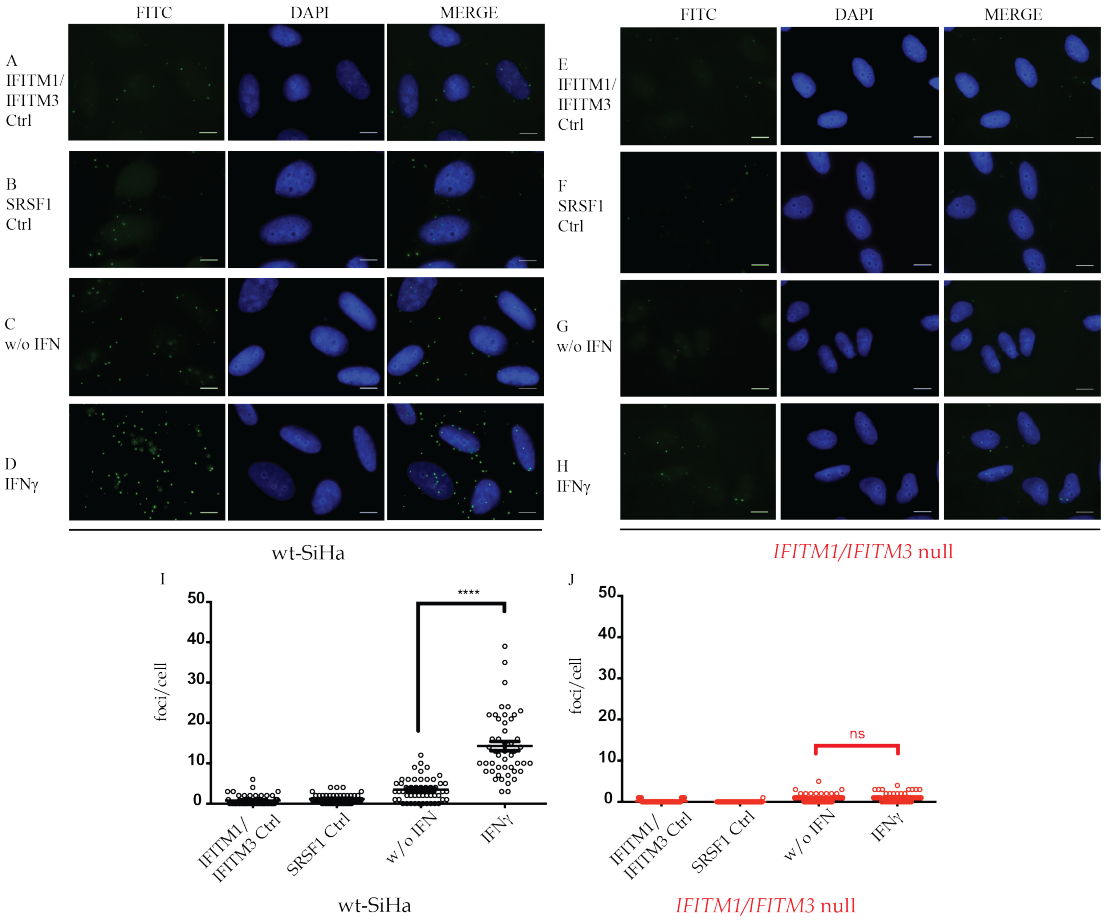

Figure 4.9: Evaluation of the IFITM1/IFITM3:SRSF1 protein–protein interaction *in situ* after stimulation with IFNγ by PLA. Proximity ligation assay was used to study the endogenous interaction between SRSF1 and IFITM1/IFITM3 proteins in wt-SiHa (A-D) and *IFITM1/IFITM3* double null cells (E-H) FITC images identify the protein–protein association foci (depicted in green) and DAPI was used for nuclear staining (depicted in blue) (A–B and E–F). Cells were incubated as negative controls using IFITM1/IFITM3 or SRSF1 antibodies only. Cells were incubated with both IFITM1/IFITM3 and SRSF1 antibodies to define protein–protein foci in non-stimulated cells (C and G). Cells were incubated with both IFITM1 and SRSF1 antibodies to define protein–protein foci in IFNγ-stimulated cells (D and H). Representative quantification of the protein–protein interaction foci per cell in presence or absence of IFNγ stimulation in wt-SiHa (I) and *IFITM1/IFITM3* double null (J). At least 50 cells were counted for each condition. Statistical study was performed with one-way ANOVA and Bonferroni correction (****$p < 0.0001$; ns, not significant). n=3. Scale bar: 10 μm.

To further validate SRSF1 association to IFITM1/IFITM3, an experiment based on immunofluorescent colocalization was designed. Initially, a small interfering RNA approach to deplete the levels of SRSF1 was tested, but SRSF1 protein levels did not decrease satisfactorily (data not shown). Instead, an assay was designed using ectopically transfected

SRSF1 with N-terminus T7-tagged peptide. Even though exogenously expressed forms of the protein may alter protein interactions, we aimed to confirm the protein–protein association using an alternative antibody. The pCG T7-SF2/ASF vector (henceforth T7-SRSF1) was kindly provided by Dr Magda Maslon in Dr Cáceres group (Cáceres *et al.*, 1997). Prior to its use, T7-SRSF1 was sequenced confirming it had the epitope T7 at N-terminal in frame with the SRF1 sequence.

Figure 4.10 A–E is a representative image of the immunofluorescence assay performed using three channels: IFITM1/IFITM3 (red channel), SRSF1 (green channel) and DAPI (blue channel) was used for nuclei staining. Overlapping red and green channels would show yellow signal suggesting IFITM1/IFITM3:T7-SRSF1 colocalization as shown in Figure 4.10 A and B.

IFITM1/IFITM3 are transmembrane proteins but they can also be internalised inside the cells under certain stimulus (Weston *et al.*, 2014). In this case, they are distributed throughout the cell and not particularly abundant in the cell membrane. Fixation with 4% paraformaldehyde may produce a cryptic epitope in the cell membrane and so the primary antibody is unable to recognize the IFITM1 and IFITM3 proteins. However, fixation with acetone:methanol (1:1) (data not shown) is able to reveal a better cell membrane staining of these proteins. In the case of SRSF1, it is mainly located in the cell nucleus (Figure 4.10 E) but, remarkably, it is also present in the cytoplasm. This isoform is able to translocate to the cytoplasm under particular circumstances (Das & Krainer, 2014) and this assay provides supporting evidence of this event.

Nonetheless, the focus of this experiment was to determine the interaction between IFITM1/IFITM3:SRSF1. In this respect, several yellow spots can be seen, corresponding to protein–protein interaction, mainly accumulated around the nucleus (Figure 4.10 B). One could speculate that at least some of them may be located at the inner nuclear compartments, but visualization using confocal microscopy was not conclusive. At this point it can only be confirmed that IFITM1/IFITM3:SRSF1 do interact in the wt-SiHa cell model.

We next examined the possible cellular redistribution of SRSF1 in presence of IFITM1/IFITM3-IFNγ stimulation compared to non-stimulated cells (Figure 4.11). Initially, we investigated whether there was any global difference in SRSF1 between wt-SiHa and *IFITM1/IFITM3* double null cells. Figure 4.11 A shows that expression of SRSF1 in wild type and null cells remains very similar.

Of note, there are two SRSF1 isoforms; isoform ASF-1 (identifier: Q07955-1) of expected 24 kDa, and isoform ASF-2 (identifier: Q07955-2) of expected 30 kDa. The major difference between them is that the isoform ASF-1 is enriched with arginine and serine residues at its C-terminus and so is predicted to be in the cytoplasm, apart from its canonical nuclear location. The SRSF1 antibody is able to recognize both isoforms, showing a double band in blots (Figure 4.11, SRSF1 long exposure panel). The lower panel corresponds to IFITM1/IFITM3 and it was included to monitor the expression of IFITM1/IFITM3 proteins as a control.

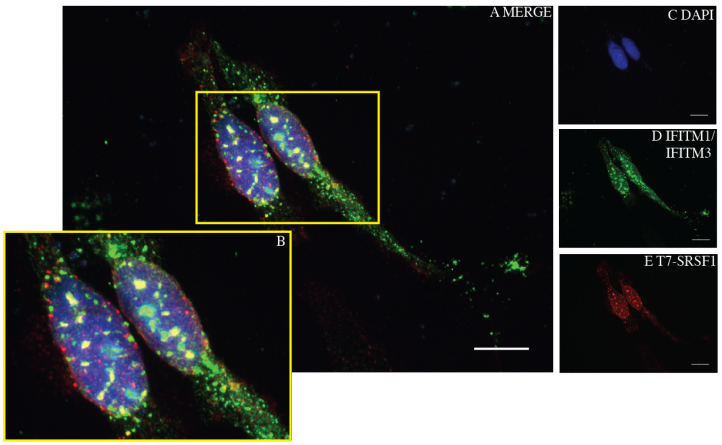

Figure 4.10: Evaluation of the IFITM1/IFITM3:SRSF1 protein–protein colocalization by immunofluorescence. Wt-SiHa cells were transfected with T7-SRSF1 for 24 hours. Immunofluorescence assay performed to assess the interaction between IFITM1/IFITM3:T7-SRSF1. Cells were fixed with 4% paraformaldehyde. (A) Merge channel, (B) ROI from (A) highlighting the overlapping channels, (C) DAPI, (D) endogenous IFITM1/IFITM3, (E) ectopically transfected T7-SRSF1. Scale bar 10 μm.

Subsequently, a cell fractionation assay was performed to determine if SRSF1 subcellular location was modulated by IFITM1/IFITM3. Coomassie blue staining was performed in parallel to the blots to show global protein loading. The total protein amount in cellular compartments, as well as buffer volume, are not the same and this is reflected between lanes (Figure 4.11 B I). Even so, similar protein amounts were loaded in the same fraction across the different samples/conditions: cytoplasmic (lanes 1, 6, 11, and 16), membrane (lanes 2 , 7, 12, and 17), nuclear (lanes 3, 8, 13, and 18), nuclear chromatin bound (lanes 4, 9, 14, and 19), and cytoplasmic (lanes 5, 10, 15, and 20).

Simultaneously, IFITM1/IFITM3 subcellular distribution was studied (Figure 4.11 B II, IFITM1/IFITM3 panel). As expected, IFITM1/IFITM3 are mainly located in the membrane fraction, increasing after IFNγ stimulation (Figure 4.11 B II, IFITM1/IFITM3 panel, lanes 2 and 12). This feature was consistent across replicates. Importantly, there is a clear increase of IFITM1/IFITM3 in the nuclear fraction obtained after IFNγ stimulation. It cannot be concluded if it is in the inner or the outer nuclear side but, nonetheless, it is interesting to observe a change in IFITM1/IFITM3 location produced by IFNγ signalling. Additionally, there is no trace of IFITM1/IFITM3 expression in *IFITM1/IFITM3* double null cells, not even after IFNγ stimulation (Figure 4.11 B II, lanes 6–10 and 16–20), confirming the knock out.

According to the supplier, this assay is limited by an established 15% cross-contamination between fractions. In that sense, it should be seen as a chemical separation rather than purely cell fractionation. Nonetheless, HSP90 (Figure 4.11 B II, HSP90 panel) for cytoplasmic fraction and H3 (Figure 4.11 B II, H3 panel) for nuclear fraction were additionally blotted as internal controls.

This first approach using SILAC identified SRSF proteins as major IFITM1 protein in-

teracting candidates, and this is found to be true association after SRSF1 validation. Even so, the confidence of detection was very poor and so we evaluated the IFITM1 interactome by employing an alternative MS method.

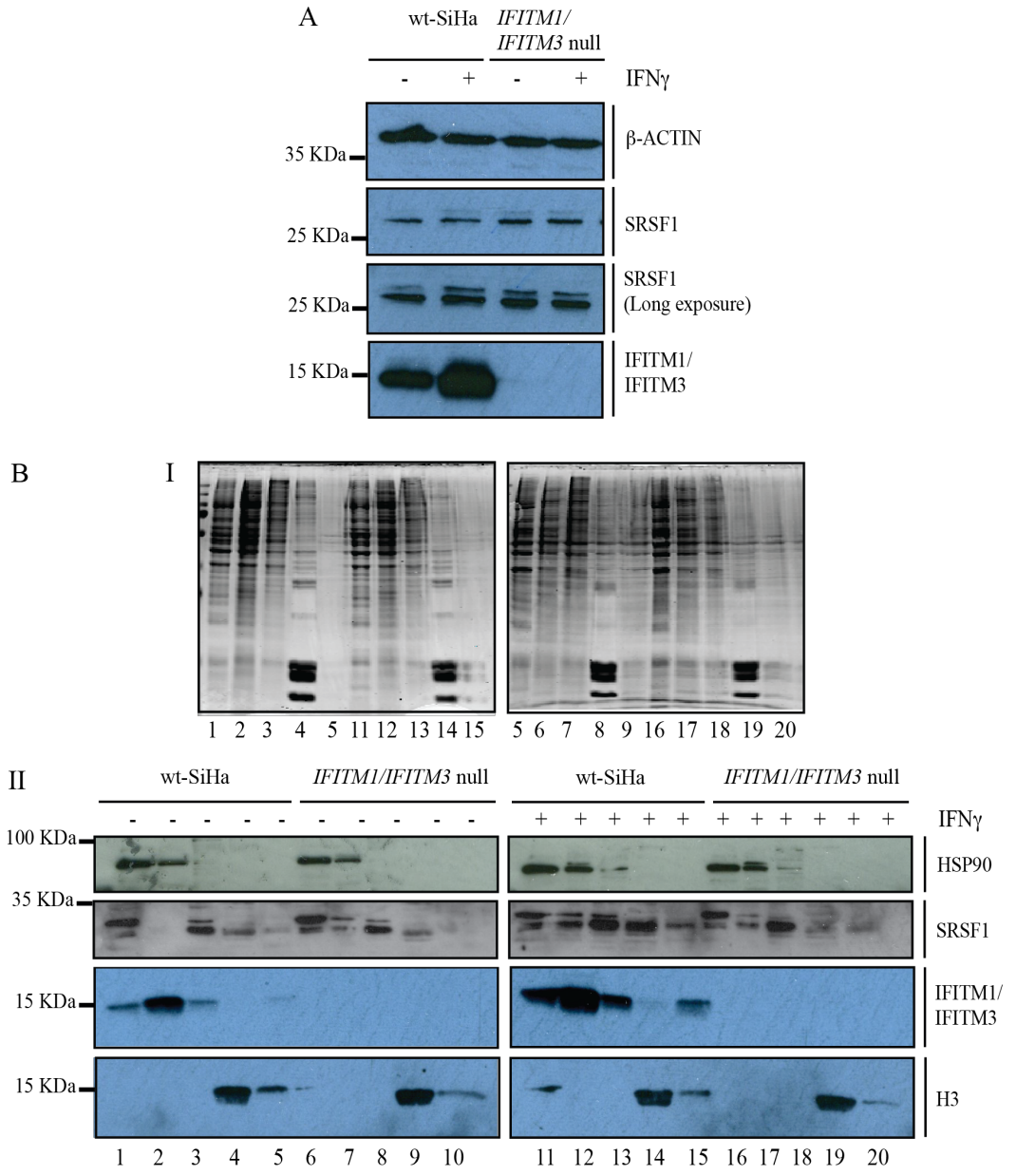

Figure 4.11: Evaluation of SRSF1 protein expression in wt-SiHa and *IFITM1/IFITM3* double null cells. (A) Immunoblots examining the endogenous levels of SRSF1 protein in wt-SiHa or *IFITM1/IFITM3* double null cells in presence or absence of IFNγ. (B) Subcellular fractionation assay with wt-SiHa or *IFITM1/IFITM3* double null cells was performed. (I) Coomassie gel of the fractions to define the distribution of dominant proteins as a loading control. (II) Immunoblot shows subcellular distribution of SRSF1 and IFITM1/IFITM3; Histone-3 (nuclear fraction) and HSP90 (cytoplasmic fraction) were used as a specific fractionation loading controls. After cellular fractionation the following fractions were obtained; cytoplasmic (lanes 1, 6, 11, and 16), membrane (lanes 2, 7, 12, and 17), nuclear (lanes 3, 8, 13, and 18), nuclear-chromatin bound (lanes 4, 9, 14, and 19), and cytoplasmic (lanes 5, 10, 15, and 20).

4.3.4 Isolation of IFITM1 interacting proteins employing label-free peptides

We employed label-free MS to see if this gave a similar dominant protein interactome signature as that obtained by SILAC – thus comparing the two methods. The experimental design was same as that followed in subsection 4.3.2 but this time wt-SiHa cells were grown in label-free media and samples were not combined prior to SWATH-MS analysis (Figure 4.12 A).

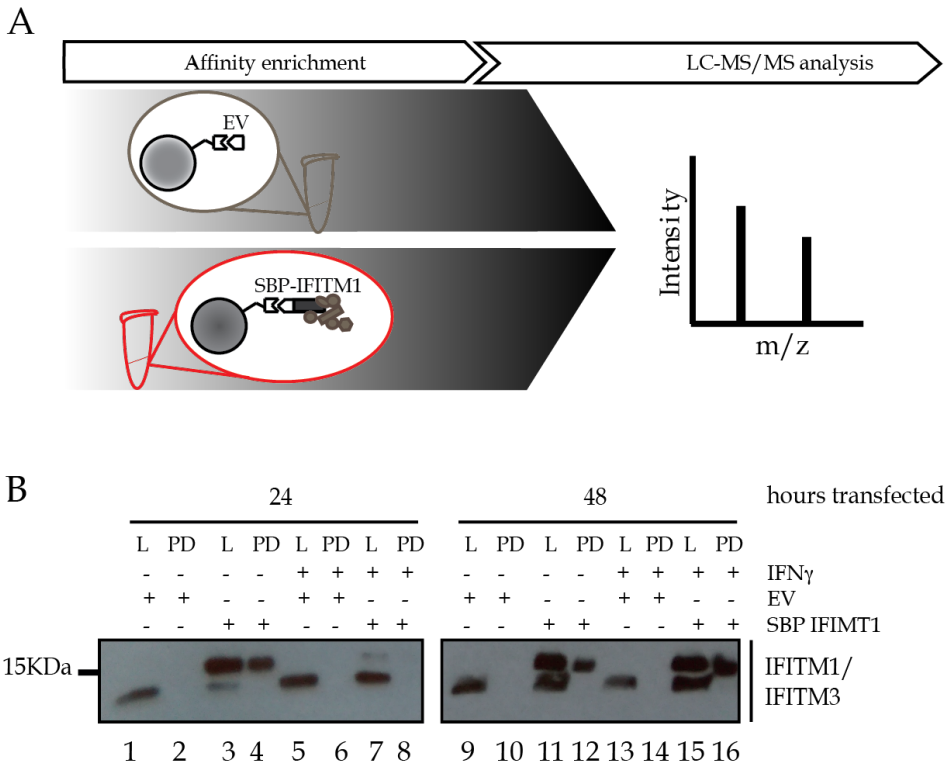

Figure 4.12: SBP-IFITM1 protein enrichment after affinity purification in label-free wt-SiHa cells. (A) Workflow describing the steps followed to perform isolation of IFITM1 interacting partners in wt-SiHa cells grown in label-free media. Cells were grown in RPMI and transfected with SBP-tagged IFITM1 or EV for 24 and 48 hours, non-stimulated and stimulated with IFNγ for 24 hours. The lysates were subjected to IFITM1 pull down by affinity enrichment using streptavidin agarose beads and the eluates were processed and analysed by LC-MS/MS analysis. (B) Immunoblot showing cells transfected with SBP-tagged IFITM1 or EV. Cells were harvested after 24 and 48 hours following SBP-IFITM1 or EV transfection. Lanes were loaded with lysate (20 μg of protein) [L] and pull down (10% v/v of total elute) [i.e. affinity enrichment; PD]. Transfections were performed in cells grown in label-free media. Using normal media with optimized serum to stimulate cell growth, the maximum IFITM1 protein enrichment was observed in 24 hour IFNγ-stimulated cells at the 48 hour post-transfection time point (lane 16) vs the 24 hour post-transfection time point (lane 8).

To find out which condition was optimal to study IFITM1 interactome, wt-SiHa cells were transfected with SBP-IFITM1 or EV for 24 hours (Figure 4.12 B, lanes 1–8) and 48 hours (Figure 4.12 B, lanes 9-16). The wt-SiHa cells were non-stimulated (Figure 4.12 B, lanes 1-4 and 9-12) or IFNγ-stimulated for 24 hours (Figure 4.12 B, lanes 5–8 and 13–16). There was no SBP-IFITM1 enrichment when cells were transfected and IFNγ-stimulated for 24

hours (Figure 4.12 B, lane 8 vs lane 16). It was suspected that IFNγ may inhibit the entry of the vector inside the cell as happens with foreign particles or pathogens. In contrast, SBP-IFITM1 transfection for 48 hours in 24 hours IFNγ-stimulated wt-SiHa cells resulted in the most significant affinity purification (Figure 4.12 B, lane 16). Due to technical problems the non-stimulated and 48 hours transfected samples had a non-satisfactory MS analysis (Figure 4.12 B, lanes 9–12). SWATH-MS analysis was performed with the affinity purified material (SBP-IFITM1 vs EV) of 24 hours post-transfection non-stimulated and 48 hours post-transfection stimulated for 24 hours with IFNγ (Figure 4.12 B, lanes 1–4 and 13-16, respectively).

These data highlight the detection of peptides belonging to a homologous sequence for IFITM1/2/3 proteins in absence of IFNγ stimulation (Figure 4.12 B, lanes 1–4) or after IFNγ stimulation (Figure 4.12 B, lanes 13–16). As previously, it was presumed that IFITM1 was the detected isoform, as it was the bait protein, and so it was considered as internal positive control (Figure 4.13 A and B, indicated as IFITM1/2/3). Nevertheless, IFITM1 may also be interacting with IFITM2 or IFITM3. Additionally, VAPA (a co-associated IFITM1/2/3 interacting protein) was non-significantly detected without IFNγ (Figure 4.13 A) whereas it was significantly detected after IFNγ stimulation (Figure 4.13 B and Table 2). It was also considered as internal positive control as its interaction with IFITM1 is further supported in studies performed by Amini-Bavil-Olyaee *et al.* (Amini-Bavil-Olyaee *et al.*, 2013). Remarkably, this result suggests that a low-confidence identified protein can be a real interacting partner.

Overall, there are more SBP-IFITM1 associated proteins with a significant p-value detected in the 48 hour post-transfection time point. This 48 hour post-transfection time point was used to highlight the SBP-IFITM1 associated proteins of interest including proteins related to cell-to-cell communication such as cornifin, galectin-7, desmocolin, JUP, hornerin and desmoglein, as well as interferon responsive proteins such as ISG15 and HLA-B (Table 4.2). A comparison between the enriched proteins identified in non-stimulated and IFNγ-stimulated wt-SiHa cells reveals that the IFITM1 interactome may be further activated after IFNγ stimulation (Figure 4.13 A vs B). We had particular interest in HLA-B and ISG-15 as they are components of the IRDS signature (related to IFNγ signalling) and they are closely associated with immune evasion and restriction of infection, as IFITM1 (Weichselbaum *et al.*, 2008a).

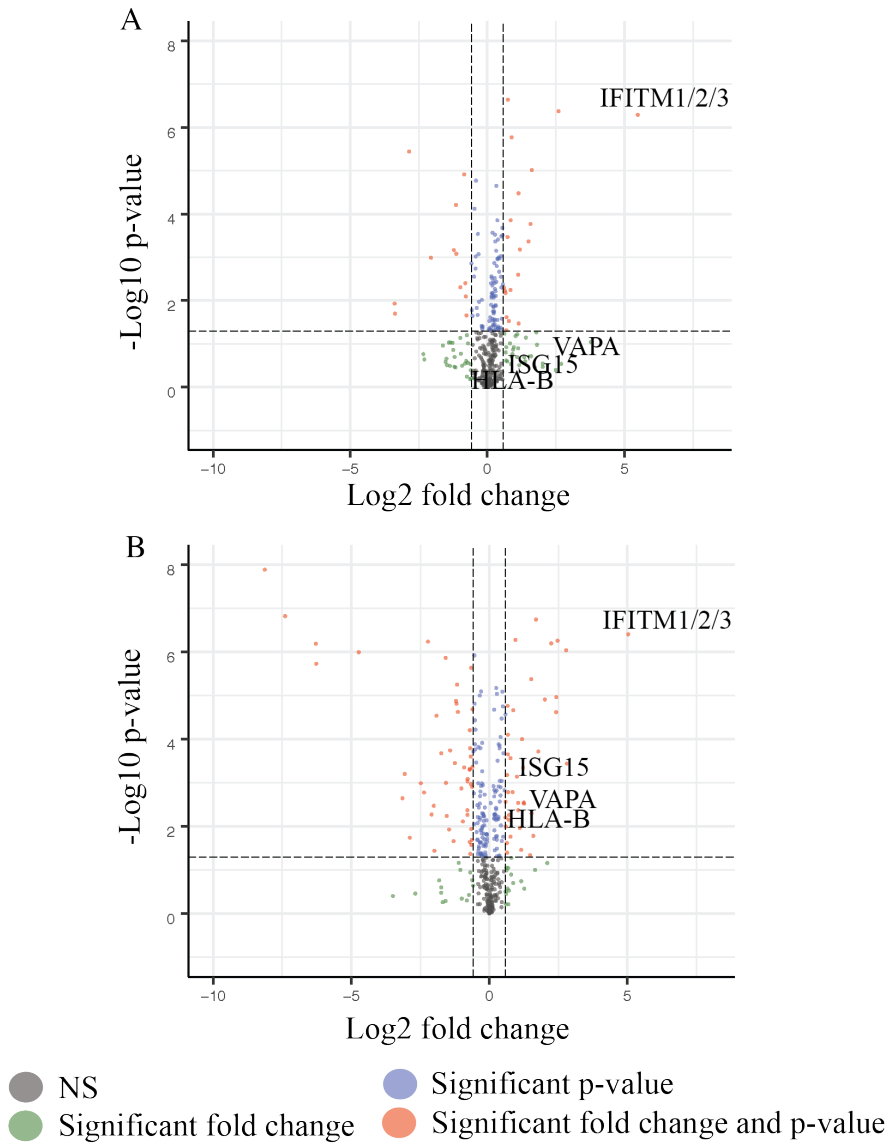

Figure 4.13: Identification of the most dominant SBP-IFITM1 interacting proteins. An affinity purification using streptavidin agarose beads was performed in non-stimulated (A) or IFNγ-stimulated (B) wt-SiHA cells. The wt-SiHa cells were either transfected with SBP-IFITM1 or EV for 24 hours (A) and 48 hours (B). Volcano plot showing the relative quantification for binding proteins by log2 fold change of cells transfected with SBP-IFITM1 versus SBP empty vector in the x-axis and -log10 p-value in the y-axis. IFITM1/2/3 is highlighted as it was used as a bait in this assay, also VAPA which is a well-known IFITM1/2/3 interacting protein. In addition, ISG15 and HLA-B are highlighted as interferon responsive proteins. The analysis was conducted in R and figures were produced using the enhanced volcano, R package version 1.0 (Blighe, 2019). Horizontal dashed lines delimit the fold-change cut-off >1.5 for upregulated and <0.5 for downregulated in the x-axis and vertical dashed line delimits the p-values cut-off <0.05 in the y-axis. Significant values for fold change and p-value are depicted in red, right quadrant as overrepresented and left quadrant as underrepresented proteins. Significant values for fold change are depicted in green. Significant values for p-value are depicted in blue. Non-significant (NS) values are depicted in grey.

Table 4.2: Selected interacting partners identified by MS for SBP-IFITM1 affinity enrichment in wt-SiHa cells stimulated with IFNγ (Figure 4.13 B) (from Table B.3)

Accession number	Protein name	p-value	Fch
E9PS44	**Interferon-induced transmembrane protein**	**3.91E-7**	**32.764**
Q01469	Fatty acid-binding protein, epidermal	1.07E-5	5.380
P22528	Cornifin-B	2.39E-05	5.364
P47929	Galectin-7	1.63E-2	3.023
Q9P0L0	Vesicle-associated membrane protein-associated protein A	5.04E-2	2.890
Q08554	Desmocollin-1	2.98E-3	2.387
P26038	Moesin	2.82E-3	2.375
P14923	Junction plakoglobin	4.5E-4	2.342
Q86YZ3	Hornerin	1.07E-2	2.153
Q02413	Desmoglein-1	2.88E-3	2.070
A0A096LPJ4	Ubiquitin-like protein ISG15	7.20E-4	1.999
Q04826	HLA class I histocompatibility antigen, B-40 alpha chain	7.01E-4	1.628
A0A0A0MTC5	Double-stranded RNA-binding protein Staufen homolog 2	1.00E-3	1.514

4.3.5 Study of IFITM1/IFITM3 implications on HLA-B and ISG15 proteins

Next, we validated ISG15 and HLA-B, two of the top protein candidates identified by SWATH-MS (Figure 4.13 A and B). First, it was tested by affinity purification if these proteins interact directly or form a complex with IFITM1 (Figure 4.14). Protein enrichment by affinity purification using ectopically transfected SBP-IFITM1 in wt-SiHa cells was unable to capture the interaction between IFITM1 with ISG15 or with HLA-B (data not shown). Alternatively, affinity purification was performed using isogenic SBP-IFITM1 SiHa cells generated by CRISPR/Cas9 system by knocking in the SBP tag to the *IFITM1* gene. A genetic study showed that these cells had SBP tag in both alleles of the *IFITM1* gene. Generation of the isogenic SBP-IFITM1 SiHa cell line was performed by Miss Erisa Nita, who kindly provided the cells.

SBP-IFITM1 SiHa cells were either non-stimulated or IFNγ-stimulated for 24 hours (Figure 4.14 A and B, lanes 2 and 3 vs lanes 4 and 5). Streptavidin agarose beads without lysate (Figure 4.14 A and B, lane 1) and wt-SiHa cells transfected with the SBP-tagged empty vector were used as negative controls (Figure 4.14 A and B, lane 6 and 7) which tested any possible non-specific interaction with the streptavidin agarose beads or SPB tag, respectively. At the same time, detection with SBP antibody was used as a positive control (Figure 4.14 A and B, bottom panel). As it can be observed in Figure 4.14 A and B, lane 3 and 5, SBP-IFITM1 is highly enriched after affinity purification whereas negative controls do not show any signal (Figure 4.14 A and B, lanes 1, 6 and 7).

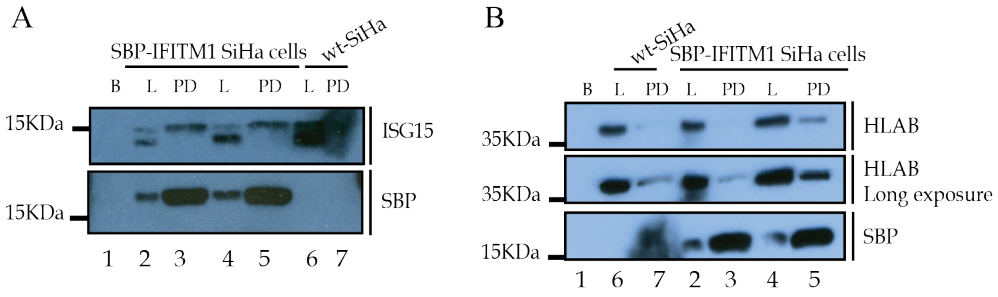

Figure 4.14: SBP-IFITM1 protein enrichment after affinity purification in wt-SiHa cells and isogenic SBP-IFITM1 SiHa cells. Immunoblot showing the pull down using wt-SiHa cells and engineered SBP-IFITM1 knock in by CRISPR/Cas9 technology. Wt-SiHa cells were transfected with SBP-tagged empty vector for 24 hours and SBP-IFITM1 SiHa cells were non-stimulated or stimulated with IFNγ for 24 hours. Lanes were loaded with streptavidin agarose beads [B], lysate (20 μg of protein) [L] and pull down (20% v/v of total elute) [affinity enrichment; PD]. Beads without lysate were carried out in parallel with the rest of the conditions (lane 1), non-stimulated SBP-IFITM1 SiHa cells (lanes 2 and 3), IFNγ-stimulated SBP-IFITM1 SiHa cells (lanes 4 and 5), SBP-tagged empty vector was transfected in wt-SiHa cells (lanes 6 and 7). (A) The upper panel was detected with ISG15 antibody, and the bottom panel was detected with SBP antibody. (B) The upper and middle panel were probed with HLA-B antibody at lower and higher exposure times. The bottom panel was probed with SBP antibody.

ISG15 protein is successfully enriched after affinity purification in the presence and absence of IFNγ stimulation (Figure 4.14 A, top panel, lanes 3 and 5). ISG15 is detected in the lysate of wt-SiHa cells but absent after affinity purification (Figure 4.14 A, top panel, lanes 6 vs 7) and not detected in the negative control with streptavidin agarose beads (Figure 4.14 A, lane 1). Notably, ISG15 shows a double band only observed after the antibody batch was changed, possibly detecting an unspecific protein.

HLA-B protein was also captured after affinity purification in the presence of IFNγ stimulation (Figure 4.14 B, top panel, lane 5). Additionally, HLA-B was very weakly detected, after long exposures, in non-stimulated SBP-IFITM1 SiHa cells (Figure 4.14 B, middle panel, lane 3). However, this could be unspecific binding to SBP tag as a similar signal is seen in wt-SiHa cells transfected with the empty vector containing SBP tag (Figure 4.14 B, middle panel, lane 7). The negative control with streptavidin agarose beads did not show any signal (Figure 4.14 B, top panel, lane 1).

The association of IFITM1/IFITM3:HLA-B was also studied by an alternative method. As previously explained, a PLA assay was designed following the same principle: wt-SiHa and *IFITM1/IFITM3* double null cells, stimulated and non-stimulated with IFNγ. As mentioned, IFITM1/IFITM3 proteins may be cooperating at the molecular level so it was used *IFITM1/IFITM3* double null cells as a negative control. As such, depleting IFITM1 only may not give a very distinct phenotype in comparison to depleting both, IFITM1 and IFITM3. The PLA results only show signal in wt-SiHa cells after IFNγ stimulation (Figure 4.15 H and J vs D and I). This result was obtained in three independent replicates. In fact, it is been previously reported that IFITM3:HLA-B interact using a colocalisation assay

in a different system, i.e IFNγ stimulated melanoma cells (Brem *et al.*, 2003).

It was investigated if IFITM1/IFITM3 could alter protein expression of HLA-B. It was tested if there was any difference in HLA-B protein expression in wt-SiHa compared to in *IFITM1/IFITM3* double null cells by immunofluorescence microscopy. IFNγ-stimulated and non-stimulated cells were also compared. Controls were performed in the absence of HLA-B primary antibody (Figure 4.16 A and D). Three independent experiments were performed, and HLA-B intensity signal was quantified using ImageJ software (version 2.0.0-rc-68/1.52e).

Although there is a basal HLA-B expression in *IFITM1/IFITM3* double null cells, it seems to be non-reactive or very attenuated after IFNγ stimulation, as intensity levels are very similar (Figure 4.16 B and C vs E and F). This observation may not be obvious in Figure 4.16 A–F, but after quantification (Figure 4.16 G and H), there is a more sustained level of HLA-B in *IFITM1/IFITM3* double null cells compared to wt-SiHa cells where it increases after IFNγ stimulation. As other MHC class I molecules also came up in the SWATH-MS screening we decided to address the same question to HLA-A and HLA-C. Similar results were obtained with HLA-A and HLA-C immunofluorescence (data not shown); there was greater induction in the null cells compared to wild type. In further work, we focused on investigating the effects of IFITM1/IFITM3 on HLA-B.

To further corroborate this result, an IFNγ time course was performed; at 0, 2, 6, 24, 48, and 72 hours, to monitor HLA-B protein changes (Figure 4.16 I). Consistently, there is a progressive induction of HLA-B after IFNγ stimulation in wt-SiHa (Figure 4.16 I, lanes 1–6). In contrast, HLA-B remains less induced after IFNγ stimulation in *IFITM1/IFITM3* double null cells (Figure 4.16 I, lanes 7–12). This result was observed in other replicates. Moreover, Dr. Marta Nekulová studied the presence of HLA-B in the cell membrane in wt-SiHa and two different *IFITM1/IFITM3* double null cells arising from two different knock out clones. There was a significantly lower expression of HLA-B on the cell surface in *IFITM1/IFITM3* double null cells (data not shown).

It was investigated whether HLA-B was relocated in an IFITM1/IFITM3-IFNγ-dependent manner. Cells were fractionated to compare cellular distribution of HLA-B in wt-SiHa and *IFITM1/IFITM3* double null cells (Figure 4.16 J). Immunoblotting shows induction of HLA-B after IFNγ stimulation, as already reported (Chang *et al.*, 1992). HLA-B is mainly located in the membrane fraction (Figure 4.16 J II, HLA-B panels, lanes 2, 7, 12 and 17). However, it appears that after IFNγ stimulation HLA-B also goes to the nuclear fraction (Figure 4.16 J II, HLA-B panels, lanes 3, 8, 13, and 18). Small differences were observed in HLA-B location between wt-SiHa and *IFITM1/IFITM3* double null; HLA-B was more extensively present in all the fractions in *IFITM1/IFITM3* double null-IFNγ, but this was not entirely consistent in all replicates.

IFITM1/IFITM3 was also detected by Western blotting to determine its subcellular distribution in wt-SiHa (Figure 4.16, IFITM1/IFITM3 panel, lanes 1–10), as well as to ensure the complete depletion of IFITM1/IFITM3 in *IFITM1/IFITM3* double null cells

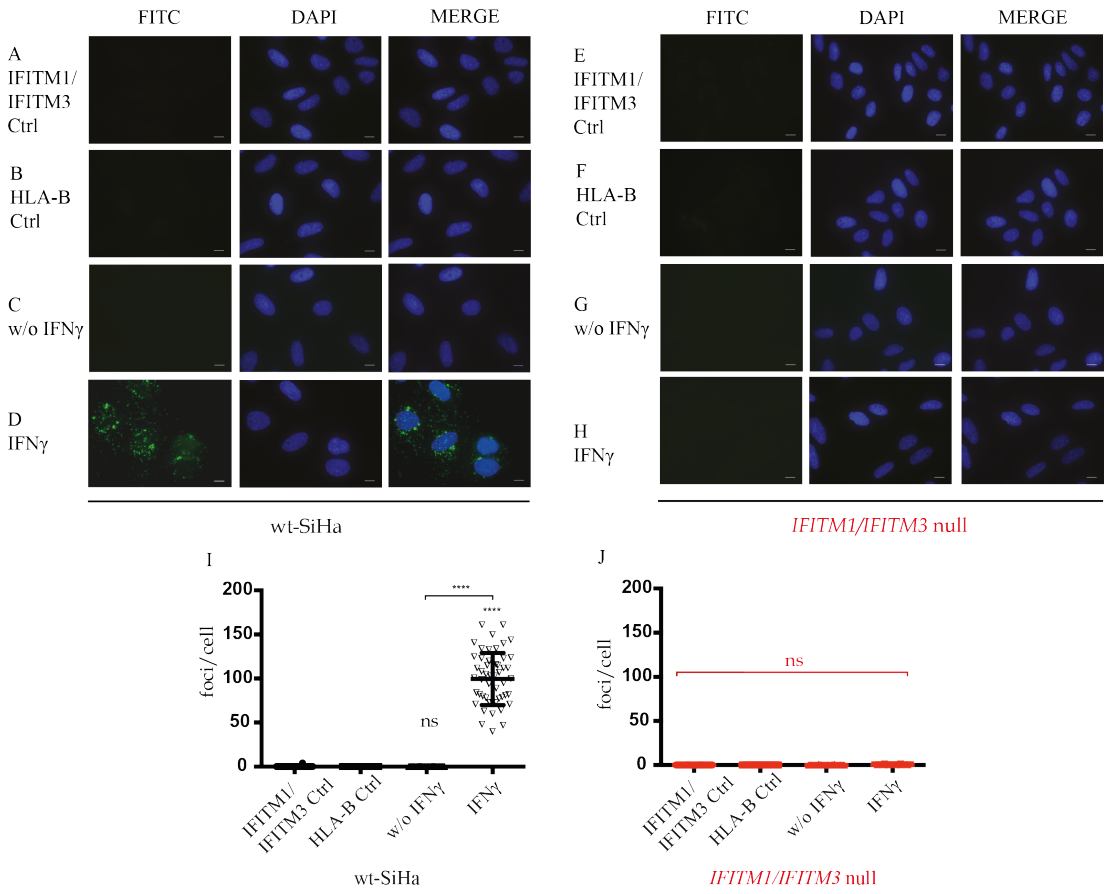

Figure 4.15: Evaluation of the IFITM1/IFITM3:HLA-B protein–protein interaction *in situ* after stimulation with IFNγ by PLA. Proximity ligation assays were used to study the endogenous interaction between IFITM1/IFITM3 and HLA-B proteins in wt-SiHa (A–D) and *IFITM1/IFITM3* double null cells (E–H). FITC images identify the protein–protein association foci (depicted in green) and DAPI was used for nuclear staining (depicted in blue). (A–B and E–F) Cells were incubated as negative controls using IFITM1/IFITM3 or HLA-B antibodies only. (C and G) Cells were incubated with both IFITM1/IFITM3 and HLA-B antibodies to define protein–protein foci in non-stimulated cells. (D and H) Cells were incubated with both IFITM1/IFITM3 and HLA-B antibodies to define protein–protein foci in IFNγ-stimulated cells. Representative quantification of the protein–protein interaction foci per cell in presence or absence of IFNγ stimulation in wt-SiHa (I) and *IFITM1/IFITM3* double null (J). At least 50 cells were counted for each condition. Statistical study was performed with one-way ANOVA and Bonferroni correction (****p < 0.0001; ns, not significant). n=3. Scale bar: 10 μm.

(Figure 4.16, IFITM1/IFITM3 panel, lanes 11–20). IFITM1/IFITM3 are mainly present in the membrane fraction and induced after IFNγ stimulation (Figure 4.16, IFITM1/IFITM3 panel, lanes 2 and 7). This observation was consistent across replicates.

Possible association of IFITM1/IFITM3:ISG15 was studied. A PLA assay was performed to validate the interaction of IFITM1/IFITM3: ISG15 in the presence or absence of IFNγ stimulation, but no signal was identified in any of the cases (data not shown). It was suspected that the ISG15 IgG antibody class was not suitable for PLA Duolink probes. Alternately, ISG15 could be part of a complex interacting indirectly with IFITM1/IFITM3. In that case, PLA is not able to recognise protein–protein associations greater than 40 nm apart.

Presented with this scenario, it was opted to study the ISG15ylation state of the isogenic cervical cell panel: wt-SiHa; *IFITM1* null; *IFITM1/IFITM3* double null cells. The rationale was that if interaction between the proteins could not be detected by PLA or immunoprecipitation, at least we may be able to identify differences in some downstream effects on the global ISG15ylation levels between wt-SiHa and *IFITM1* null and/or IFITM1/IFITM3 double null cells. Although ISG15 synthesis by IFN stimulation is very rapid, ISGylation needs between 18 to 24 hours to be detected (Loeb & Haas, 1992). Actually, it is thought that E1, E2 and E3 enzymes are expressed at much lower levels (Dastur *et al.*, 2006). The pT-Rex-DEST30TM SBP-tagged wild type ISG15, pT-Rex-DEST30TM SBP-tagged mutated ISG15 and empty vector were a gift from Miss Ainhoa González Urionabarrenetxea. Throughout this thesis they will be called SBP-ISG15, SBP-ISG15AA, and EV, respectively. SBP-ISG15AA has a diglycine mutated C-terminus; these mutated residues are responsible for conjugating ISG15 to target proteins and therefore, ISG15ylation will be inhibited in this construct, serving as a negative control.

Cells were transfected with SBP-ISG15 for 48 hours and stimulated with IFNγ for 24 hours. Two experimental approaches were designed: firstly, transfecting cells with EV to enhance ISG15ylation (Figure 4.17) and, secondly transfecting SBP-ISG15 or SBP-ISG15AA constructs (Figure 4.18 A and B, respectively). Additional conditions were included in which null cells were complemented with full-length IFITM1 or IFITM3 constructs; untagged IFITM1 and IFITM3 were added back by transfection to asses if the wild type phenotype could be rescued (Figure 4.18 A, lanes 5, 8, 9, and 10). Prior to this, IFITM3 cDNA was cloned from pCMV-myc-hIFITM3 (Oxford Genetics) to pSF-CMV untagged backbone, following a similar strategy as in section 2.5.5. IFITM1 cDNA was kindly borrowed from the Hupp group.

The initial approach was to maintain the cellular system without major perturbations: ISG15 conjugation was assessed by examining endogenous levels before and after IFNγ stimulation in wt-SiHa and *IFITM1/IFITM3* double null cells (data not shown). Differences were subtle, and it was not possible to determine if the changes were significant. The next strategy was to transfect with EV in IFNγ-stimulated wt-SiHa and *IFITM1/IFITM3* double null cells (Figure 4.17). The mere transfection with EV induces the activation of the

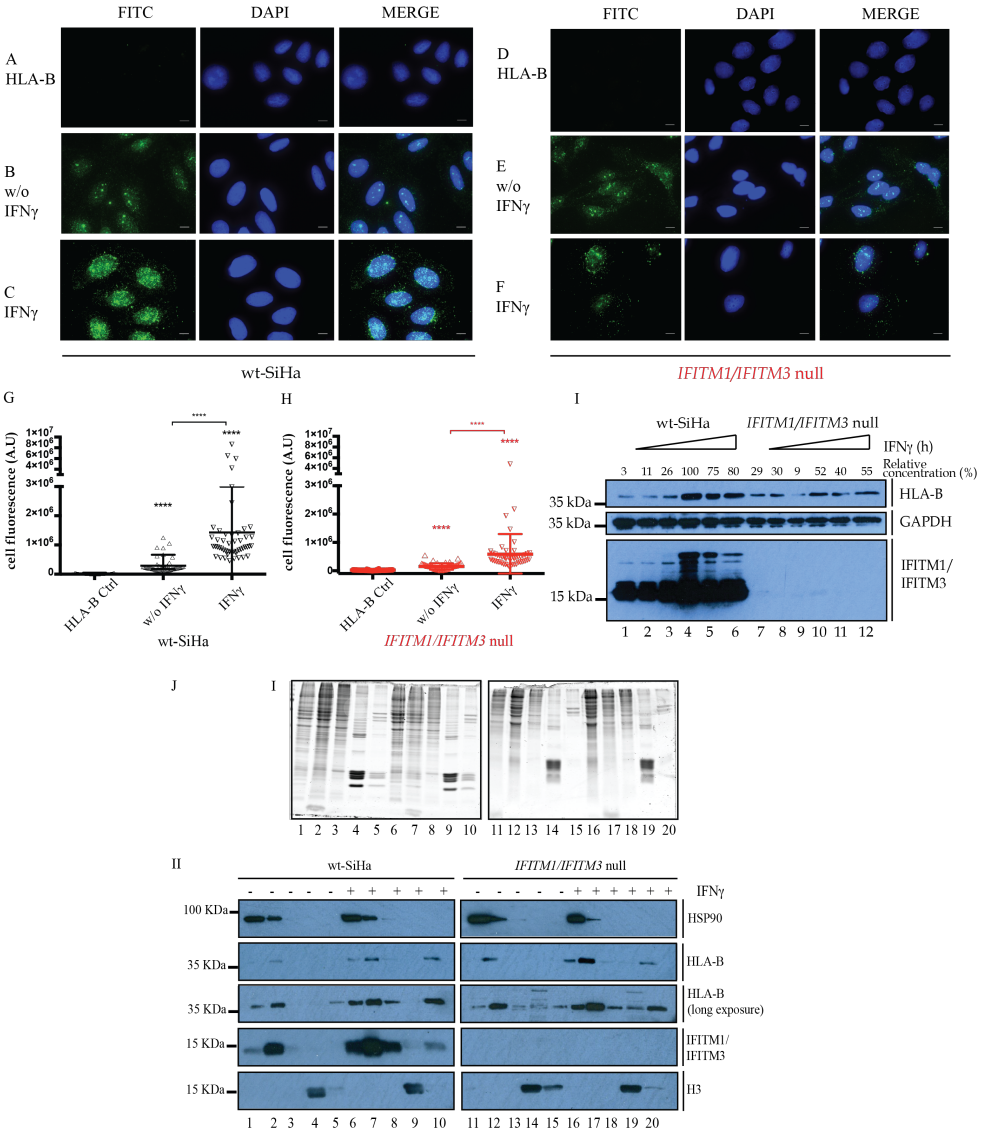

Figure 4.16: Evaluation of HLA-B levels in wt-SiHa and *IFITM1/IFITM3* double null cells. (A-F) SiHa cells were non-stimulated (B and E) or IFNγ-stimulated for 24 hours (C and F) prior to 4% paraformaldehyde fixation. Cells were incubated with HLA-B specific antibody overnight. FITC images identify HLA-B (green) and DAPI was used for nuclear staining (blue). n=3. Scale bar: 10 μm. Representative quantification of HLA-B total fluorescence per cell in presence or absence of IFNγ stimulation in wt-SiHa (G) and *IFITM1/IFITM3* double null cells (H). At least 50 cells were measured in each condition. Statistical study was performed with 1-way ANOVA and Bonferroni correction (****p < 0.0001). (I) A time course of 0, 4, 6, 24, 48, and 72 hours with 100 ng/ml INFγ stimulation in wt-SiHa and *IFITM1/IFITM3* double null cells to measure levels of HLA-B and IFITM1/IFITM3. GAPDH was used as loading control. Relative concentration (%) was measured using Fiji software by taking the higher IFITM1/IFITM3 intensity (lane 4) as 100% intensity, and other lanes were normalised to lane 4 (indicated on top of HLA-B panel). (J) Subcellular fractionation assay in wt-SiHa or *IFITM1/IFITM3* double null cells was performed. (I) Coomassie gel was run to define the distribution of dominant proteins as a loading control. (II) Immunoblot shows subcellular distribution of HLA-B and IFITM1/IFITM3; Histone-3 (nuclear fraction) and HSP90 (cytoplasmic fraction) were used as a specific fractionation loading controls. After cellular fractionation the following fractions were obtained; cytoplasmic (lanes 1, 6, 11, and 16), membrane (lanes 2, 7, 12, and 17), nuclear (lanes 3, 8, 13, and 18), nuclear chromatin-bound (lanes 4, 9, 14, and 19), and cytoplasmic (lanes 5, 10, 15, and 20).

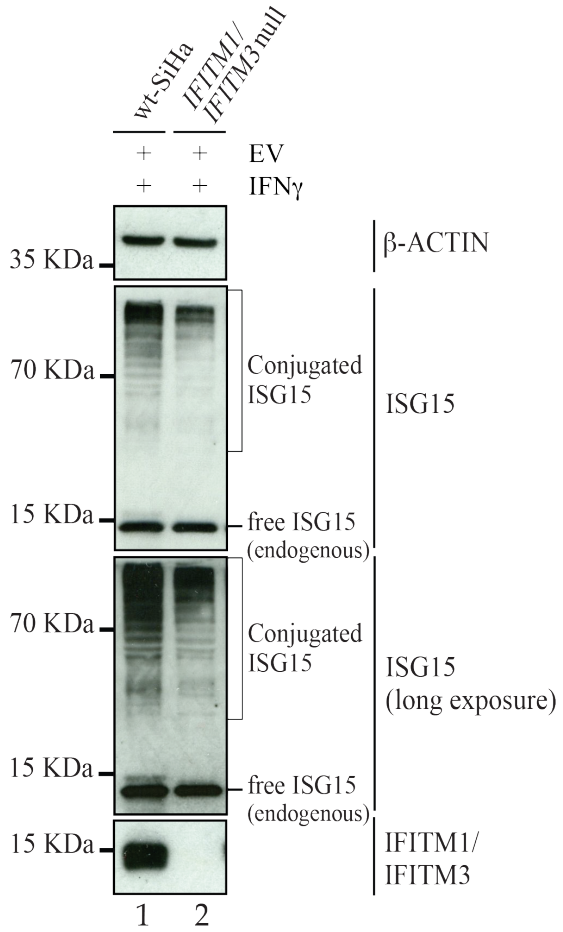

Figure 4.17: Study of endogenous ISG15ylation levels in wt-SiHa and *IFITM1/IFITM3* double null cells. Wt-SiHa cells (lane 1) and *IFITM1/IFITM3* double null (lane 2) cells were transfected with EV for 48 hours and IFNγ-stimulated for 24 hours. Detection of conjugated ISG15 was performed using ISG15 antibody (middle panels). β-ACTIN was used as a loading control (top panel) and IFITM1/IFITM3 antibody determined depletion of IFITM1/IFITM3 proteins (bottom panel).

IFN signalling cascade and *ISG15* is one of the downstream induced genes (Huerfano *et al.*, 2013). On this occasion, there was a clear increase of ISG15ylation in wt-SiHa, compared to *IFITM1/IFITM3* double null cells. There was a 50% reduction of conjugated ISG15 in *IFITM1/IFITM3* double null cells, compared to wt-SiHa, and a similar reduction was observed in replicates. Measurement of the signal intensity was performed using ImageJ software (version 2.0.0-rc-68/1.52e). A loading control with β-ACTIN shows that the protein loading was the same in both cell lines, and detection with IFITM1/IFITM3 antibody shows that IFITM1/IFITM3 proteins are depleted in *IFITM1/IFITM3* double null cells.

Next, it was studied whether ectopic ISG15 leads to the same effect. For this, wt-SiHa, *IFITM1* null, and *IFITM1/IFITM3* double null cells were transfected with tagged SBP-ISG15 (Figure 4.18). The expected molecular weight for ISG15, around 15 kDa, is indicated as free ISG15 (endogenous) in the ISG15 panel (Figure 4.18 A). Additionally, the transfected free ISG15 (SBP-ISG15) is detected 5 kDa above it (Figure 4.18 A, lanes 2, 4, 5, 7, 8, 9, and 10)

and is absent when transfected with EV (Figure 4.18 A, lanes 1, 3, and 6). The ladder at the top of the lane corresponds to the ISG15 conjugated proteins (Figure 4.18 A). Absence of free ISG15 (endogenous) is observed in the SBP panel.

In contrast to the previous experiment (Figure 4.17), ISG15ylation levels in wt-SiHa are lower than in *IFITIM1/IFITM3* double null cells when detected by SBP (Figure 4.18 A, lanes 2 vs 6). Nonetheless, ISG15ylation in wt-SiHa is higher than in *IFITM1* null cells (Figure 4.18 A, lanes 2 vs 4). In addition, ISG15ylation decreases once IFITM1 or IFITM3 (individually) were complemented in *IFITM1/IFITM3* double null cells (Figure 4.18 A, lane 7 vs 8 and 9). Furthermore, ISG15ylation reduction is observed when *IFITM1/IFITM3* double null cells are complemented with IFITM1 and IFITM3 constructs (Figure 4.18 A, lane 1 vs 10). This further supports the suspicion, stated previously, that IFITM1/IFITM3 proteins may be cooperating.

Moreover, complementation of IFITM1 in *IFITM1* null cells does not rescue the ISG15ylation state of wt-SiHa (Figure 4.18 A, lane 5 vs 2). Profound genetic and epigenetic changes in this isogenic cell line or the nature of transfection as well as vector used may interfere in the regulation of conjugated ISG15, consequently no major differences are seen in SBP-ISG15 complemented with EV or IFITM1 (Figure 4.18 A, lane 4 vs 5). Additionally, expression of IFITM1 in rescued *IFITM1* null cells is lower than in wt-SiHA (Figure 4.18 A, IFITM1 panel, lane 5 vs 2). Likewise, deficiencies in posttranslational modification of transfected IFITM3 are also observed (Figure 4.18 A, IFITM3 panel, lane 2 vs 9 and 10). That indicates that the system cannot be completely and fully restored.

Surprisingly, the ISG15 panel did not show similar ISG15ylation. There was a depletion of conjugated ISG15 in *IFITM1* null cells and *IFITM1/IFITM3* double null cells that was not rescued after complementation (Figure 4.18 A, ISG15 panel, lanes 3-5 and lanes 6-10). This correlates with the result observed in Figure 4.17. To shed some light to this observation, mutated SBP-ISG15, indicated as SBP-ISG15AA, was transfected to assess if the SBP antibody was detecting specific conjugated ISG15 proteins (Figure 4.18 B). As predicted, there was a large depletion of global ISGylation of the aberrant SBP-ISG15AA form (Figure 4.18 B, lanes 2 vs 3). Possibly, SBP-ISG15 competes with endogenous ISG15 and, additionally, SBP-ISG15 may have a cryptic peptide not recognised by the ISG15 antibody.

Even though contradictory, these observations were consistent across replicates. At this point it should be noted that both systems, endogenous (Figure 4.17) vs transfected (Figure 4.18), are fundamentally different and should not be compared. We should rely on the outcome in Figure 4.17 as the system remains less manipulated. Nonetheless, the assay in Figure 4.18 A suggests a profound IFITM1/IFITM3 influence on global ISGylation. Moreover, major ISGylation change observed in the absence of IFITM1 or IFITM1/IFITM3 cannot be underestimated. Additionally, complementation by transfection suggests that this effect is due to the action of IFITM1/IFITM3 proteins, and rules out the possibility of it being a CRISPR clone-dependent artifact.

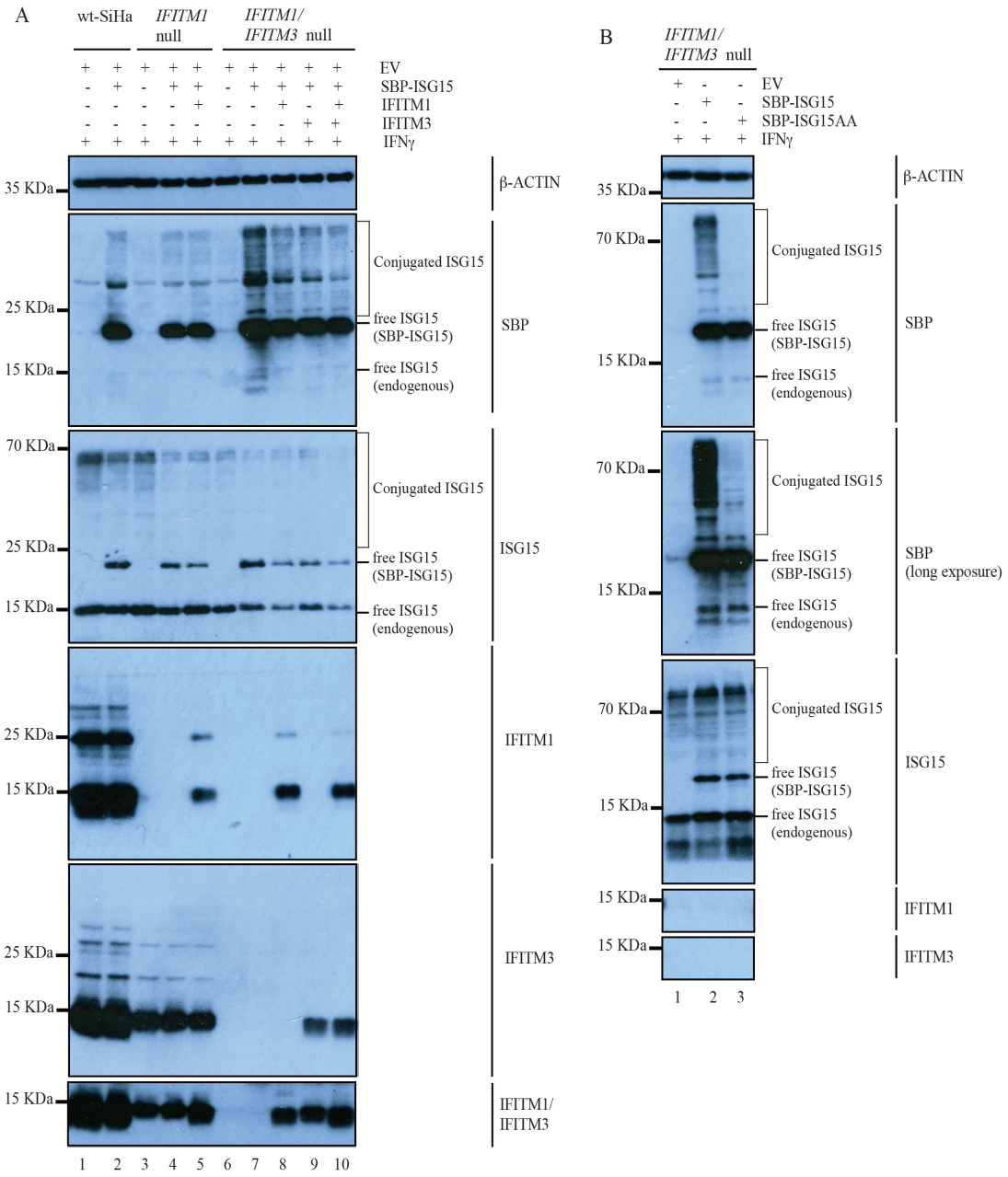

Figure 4.18: Study of exogenous ISG15ylation levels in wt-SiHa, *IFITM1* single null, and *IFITM1/IFITM3* double null cells. (A) Wt-SiHa (lanes 1 and 2), *IFITM1* null (lanes 3-5), and *IFITM1/IFITM3* double null (lanes 6–10) cells were ectopically transfected with tagged SBP-ISG15 and occasionally complemented with full length IFITM1 (lanes 5, 8, and 10) and IFITM3 (lanes 9 and 10) for 48 hours and IFNγ-stimulated for 24 hours. Transfections were carried out with EV to maintain the same total amount of DNA in all conditions. (B) *IFITM1/IFITM3* double null cells were transfected with SBP-ISG15 (lane 2) or mutated SBP-ISG15AA (lane 3). Conjugated and free ISG15 are indicated in SBP and ISG15 panels. Protein loading control is assessed in β-ACTIN panel.

4.4 Discussion

This chapter is entirely dedicated to identifying new proteins associated with IFITM1. For this purpose, affinity purification of SBP-tagged IFITM1 was used to identify enriched proteins using SILAC (subsection 4.3.2) and label free-MS (subsection 4.3.4) approaches in a SiHa cervical cancer cell model.

Firstly, the SILAC methodology was applied. Among the proteins listed, an interesting group of splicing factors, SRSF, was recognised as IFITM1 interacting proteins (Figure 4.7). Splicing is a crucial and complex mechanism that allows generation of protein diversity. Altering this sophisticated system may lead to the production of deleterious splice variants that may impede and/or modify proper protein expression, including the generation of protein variants associated with cancer.

The splicing factor proteins SRSF1, SRSF2, SRSF3, SRSF6 and U2AF were identified in the overlapping top 50 protein candidates at two time points: transfected SBP-IFITM1 for 24 and 48 hours (Table 4.1). These proteins are part of the SR protein family. Its basic structure comprises one or two domains for RNA recognition motifs (RRM) and a C-terminal RS domain of multiple arginine and serine repeats (Long & Caceres, 2009). It is remarkable that most of the isoforms identified in our study have this C-terminal domain enriched in arginine and serine residues (Figure 4.7). These have been classically implicated in alternative splicing and pre-mRNA splicing. In addition to their canonical function, they also have an important role in post-splicing activities. In this regard, some studies show that some SRSF proteins have roles not only involving nuclear splicing but also in processes occurring in the cytoplasm, such as mRNA nuclear export, nonsense-mediated mRNA decay (NMD) and mRNA translation (Das & Krainer, 2014).

SRSF is a family of 12 proteins predominantly located in the nucleus, where six of them (including SRSF1 and SRSF3) shuttle continuously between the nucleus and the cytoplasm to export mRNA out of the nucleus (Cáceres *et al.*, 1998). The presence of some SRSF proteins in the cytoplasm is not well understood. Nonetheless, it is been postulated that SRSF1 (the prototypical SRSF protein) transitions between nucleus and cytoplasm is closely related to its phosphorylation state. Phosphorylation in the RS domain is crucial to initiate export activity; extensive posttranslational phosphorylation of SRSF1 in the nucleus enhances splicing reactions. During splicing it returns to the hypophosphorylated state and is directly transported to the cytoplasm by interaction with the nuclear export factor TAP. Shuttling SRSF proteins are dephosphorylated after splicing and remain associated with spliced mRNA during mRNA export. Repeated SRSF1 dephosphorylation in the cytoplasm produces intermediate phosphorylation states that allow interaction with other proteins until the protein is hypophosphorylated. It is then imported back into the nucleus, interacting with the transportin-SRSF protein and accumulating until the cycle is initiated again (Ding *et al.*, 2006; Huang *et al.*, 2004).

To shed some light on this matter, IFITM1/IFITM3:SRSF1 interaction was validated

by PLA. Remarkably, there was a higher association between IFITM1/IFITM3:SRSF1 after IFNγ stimulation, whereas in absence of IFNγ there was a very low signal, very similar to the background signal obtained in the controls (Figure 4.9). Interestingly, the signal was present mainly in the cytosol suggesting that IFITM1/IFITM3 association with SRSF1 may be implicated in protein synthesis. To provide more corroboration, a colocalization assay was designed to characterize association between ectopically transfected SRSF1 tagged with T7 at its N-terminus with endogenous IFITM1/IFITM3 (Figure 4.10). An overlap between both signals was observed, also located in the cytosol.

To give a wider view of this protein, SRSF1 has been also reported to function in translation and IRES-mediated translation of viral RNA (Bedard *et al.*, 2007). It is been postulated that SRSF1 binds with the cellular RNA binding protein PCBP2 that in turn binds to an IRES sequence within the genomic RNA of particular RNA-viruses and is furthermore required for translation. The new role identified here suggests a new function for SRSF proteins in mediating cap-independent translation initiation (Bedard *et al.*, 2007). This finding links with IFITM1 canonical function as a viral restriction factor. As mentioned previously, IFITM1 is implicated in viral inhibition. Interestingly, most of the viruses described have ssRNA and normally replicate in the cytosol. Taken together, it may be possible that IFITM1 interferes with viral replication, altering the splicing of the virus in the cytosol but also affecting the expression of oncoproteins. During the course of this research, Lee *et al.* proposed that IFITMs are able to interfere in HIV-1 protein synthesis. That finding consolidated our speculation regarding IFITM1 implications in protein translation (Lee *et al.*, 2017). There are further examples in which SRSF proteins modulate viral gene expression, such as herpes simplex virus 1 protein ICP27 interaction with SRSF protein and SRSF protein kinases (responsible of SRSF protein regulation) (Sciabica *et al.*, 2003). In addition, they interact with binding sites that are required for export of un-spliced herpesvirus mRNAs, and influence other viruses such as human rhinovirus and hepatitis A virus.

To further investigate whether IFITM1/IFITM3 could have some additional effect on SRSF1, we looked at the global protein levels for SRSF1 but did not find any major difference between wt-SiHa and *IFITM1/IFITM3* double null cells. We next asked if, instead of altering the total SRSF1 protein amount, it may be influencing its subcellular localization; to answer this we carried out a cell fractionation assay (Figure 4.11). Several replicates of this experiment were performed, and no major difference in SRSF1 subcellular location was identified. Even though minor difference between fractions may be caused by IFITM1/IFITM3, it can also be due to technical variability or small cross-contamination between fractions. In that respect, these results suggest that IFITM1/IFITM3 cooperates with SRSF1 rather than SRSF1 being a downstream effector of IFITM1/IFITM3. Even so, it is remarkable that SRSF1 was also found in the cytoplasmic fraction where it interacts with IFITM1/IFITM3.

Nevertheless, SRSF1 serves as a good example of how low significance proteins identified by MS methodology could have a real biological impact. In summary this is the first

evidence suggesting that IFITM1 may have an active role in protein translation. At that stage we aimed to redefine the biological importance of IFITM1, describing implications of this protein in a novel cellular role.

SWATH-MS was also applied to compare it with Orbitrap-MS methodology. Ideally, we would expect these to identify the same interacting partners, but these instruments are fundamentally different. Initially, we choose SILAC labelling as it allows combining of samples at an early stage and processing them in the same sample mixture, thus minimizing handling errors. The expression of the SBP-IFITM1 construct in cells labelled with light or heavy isotopic amino acids (SILAC media) resulted in the efficient capture of IFITM1 protein. However, a limitation of the SILAC-MS methodology was found as the dialyzed serum used in combination with spiked SILAC compatible amino acids produced pronounced morphological changes in the wt-SiHa cells. Alternatively, it was used a label-free method (SWATH-MS) that included the use of non-dialyzed serum, which maintained normal cell morphology. These effects could have given rise (at least partially) to observed differences in the SiHa cell model proteome, and so impact on the IFITM1 interactome.

Applying label-free methodology, a new interesting set of cell membrane-localized proteins (Table 4.2) were identified, suggesting a role for IFITM1 in cell–cell communication. These proteins were not validated as they were beyond the scope of the current study, although their p-values were more significant in IFNγ-stimulated cells. This might suggest that the interactions are induced by IFNγ and that they are not constitutive. We focused more on the possible significance of the co-association of IFITM1 with some of the classic IFN-inducible proteins, HLA-B and ISG15 (Table 4.2 and subsection 4.3.5).

Results show that IFITM1/IFITM3 are not totally responsible for the HLA-B fate in subcellular compartments. Nonetheless, it may be ventured that it may have some impact on stability, consequently altering the appropriate trafficking of HLA-B and potentially the half-life of this protein. In this regard, 2D-gels were performed by our collaborator Prof. Lenka Hernychova in wt-SiHa and *IFITM1/IFITM3* double null cells (data not shown). There was a shift to the left of HLA-B on comparing *IFITM1/IFITM3* double null cells to wt-SiHa cells, suggesting a deficiency in the integrity of HLA-B in absence of IFITM1/IFITM3 expression. One can speculate that in the absence of IFITIM1/IFITM3 expression, post-translational modification of some residues (i.e. phosphorylation) may be facilitated, increasing protein stability. On taking a close look at HLA-B in *IFITM1/IFITM3* double null cells by immunofluorescence, HLA-B shows aberrant distribution in *IFITM1/IFITM3* double null cells compared to that in wt-SiHa cells (Figure 4.16 A-F).

Disclosing results from chapter 5, IFITM1/IFITM3 may have an active role in HLA-B translation in the presence of IFNγ. If this is true, IFITM1/IFITM3 would not be totally responsible for activating the expression of HLA-B. They would be enhancing HLA-B expression in a very particular circumstance i.e. in the presence of IFNγ stimulation, boosting the antigen presentation machinery. In this respect, affinity purification and the IFITM1/IFITM3: HLA-B proximity ligation assay supports the hypothesis that there is di-

rect interaction between these proteins only after IFNγ stimulation (Figure 4.14 and Figure 4.15). Supporting evidence by an independent study concluded that IFITM3 may be associated with MHC class I molecules, HLA B included, by immunostaining assays. Both proteins colocalized along with CD81 in exosome-like organelles, particularly after IFNγ stimulation (Brem *et al.*, 2003). In turn, CD81 is known to be an IFITM1 interacting partner (Deblandre *et al.*, 1995; Matsumoto *et al.*, 1993; Takahashi *et al.*, 1990) . This matter will be further discussed in chapter 5.

Significant effort was made to identify differences in the ISG15ylation state in wt-SiHa and *IFITM1/IFITM3* double null cells. We aimed to keep the system as endogenous as possible, and cells were only stimulated with IFNγ. That proved not enough to activate the system and thus SiHa cells were additionally transfected with EV to enhance IFNγ signalling activation (Figure 4.17). Under these conditions, a substantial decrease in total ISG15ylation levels in *IFITM1/IFITM3* double null compared to wt-SiHa cells was found. This result suggests that IFITM1 and/or IFITM3 are modulating ISG15 conjugation to target proteins. Nonetheless, it was not determined whether this happened at the protein level, during protein synthesis or at an even earlier stage. To start assessing this, next chapter will study the implication of IFITM1/IFITM3 dependencies on ISG15 protein production.

Another experiment provided conflicting evidence regarding global ISG15 conjugation. In this case cells were transfected with SBP-ISG15 construct for 48 hours and IFNγ-stimulated for 24 hours. The outcome of this experiment was consistent between replicates but here ISG15ylation was considerably higher in *IFITM1/IFITM3* double null cells than in wt-SiHa cells (Figure 4.18 A, lane 2 vs lane 7). More evidence comes from the observation that ISG15ylation is reduced in the presence of IFITM1 or IFITM3 by complementation and this phenotype is more dramatic with the additional loss of the other IFITM (IFITM1 or IFITM3), artificially resembling the wt-SiHa phenotype (Figure 4.18 A). Moreover, SBP-ISG15AA (unable to conjugate ISG15) clearly shows a global inhibition of ISG15ylation (Figure 4.18 B).

What remains consistent between experiments is that IFITM1/IFITM3 directly affects the levels of global ISG15ylation. Nonetheless, results are contradictory and so it is necessary to think about both experimental designs. Transfected SBP-ISG15 will by-pass some steps of natural protein synthesis and additionally it does not provide the usual endogenous regulatory gene induction, and thus the system is over-saturated with enormous amounts of synthetized protein. For these reasons, studying endogenous ISG15 is more reliable (Figure 4.17).

In summary, we took the results from both MS methodologies and focused on validating some interesting IFITM1 interacting partners; SRSF1, HLA-B, and ISG15. Taking everything together, and considering previous work performed in our lab (Figure 3.2), we suspected that IFITM1 could have a major role in modulating some IRDS, the subset of ISG proteins found upregulated in chemoresistant tumours (Cheon *et al.*, 2014; Weichselbaum

et al., 2008a). Furthermore, in this work it is noted that with siRNA depletion of IFITM1 (Figure 3.2), IFITM3 expression was also decreased. Nonetheless, due to high homology it cannot be completely assured that the protein identified was in fact IFITM1. In any case, protein interactions have been studied from the IFITM1 perspective, but it remains unknown if IFITM3 also contributes to IFTIM1 functions. For instance, ISG15 is initially proposed as an interacting partner of IFITM1 by MS (Figure 4.13) but it can be observed that IFITM3 can also play an active role on ISG15ylation by Western blotting (Figure 4.17 and Figure 4.18). This would imply that both proteins have synergetic effects over their effectors. Moreover, association of IFITM1 with SRSF1 may be implicated in mediating mRNA guidance to the ribosome.

All-in-all, it could be argued that IFITM1 (maybe in cooperation with IFITM3) may have an effect on protein production, possibly by altering either trafficking or protein translation. As such, in the upcoming chapter 5, we will concentrate on understanding the impact of the IFITM1 pathway on IFNγ mediation of protein synthesis.

Chapter 5

Analysis of IFITM1/IFITM3 roles in ribosomal integrity and protein synthesis in the SiHa cervical cancer cell model

5.1 Introduction

The cytokine IFNγ is able to induce expression of a wide range of genes, and the aim of this study was to investigate the potential IFITM1/IFITM3-dependent expression of some of these genes. In the last chapter, we showed that IFITM1 could be involved in the process of protein translation. Firstly, we described SRSF1 as a novel interacting partner of IFITM1/IFITM3. This association occurs in the cytoplasm and is significantly increased after IFNγ stimulation (Figure 4.9). An alternative role of the SRSF1 splicing factor relates to guiding of mRNA to the ribosome. Together, these findings highlight the importance of studying protein synthesis. Secondly, two other novel IFITM1 interaction partners, HLA-B and ISG15, were found to be associated with IFITM1/IFITM3 proteins in IFNγ-stimulated wt-SiHa cells. Both proteins are encoded by IRDS genes, which represent a subset of 32 interferon-stimulated genes including IFITM1, but not IFITM3, proteins. The data presented in chapter 4 demonstrated that loss of IFITM1/IFITM3 expression results in alterations in HLA-B protein abundance and globally they also change protein ISG15ylation (subsection 4.3.5).

Thus far, these results have been considered from a proteomic perspective. However, protein synthesis is the final stage of gene expression, which is a highly regulated process influenced at various stages by physiological and/or pathological factors. As such, IFITM1, along with IFITM3, may interact with and regulate ISG15 and HLA-B (and potentially other molecules) at different stages. Nonetheless, previous empirical work has served to focus

attention on translation at the ribosome, one of the core events of protein regulation. We hypothesised that IFITM1, along with IFITM3, may control the protein synthesis of particular ISG genes. To study this possibility, we examined the ribosomal status in wt-SiHa cells and *IFITM1/IFITM3* double null cells after IFNγ stimulation.

5.1.1 Defining the approach applied to study ribosome integrity

Translation is a complex multi-step process which takes place on the ribosome. Ribosomes are composed of two major ribonucleoprotein structures, the 40S and 60S subunits. In brief, the 40S subunit facilitates the appropriate codon-anticodon pairing to determine the correct amino acid sequence while the 60S subunit contains the peptidyl transferase centre which catalyses peptide bond formation in the synthesised peptide (Wilson & Doundna Cate, 2012). Being a fundamental biological process, translation requires the active and precise participation of many proteins, and even subtle defects in the translational machinery can lead to catastrophic effects which may compromise cell health.

Sucrose density gradient ultracentrifugation is a technique that enables the separation of mRNA and ribosomal subfractions. In the present study, this technique was used to investigate the roles of IFITM1/IFITM3 proteins at the ribosome. Polysome profiling was then used to identify and distinguish actively translated mRNAs from those that remain untranslated. Additionally, this technique provides some insights into possible alterations in ribosomal proteins in the absence of IFITM1/IFITM3 protein expression. The assay is based on a sucrose gradient separation of ribosomes and associated mRNAs. Sub-ribosomal fractions (40S, 60S, 80S and polysome) separate based on their sedimentation coefficient along the sucrose gradient in the following order from bottom to top of the gradient: polysome, 80S, 60S, 40S and free mRNAs (Figure 5.2 II). Finally, the sub-ribosomal fractions were analysed by SWATH-MS.

5.1.2 Pulse SILAC, an emergent technique to study protein turnover

The results relating to ribosomal status highlighted the need to investigate whether IFITM1/IFITM3 proteins are involved in the control of protein synthesis. Analysis of the correlation between mRNAs and protein expression levels is challenging. Protein expression and regulation are influenced by many described cell perturbations (including IFNγ signalling). Expressed proteins undergo posttranslational modifications, and degradation rate changes alter their half-life, therefore it is difficult to predict the protein fate. We are particularly interested in the rapid IFITM1/IFITM3-dependent protein expression that occurs in response to IFNγ stimulation, and therefore aimed to explore the capacity of IFITM1/IFITM3 proteins to precisely regulate protein synthesis.

Applying MS methodologies that analysed the whole cell proteome provide little information about the proteins that are being actively translated during IFNγ stimulation. Thus, label-free SWATH-MS and SILAC-Orbitrap-MS (subsection 4.3.4 and subsec-

tion 4.3.2) cannot be used as they measure the accumulated abundance of proteins. An alternative MS approach is therefore required to measure protein abundance in a more dynamic way.

Pulse SILAC is a relatively new MS technique, which allows the measurement of protein turnover. It follows the same principles as conventional SILAC labelling but, in this case, cells are labelled (spiked) with SILAC media for a short period of time. This allows the incorporation of isotopic amino acids only in newly synthesized polypeptides (Figure 5.1). In this experimental approach, the cell proteome is partially labelled (previously translated proteins in light media and new synthesized proteins in heavy media). As in conventional SILAC, protein quantification is determined by the fold-change ratio of heavy/light labelled proteins. Fold-change ratio is a relative measurement, and it is limited by the individual amount of protein present in cells. By applying this methodology it is possible to determine the immediately translated proteins on a global scale (Doherty *et al.*, 2009; Doherty & Beynon, 2006).

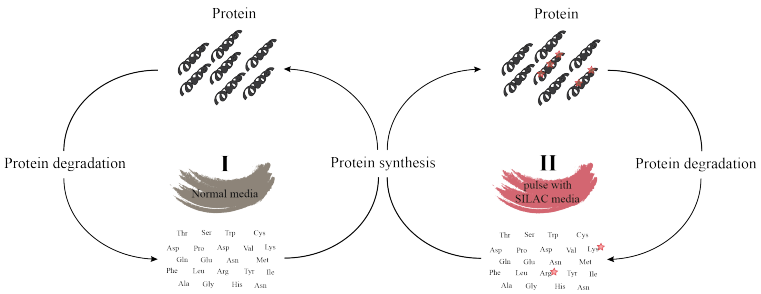

Figure 5.1: Schematic of pulse SILAC principle for measuring protein turnover. Protein turnover is a very dynamic process in which protein levels are constantly balancing between protein synthesis and degradation to maintain cellular homeostasis. (I) Schematic representation of the continuous cellular renewal of proteins from assembly (protein synthesis) to breakdown (protein degradation). (II) To analyse protein turnover, cells were labelled with SILAC media for a short time (spiked) to isotopically label arginines and lysines. Only newly synthesized proteins contain the isotopically labelled amino acids.

5.2 Aims of the chapter

In the previous chapter it was speculated that IFITM1/IFITM3 proteins may have a role in the translation process. To further study whether ISG/IRDS gene synthesis is modulated by IFITM1/IFITM3 proteins, sucrose density gradient separation coupled to MS-SWATH and pulse SILAC experiments were performed to evaluate the implications of IFITM1 and IFITM3 proteins in the IFNγ gene expression pathway.

CRISPR/Cas9 engineered *IFITM1* null cells, and *IFITM1/IFITM3* double null cells (chapter 3) along with wt-SiHa cells were used to define IFITM1 and IFITM3 effects on ribosomal integrity, to understand whether IFITM1/IFITM3 proteins interact with polysomal fractions, to determine whether the interactions are IFNγ-dependent, and whether IFITM1/IFITM3 are required for protein synthesis of IFNγ-responsive proteins.

5.3 Results

5.3.1 Study of ribosomal integrity in IFNγ-stimulated wt-SiHa cells vs IFNγ-stimulated *IFITM1/IFITM3* double null cells and the IFITM1/IFITM3 location in the ribosome

First, we aimed to define ribosomal integrity by studying its structural protein components. To address this, ribosomal profiles were analysed in IFNγ-stimulated wt-SiHa cells, compared with IFNγ-stimulated *IFITM1/IFITM3* double null cells; both cell types were stimulated with 100 ng/ml IFNγ for 24 hours (Figure 5.2). It was predicted that wt-SiHa cells would differ significantly in comparison to *IFITM1/IFITM3* double null cells. The *IFITM1/IFITM3* double null cells (instead of *IFITM1* null cells) were used, as it was suspected that IFITM3 can partially replace or compensate for some IFITM1 molecular functions. This isogenic cell model has only depleted the expression of two proteins, IFITM1 and IFITM3. In addition, the ribosome machinery has compensatory mechanisms to bypass malfunctions, consequently identification of ribosomal integrity defects (even subtle ones) is difficult.

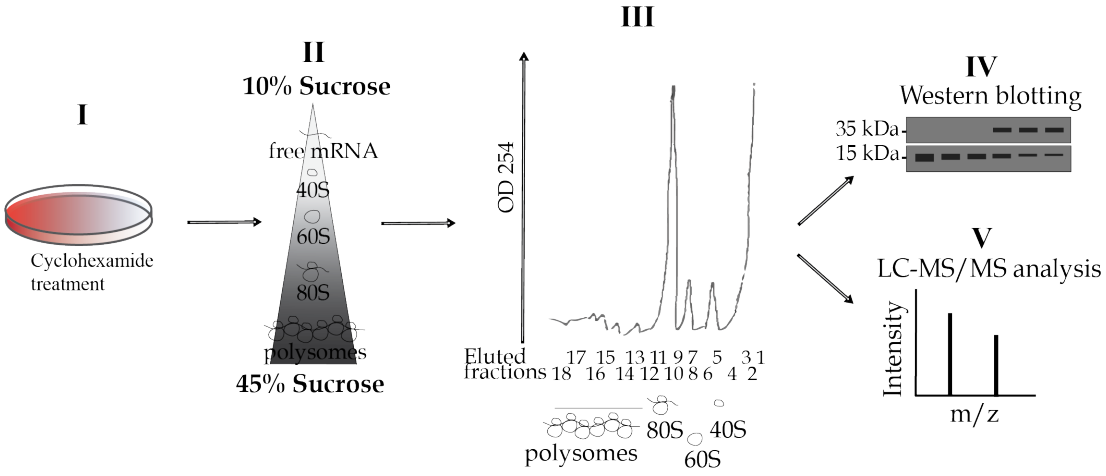

Figure 5.2: Overview of ribosomal profiling method to study ribosomal integrity. (I) Cells were treated with cycloheximide for 30 minutes. (II) Ribosomal subunits were separated by sucrose density gradient ultracentrifugation and followed by fractionation (III). Fractions of the same ribosomal subunits were combined and sequentially analysed by Western blotting after trichloroacetic acid (TCA) protein precipitation (IV) or by SWATH-MS (V).

The IFNγ-stimulated wt-SiHa cells and IFNγ-stimulated *IFITM1/IFITM3* double null cells were treated with cycloheximide for 30 min prior to collection, to maintain interaction of ribosome-associated proteins and retain ribosomal integrity, as cycloheximide prevents polysome run-off during cell lysis (Figure 5.2 I). Cycloheximide is a translation elongation inhibitor that binds to the 60S ribosomal subunit and stops the translation elongation step by blocking the release of deacylated tRNA from the ribosome E site (Del Prete *et al.*, 2007). The lysis buffer contained EGTA and a high salt concentration to preserve RNA (Brand-

horst, 2004), and an anti-protease cocktail to prevent protein degradation.

Fractions containing ribosomal subunits, were monitored by absorbance at 254 nm. The representative A254 peaks of 40S, 60S, 80S and polysomal ribosomes are depicted in the absorbance profile for the RNA in Figure 5.2 III. The major difference observed was a significantly lower 80S subunit fraction in IFNγ-stimulated *IFITM1/IFITM3* double null cells compared to IFNγ-stimulated wt-SiHa cells; this was seen in three independent replicates (Figure 5.3). Furthermore, the 80S peak difference was partially recovered after transfecting IFITM1 and IFITM3 in the *IFITM1/IFITM3* double null cells, resembling the 80S peak in wt-SiHa cells in three independent replicates (Figure 5.4, wt-SiHa cells transfected with empty vectors vs *IFITM1/IFITM3* double null cells transfected with IFITM1 and IFITM3). These results are of great interest, even though transfection efficiency was not good enough, transfected cells with IFITM1 and IFITM3 were enough to partially restore the 80S peak (Figure 5.4, *IFITM1/IFITM3* double null cells transfected with empty vectors vs *IFITM1/IFITM3* double null cells transfected with IFITM1 and IFITM3). These data indicate an impairment in the 80S monosome subunit after losing IFITM1/IFITM3 protein expression.

Then, ribosomal fractions from a representative replicate were combined (Figure 5.3 A); fractions belonging to the same ribosomal subunit were pooled. Protein was sequentially concentrated by trichloroacetic acid (TCA) protein precipitation, and immunoblots (Figure 5.2 IV) were performed to validate the appropriate ribosomal subunit separation; IFITM1/IFITM3 proteins were present but, progressively decreasing in amounts, in all ribosomal fractions; 40S, 60S, 80S, and polysome, from IFNγ stimulated wt-SiHa cells. There was no trace, in any fraction, of IFITM1/IFITM3 proteins in the IFNγ-stimulated *IFITM1/IFITM3* double null cells (Figure 5.5 B). As a positive control, RPL7a protein was included; this is a component of the 60S ribosomal (Robledo *et al.*, 2008) and is associated with the endoplasmic reticulum (Wei-Cheng *et al.*, 2007). RPL7a was detected in IFNγ-stimulated wt-SiHa cells and IFNγ-stimulated *IFITM1/IFITM3* double null cells (Figure 5.5 B). As indicated in Figure 5.5 A, fractions 7–9 correspond to 60S subunit in the cartoon.

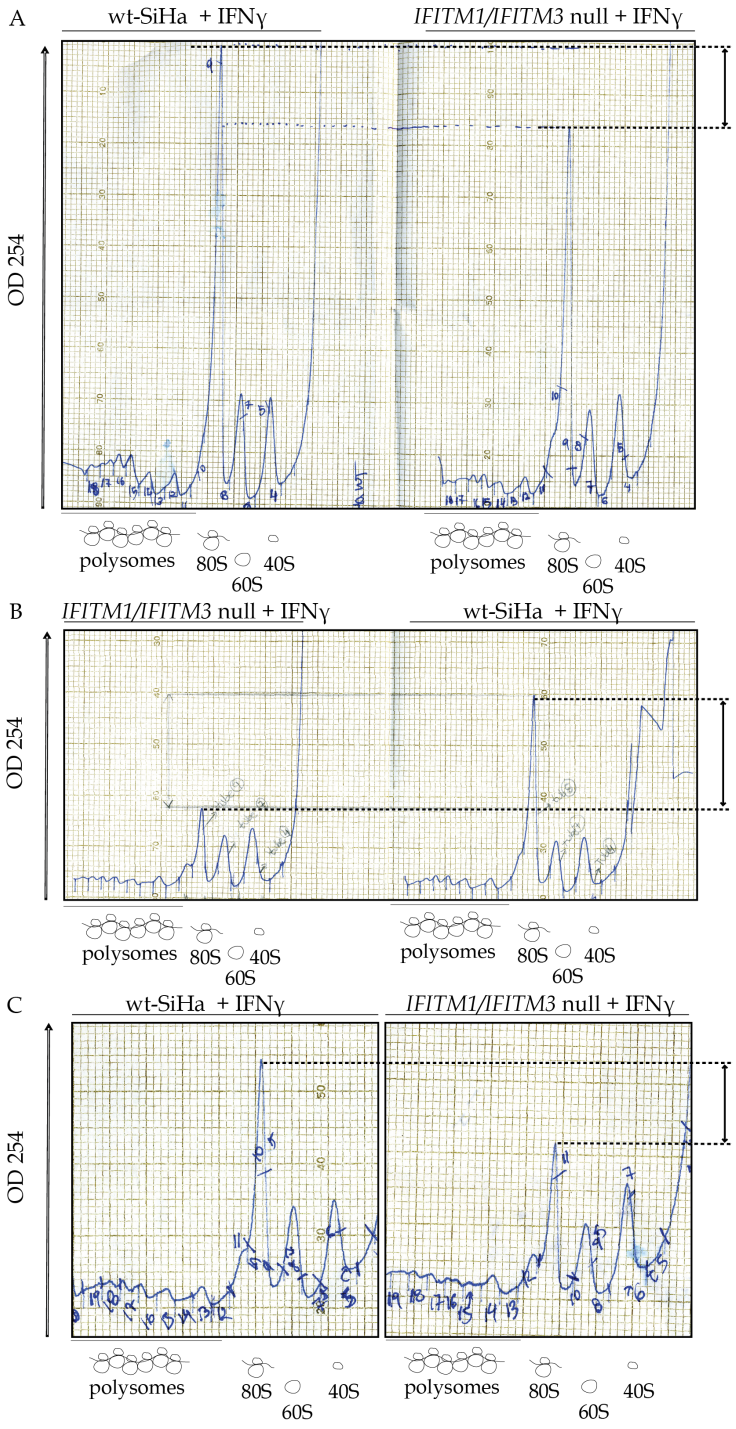

Figure 5.3: Original scans of the mRNA trace after sucrose density gradient fractionation in three independent replicates. (A–D). Sucrose density gradient was performed in wt-SiHa cells and *IFITM1/IFITM3* double null cells stimulated with IFNγ for 24 hours to activate the IFN-protein synthesis response. The original mRNA trace depicted in (A) is the replicate used to perform the ribosomal SWATH-MS (Figure 5.5). (A). A higher 80S peak (A254) was observed in wt-SiHa cells compared to in *IFITM1/IFITM3* double null cells in all three replicates (A-C).

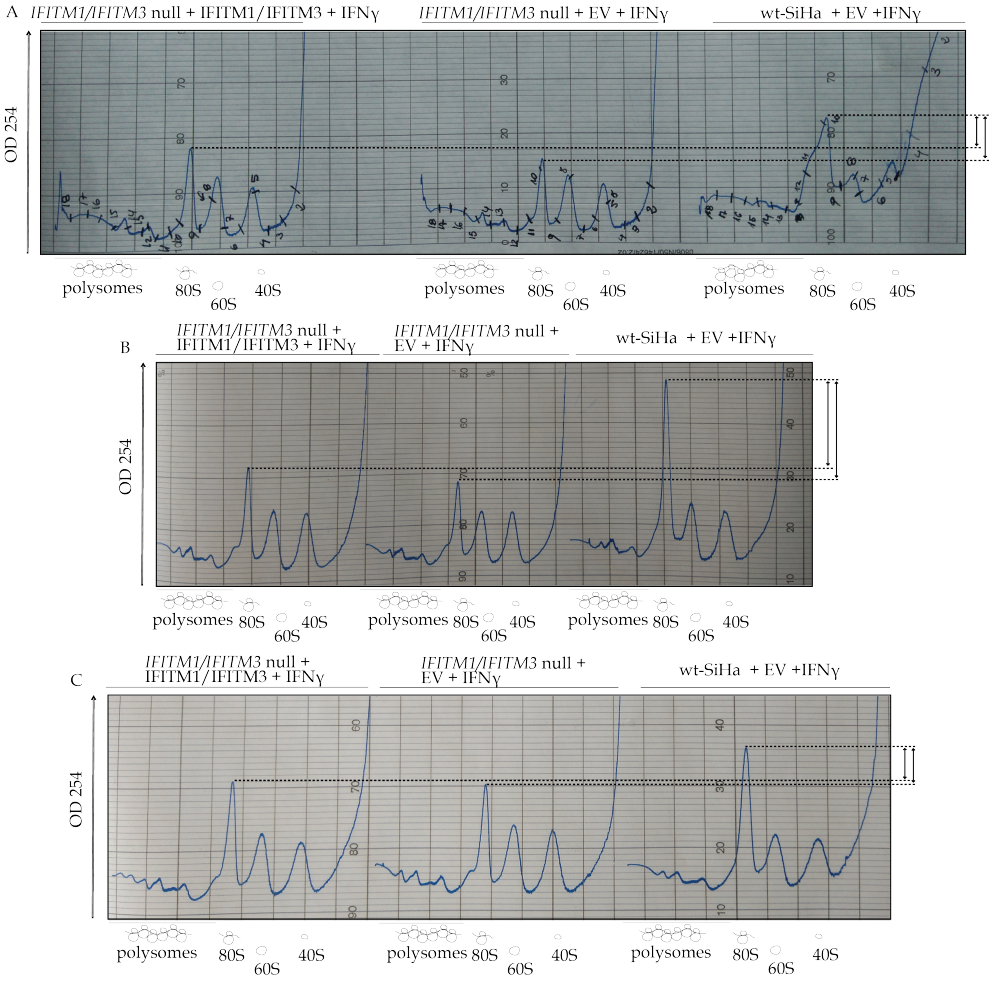

Figure 5.4: Original scans of the mRNA trace after sucrose density gradient fractionation to recapitulate the wt-SiHa 80S peak in IFITM1/IFITM3 transfected *IFITM1/IFITM3* double null cells. (A-C) Sucrose density gradient was performed in wt-SiHa cells and *IFITM1/IFITM3* double null cells stimulated with IFNγ for 24 hours to activate the IFN-protein synthesis response. The *IFITM1/IFITM3* double null cells were transiently transfected with IFITM1 or IFITM3 to recapitulate the 80S peak seen in the wt-SiHa cells. The wt-SiHa cells as well as *IFITM1/IFITM3* double null cells were transfected with EV to compensate possible change in the protein synthesis induced by the transfection method or presence of plasmid inside the cell.

Another representative replicate was processed by label-free SWATH-MS (Figure 5.2 V). Analysis was performed in three technical replicates. The purpose was to define whether there were global proteomic changes in the protein constituents of the ribosome following depletion of IFITM1/IFITM3 proteins in the IFNγ-stimulated cells. A volcano plot was used to quickly identify differential expression of ribosomal proteins and newly synthesised polypeptides between IFNγ-stimulated wt-SiHa cells and IFNγ-stimulated *IFITM1/IFITM3* double null cells. The differential protein expression of the quantified fold-change ratio (heavy/light) in IFNγ-stimulated wt-SiHa cells vs IFNγ-stimulated *IFITM1/IFITM3* double null cells is represented in Figure 5.5 C-F. The 40S associated proteins throughout the ribosomal peak fractions were similar in IFNγ-stimulated wt-SiHa and IFNγ-stimulated *IFITM1/IFITM3* double null cells (Figure 5.5 C), with only a few 40S

components over-represented (Figure 5.5 C). Similarly, the 60S protein family members were almost equivalent, with a few over-represented proteins (Figure 5.5 D, polysome fraction). Other over-represented non-related ribosome structure proteins were evaluated in IFNγ-stimulated wt-SiHa cells.

Interestingly, CAV1 protein, identified in the 80S and polysome fraction, was over-represented in the IFNγ-stimulated wt-SiHa cells compared to IFNγ-stimulated *IFITM1/IFITM3* double null cells and it served as internal positive control as it is been proposed an IFITM1 interacting partner (Novita Sari *et al.*, 2016; Yu *et al.*, 2015) (Figure 5.5 E and F). CAV1 was validated by PLA, however these IFITM1-associated proteins were beyond the scope of the current study and they were not further investigated (data not shown). Likewise, VAPB protein was also detected in the 40S and the polysome fraction and it is also a well-defined IFITM1-associated protein (Amini-Bavil-Olyaee *et al.*, 2013) (Figure 5.5 C and F).

The 40S ribosomal fraction had over-represented U2AF1 in IFNγ-stimulated wt-SiHa vs IFNγ-stimulated *IFITM1/IFITM3* double null cells (Figure 5.5 C). This is a splicing factor that has been proposed as interacting partner for IFITM1 (Table 4.1). In fact, U2AF1 can associate with mature RNAs to guide them to the ribosome. Once on the ribosome, Palangat *et al.*, 2019 proposed that U2AF1 can also function as a translation regulator by inhibiting the synthesis of selected peptides. It is suggested that U2AF1 forms a heterodimer with U2AF2 factor and binds in a region close to the mRNA start codon, possibly regulating the initiation of specific transcripts (Palangat *et al.*, 2019). Our results show higher U2AF1 association to the 40S fractions of IFNγ-stimulated wt-SiHa cells (Figure 5.5 C), fraction where the mRNA is initially loaded into the ribosomes (Walsh & Mohr, 2013).

To our surprise, STAT1 was also over-represented in the wt-SiHa vs *IFITM1/IFITM3* double null cells, both stimulated with IFNγ. This is a key factor in the IFNγ pathway and was identified in the 40S, 60S, and 80S fractions. Little is known about the role of STAT1 in protein translation, but Wang *et al.* propose that it can regulate mRNA translation by induction of the phosphoinositide 3-kinase (PI3K) and 4E (eI4E)-binding protein 1 (4EBP1), a repressor of the translation initiation. These leads to increase in the translation of cap-independent transcripts (Wang *et al.*, 2015). STAT1 has not been reported as having a direct association with the ribosome.

The results suggested that IFITM1/IFITM3 were present in the ribosome fractions (Figure 5.5 B), so we explored the possibility that IFITM1/IFITM3 could associate to ribosome proteins by studying the protein–protein interaction between IFITM1/IFITM3 and RPL7a. RPL7a is a ribosome-specific protein used as a marker to identify the ribosomes in the cell. It is a component of the 60S ribosomal subunit and it contains two nucleic acid-binding domains, one at the N-terminus and the other at the C-terminus. Interestingly, RPL7a is involved in translation and so it can also regulate the expression of some mRNAs (Neumann & Krawinkel, 1997; Neumann *et al.*, 1995). Moreover, it is also implicated in ribosomal biogenesis (Robledo *et al.*, 2008) and translation (Neumann *et al.*, 1995).

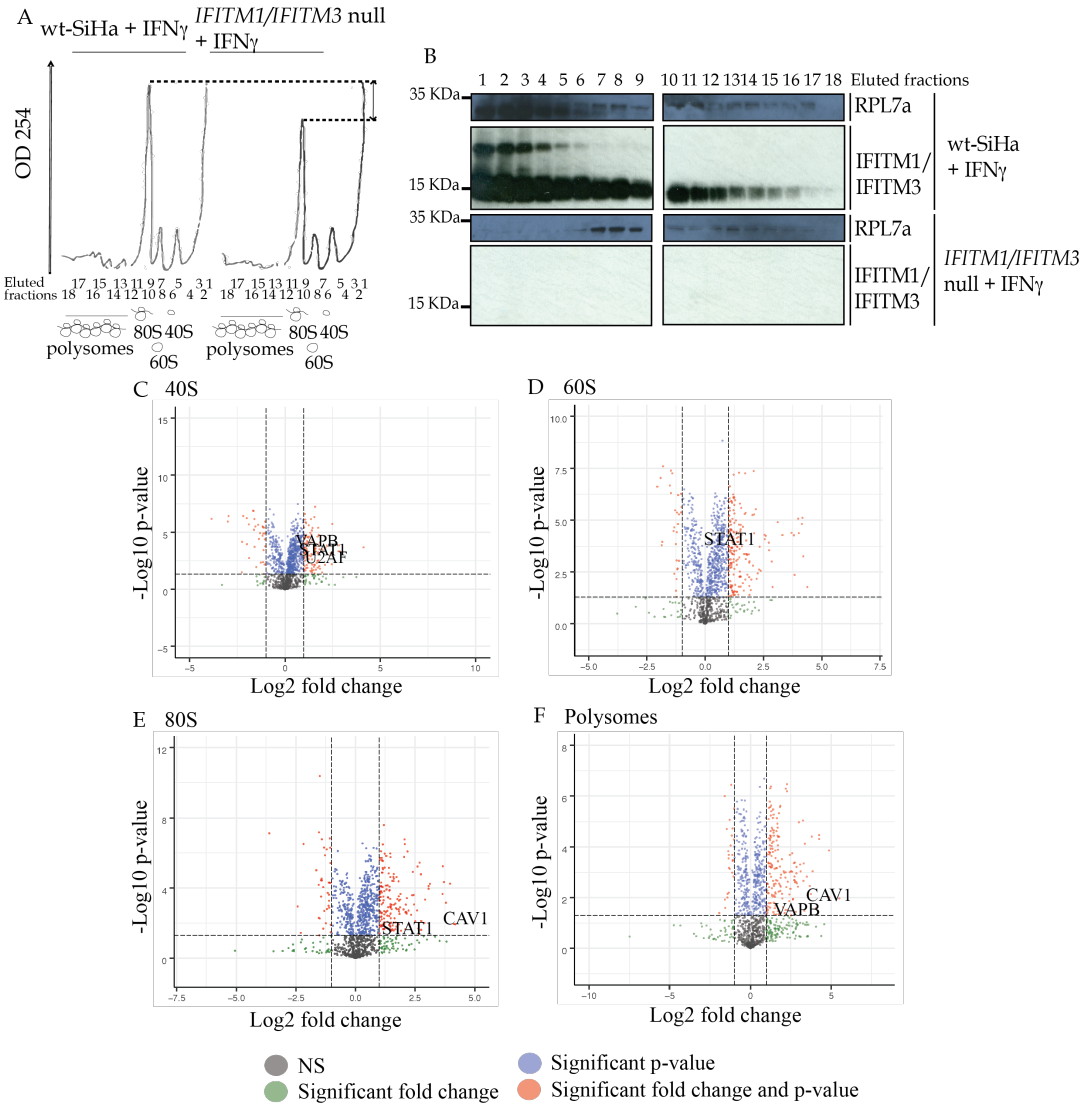

Figure 5.5: Ribosomal analysis by SWATH-MS in wt-SiHa IFNγ-stimulated cells and *IFITM1/IFITM3* double null IFNγ-stimulated cells. (A) Following the stimulation of wt-SiHa cells and *IFITM1/IFITM3* double null cells with IFNγ for 24 hours, cells were lysed with ribosome stabilization buffer, and applied to a sucrose gradient to separate individual components of the large and small ribosomal subunits, and polysomes. Eluted fractions were scanned at A254 nm. As indicated in the diagram; 40S subunit was eluted in fractions 3–5, 60S subunit in fractions 6–8, 80S subunit in fractions 9–11, and polysomes in fractions 12-18. The dotted line highlights the reproducible 80S peak reduction in the A254 signal in eluates from *IFITM1/IFITM3* double null cells. (B) Following fractionation, samples from fractions 1–18 were precipitated by trichloroacetic acid (corresponding to samples in Figure 5.3 A) and were analysed for key proteins as indicated, including RPL7a (enriched from 60S as defined by sucrose gradient), and IFITM1/IFITM3 proteins (enriched in all wt-SiHa fractions). Following SWATH-MS of eluted samples from IFNγ-stimulated wt-SiHa cells and IFNγ-stimulated *IFITM1/IFITM3* double null cells (Table B.4). Visualisation of the volcano plot by plotting the log2 fold-change ratio (wt/null) of 40S (C) 60S (D) 80S, (E) and polysome (F) fractions represented on the x-axis and -log10 p-value on the y-axis. (C-F) The analysis was conducted using R software and figures were produced using the Enhanced volcano, R package version 1.0 (Blighe, 2019). Horizontal dashed lines delimit the fold-change cut-off > 2 for upregulated and <0.5 for downregulated in the x-axis and vertical dashed line delimits the p-values cut-off <0.05 in the y-axis. Significant values for fold-change and p-value are depicted in red, right quadrant as overrepresented and left quadrant as under-represented proteins. Significant values for fold-change are depicted in green. Significant values for p-value are depicted in blue. Non-significant (NS) values are depicted in grey.

In the attempt to validate IFITM1/IFITM3 protein presence in the ribosome, IFNγ-stimulated and non-stimulated wt-SiHa cells were fixed for a proximity ligation assay (Figure 5.6 A-D). The *IFITM1/IFITM3* double null cells were used as a negative control (Figure 5.6 E-H). The Figure 5.6 D shows a representative image of IFNγ-stimulated wt-SiHa cells in which there is a high association between IFITM1/IFITM3-RPL7a proteins in the cytosol. The assay shows a significantly increased protein–protein association between IFITM1/IFITM3-RPL7a after IFNγ-stimulation compared to that in non-stimulated wt-SiHa cells (Figure 5.6 C vs D and I). In contrast, there is no detectable signal in IFNγ-stimulated *IFITM1/IFITM3* double null cells (Figure 5.6 H and J).

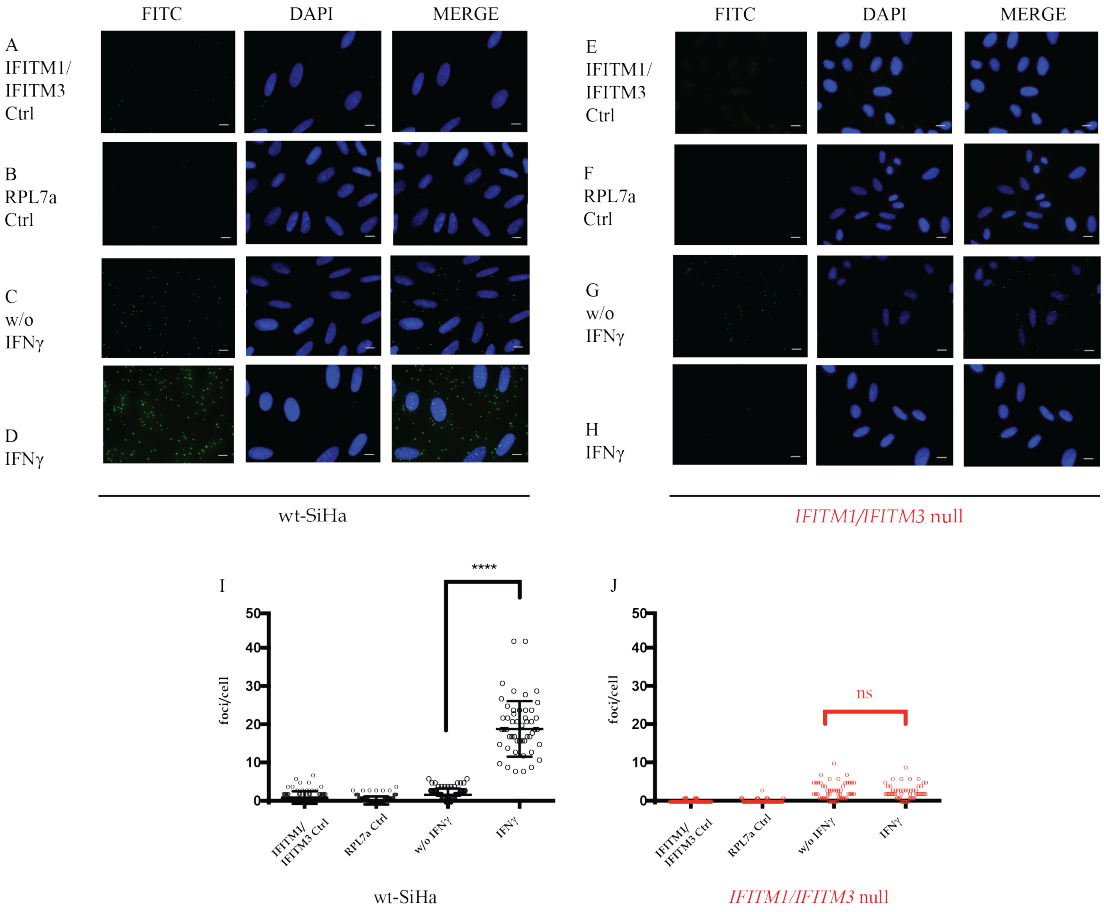

Figure 5.6: Evaluation of the IFITM1/IFITM3:RPL7a protein–protein expression and interaction *in situ* after stimulation with IFNγ. Proximity ligation assays were used to study the endogenous interaction between RPL7a and IFITM1/IFITM3 proteins in wt-SiHa (A–D) and *IFITM1/IFITM3* double null cells (E–H) FITC images identify the protein–protein association foci (green) and DAPI was used for nuclear staining (blue). (A–B and E–F) Cells were incubated as negative controls using IFITM1/IFITM3 or RPL7a antibodies only. (C and G) Cells were incubated with both IFITM1/IFITM3 and RPL7a antibodies to define protein–protein foci in non-stimulated cells. (D and H) Cells were incubated with both IFITM1 and RPL7a antibodies to define protein–protein foci in IFNγ-stimulated cells. Representative quantification of the protein–protein interaction foci per cell in presence or absence of IFNγ stimulation in wt-SiHa (I) and *IFITM1/IFITM3* double null (J). At least 50 cells were counted for each condition. Statistical study was performed with one-way ANOVA and Bonferroni correction (****p < 0.0001; ns, not significant). n=3. Scale bar: 10 μm.

5.3.2 Pulse SILAC to identify IFITM1- and IFITM1/IFITM3- dependent protein synthesis in response to IFNγ signalling

The cytokine IFNγ is capable of inducing expression of a wide range of genes through the activation of the JAK kinase–STAT pathway (Darnell *et al.*, 1994; Williams, 1991). We evaluated whether IFNγ responsive protein synthesis is impaired by loss of IFITM1/IFITM3 protein expression. The wt-SiHa cells, *IFITM1* null cells, and *IFITM1/IFITM3* double null cells were grown in parallel with SILAC heavy isotopic amino acid labelling media for 6 or 24 hours, non-stimulated or stimulated with 100 ng/ml IFNγ for 6 or 24 hours, respectively (Figure 5.7 A). The 24-hour time point was the maximum IFITM1 peak induction on IFNγ stimulation (Figure 4.16 I). The earlier 6-hour time point was included to study which proteins were initially activated and if their induction varied with time. This time point was a compromise between capturing the first wave of IFNγ-activated effectors but not so early that there would not be enough heavy-isotope-labelled newly synthetized proteins to be identified in the MS analysis (Figure 5.7). Moreover, the classic IFNγ-responsive synthesis of proteins is observed in this SiHa cell line (Figure 5.8), indicating that these cells are a good model to dissect the IFNγ-signalling cascade. Cell lysates were processed by FASP section 2.8.1 and analysed by MS for IFNγ and IFITM1/IFITM3-dependent protein synthesis (Figure 5.8 B, D, F vs A, C, E; Figure 5.9B, D, F vs A, C, E).

This experiment was designed to determine those proteins after IFNγ stimulation that are IFITM1/IFITM3-dependent. The induced proteins identified in IFNγ stimulated wt-SiHa cells were compared to those in IFNγ stimulated *IFITM1/IFITM3* double null cells.It was determined whether these identified IFNγ-induced proteins were indeed IFITM1-dependent. Hence, the induced proteins identified in IFNγ stimulated wt-SiHa cells were compared to those in *IFITM1* null-IFNγ stimulated SiHa cells.

The first step was determining which proteins are significantly induced after IFNγ stimulation in wt-SiHA cells. A preliminary analysis to address this question was kindly performed by Prof. Lenka Hernychová using the Proteome Discoverer 2.2 platform (Thermo Fisher Scientific). This was used to compare those proteins significantly expressed in wt-SiHa cells with or without IFNγ stimulation. Strikingly, MHC class I molecules (HLA-A, HLA-B, and HLA-C) were the major dominant ISG genes induced (Figure 5.7 B and C) and were consistently identified across all three replicates. Two additional proteins were heavily induced; B2M which is the light chain of MCH class I complex, and STAT1 which is the key transducer effector of the IFNγ signalling pathway. Several studies have demonstrated that these proteins are upregulated upon IFNγ stimulation (subsection 1.5.3).

The novelty of this experimental approach is determining whether these differences are IFITM1 and/or IFITM1/IFITM3-dependent. For this reason, the same comparison of stimulated and non-stimulated cells was made in both isogenic knock out SiHa cell lines.

In this case, a more exhaustive analysis was performed on all the proteins identified by MS (Figure 5.8 for 6 hours IFNγ stimulation and Figure 5.9 for 24 hours IFNγ stimulation). Interestingly, not many over-represented proteins were identified, suggesting that IFITM1 and IFITM1/IFITM3 are modulating very specific targets. This finding supports the previous outcome where global ribosomal integrity was not drastically perturbed but the 80S peak was decreased, denoting a certain limited impairment in protein synthesis (Figure 5.3).

The experiment was designed with two different time points; initially 6 hours of pulse SILAC was analysed. The first dominant protein of note is STAT1 which was only induced after IFNγ-stimulation in the entire cervical cancer cell panel i.e. wt-SiHa cells, *IFITM1* null cells, and *IFITM1/IFITM3* double null cells (Figure 5.9 A-F and I). STAT1 was used as an internal positive control as an example of a protein that is IFNγ-dependent but IFITM1/IFITM3 independent.

Other proteins whose synthesis rates were evaluated at 6 hours post-labelling included: ISG15, EIF1, B2M, and HLA-B (Figure 5.8 G, J, K, and L). Peptides identified from EIF1 and B2M were not substantially different between wild type and both isogenic null cells. EIF1 is a key component for the assembly of the translation initiation complex. It facilitates 40S conformation and, consequently, allows the mRNA scan to precisely select the AUG start codon (Cheung *et al.*, 2007; Passmore *et al.*, 2007; Pestova *et al.*, 2001). B2M is the light chain of MHC molecules (Neefjes *et al.*, 2011). In addition, ISG15 and HLA-B were not detected at early stages. Likewise, another member of MHC class I molecules, HLA-C, was not detected (Figure 5.9 A-F).

IRF1 protein synthesis was IFNγ-dependent after 6 hours post-labelling in wt-SiHa cells, but IRF1 peptide recovery was attenuated in all triplicates in *IFITM1/IFITM3* double null cells (Figure 5.8 H). This suggested that IRF1 is partially dependent upon IFITM1/IFITM3 signalling at a very early stage. IRF1 is an IFN regulatory factor induced by type I and type II IFN and it is involved in mediating antiviral and immunomodulatory roles(Harada *et al.*, 1994; Tamura *et al.*, 2008).

Overall, very few proteins were overrepresented in the 6 hour pulse SILAC. Possibly, there was not enough time to fully induce all the dominant effectors. Moreover, protein synthesis is evaluated by comparing the fold-change rate between heavy (already synthesized proteins) vs light (newly synthesized proteins). Taking this into consideration, it may occur that even if the cell is synthesizing new proteins, these are not significantly increased enough to be compared to the total amount of protein present in the cell and consequently the ratio heavy/light is very low. Therefore, the 24 hour pulse SILAC was analysed.

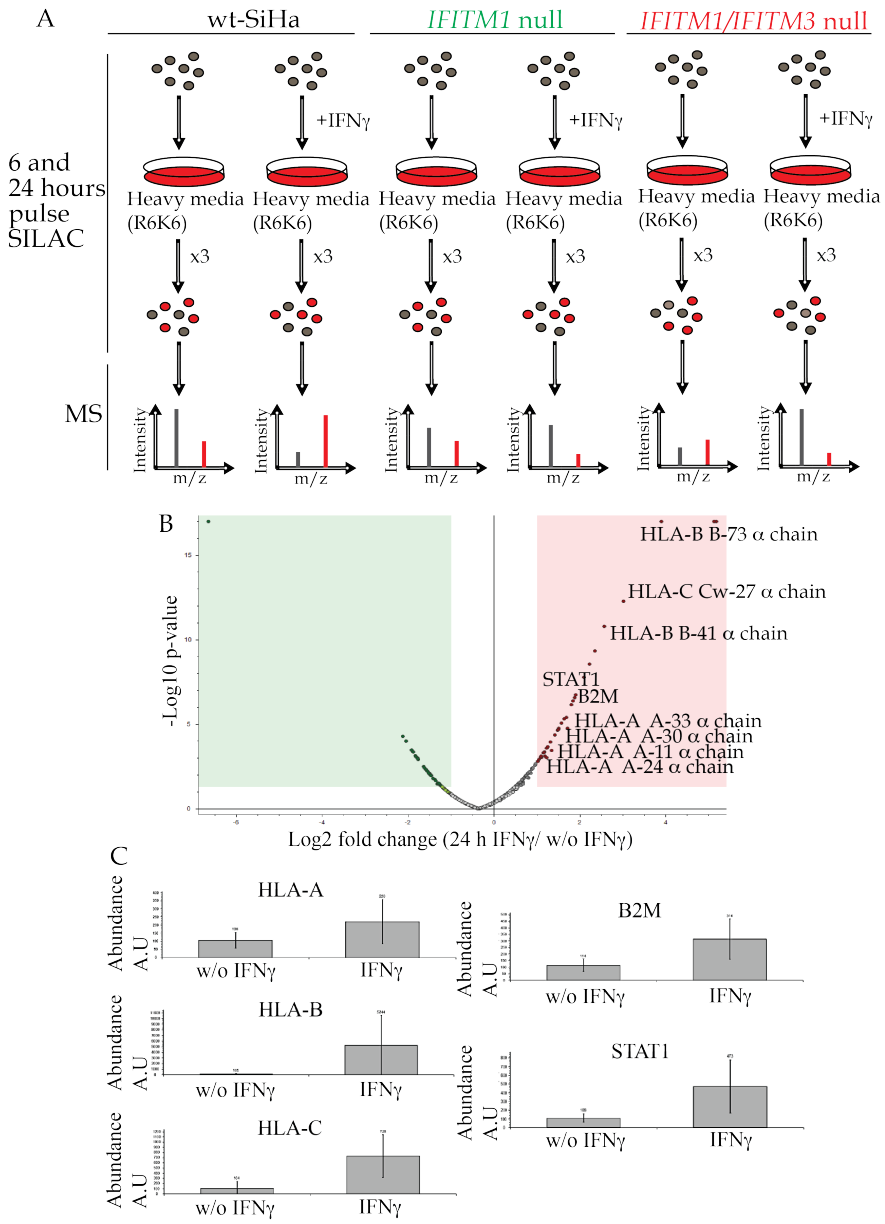

Figure 5.7: Pulse SILAC to identify global changes in protein synthesis in wt-SiHa cells, *IFITM1* null cells, and *IFITM1/IFITM3* double null cells. (A) Workflow describing the steps followed to perform pulse SILAC; SILAC heavy medium was introduced for 6 and 24 hours to non-stimulated and IFNγ-stimulated cells for 6 and 24 hours. (B) Volcano plot was used for quick identification of protein changes of wt-SiHa cells cultivated for 24 hours in heavy SILAC media (Table B.5). This analysis was performed using the Proteome Discoverer 2.2 platform (Thermo Fisher Scientific). The right upper quadrant (highlighted in red) displays significantly upregulated proteins that were newly synthesized in 24 hour INFγ-stimulated wt-SiHa cells compared to non-stimulated wt-SiHa cells. The x-axis displays the abundance ratio (fold-change) in log2 with initial setting 1, and the y-axis displays p-values in log10 with initial setting 0.05. (C) The quantification channel values plot for precursor ion quantification displays the relative peak area with the standard deviation of the biological replicate measurements for HLA-A, HLA-B, HLA-C, B2M, and STAT1 proteins with the heavy isotope labels (non-stimulated and IFNγ-stimulated for 24 hours). The x-axis displays the quantification channel and the y-axis displays the detected area of the selected protein for the given quantification channel defined by counts x seconds.

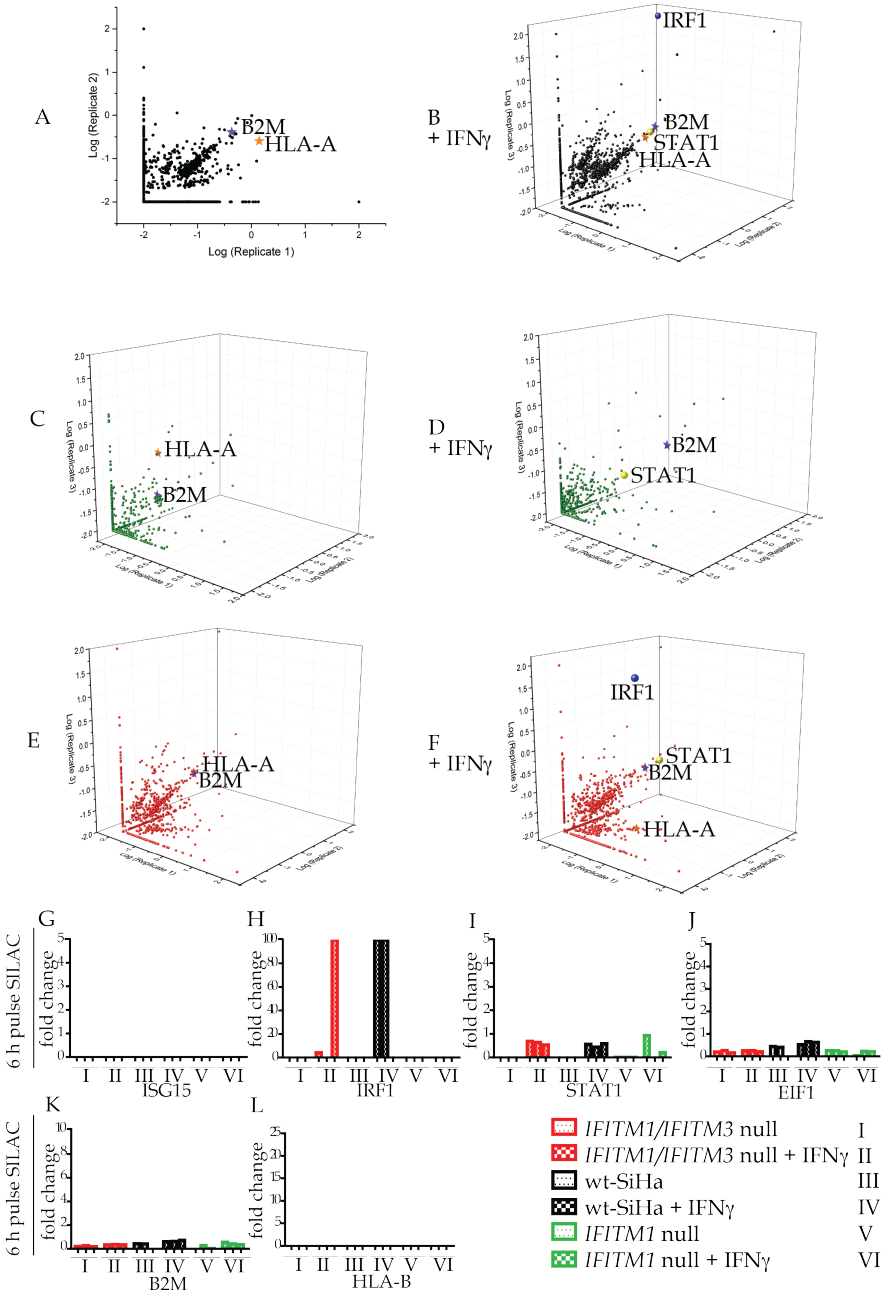

Figure 5.8: Defining dominant proteins whose synthesis is IFITM1/IFITM3-IFNγ attenuated at an early stage. SILAC pulse labelling was performed in wt-SiHa cells (A–B); in *IFITM1* null cells (C–D); and in *IFITM1/IFITM3* double null cells (E–F) (Table B.5). Cells were stimulated with IFNγ for 6 hours in B, D and F. Samples were plotted as a function of log10 fold-change of heavy/light peptide intensities. Biological triplicates are represented in the x, y, and z- axis (B–F), whereas only two biological replicates were available in (A). Graph bars showing the most significant synthetized protein in each of the three biological replicates for 6 hours pulse labelling: IRF1 (H); non-stimulated at early stage: ISG15 and HLA-B (G and L); proteins that were taken as internal controls at the indicated pulse labelling time points such as: STAT1, EIF1, and B2M (I–K).

By 24 hours of IFNγ stimulation (Figure 5.9 A-F), the isotopically labelled IRF1 peptides recovered were attenuated (Figure 5.9 H). This is consistent with the early and tran-

sient induction of IRF1 by IFNγ. Previous work performed by Dr Elisabeth Sinclair confirmed, using a luciferase reporter assay, that IRF1 transcription activity is attenuated in cells with a targeted depletion of IFITM1 (data not shown). In contrast to IRF1, the elevation in STAT1 (internal positive control) synthesis after 24 hours with IFNγ appears largely IFITM1/IFITM3-independent (Figure 5.9 B, D, F, and I). Another well-known inducible IFNγ protein, B2M, also appears to be IFITM1/IFITM3-independent (Figure 5.9 A–F and K). Moreover, there is an elevation in amount of HLA-A, HLA-B, and HLA-C at 24 hours of IFNγ stimulation in wt-SiHa cells (Figure 5.9 A vs B). Together, these data indicate that the SiHa cervical cancer cell model activates the classic IFNγ response i.e. able to induce STAT1, IRF1, B2M, and MHC class I molecules.

Strikingly, there was an absence of HLA-A, HLA-B, and HLA-C protein synthesis after 24 hours with IFNγ in the *IFITM1/IFITM3* double null cells compared to wt-SiHa cells (Figure 5.9 B vs F). Similar results were observed in the *IFITM1* null cells (Figure 5.9 B vs D). Furthermore, isotopically labelled ISG15 tryptic peptides are not observed in the early IFNγ response (Figure 5.8 A-G), but the isotopically labelled ISG15 peptide recovery after 24 hours with IFNγ is elevated in the wt-SiHa cells (Figure 5.9 B and G) and not seen in *IFITM1* null cells or *IFITM1/IFITM3* double null cells (Figure 5.9 D, F and G) suggesting that ISG15 protein synthesis is largely IFITM1/IFITM3 dependent in the late stage.

MHC class I molecules (HLA-A, HLA-B, HLA-C) along with ISG15 were by far the major dominant proteins induced by IFITM1/IFITM3-IFNγ stimulation. Considering that HLAs have homologous regions, peptides identified by MS methodology were manually validated and unique peptides for each HLA type are indicated with a red asterisk in Figure 5.10.

In summary, IFNγ-dependent induction of IRF1 protein synthesis is attenuated at 6 hours post-labelling in *IFITM1/IFITM3* double null cells but also in *IFITM1* null cells (Figure 5.8 H). This suggests that IRF1 is dependent upon IFITM1. ISG15 tryptic peptides are not observed in the early IFNγ response (Figure 5.8 G) but are only overexpressed as a late response in wt-SiHa IFNγ-stimulated cells (Figure 5.9 G). In contrast, elevations in STAT1 protein synthesis are IFITM1-independent, based on the equivalent induction of STAT1 in the *IFITM1* null cells and *IFITM1/IFITM3* double null cells in comparison with wt-SiHa cells (Figure 5.9 I). HLA-A, HLA-B, and HLA-C protein synthesis is also attenuated after 24 hours IFNγ stimulation in the *IFITM1* null cells and *IFITM1/IFITM3* double null cells (Figure 5.9). Together, these data indicate that MHC class I family members, as well as ISG15, require IFITM1 for rapid IFNγ-induced protein expression.

These results provide further evidence to support previous work performed in our group (Figure 3.2) where attenuation of IFITM1 by siRNA decreased protein levels of MHC class I molecules as well as ISG15. Moreover, it is consistent with findings described in the previous chapter where HLA-B and ISG15 were identified as novel interacting partners for IFITM1. Nonetheless, the possibility cannot be ruled out that IFITM1 and IFITM3 proteins are modulating HLA-B and ISG15 at stages other than protein synthesis.

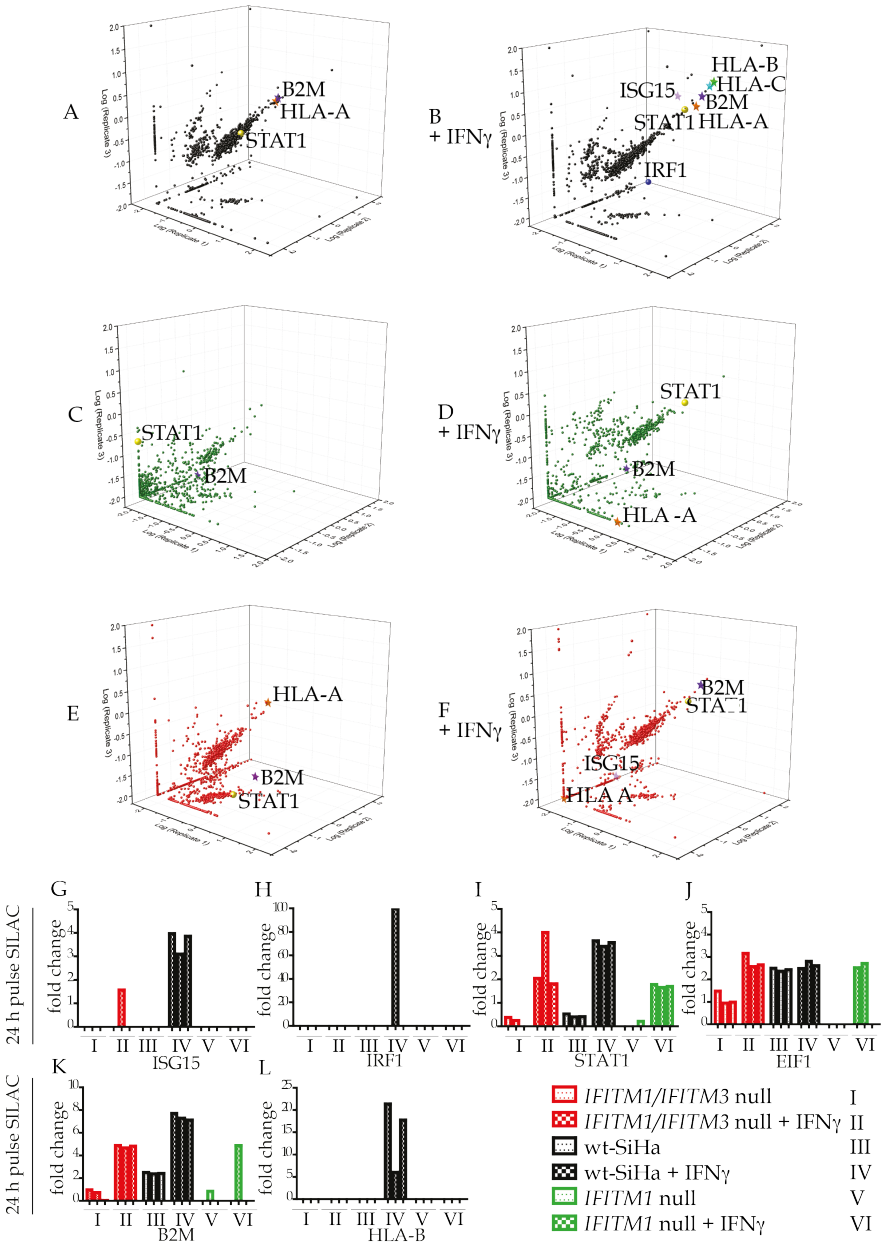

Figure 5.9: Defining dominant proteins whose synthesis is IFITM1/IFITM3-IFNγ attenuated in the late stage. SILAC pulse-labelling was performed in wt-SiHa cells (A, B); in *IFITM1* null cells (C, D); and in *IFITM1/IFITM3* double null cells (E, F) (Table B.5). Cells were stimulated with IFNγ for 24 hours in B, D and F including the pulse label. Data were plotted as a function of log10 fold change of heavy/light peptide intensities. Biological triplicates were represented in x, y, and z- axis. In samples (G–I), representative peptides used for quantification in biological triplicates are highlighted to demonstrate a protein that is induced independent of IFITM1/IFITM3 (STAT1; I, EIF1; J, and B2M; K), IFITM1/IFITM3-dependent at a later time point (ISG15; G vs Figure 5.8 G and HLA-B; L vs Figure 5.8 L), and IFITM1/IFITM3-dependent at an earlier time point (IRF1; H vs Figure 5.8 H).

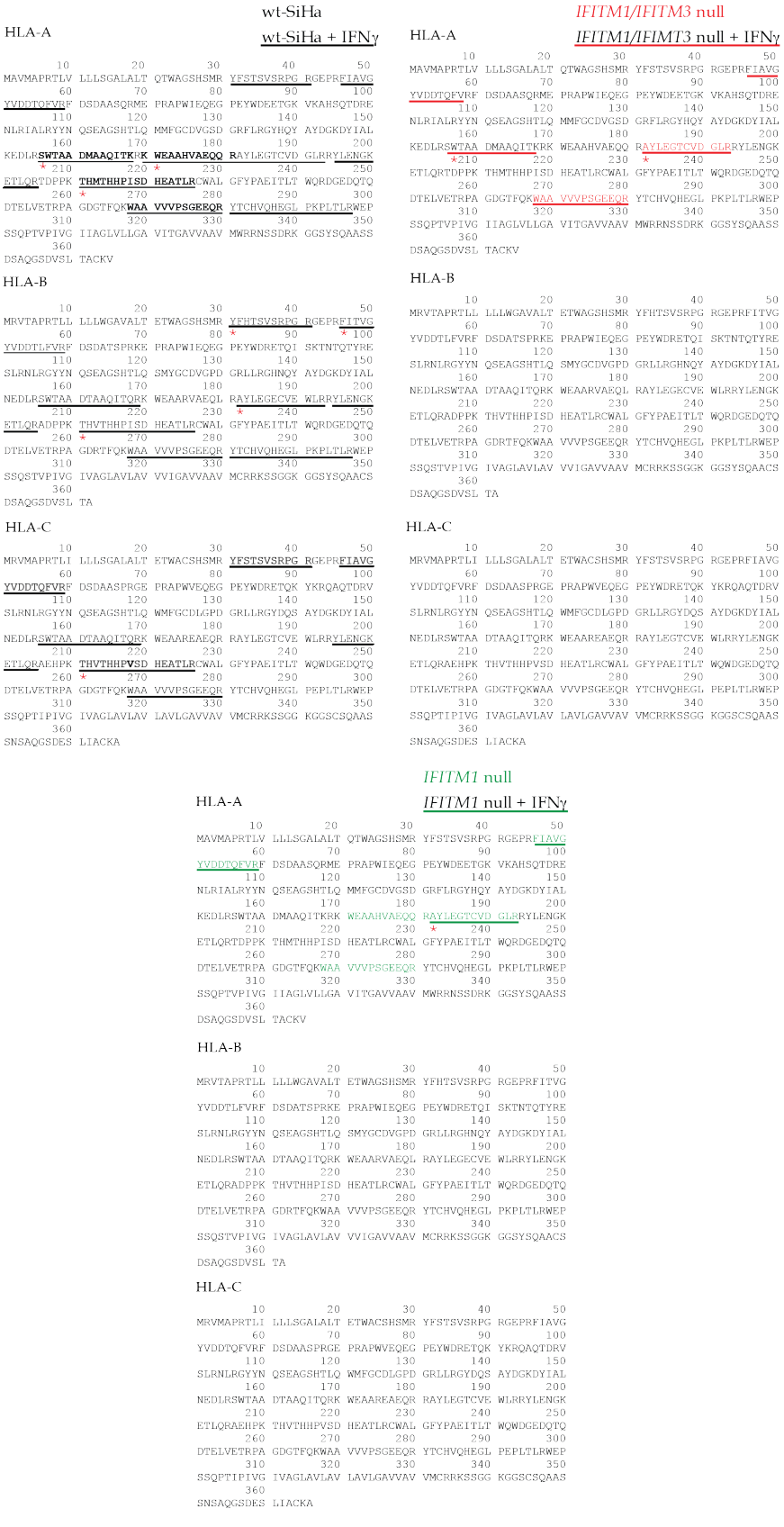

Figure 5.10: Tryptic peptides identified for HLA-A, HLA-B and HLA-C. Underlined are the peptides identified in HLA-A, HLA-B and HLA-C for wt-SiHa cells, wt-SiHa-IFNγ stimulated cells, *IFITM1* null cells, *IFITM1* null-IFNγ stimulated cells, *IFITM1/IFITM3* double null cells, and *IFITM1/IFITM3* double null-IFNγ stimulated cells. Additionally, highlighted (*) are the unique peptides characteristic for each MHC class I orthologue.

5.3.3 Dissecting IFITM1/IFITM3-IFNγ dependencies in the SiHa cervical cancer cell model by Western blot analysis

The IFN signalling pathway is a complicated system in which many components interact throughout a cellular cascade of events. Though this project has a particular focus on IFNγ signalling, it is known that all three IFN types can affect each other, promoting cross-activation of their pathways. As a result, effectors may have redundant roles, making it complicated to dissect individual protein functions (Dunn *et al.*, 2006).

We tested our SiHa cancer cell model (comprised of wt-SiHa cells, *IFITM1* null cells, and *IFITM1/IFITM3* double null cells) to determine if there were any differences in the IFNγ activation cascade as well as in IFITM1/IFITM3 protein expression. In brief, the IFNγ signalling pathway initiates with the cross-tyrosine phosphorylation of JAK-kinases that facilitate dimerization of signal transducer STAT1. The STAT1 dimers forms a complex with the regulatory factor IRF9 and this induces expression of the first wave of ISG genes, among them IRF1 transcription factor (Boehm *et al.*, 1997).

Cells were IFNγ stimulated for 6 and 24 hours to determine early and more sustained responses, respectively. In this sense, IFNγ stimulation mimics the same conditions performed for the pulse SILAC (subsection 5.3.2). Importantly, this experiment evaluates the total amount of protein present in the cell. This approach does not take into account any possible cellular compensatory effects to overcome the absence of IFITM1 or IFITM1/IFITM3.

There is a subtle reduction in STAT1 induction in *IFITM1/IFITM3* double null cells compared to wt-SiHa cells (Figure 5.11, STAT1 panel). Similarly, there is a pronounced reduction of IRF1 expression in *IFITM1/IFITM3* double null cells, more noticeable in the long exposure panel (Figure 5.11, IRF panel). A delay in the STAT1 induction, in comparison to IRF1, is also observed (Figure 5.11, STAT1 and IRF1 panel), and there is a reduction in HLA-B as well as ISG15 expression in *IFITM1/IFITM3* double null cells compared to wt-SiHa cells. Overall, the IFNγ system is attenuated in *IFITM1/IFITM3* double null cells, whereas *IFITM1* null cells resemble wt-SiHa cells in terms of IFNγ signature expression. These observations are not comparable with the results of the pulse SILAC experiments in the previous section as total protein expression is assessed in this section whereas pulse SILAC experiments study the synthesized proteins after IFNγ stimulation.

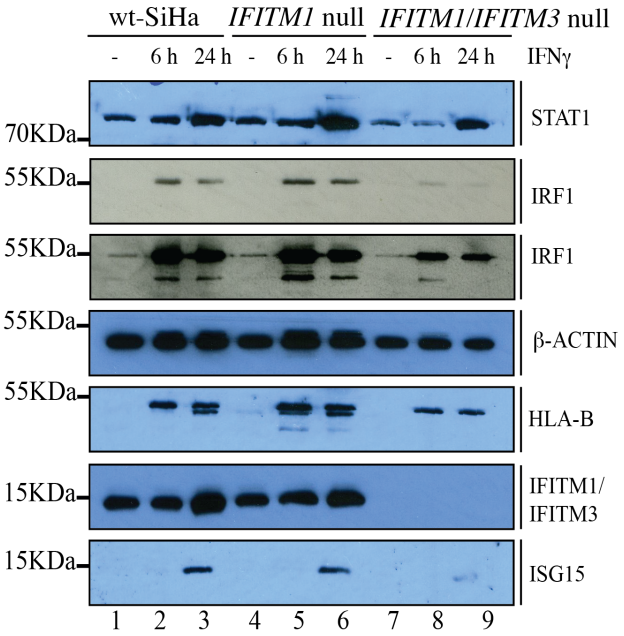

Figure 5.11: Identifying global changes in IFN signature in wt-SiHa cells, *IFITM1* null cells, and *IFITM1/IFITM3* double null cells after IFNγ stimultaion. Wt-SiHa cells (lanes 1-3), *IFITM1* null cells (lanes 4-6), and *IFITM1/IFTIM3* double null cells (lanes 7-9) were stimulated in absence or with 100 ng/ml IFNγ for 6 hours (lanes 2, 5, and 8) and 24 hours (lanes 3, 6, and 9). Western blotting was used to characterize the expression of key IFN-induced proteins; STAT1, IRF1, HLA-B, IFITM1/IFITM3, and ISG15. β-ACTIN was used as a loading control.

5.4 Discussion

It has been widely argued that overexpression of the IFITM1 receptor has a pro-oncogenic role. Besides, evidence shows that IFITM1 mediates pleiotropic effects: on one hand, it is involved in antiproliferative programmes causing growth arrest, enhanced by IFNγ-stimulation, and on the other hand, IFITM1 also inhibits NK-mediated cytotoxicity signalling, allowing tumour cell immune evasion (Yang *et al.*, 2005). Several studies found IFITM1 overexpressed in many cancer types (Akyerli *et al.*, 2005; Borg *et al.*, 2016; Hach *et al.*, 2013; Ogony *et al.*, 2016; Yu *et al.*, 2015), but it remains poorly understood why the opposite situation i.e. absence of IFITM1 also induces metastatic outcomes. In this respect, a study found significant differences in the IFITM1 expression profiles of cervical squamous cell carcinoma compared to normal tissue and *IFITM1* mRNA in cervical cancer tissues was decreased in comparison to chronic cervicitis tissue. This is possibly explained by elevated methylation in the *IFITM1* gene promoter in cervical cancer tissues compared to normal cervical tissues and that may affect cell proliferation, suggesting implication for cervical carcinogenesis. Additionally, ectopically transfected IFITM1 in HeLa cells reduced cell migration and invasion, but promoted apoptosis and cell arrest in S phase (Zheng *et al.*, 2017).

Each cancer type has a unique physiology, and dysfunction of particular molecular pathways may be favourable or disadvantageous to its development and progression. In this context, it is possible that IFITM1/IFITM3 proteins promote pleiotropic functions, and this chapter gives some insights on how loss of IFITM1/IFITM3 protein expression may be also implicated in poor cancer prognosis.

Data from the polysome analysis suggests that there is a defect in the assembly of the RNA components of the 80S ribosomal complex when IFITM1/IFITM3 proteins are not expressed, recapitulated with ectopic transfection of IFITM1/IFITM3 (Figure 5.4). Additionally, CAV1, U2AF1, and VAPB are examples of non-ribosomal proteins significantly overrepresented during IFNγ-stimulation of wt-SiHa cells vs *IFITM1/IFITM3* double null cells (Figure 5.5 C-F). In particular, U2AF1 was proposed as a novel IFITM1 interacting partner (Table 4.1) and is implicated the regulation of the protein synthesis (Palangat *et al.*, 2019). Along with its association with the 40S ribosomal subunit, this emphasizes the hypothesis that IFITM1/IFITM3 proteins guide and regulate specific transcripts. This study also locates IFITM1/IFITM3 to the ribosome by studying the association between IFITM1/IFITM3 and RPL7a ribosomal protein (Figure 5.6)

The fact that protein translation is not globally affected suggested that IFITM1 (and IFITM3) loss may act as exclusion binding proteins for certain mRNA targets. In the pulse SILAC assay, HLA-B in coordination with other MHC class I molecules is expressed in an IFITM1/IFITM3-IFNγ dependent manner (Figure 5.9 B, D, F, L). MHC class I molecules are the core components of the antigen presentation pathway, having an important involvement in tumour–antigen presentation, recognition and elimination. In addition, IFNγ is one of the best-characterised immune regulatory cytokines, with a key role in tumour neoantigen recognition and elimination. Any malignant cell with immune-evasive capability will be positively selected and expanded during tumour evolution (Pettit *et al.*, 2000). Among many other mechanisms, it has been extensively reported that downregulation of MHC class I molecules leads to immune-therapy failure (Garrido *et al.*, 2016; Garrido *et al.*, 1993; Garrido *et al.*, 2017; Seliger *et al.*, 2002).

In this context, HLA-B protein synthesis would be increased as part of a rapid IFNγ response in addition to its constitutive expression. In fact, IFNγ signalling would be activated by any molecule recognized as “non-self” such as pathogen attack or tumour. HLAs are physiologically over-induced for a short time under particular circumstances and then restored to their basal expression levels. But, constitutive exposure to discrete levels of IFNs induced by infection (i.e. HPV), or other causes, may contribute to increased resistance to DNA damage by expression of IRDS gene products (Cheon *et al.*, 2014). Under pathological conditions, such as cancer, it may sustain the activated signalling pathway conditioning immune-escape and therefore risking the host survival.

IFNγ is a good candidate for immunotherapy as it induces tumour antigen–MHC complex presentation (Propper *et al.*, 2003). In addition, it enhances tumour-specific cytotoxic T lymphocyte (CTL) which in turn is dependent on appropriate MHC class I expression.

But what happens if there are some defects in the IFNγ pathway? In the SiHa model we see deficiencies in MHC class I molecule expression when IFITM1/IFITM3 protein expression is lost. Depletion of key factors in mouse models result in blockage of the MHC class I induction, rapid tumour growth and more resistance to immunotherapy (Manguso *et al.*, 2018). Actually, SiHa cells express low levels of MHC class I molecules in comparison to other cervical cell lines. Downregulation of MHC class I expression (not found for MHC class II) affects tumour elimination activity by tumour-specific cytotoxic T lymphocytes (CTLs). These CTL-resistant tumour cells survive by positive selection even if they are surrounded by tumour-specific CTLs (Street *et al.*, 1997).

Nevertheless, such a fundamental cellular mechanism must be robustly regulated by other alternative pathways to guarantee appropriate protein expression. Absence of IFITM1/IFITM3 protein expression may not abolish exposure of antigen presentation on the cell membrane completely, but may contribute to its impairment . Impairment of antigen presentation complexes by decreasing the MCH class I protein expression (or other associated molecules) may lead to aberrant recognition of cancer neo-antigens by the $CD8^+$ T cell, promoting immune evasion and causing immunotherapy failure.

In summary, IFITM1/IFITM3 are viral restriction factors and HPV infection is correlated with development of cervical cancer. There is a close relationship between persistent viral infection, development of cancer and failure in immune response. For example, cervical and vulvar intraepithelial neoplasias are pre-cancerous conditions characterized by sustained HPV-16 infection. A clinical study showed a favourable prognosis related to an increase in IFNγ-producing $CD8^+$ cytotoxic T cells following a robust cell response induced by vaccination (Kenter *et al.*, 2009). Vaccination delivered a high dose of specific antigen for HPV-16 oncoproteins E6 and E7 and mediated MHC-binding peptide complex presentation (Melief & Van Der Burg, 2008). A similar outcome was also observed after vaccination of a preclinical mouse model of HPV-positive cervical cancer (Zwaveling *et al.*, 2002). There is a significant correlation between MHC class I (not MHC class II) expression on malignant cells and T-cell infiltrates (TIL) in human ovarian cancer (Kooi *et al.*, 1996) and is a positive prognostic factor (Hamanishi *et al.*, 2007). An independent study also correlated viral infection with cancer pathology; bioinformatic analysis of gene expression in several lymphoblastic leukaemia types identified a cluster of IFN-induced genes in 40% of patients, corresponding to those leukemic types more susceptible to infection. Similar proportions were found in breast and ovarian cancer analyses. Actually, many of these IFN-stimulated genes are members of the IRDS signature. Additionally, UBE2L6, the ubiquitin/ISG15-conjugating enzyme, is also found amongst these genes (Einav *et al.*, 2005).

Interestingly, ISG15 was also identified as a dominant protein expressed in a IFITM1/IFITM3-IFNγ dependent manner (Figure 5.9 B, D, F and G). Integrating cellular functions between ISG15 and MHC class I, Burks *et al.* proposed that free extracellular ISG15 has anti-tumour properties, promoting increased infusion of MHC class I presenta-

tion molecules on the cell surface in breast cancer cells (Burks *et al.*, 2015).

ISG15 gene expression by IFN type I has been widely explored but there is little experimental work in relation to IFNγ signalling. An ISG15 study revealed that free, as well as conjugated, ISG15 levels are increased upon IFNγ stimulation (Tecalco-Cruz & Cruz-Ramos, 2018). Interestingly, they stimulated breast cancer cells with IFNγ using the same conditions as in the present thesis. ISG15 is coupled to the translation machinery and so it directly conjugates to target proteins that are newly synthesized. Herc5, the E3 ligase for ISG15 conjugation, is proven to be associated with the polysomes. As postulated by Durfee & Huibregtse, ISG15 is able to specifically target a small pool of viral proteins in IFN-stimulated cells. Even if ISG15 conjugates to few viral proteins, that would have major consequences for correct viral protein assembly and activity. To support this hypothesis, they studied the ISGylation of HPV-L1 capsid protein, a viral component of the HPV16 virus and one of the two major viral strains involved in cervical cancer (Durfee *et al.*, 2010). Similarly, HERC5 also restricts HIV-1 infection through ISGylation of viral Gag protein (Woods *et al.*, 2011). These studies suggest that perturbation of IFITM1/IFITM3 protein expression may reduce viral protein ISGylation resulting in decreased cell protection from HPV-16 infectivity, and that in the long term they facilitate cervical carcinogenesis.

One can speculate that interaction of IFITM1/IFITM3 with ISG15 may occur immediately after ISG15 is synthesized, as IFITM1/IFITM3 may be in close association with the ribosomes. In this regard, it has been postulated that ISG15 is also located in the ribosome and actually modifies target proteins (including viral proteins) right after their synthesis. Analysis of global ISGylation by Western blotting analysis has identified a defect in ISG15 conjugation in the absence of IFITM1/IFITM3 proteins (Figure 4.17). Maybe there is less ISG15 expressed under these conditions. Besides contributing to ISG15 synthesis, IFITM1/IFITM3 may also be implicated in the conjugation of target proteins to ISG15.

This experimental work shows that IFITM1/IFITM3 proteins govern, at least partially, the fate of ISG15. In the first place, IFITM1/IFITM3 controls the expression of ISG15 by its protein synthesis. It is still to be determined how absence of IFITM1/IFITM3 protein expression precisely affects the protein synthesis of ISG15 and other ISG proteins from mRNA, such as by exclusion of the mRNA loading into the ribosome or appropriate guidance to the ribosome. For this reason, the next chapter investigates IFITM1/IFITM3-IFNγ dependencies on mRNA production and regulation.

Bringing everything together, IFITM1 and ISG15 may be related at two different cell stages; firstly, IFITM1 affects ISG15 synthesis (Figure 5.9), and secondly, IFITM1 associates with ISG15 (Table 4.2). It is still to be determined if there is a direct interaction or if they form a complex. This study was performed after IFNγ stimulation, but these findings may not be exclusive to type II IFN, and may also happen with other IFN types.

In summary, we investigated to what extent loss of IFITM1/IFITM3 protein expression changed the proteome in a SiHa-IFNγ stimulated cancer cell model panel. Presumably, the perturbation of protein translation machinery would be conferred by a combina-

tion of several proteins. Thus, it is relevant that there is a consistent impairment of IRDS protein expression, particularly HLA-B and ISG15, with depletion of only IFITM1/IFITM3 proteins. This observation has been demonstrated in several experiments in this thesis: IFITM1 siRNA depletion coupled to SWATH-MS (performed in a prior study by Dr Elisabeth Sinclar, section x introduction); SBP-IFITM1 interactomics (chapter 4); and in this chapter by sucrose density gradient ultracentrifugation coupled to SWATH-MS (subsection 5.3.1) and pulse SILAC coupled to Orbitrap-MS (subsection 5.3.2). Additional immunofluorescence assays (subsection 4.3.5) and Western blotting analysis (subsection 5.3.3) support HLA-B and ISG15 protein alterations in absence of IFITM1/IFITM3 protein expression.

To conclude, the evidence suggests that IFITM1/IFITM3 are key regulation factors for the expression of a specific subset of proteins induced in IFNγ signalling. To the best of available knowledge there is only one study that hypothesises IFITM1 being involved in a translational role (Lee *et al.*, 2018) . In that case the study was performed in a virus context where they propose that IFITMs attenuate HIV replication through inhibition of viral protein translation. In this sense, IFITMs may be able to modulate (enhancing or attenuating) particular target proteins according to the cells needs. All-in-all, these findings provide more evidence for the pivotal function of IFITM1 (and IFITM3); expanding the range of IFITM1 roles in cancer pathology and pathogen protection.

Chapter 6

Transcriptomic analysis to identify dominant IFITM1/IFITM3-dependencies in protein expression

6.1 Introduction

In chapter 4, SRSF1 protein was identified as a protein that binds IFITM1 (Table 4.1 and Figure 4.9). This novel interacting partner can guide mRNA to the ribosome. In chapter 5, the analysis of ribosomal integrity showed an impairment of the 80S ribosomal subunit in IFNγ-stimulated *IFITM1/IFITM3* double null cells compared to wt-SiHa cells (Figure 5.3). In addition, there was also a major defect in the production of HLA-B and ISG15 proteins in IFNγ-stimulated *IFITM1/IFITM3* double null cells compared to wt-SiHa cells (Figure 5.9).

Taken together, these results suggest that IFITM1/IFITM3 may be implicated in protein synthesis, but it may also be possible that these observations are a consequence of a reduction in transcript synthesis, and decreased mRNA production would thus decrease the synthesis of protein. To investigate this hypothesis RNA-Seq and RT-qPCR methodologies were applied.

6.1.1 Next Generation Sequencing as a tool to study RNA

The RNA profile is dynamic and highly dependent on physiological and pathological stimuli. So far, many different types of RNA have been identified. Collectively they are categorised as coding and non-coding RNA (Ewing & Green, 2000; Eddy, 2001). Coding RNAs are those species that will ultimately code for a protein. Non-coding RNAs have been further subdivided into many more types of which two representative subtypes are transfer RNA (tRNA) and ribosomal RNA (rRNA), both involved in translation (Eddy, 2001). In some

contexts, the term transcriptome may be defined as all the RNA molecules expressed, including non-coding RNAs. This chapter will study only those polyadenylated and messenger RNA (mRNA) species that encode proteins. Consequently, in this thesis, transcriptome will refer to the polyadenylated and mRNA molecules exclusively.

Multiple methods have been developed to investigate and understand the complexity of RNA species. RNA sequencing (RNA-Seq) is a very powerful tool that allows the study of the transcriptome by accurately measuring gene expression. In addition, RNA-Seq is a deep-sequencing technology that gives information on the RNA sequences. Due to its potential, and the simplified workflows, RNA-Seq is used in a broad range of studies; it is a high-throughput methodology based on next-generation sequencing (NGS), and is composed of a multi-step process where a sample library of RNA is prepared, amplified, and finally sequenced (Figure 6.1) (Buermans & Dunnen, 2014; Dijk *et al.*, 2014).

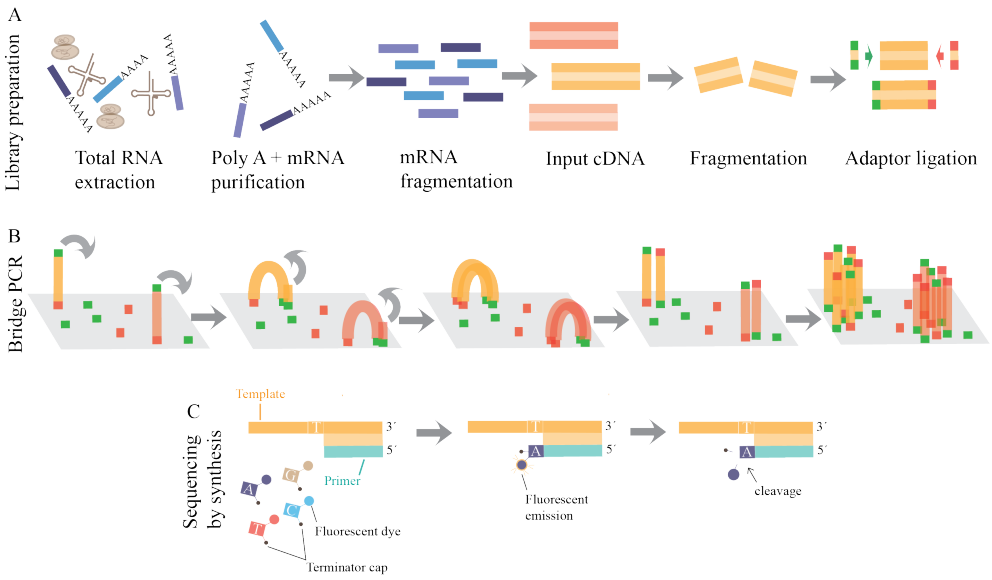

Figure 6.1: Workflow of RNA sequencing by synthesis. The Illumina process is composed of three steps: sample library preparation (A), cluster generation by bridge PCR (B), and sequencing by synthesis (C). Total RNA is extracted and polyadenylated and mRNA transcripts are purified. The input DNA is obtained by reverse transcription and then fragmented. Adaptors are added at the end of the cDNA fragments to allow amplification, and additional motifs are introduced to the adaptors, such as the sequencing binding site and regions complementary to the flow cell oligos (A). Clustering is a process where each fragment molecule is amplified. The cell contains two types of oligos that hybridize with one adaptor of the DNA fragment. A complementary strand will by synthesized by polymerisation. Then, the two fragments are denatured, and the template is washed away. Amplification occurs by bridge PCR, in which a DNA fragment bends over to bind the neighbouring complementary oligo displayed on the flow cell. Next, a polymerase produces two identical copies that are sequentially denatured, resulting in two single stranded copies bound on one end to the flow cell. The process is repeated sequentially for all the clusters of DNA present in the flow cell (B). After the clonal expansion of all the clusters of DNA the sequencing begins. Fluorescent nucleotides are tagged with different dyes and they bind by complementation to the single strand. In each cycle one fluorescent nucleotide will be added and detected when a fluorescence signal is emitted. All clusters are read simultaneously (C). [a]

[a]https://www.illumina.com/documents/products/illumina-sequencing-introductiOn.pdf

6.2 RT-qPCR using SYBR green dye

The real-time reverse transcription polymerase chain reaction (RT-qPCR) is a quantitative technique used to quantify nucleic acids (Gibson *et al.*, 1996). The RNA material must be previously transcribed into complementary DNA (cDNA). This is based on the same principle as PCR, where the DNA is amplified by denaturation, annealing and elongation, but in RT-qPCR, the addition of a fluorescent reporter allows the detection and quantification of the cDNA material in each cycle of amplification (Figure 6.2) (Nolan *et al.*, 2006).

Real-time PCR (qPCR) requires a fluorescent reporter dye to detect the amplified PCR product in each cycle of the reaction. There are many available types of dye to detect and quantify the amplified cDNA. We used SYBR green which is a non-specific detection fluorescent dye that allows the measurement of new strands of DNA in a quantitative manner during each cycle of amplification. The SYBR green probe can only bind to the minor groove of the double stranded DNA (dsDNA). It has a weak binding affinity with ssDNA producing only a very weak green fluorescent signal but when bound to the dsDNA it becomes strongly fluorescent. One disadvantage is that it can also bind to unspecific dsDNA (Pochel *et al.*, 2003)).

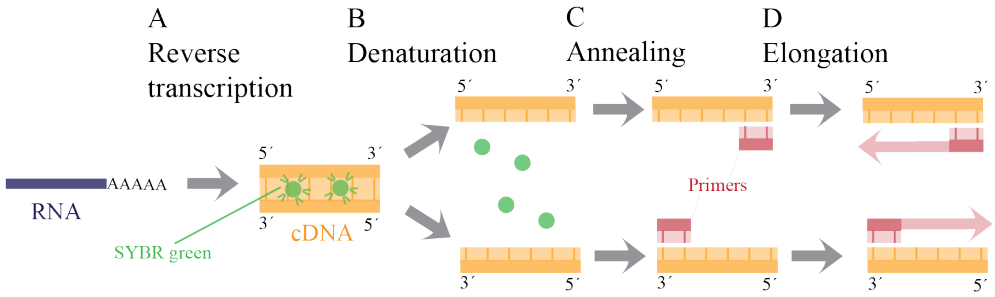

Figure 6.2: RT-qPCR amplification principle. This method has four steps: reverse transcription (A), denaturation (B), annealing (C), elongation (D). Reverse transcriptase takes the initial RNA material as a template to generate complementary DNA (cDNA) (A). The following steps are common to standard PCR. The cDNA is denatured by increasing the temperature to 95ºC to separate the double strand cDNA (B). The next step allows the annealing of the primers to the single strand. One primer is specifically designed to bind by complementation to the forward strand and the other binds the reverse strand. The annealing temperature varies depending on the composition of the primers but typically it is carried out at 55–65ºC. (C). The extension step is carried out around at 72ºC and synthesizes the new complementary cDNA strand (D). Steps (B), (C), and (D) are repeated for several cycles to amplify the starting cDNA material. SYBR green dye fluoresces when it binds to the dsDNA and allows DNA quantification.

SYBR green dye gives a relative quantification of how much cDNA material is present in each cycle of amplification. The amplification curve is a representation of the accumulated synthesised cDNA over the PCR cycles (Figure 6.3). The plot in Figure 6.3 shows the PCR cycle number (x-axis) versus fluorescent signal (y-axis). Each reaction will define a PCR cycle at which fluorescence exceeds an established background fluorescence; this corresponds to the threshold cycle (Ct) (Nolan *et al.*, 2006). Prior to the comparison it is

crucial to normalise the genetic material between samples and remove any technical errors while preparing the samples. For this purpose, the measurement of a housekeeping gene, that is expected to maintain the same expression in all conditions, is included. We used β*-ACTIN*. Relative expression between samples is compared by the cycle in which they reach the threshold (Ct). If the starting material is very low, it will take many cycles to reach the threshold giving a high Ct number.

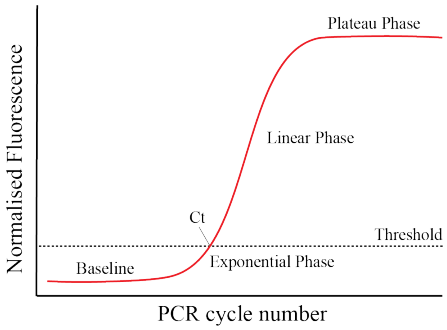

Figure 6.3: Amplification curve. RT-qPCR amplification curve (in red) is divided into four stages: baseline, early exponential phase, linear exponential phase, and plateau phase. In the baseline stage the PCR is in the early cycles and fluorescent signal is below the threshold (dashed line). The early exponential phase is where the signal is just above the threshold, also referred as cycle threshold (Ct). In the linear exponential phase, conditions are optimal and the amplification products double in each cycle. In the plateau phase, there is not enough substrate available and the fluorescent signal stops increasing.

6.3 Aims of the chapter

In this chapter we aim to study whether there is any observable change in the transcriptome when IFITM1/IFITM3 protein expression is lost. RNA-Seq analysis will provide some insights into the expressed genes and whether there are major differences between wt-SiHa cells, *IFITM1* null cells and *IFITM1/IFITM3* double null cells. Relative comparison of the transcripts of interest by RT-qPCR will provide further validation of the analysis.

6.4 Results

6.4.1 Transcriptome analysis of differentially expressed genes after IFITM1/IFITM3 loss

We aimed to investigate whether there are major differences in the transcript expression. RNA-Seq analysis was performed to reveal the global RNA quantity in non-stimulated and IFNγ-stimulated wt-SiHa cells, *IFITM1* null cells, and *IFITM1/IFITM3* double null cells. RT-qPCR technique was used for validation of some transcripts of interest. Figure 6.4 is a representation of the steps followed to extract the RNA and the sample analysis workflow.

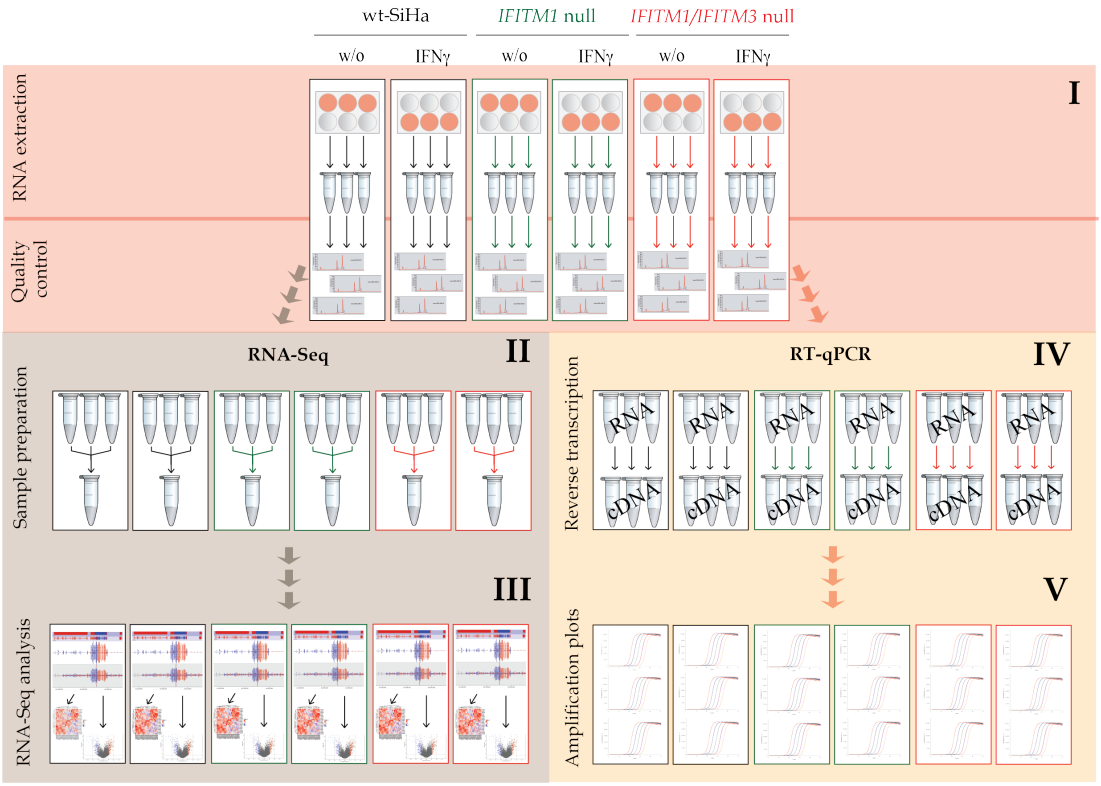

Figure 6.4: Workflow followed to analyse the transcript levels in wt-SiHa cells, *IFITM1* null cells and *IFITM1/IFITM3* double null cells non-stimulated or IFNγ-stimulated for 24 hours. Workflow followed to analyse the transcriptome in wt-SiHa cells, *IFITM1* null cells and *IFITM1/IFITM3* double null cells. RNA was extracted from non-stimulated or IFNγ-stimulated cells. All samples passed the quality control with a RIN number above 7.5 (I). Three biological replicates were used for RNA-Seq analysis (II) and RT-qPCR validation (IV). Equal amounts of RNA were combined and sequenced by Otogenetics. Further steps include mRNA purification and stranded cDNA synthesis; Ilumina sequencing library preparation; and PE100-125 and HiSeq2500 sequencing (II). Amplified sequences were analysed using CLC Genomics Workbench, using GRCh38 as a reference genome (III). Transcripts of interest were further validated by RT-qPCR using the same three biological replicates. For this purpose, the RNA was reverse transcribed into cDNA (IV), and sequentially quantified and compared between samples (V).

The purity of the RNA was assessed after RNA extraction (Figure 6.4 I). Purity and quantity of the RNA are crucial to obtaining high quality results. To ensure optimal conditions, standardization of the RNA quality is obtained by measuring the RNA integrity number (RIN). For this reason, after RNA extraction RNA quality was assessed by measuring RIN values (Figure 6.4 I). Samples were tested by the Sequencing Group, a technical service in the IGMM. The measurement of RNA was carried out in the Agilent 2100 bioanalyzer in combination with the RNA 6000 Nano LabChip. The Figure 6.5 A and B shows the replicate 1 of the *IFITM1* null cells as a representative example of the quality control output.

The RIN is an algorithm for assigning integrity values to RNA measurements (Schroeder *et al.*, 2006). The integrity of RNA is crucial for generating successful gene expression studies and traditionally it has been evaluated using the 28S to 18S rRNA ratio. RIN numbers greater or equal to 7 are considered sufficient, but it is desirable to have RIN

values above 8. In the present study all replicates have a RIN value above 8, except sample 2 *IFITM1* null cells with RIN 7.5 (Figure 6.5 C).

A

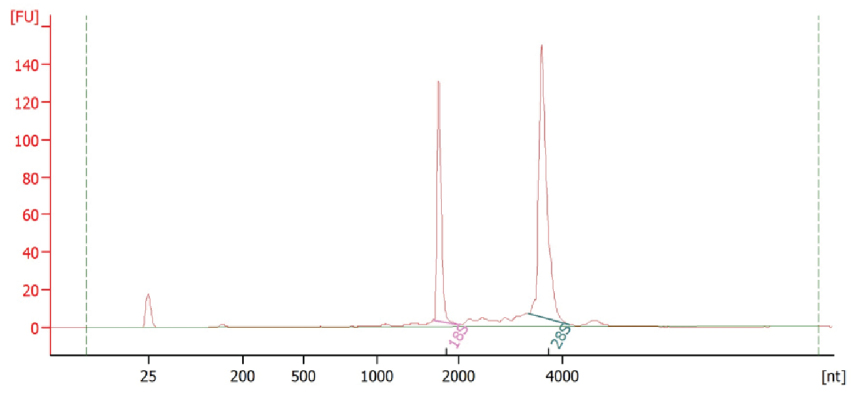

B

Overall Results for sample 1

RNA Area:	370.5	RNA Integrity Number (RIN):	10 (B.02.08)
RNA Concentration:	255 ng/µl	Result Flagging Color:	
rRNA Ratio [28s / 18s]:	1.9	Result Flagging Label:	RIN:10

Fragment table for sample 1

Name	Start Size [nt]	End Size [nt]	Area	% of total Area
18S	1,694	2,006	96.1	25.9
28S	3,336	4,151	180.0	48.6

C

	RIN		RIN		RIN
1 wt-SiHa	9.40	1 *IFITM1* null	10	1 *IFITM1/IFITM3* null	10
2 wt-SiHa	9.80	*2 IFITM1* null	7.5	*2 IFITM1/IFITM3* null	10
3 wt-SiHa	9.90	*3 IFITM1* null	8.40	*3 IFITM1/IFITM3* null	10
1 wt-SiHa +IFNγ	9.80	*1 IFITM1* null +IFNγ	9.70	*1 IFITM1/IFITM3* null +IFNγ	10
2 wt-SiHa +IFNγ	8.50	*2 IFITM1* null +IFNγ	10	*2 IFITM1/IFITM3* null +IFNγ	9.90
3 wt-SiHa +IFNγ	10	*3 IFITM1* null +IFNγ	9.90	*3 IFITM1/IFITM3* null +IFNγ	10

Figure 6.5: Quality control of the total RNA extracted using the Agilent 2100 bioanalyzer. Samples were heated at 70ºC for 2 min and immediately placed on ice prior to quality control analysis. This is based on gel electrophoresis in a chip format. RNA molecules have an intrinsic charge and will be electrophoretically moved and separated by size using a voltage gradient. (A) Electropherogram is displayed by plotting fluorescence intensity versus migration time. (B) Output is also represented as a densitometry plot, resembling a gel. (C) RIN values for each sample.

There are three biological replicates for each condition and all of the samples have RNA concentrations between 150–200 ng/ml. Equal amounts of RNA for each condition were combined in a single Eppendorf tube (Figure 6.4 II). Samples were then processed to RNA-Seq by Otogenetics Corporation (Atlanta, USA). Remaining RNA was stored at -80ºC for future validation by RT-qPCR.

One of the main aims was to investigate whether the loss of IFITM1/IFITM3 expression drastically impacts on gene induction. To address this question, we performed a global study of the transcriptome. Bioinformatic analysis was carried out by Mr Marcos Yébenes Mayordomo (Table B.6). The RNA-Seq analysis was performed using CLC Genomics Work-

bench software (Figure 6.4 III). Transcriptomic analysis is represented in plots comparing two by two the total transcript count (expressed in transcripts per million) in the different conditions (Figure 6.6). All-in-all, there were no major differences between wt-SiHa cells and isogenic *IFITM1* null cells and *IFITM1/IFITM3* double null cells (Figure 6.6 B-E). Interestingly, there was clear gene induction in all three cell lines after IFNγ stimulation (Figure 6.6 A, F and G). Transcripts of *IFITM1, ISG15, HLA-B, STAT-1,* and *IRF1* are also higher after IFNγ-stimulation (Figure 6.6 A, F and G, transcripts are labelled in red).

Loss of IFITM1/IFITM3 protein expression does not decrease transcript induction. On the contrary, most of the highly-induced transcripts after IFNγ stimulation are IFITM1/IFITM3-independent, such as *HLA-DRB1, HLA-DRA, CXCL10* and *GBP5* (Figure 6.6 A vs F and G, transcripts are labelled in black). All of them are well established IFNγ-inducible genes related to tumour immunity or pathogen restriction (Feng *et al.*, 2017; Mach *et al.*, 1996; Soejima & Rollins, 2001). They provided a good internal control to test gene induction after IFNγ-stimulation and emphasised that loss of IFITM1/IFITM3 protein expression is not sufficient to inhibit IFN signalling.

Next, we concentrated on understanding the induction of some transcripts of interest, and in particular the pattern of transcript induction in the IRDS genes (Figure 6.7 A). Overall, there is a clear induction of IRDS genes after IFNγ-stimulation regardless of the expression of IFITM1/IFITM3 proteins (Figure 6.7 A). Some genes are particularly induced after IFNγ stimulation such as M*X1, MX2, OASL, IFIT1*, and *IFIT3*. In contrast, other transcripts, such as *BST2* and *OAS3*, remain similarly induced with or without IFNγ-stimulation. In this case again there is no major difference between wt-SiHa cells, *IFITM1* null cells, and *IFITM1/IFITM3* double null cells.

Moreover, it was investigated the induction of *STAT1, IFITM1, IFITM3, ISG15, IRF1, B2M*, and *HLA-B* (Figure 6.7 B and C). Remarkably, *ISG15* and *IRF1* are highly induced after IFNγ-stimulation. Often, the analysis is done as a sum of all the transcripts identified in the RNA-Seq library. However, there is particular interest in the transcripts that code for proteins as these will ultimately determine the expression of the protein. For this reason, the total transcript was compared to expression of the transcript that codes for the protein (Figure 6.7 B vs C). Overall, the induction remains very similar except in *B2M* where it is much less induced.

Interestingly, *IFITM1/IFITM3* double null cells have a very low induction of IFITM1 and IFITM3 transcripts (Figure 6.7 C). On the contrary, *IFITM1* null cells do induce IFITM1 transcript after IFNγ-stimulation (Figure 6.7 C). Nonetheless, this feature does not imply that IFITM1 protein will be expressed. IFITM3 transcript levels were similar to *IFITM1* null cells compared to wt-SiHa, even after IFNγ-stimulation (Figure 6.7 C).

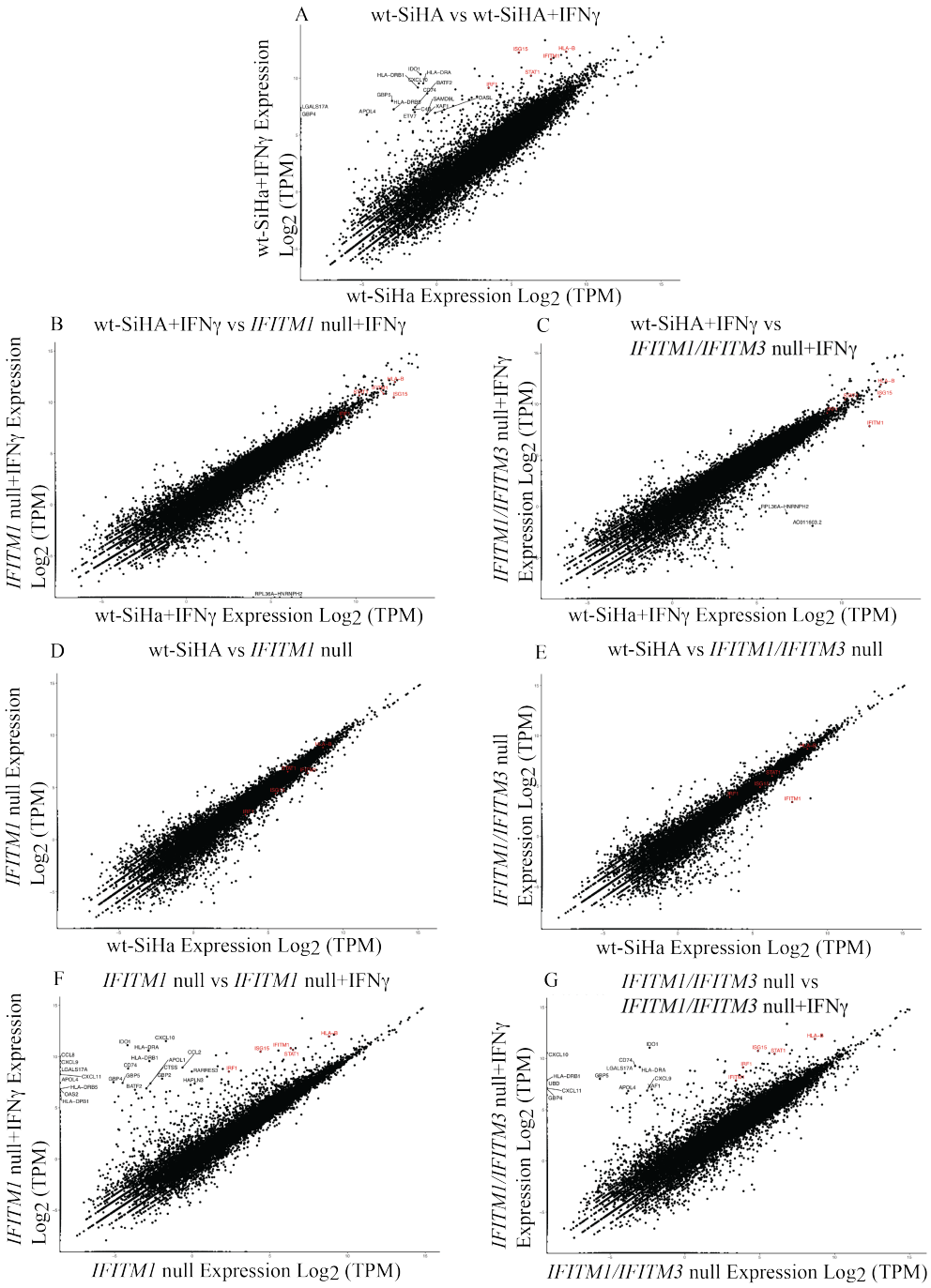

Figure 6.6: Comparison of total transcript count in wt-SiHa cells, *IFITM1* null cells and *IFITM1/IFITM3* double null cells. All transcript reads detected were taken to generate the final transcript count for each gene (Table B.6). Comparisons of all transcripts identified are plotted for the following conditions: (A) non-stimulated wt-SiHa cells vs IFNγ-stimulated wt-SiHa cells, (B) IFNγ-stimulated wt-SiHa cells vs IFNγ-stimulated *IFITM1* null cells, (C) IFNγ-stimulated wt-SiHa cells vs IFNγ-stimulated *IFITM1/IFITM3* double null cells, (D) non-stimulated wt-SiHa cells vs non-stimulated *IFITM1* null cells, (E) non-stimulated wt-SiHa cells vs non-stimulated *IFITM1/IFITM3* double null cells, (F) non-stimulated *IFITM1* null cells vs IFNγ-stimulated *IFITM1* null cells, (G) non-stimulated *IFITM1/IFITM3* double null cells vs IFNγ-stimulated *IFITM1/IFITM3* double null cells. Each plot has highlighted in red *STAT1*, *IFITM1*, *IRF1*, *ISG15* and *HLA-B* transcripts. Other significantly induced transcripts are additionally highlighted in black. Transcript expression is measured in log2 of transcripts per million (TPM).

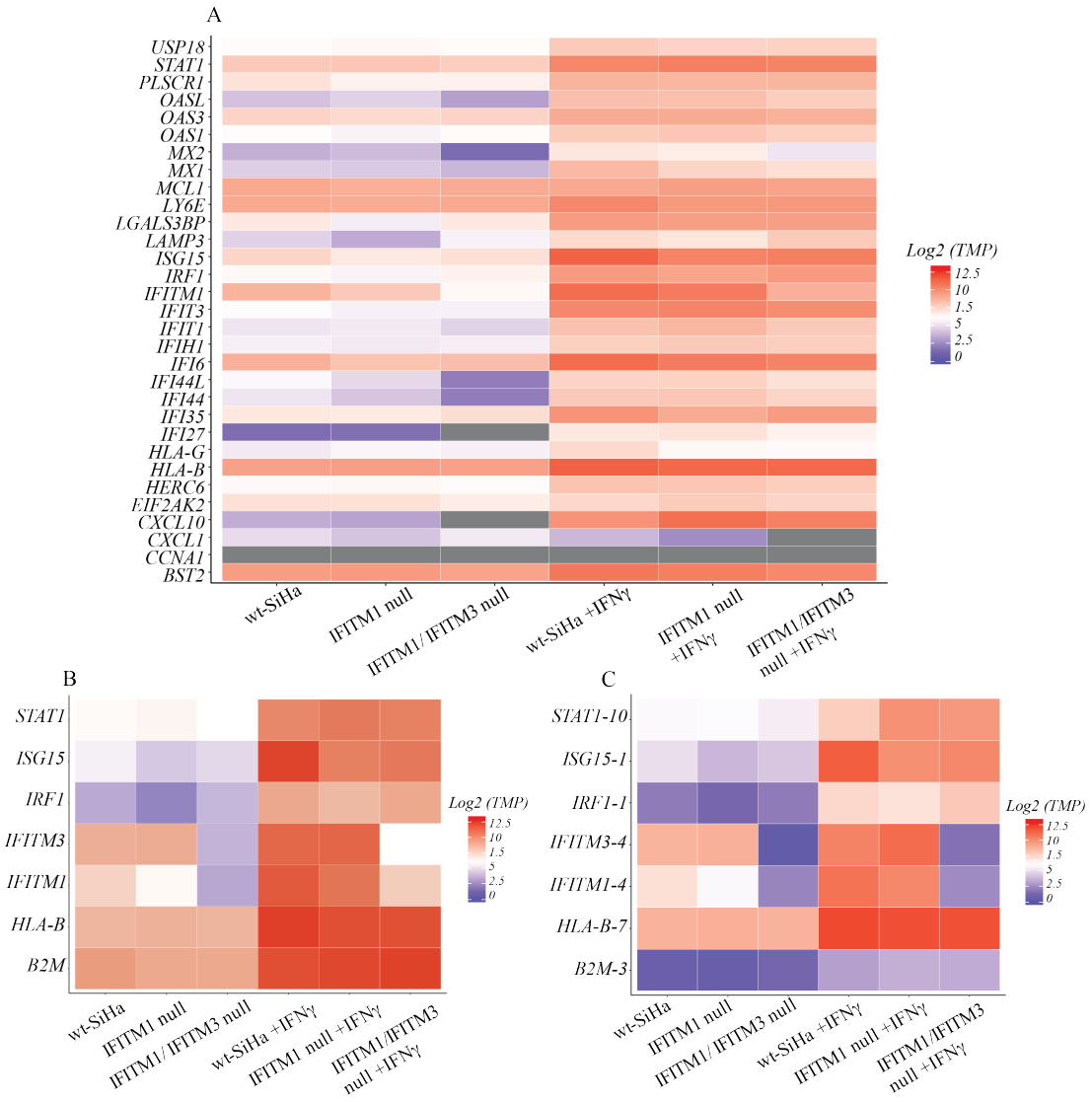

Figure 6.7: Heat map of the IRDS transcripts for wt-SiHa cells, *IFITM1* null cells and *IFITM1/IFITM3* double null cells. (A) Heat map representation of the expression of the 31 IRDS genes. In the y-axis is the transcript expression corresponding to the 31 IRDS genes (Table B.6). Values in grey correspond to genes where the transcript per million (TPM)= 0. (B) Heat map representation of *IFITM1* and *IFITM3* transcripts, the genes that came up less expressed in the absence of IFITM1/IFITM3 protein expression (ISG-15, IRF1, HLA-B), and their controls (STAT1, B2M) (Figure 5.9). (C) Heat map representation of the transcript that translates into the full-length protein for the genes in B. (B and C) In the y-axis there are the transcripts *STAT1, ISG15, IRF1, IFITM3, IFITM1, HLA-B*, and *B2M*. (A, B and C) In the x-axis are represented wt-SiHa cells , *IFITM1* null cells, and *IFITM1/IFITM3* double null cells non-stimulated or IFNγ-stimulated with 100 ng/ml for 24 hours. Colour scale units are log2 (TMP), becoming red when it is highly expressed and purple to blue for non-expressed and under-expressed values.

6.4.2 Quantification of mRNA using real-time RT-qPCR

An RT-qPCR assay was performed to further investigate whether there are transcript differences in our isogenic knock out cervical cell models. The aim was to establish if *ISG15, HLA-B* and *IRF1* transcripts were similarly abundant after loss of IFITM1/IFITM3

proteins compared to wt-SiHa cells, but, the gene selection was also expanded to quantify other gene transcripts. We included *IFITM1* and *IFITM3* to find out if the gene editing in the knock out cells alters mRNA transcription. Additionally, STAT1 and B2M protein synthesis were IFITM1/IFITM3-independent (Figure 5.9). We anticipated that their mRNA levels would remain similar in the absence of IFITM1/IFITM3 protein expression. Finally, *β-ACTIN* was used as housekeeping gene to normalize the output between samples.

Primer design is a crucial step in this assay; primers have to exclusively bind to the region of interest without amplifying non-specific regions. The following parameters were considered while designing the primers: Firstly, primers were designed to the coding region of *IFITM1, IFITM3, IRF1, ISG15, HLA-B, B2M, STAT1*, and *β-ACTIN* genes; additional parameters were that all amplicons were expected to have a product size around 150–250 bp and with a melting temperature difference under 1°C between primers, as multiple genes were run in parallel using the same PCR plates. Primer pairs were designed using available public sequences on ENSEMBL (Table 6.1). Designed primer sequences were checked by BLAST to make sure there were no additional amplicons.

Table 6.1: ENSEMBL accession number of the genes and transcript sequence used to design the primers used in RT-qPCR.

Gene symbol	Gene number	Transcript	Transcript number
IFITM1	ENSG00000185885	*IFITM1-202*	ENST00000408968.4
IFITM3	ENSG00000142089	*IFITM3-201*	ENST00000399808.5
IRF1	ENSG00000125347	*IRF1-201*	ENST00000245414.9
ISG15	ENSG00000187608	*ISG15-201*	ENST00000379389.4
HLA-B	ENSG00000234745	*HLA-B-249*	ENST00000412585.7
B2M	ENSG00000166710	*B2M-204*	ENST00000558401.6
STAT1	ENSG00000115415	*STAT1-201*	ENST00000361099.7
β-ACTIN	ENSG00000075624	*ACTB-201*	ENST00000331789.11

Designing IFITM1 and IFITM3 primers was more complicated as IFITM proteins are highly homologous. Nonetheless, IFITM1 and IFITM3 have a unique C-terminus and N-termius, respectively, and so primers were designed in these regions. Likewise, HLA-B sequence is very similar to the other HLA molecules, but a unique region for HLA-B was carefully selected. RT-qPCR was run under the same conditions for all the different transcripts.

Three technical and three biological replicates were set for each sample condition, the raw Ct values of all samples are listed in Figure 6.8. To allow a stringent analysis, Ct expression values with less than one unit difference between each technical triplicate were used for analysis. Relative Ct expression values were normalised by a housekeeping gene, *β-ACTIN*. Ct values obtained by RT-qPCR (Figure 6.9) were changed into relative expression using the formula $2^{-\Delta Ct}$ where ΔCt is the difference between the Ct of the transcript

A

IFITM1	Ct Technical Replicate		
	1	2	3
1 wt-SiHa	21.5	22.2	22
2 wt-SiHa	21.9	21.9	21.9
3 wt-SiHa	21.6	21.7	21.7
1 wt-SiHa +IFNγ	18	18.2	18.2
2 wt-SiHa +IFNγ	18	17.9	17.9
3 wt-SiHa +IFNγ	16.5	18.1	18.2
1 IFITM1 null +IFNγ	19.3	19.3	18.8
2 IFITM1 null +IFNγ	18.8	18.9	18.8
3 IFITM1 null +IFNγ	19	19.5	19
1 *IFITM1/IFITM3* null	26.5	26.3	26.1
2 IFITM1/IFITM3 null	26.2	26.8	26
3 IFITM1/IFITM3 null	26.2	26	26
1 IFITM1/IFITM3 null +IFNγ	22.1	22.1	22
2 IFITM1/IFITM3 null +IFNγ	23.2	22.1	22.4
3 IFITM1/IFITM3 null +IFNγ	21.3	21.3	21.4

B

IFITM3	Ct Technical Replicate		
	1	2	3
1 wt-SiHa	22	22.3	22.2
2 wt-SiHa	22	23	-
3 wt-SiHa	22.5	22.5	22.5
1 wt-SiHa +IFNγ	21.6	21.8	21.5
2 wt-SiHa +IFNγ	21	20.5	20.8
3 wt-SiHa +IFNγ	21.5	21.3	21.5
1 IFITM1 null +IFNγ	22	22	22.3
2 IFITM1 null +IFNγ	21.4	21.5	21.3
3 IFITM1 null +IFNγ	22	22.3	22
1 *IFITM1/IFITM3* null	36.2	37.1	37
2 IFITM1/IFITM3 null	35.3	36.4	35.8
3 IFITM1/IFITM3 null	26.8	36	36.5
1 IFITM1/IFITM3 null +IFNγ	35	35.9	-
2 IFITM1/IFITM3 null +IFNγ	35	-	36
3 IFITM1/IFITM3 null +IFNγ	33.6	34.3	34.4

C

IRF1	Ct Technical Replicate		
	1	2	3
1 wt-SiHa	33.4	33.6	34.2
2 wt-SiHa	-	33.3	33.9
3 wt-SiHa	33	33.3	33.6
1 wt-SiHa +IFNγ	27.3	37.4	27.4
2 wt-SiHa +IFNγ	28	27.8	27.8
3 wt-SiHa +IFNγ	27.5	27.1	27
1 IFITM1 null +IFNγ	29.7	29	29
2 IFITM1 null +IFNγ	-	29.1	29.1
3 IFITM1 null +IFNγ	28.9	28.7	28.2
1 *IFITM1/IFITM3* null	33.3	32.6	-
2 IFITM1/IFITM3 null	33.3	33.5	33.5
3 IFITM1/IFITM3 null	33	33	33.3
1 IFITM1/IFITM3 null +IFNγ	27.6	27	27.4
2 IFITM1/IFITM3 null +IFNγ	27.8	27.5	28
3 IFITM1/IFITM3 null +IFNγ	27.8	27.7	27

D

ISG15	Ct Technical Replicate		
	1	2	3
1 wt-SiHa	25.5	25.7	25.6
2 wt-SiHa	23.6	25.9	25.1
3 wt-SiHa	25.4	26	25.6
1 wt-SiHa +IFNγ	20.6	20.4	20.3
2 wt-SiHa +IFNγ	20.1	20.3	20.2
3 wt-SiHa +IFNγ	20.5	20.5	20.7
1 IFITM1 null +IFNγ	22.2	22	21.7
2 IFITM1 null +IFNγ	21.2	21.5	21.4
3 IFITM1 null +IFNγ	22	21.9	22.2
1 *IFITM1/IFITM3* null	27.5	27.4	27.3
2 IFITM1/IFITM3 null	27.5	27.4	27.3
3 IFITM1/IFITM3 null	27	27	27
1 IFITM1/IFITM3 null +IFNγ	21.9	21.6	21.7
2 IFITM1/IFITM3 null +IFNγ	22.1	21.9	22
3 IFITM1/IFITM3 null +IFNγ	21.3	20.6	21.7

E

HLA-B	Ct Technical Replicate		
	1	2	3
1 wt-SiHa	22.4	22.8	22.8
2 wt-SiHa	23.2	23.6	23.6
3 wt-SiHa	23	23	23
1 wt-SiHa +IFNγ	21	20.5	20.2
2 wt-SiHa +IFNγ	20	20	19.3
3 wt-SiHa +IFNγ	19.6	20.4	20
1 IFITM1 null +IFNγ	21.7	21	21
2 IFITM1 null +IFNγ	20.6	20.6	20.2
3 IFITM1 null +IFNγ	21	21	21
1 *IFITM1/IFITM3* null	24.1	24.1	24
2 IFITM1/IFITM3 null	24	23.9	23.9
3 IFITM1/IFITM3 null	23.8	23.8	23.3
1 IFITM1/IFITM3 null +IFNγ	21.2	21	20.7
2 IFITM1/IFITM3 null +IFNγ	21.5	21.3	21.4
3 IFITM1/IFITM3 null +IFNγ	20	19.9	19.9

F

B2M	Ct Technical Replicate		
	1	2	3
1 wt-SiHa	20.8	20.9	21
2 wt-SiHa	21.4	21.1	20.9
3 wt-SiHa	21.3	21.2	22.2
1 wt-SiHa +IFNγ	18	18.1	18.3
2 wt-SiHa +IFNγ	18.3	18	18
3 wt-SiHa +IFNγ	8.4	18.5	18.5
1 IFITM1 null +IFNγ	18.7	18.4	18.6
2 IFITM1 null +IFNγ	18.5	18.6	18.5
3 IFITM1 null +IFNγ	18.2	18.4	18.5
1 *IFITM1/IFITM3* null	21.8	21.5	21.7
2 IFITM1/IFITM3 null	22.3	22.1	21.8
3 IFITM1/IFITM3 null	21.7	21.3	21.4
1 IFITM1/IFITM3 null +IFNγ	19	18.9	18.8
2 IFITM1/IFITM3 null +IFNγ	18.6	18.6	18.7
3 IFITM1/IFITM3 null +IFNγ	18.8	18.7	18.4

G

STAT1	Ct Technical Replicate		
	1	2	3
1 wt-SiHa	22.1	22.5	22.7
2 wt-SiHa	23.8	24	24.7
3 wt-SiHa	23	22.6	22.9
1 wt-SiHa +IFNγ	20.5	20.3	20.3
2 wt-SiHa +IFNγ	19	19.3	19.4
3 wt-SiHa +IFNγ	20.1	20.1	20.2
1 IFITM1 null +IFNγ	20.9	20.9	20.9
2 IFITM1 null +IFNγ	20.4	20.1	20
3 IFITM1 null +IFNγ	21.2	21	21.6
1 *IFITM1/IFITM3* null	25.7	25.6	24.8
2 IFITM1/IFITM3 null	25.5	25.8	25
3 IFITM1/IFITM3 null	24.9	24.8	24.8
1 IFITM1/IFITM3 null +IFNγ	21	21.1	21
2 IFITM1/IFITM3 null +IFNγ	21.1	21.5	21.2
3 IFITM1/IFITM3 null +IFNγ	18.5	18.3	19.1

H

β –ACTIN	Ct Technical Replicate		
	1	2	3
1 wt-SiHa	13.4	13.5	13.6
2 wt-SiHa	14.3	14.7	14.4
3 wt-SiHa	14	13.7	13.7
1 wt-SiHa +IFNγ	16.7	17	17.1
2 wt-SiHa +IFNγ	16	16.1	16.2
3 wt-SiHa +IFNγ	17.1	17	17.2
1 IFITM1 null +IFNγ	16.9	16.9	16.7
2 IFITM1 null +IFNγ	16.4	16.3	16.1
3 IFITM1 null +IFNγ	17.4	17.2	17
1 *IFITM1/IFITM3* null	15.6	15.9	-
2 IFITM1/IFITM3 null	15.2	14.9	14.8
3 IFITM1/IFITM3 null	14.5	14.4	14.5
1 IFITM1/IFITM3 null +IFNγ	17.7	16.7	17.7
2 IFITM1/IFITM3 null +IFNγ	17.9	17.8	17.9
3 IFITM1/IFITM3 null +IFNγ	15.7	15.6	15.4

I

β –ACTIN (IRF1)	Ct Technical Replicate		
	1	2	3
1 wt-SiHa	18	18	17.5
2 wt-SiHa	18.3	18.4	18.3
3 wt-SiHa	17.8	17.9	19
1 wt-SiHa +IFNγ	20	20.2	20
2 wt-SiHa +IFNγ	19.8	19.8	19.6
3 wt-SiHa +IFNγ	19.6	19.6	20
1 IFITM1 null +IFNγ	19.5	19.6	19.4
2 IFITM1 null +IFNγ	19.2	19.5	19.4
3 IFITM1 null +IFNγ	19.4	19.3	19.2
1 *IFITM1/IFITM3* null	18	18	17.8
2 IFITM1/IFITM3 null	17.8	18	17.9
3 IFITM1/IFITM3 null	17.8	17.4	17.8
1 IFITM1/IFITM3 null +IFNγ	20.4	20.6	20.5
2 IFITM1/IFITM3 null +IFNγ	19.8	20.5	20.5
3 IFITM1/IFITM3 null +IFNγ	20.1	20.5	20.5

J

	Ct Technical Replicate			
	1	2	3	
1 *IFITM1* null	24.3	23.8	23.8	IFITM1
2 IFITM1 null	24	24	24.1	
3 IFITM1 null	24.1	24	24.1	
1 *IFITM1* null	25	-	25	IFITM3
2 IFITM1 null	25.1	26.1	26	
3 IFITM1 null	27.2	27.7	-	
1 *IFITM1* null	36.9	36.5	36	IRF1
2 IFITM1 null	36.8	36.7	36.2	
3 IFITM1 null	37.3	37.5	37.4	
1 *IFITM1* null	27.6	27.3	27.3	ISG15
2 IFITM1 null	27.5	27.3	27.4	
3 IFITM1 null	27.5	27	27.4	
1 *IFITM1* null	22.8	22.7	22.8	HLA-B
2 IFITM1 null	22.9	22.6	22.6	
3 IFITM1 null	22.8	22.8	23	
1 *IFITM1* null	22	22.2	22.1	B2M
2 IFITM1 null	22.4	22.1	22.1	
3 IFITM1 null	22.1	22.2	22.3	
1 *IFITM1* null	26	26.1	26	STAT1
2 IFITM1 null	26.2	26.1	26.1	
3 IFITM1 null	26.5	26.3	26.2	
1 *IFITM1* null	18.8	19	19	β –ACTIN
2 IFITM1 null	19.1	19.1	18.9	
3 IFITM1 null	19.4	19.3	19.2	

Figure 6.8: Cycle threshold values. Ct values for three biological replicates in *IFITM1* (A and I), *IFITM3* (B and I), *IRF1* (C and I), *ISG15* (D and I), *HLA-B* (E and I), *B2M* (F and I), *STAT1* (G and I), and *β-ACTIN* (H, I, and J) genes. Columns 1, 2 and 3 correspond to three technical replicates. Replicate with a Ct value one unit different from the other two replicates were excluded from the analysis (indicated as -).

of interest and the Ct of *β-ACTIN* (Figure 6.8).

The results show good reproducibility as the Ct is very similar between replicates (Figure 6.8). As a consequence, the standard deviation between triplicates is very low in most of the genes studied (Figure 6.10). This feature gives more power to the RNA-Seq analysis where a combination of all three biological replicates were run as a single sample (Figure 6.6).

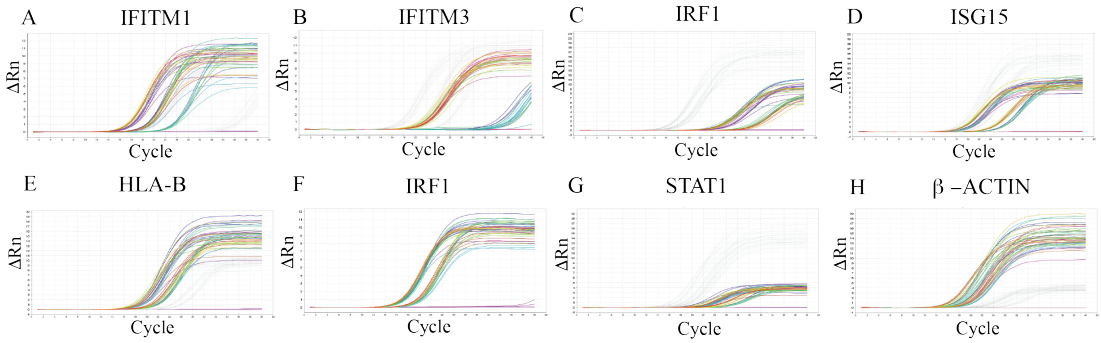

Figure 6.9: Amplification plots. Amplification plots in *IFITM1* (A), *IFITM3* (B), *IRF1* (C), *ISG15* (D), *HLA-B* (E), *B2M* (F), *STAT1* (G), and *β-ACTIN* (H) genes. The x-axis shows the Ct cycle and the y-axis (ΔRn) represents the fluorescence emitted by the SYBR safe reporter. Each coloured line represents a single sample (triplicates are grouped in one colour). Basal purple line corresponds to the negative control where there was no cDNA (template).

Overall, the transcript content is very low without stimulation and rapidly increases after IFNγ stimulation (Figure 6.10 A-G, three first columns vs three last columns). As expected, *STAT1* and *B2M* are responsive to IFNγ-stimulation in wt-SiHa cells (in black) as well as *IFITM1* null cells (in green) and *IFITM1/IFITM3* double null cells (in red) (Figure 6.10 A and G). This observation denotes that loss of IFITM1/IFITM3 protein expression does not affect the gene induction of *STAT1* and *B2M* after IFNγ stimulation. *ISG-15* is also more abundant after IFNγ stimulation and is especially inducible in wt-SiHa cells (in black) compared to *IFITM1* null cells (in green) and *IFITM1/IFITM3* double null cells (in red) (Figure 6.10 D).

Remarkably, *HLA-B* mRNA is very abundant in the non-stimulated *IFITM1* null cells and does not increase after IFNγ stimulation. In comparison, *HLA-B* mRNA in *IFITM1/IFITM3* double null cells is sensitive to IFNγ stimulation (Figure 6.10 F). Likewise, a similar effect is seen in *IRF-1* mRNA (Figure 6.10 E).

Interestingly, *IFITM1* mRNA is detected in *IFITM1* null cells and increases after IFNγ-stimulation (Figure 6.10 B, green bars). Nonetheless, it is not as inducible as in wt-SiHa cells (Figure 6.10 B, black bars). *IFITM3* mRNA levels are similar in wt-SiHa cells compared to *IFITM*1 null cells (Figure 6.10 C, black bars vs green bars). Loss of *IFITM1* does not affect the *IFITM3* mRNA transcription and IFNγ-stimulation.

Furthermore, *IFITM1* mRNA is barely observed in non-stimulated cells and only slightly induced after IFNγ-stimulation in *IFITM1/IFITM3* double null cells (Figure 6.10 B,

red bars). In the same way, *IFITM3* mRNA is almost undetected in non-stimulated cells and slightly induced after IFNγ-stimulation in *IFITM1/IFITM3* double null cells (Figure 6.10 C, red bars).

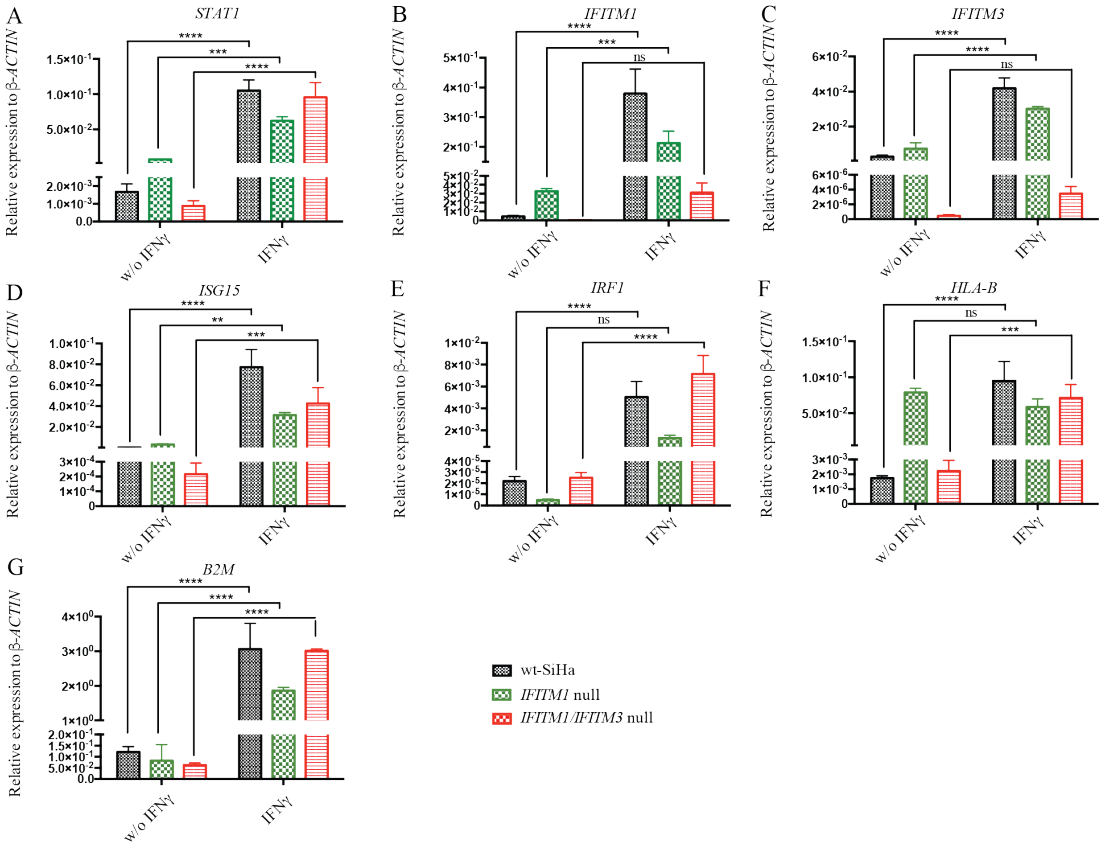

Figure 6.10: Validation of the transcript levels of IFNγ-stimulated genes of interest in wt-SiHa cells, *IFITM1* null cells and *IFITM1/IFITM3* double null cells non-stimulated or IFNγ-stimulated for 24 hours. *STAT1* (A), *IFITM1* (B), *IFITM3* (C), *ISG15* (D), *IRF1* (E), *HLA-B* (F), *B2M* (G) mRNA quantification by RT-qPCR in wt-SiHa (in black), *IFITM1* null (in green) and *IFITM1/IFITM3* double null (in red) cells. Measurements were performed in non-stimulated cells and after stimulation with IFNγ for 24 hours. Error bars are a representation of the variability between three biological replicates. Each biological sample was run in three technical replicates. β*-ACTIN* was used to normalise the mRNA expression between samples. Statistical study was performed with two-way ANOVA and Bonferroni correction (****p < 0.0001; ***p < 0.001; ** p <0.01; ns, not significant).

6.4.3 Study of the IFITM1/IFITM3 association to mRNA

Results from the previous section suggest that global gene induction by IFNγ is not compromised in the absence of IFITM1/IFITM3 protein expression. Nonetheless, it is still unclear if IFITM1/IFITM3 has some effect on the guidance of the mRNA to the ribosome. Given that IFITM1/IFITM3 associates with the splicing factor SRSF1 (Figure 4.9), we aimed to investigate whether it is possible that IFITM1/IFITM3 proteins associate with mRNA. To study the protein:RNA complexes we took advantage of RNA *in situ* hybridization–PLA methods (Zhang *et al.*, 2016). It follows the same principle as PLA (described in Figure 4.8)

but includes an additional first step in which a biotinylated DNA probe hybridizes to the mRNA of interest (Figure 6.11).

As HLA-B is one of the main proteins depleted in the absence of IFITM1/IFITM3 protein expression, we designed a specific probe to hybridize with the *HLA-B* mRNA. Additionally, interaction between *ISG15* mRNA and IFITM1/3 protein was also studied. There was no significant signal identified (data not shown).

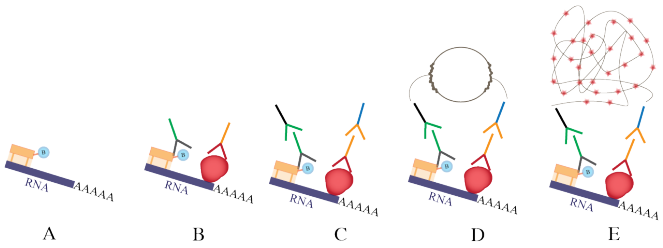

Figure 6.11: Principle of RNA *in situ* Hybridization–PLA. (A) The mRNA of interest is annealed with a specifically designed probe that is complementary to its sequence to create a double stranded DNA:RNA hybrid. The DNA probe is biotinylated to allow its detection. (B) Binding of the specific primary antibodies (of different species) to the proteins of interest (i.e. mouse anti-IFITM1/IFITM3 and rabbit anti-Biotin). (C) Binding of the secondary antibody, named as probe MINUS (mouse) and PLUS (rabbit). (D) Proteins closer than 30–40 nm will allow oligos to hybridize and amplify by rolling circular amplification. (E) Further amplification and increase of the signal by adding a fluorophore labelled probe.

Regarding IFITM1/3:*HLA-B* protein:RNA interaction in wt-SiHa cells, the negative control without primary antibody (Figure 6.12 B) and the negative control without secondary antibody (Figure 6.12 C) showed no signal. On the contrary, it was not easy to quantify the signal in the negative control without RNA probe (Figure 6.12 A) as there was some background. To show the true positive signal in Figure 6.12, the exposure time was set when the signal was completely absent in the negative control without RNA probe (Figure 6.12 A). A significant protein:RNA association was observed in the IFNγ-stimulated wt-SiHa cells (Figure 6.12 E and K) and not observed in the IFNγ-stimulated *IFITM1/IFITM3* double null cells (Figure 6.12 J and L).

These data suggest that IFITM1/IFITM3 associate with *HLA-B* mRNA after IFNγ stimulation. This serves as a proof of concept that IFITM1/IFITM3 may be playing a role in the RNA guidance to the ribosome. In fact, IFITM1/IFITM3 proteins might also associate with other transcripts, but this possibility has not been further explored.

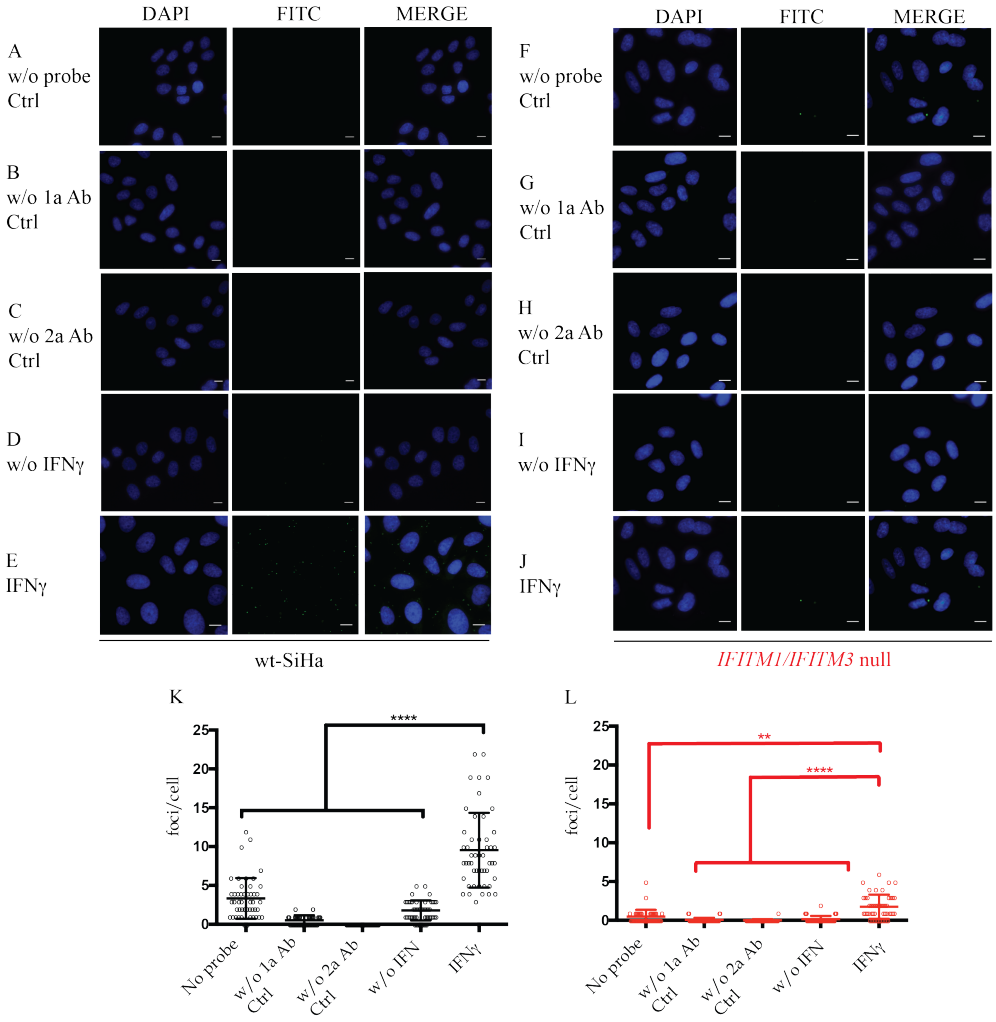

Figure 6.12: Evaluation of the IFITM1/IFITM3:*HLA-B* protein-RNA interaction *in situ* after stimulation with IFNγ by rISH–PLA. RNA in situ hybridization–PLA assays were used to study the endogenous interaction between *HLA-B* mRNA and IFITM1/IFITM3 proteins in wt-SiHa cells (A–E) and *IFITM1/IFITM3* double null cells (F-J). *HLA-B* mRNA was detected with a biotinylated probe. FITC images identify the protein–RNA association foci (green) and DAPI was used for nuclear staining (blue). (A–C and F-H) Cells were incubated as negative controls; without the RNA probe (A and F), using primary antibodies only (B and G), or secondary antibodies only (C and H). (D and I) Cells were incubated with both IFITM1/IFITM3 and biotin antibodies to define protein–RNA foci in non-stimulated cells. (E and J) Cells were incubated with both IFITM1 and biotin antibodies to define protein–RNA foci in IFNγ-stimulated cells. Representative quantification of the protein–RNA interaction foci per cell in presence or absence of IFNγ stimulation in wt-SiHa cells (K) and *IFITM1/IFITM3* double null cells (L). At least 50 cells were counted in each condition. Statistical study was performed with one-way ANOVA and Bonferroni correction (****$p < 0.0001$). n=3. Scale bar: 10 μm.

6.5 Discussion

In the previous chapter we showed that loss of IFITM1/IFITM3 protein expression attenuates the protein synthesis of HLA-B and ISG15. There are many reasons why this can happen. For instance, it could be a reduction of the gene induction, degradation of the mRNA or misguiding mRNA to other subcellular locations. At that time, we had no information about the mRNA abundance in the wt-SiHa, *IFITM*1 null or *IFITM1/IFITM3* double null cells. For this reason, the first question addressed was to establish if there were any major differences in the transcriptomes of wt-SiHa cells compared to *IFITM1* null cells and *IFITM1/IFITM3* double null cells.

The RNA-Seq analysis showed no major differences in the transcriptome of *IFITM1* null cells or *IFITM1/IFITM3* double null cells compared to wt-SiHa cells (Figure 6.6). In addition, a similar phenomenon was observed with the IRDS genes, where most of the genes were equally induced regardless of the expression of IFITM1/IFITM3 proteins (Figure 6.7 A). Similarly, *ISG15* and *HLA-B* transcripts are induced after IFNγ-stimulation in wt-SiHa cells as well as in the isogenic *IFITM1* and *IFITM1/IFITM3* knock out cells. Therefore, it seems that transcript synthesis is not the limitation resulting in defective expression of ISG15 and HLA-B proteins (Figure 5.9).

IFITM1/IFITM3 proteins are responsible for modulating, at least partially, the protein expression of HLA-B and ISG15. There are many possibilities by which their mRNA is not translated into protein; translation repression as well as mRNA decay are two key factors in gene expression. For a long time, scientific efforts have concentrated on how transcription regulation functions, but posttranscriptional regulation is equally important in determining the fate of the nascent mRNAs. The mRNA is protected from exonuclease attack by the 5' 7-methylguanosine cap and the 3' poly(A) tail. Nonetheless, the mRNA decay pathway is able to recognise and eliminate aberrant mRNAs (Garneau *et al.*, 2007).

But this does not seem to be the case: the evidence suggests that IFITM1/IFITM3 modulates HLA-B at the translational level. On the one hand, there is no detectable difference in *HLA-B* gene induction between wt-SiHa cells, *IFITM1* null cells and *IFITM1/IFITM3* double null cells in our study. In fact, *HLA-B* mRNA in non-stimulated *IFITM1* null cells is highly abundant (Figure 6.10 F). But looking at protein synthesis, there is a large inhibition by IFITM1/IFITM3 proteins (Figure 5.9). Therefore, the data suggests that the inhibition of HLA-B synthesis is regulated during translation. Even though the mechanism is not completely understood, translation is usually regulated at the initial stage, at which it is clear that eIFs factors, but also RNA-binding proteins, play a fundamental role. The stabilization of the mRNA on polysomes is essential to activate the translation and, interestingly, IFITM1/IFITM3 are localised at the ribosomal subunits (Figure 5.5 B) (Jackson *et al.*, 2010).

The RT-qPCR assay is an efficient, sensitive and specific method to quantify the mRNA abundance of particular genes. Based on this technique, we have reasons to believe that *IFITM1* and *IFITM3* mRNA in the knock out cells are transcribed. It is possible that the

CRIPSR indel, in the respective knock out cell lines, does not inhibit completely the transcription of the *IFITM1* and *IFITM3* genes. In fact, cells are able to compensate genetic mutations by upregulating the transcription of related genes or the mutated gene itself (El-Brolosy *et al.*, 2019). But somehow the aberrant mRNA is not being translated or at least not functional.

The cell has multiple mRNA-surveillance mechanisms to specifically recognise and degrade aberrant mRNA, for instance the recognition of a premature stop codon. In fact, CRISPR/Cas9 indels for IFITM1 in *IFITM1* null cells and IFITM3 in *IFITM1/IFITM3* double null cells do contain premature stop codon sequences (Figure 3.6 and Figure 3.9). Presumably, the aberrant mRNA associates with the ribosome but gets stalled upon recognition of the premature termination codon. The SURF complex is implicated in the recognition and dissociation of the aberrant mRNA from the ribosome and facilitates its degradation (Garneau *et al.*, 2007). This could explain why we are able to detect *IFITM1* and *IFITM3* transcripts (Figure 6.10 B and C) but their protein synthesis is inhibited (Figure 5.9).

This does not apply to the *IFITM1* gene that has an intron deletion in the *IFITM1/IFITM3* double null cells. An alternative process must be happening. It is important to highlight that transcription, splicing machinery and nonsense-mediated decay pathways are closely interconnected. On this note, the intron deletion may alter the natural processes of transcription initiation and the pre-mRNA maturation to mRNA(Chorev & Carmel, 2012). In fact, intron sequence *per se* can have an inherent role in transcription initiation being able to modulate the gene expression (Vasil *et al.*, 1989). For instance, it may change the exon-junction complexes whose formation is required to facilitate recruitment of export factors and is implicated in mRNA degradation via nonsense-mediated decay (Popp & Maquat, 2016). Another possibility is that intron loss changes the natural 3D structure of the gene, affecting its folding and impacting on the processing and maturation of the mRNA, generating a faulty transcript (Wang *et al.*, 2013).

All-in-all, the evidence suggests that there is a selective mRNA exclusion at the ribosome that inhibits the translation of particular transcripts such as *ISG15* and *HLA-B*. In addition, IFITM1/IFITM3 proteins are mRNA-binding proteins for the *HLA-B* transcript (Figure 6.12).

Chapter 7

Final remarks

IFITM1 is implicated in multiple types of cancer. However, the molecular implications of this phenomenon are not well characterized. The focus of this project was to expand our limited understanding of the cellular role of IFITM1. Previous work with immunohistochemical staining of FFPE cervical cancer tissue identified a distinct subgroup of cervical cancer patients where IFITM1/IFITM3 protein expression inversely correlates to metastasis. From there, we aimed to understand why patients who are IFITM1/IFITM3 double negative are also susceptible to developing aggressive tumours. As IFITM1 is the main isoform described as a pro-oncogene, we started studying its interactome (chapter 4). During the course of this study, we realized that IFITM1 and IFITM3 are closely related, orchestrating overlapping functions and/or having synergistic effects, thus we needed to study both proteins together. Some experimental work on this matter was done in our group prior to the present study; SWATH–MS proteomic screens in cervical cancer cells treated with IFITM1-targeted siRNA resulted in the attenuation of an IFN regulated protein subpopulation including MHC class I molecules (Figure 3.2).

Initially, SiHa cells were chosen as a cancer cell model as they had highly activated effectors of the IFNγ signal transduction pathway, including IFITM1/IFITM3 proteins. Remarkably, these human-derived cells from cervical cancer are infected by HPV-16 virus. The study of IFITM1/IFITM3 proteins as restriction factors was not our focus of interest, nevertheless the fact that these cells are infected may have an impact on the cancer progression, where persistent infection may lead to a sustained low activation of IFN signalling (Cheon & Stark, 2009; Cheon *et al.*, 2011). Notoriously, this is a favourable context where an IRDS signature could be induced. However, it is difficult to provide direct evidence to support this argument.

This thesis has begun to unravel new underlying cellular functions for IFITM1 by studying its interactome. SRSF1 was identified as one of the major binding partners for IFITM1 (Table 4.1). Even though we did not continue studying the cellular implications of this interaction, it provided some evidence to prompt a study of IFITM1 function in protein biogenesis on the ribosome (chapter 4). Ultracentrifugation sedimentation analysis of

cell lysates from IFNγ-stimulated wt-SiHa cells and *IFITM1/IFITM3* double null cells was carried out to isolate ribosomal constituents. The results suggested a specific role for IFITM1/IFITM3 in regulating the integrity of the 80S ribosomal subunit (chapter 5). The subcellular localization of IFITM1/IFITM3 in the ribosome (Figure 5.5 B and Figure 5.6) prompted an analysis of IFNγ-dependent protein synthesis using pulse SILAC-MS (Figure 5.8 and Figure 5.9). It was identified that ISG15 and MHC class I synthesis, particularly HLA-B, requires IFITM1/IFITM3-IFNγ-mediated signal transduction (chapter 5). To consolidate the results, HLA-B as well as ISG15 were identified as major interacting partners for IFITM1 (Table 4.2). Additional experimental work conducting immunohistochemistry and proximity ligation assays indicated that HLA-B interacts with IFITM1/IFITM3 in wt-SiHa cells and that HLA-B induction was attenuated in the *IFITM1/IFITM3* double null cells (chapter 4). In the case of ISG15, it was not possible to study its association with IFITM1/IFITM3 by the same techniques. Nonetheless, it was noted that in the absence of IFITM1/IFITM3 protein expression there is a decrease in global ISGylation (Figure 4.17).

Further analysis of the transcriptome in wt-SiHa cells compared to the knock out cell lines did not find any remarkable inhibition in the synthesis of the *HLA-B* mRNA (Figure 6.10 F). Thus, it seems as though the abundance of the *HLA-B* mRNA is not a limiting factor when IFITM1/IFITM3 proteins are not expressed. Similarly, *ISG15* mRNA is also present in the knock out cells (Figure 6.10 D).

Our findings also emphasize the importance of IFITM1/IFITM3 in increasing HLA-B expression and that would greatly impact on the global number of neo-antigens presented to $CD8^+$ T cells, otherwise promoting immune-escape. In a broad cellular context, impairment of antigen presentation complexes by decreasing the MHC class I expression may lead to an aberrant recognition of oncopeptides by the $CD8^+$ T cell, causing immunotherapy failure, promoting immune evasion, and leading to metastatic events. In other words, it may be possible that absence of IFITM1/IFTITM3 could contribute to acquisition of a new cellular mechanism to decrease MHC class I molecules, resulting in immunotherapy resistant tumours.

In fact, the identification of tumour-specific antigens, suitable to be good immunotherapeutic targets, has generated great interest. But this effect relies on the premise that HLA phenotypes remain unaltered and so optimal antigen presentation is required to effectively eliminate cancer cells via cytotoxic T lymphocyte activation. The principle of immunotherapy is to activate specifically those tumour-specific T cells that ultimately will be able to target and eliminate tumour cells. Cancer vaccines that boost CTL-mediated cytolysis will be effective if key effectors remain fully active. For instance, some cancer vaccines are designed to increase $CD4^+$ and $CD8^+$ T-cell populations capable of recognising tumour-associated antigens (Guo *et al.*, 2013). On the contrary, immune check points are largely dysregulated in cancer; tumours adapt rapidly to their microenvironment and so develop strategies to escape immune surveillance and propagate. For instance, several tumours are able to decrease MHC class I expression (Garrido *et al.*, 2010; Restifo *et*

al., 2002); evidence of this is found even in spontaneously originating tumours (Garrido *et al.*, 1997). In contrast, several tumours consistently upregulate nonclassical MHC class I molecules such as HLA-E which prevents NK-tumour cell recognition, and so they evade cell lysis (Monaco *et al.*, 2011). Therefore, it is crucial to define the underlying cellular and molecular signalling targets for immunotherapy. A lack of understanding of how some tumour subclones become resistant as a result of bypassing natural immune pathways leads to therapeutic failure.

HLA-B depletion greatly correlates with the proposed natural selection mechanism to successfully promote tumour immune-evasion (Khong & Restifo, 2002). Tumour heterogeneity by genomic instability is a property widely spread in all cancer types. Those traits that confer a positive advantage over other tumour variants will be selected and so only these will undergo clonal expansion. In fact, suppression of the HLA-B locus is observed in multiple colon cancer cell types (Soong & Hui, 1992). Further *in silico* analysis identified loss of heterozygosity in HLA haplotypes in non-small-cell lung cancers. Evidence suggests that it is a result of positive advantage in the face of strong tumour selection by microenvironmental pressure (Algarra *et al.*, 1997; Cabrera *et al.*, 1996). Actually, tumour evasion mechanisms are in concordance with the study of how viruses also escape from being eradicated by the immune system. It would seem logical to predict that immune recognition and destruction of tumour cells and viruses are active in both cases.

From the cervical cancer perspective, MHC class I depletion is not correlated with HPV positive tissues (Connor & Stern, 1990; Cromme *et al.*, 1993). It is suggested that these events originated at different stages of the cervical cancer progression. On the contrary, independent studies have identified impaired MHC class I expression in cervical tumours (and other cancer types), particularly loss of MHC class I in metastatic lesions compared to primary tumours (Honma *et al.*, 1994; Torres *et al.*, 1993), including chromosomal aberrations (Koopman *et al.*, 2000; Vermeulen *et al.*, 2005). This is of particular relevance for this thesis as it consolidates the hypothesis that IFITM1 is able to regulate, at least partially, the expression of MHC class I. Remarkably, several studies revealed HLA expression deficiencies in lymph node metastases, compared with primary tumours (Cromme *et al.*, 1994; Ferns *et al.*, 2016; Hilders *et al.*, 1995), which fits with the idea that lack of IFITM1/IFITM3 would lead to diminished HLA expression, as seen in Figure 4.16.

In summary, these data provide a novel biochemical pathway that correlates with the IFN-responsive nature of IFITM1. It can mediate IFNγ-dependent protein production of MHC class I proteins as well as ISG15, whilst the maintenance of STAT1 protein in response to IFNγ involves a different signalling mechanism that is IFITM1-independent (Figure 5.9). This work can also be used to predict that IFITM1 can mediate MHC class I antigen presentation pathways as well as ISG15 conjugation pathways. Both antigen presentation and ISGylation signalling events are important for anti-viral signalling as well as for immune regulation of cancer cells at the immune-cancer synapse (Bassani-Sternberg *et al.*, 2016; Burks *et al.*, 2015; Santos & Mansur, 2017; Okumura *et al.*, 2006; van Montfoort *et al.*, 2014;

Wahl *et al.*, 2009). However, one should imagine these events in their natural context, and so IFNγ stimulus is not present in cellular "steady-state". Its signalling is activated in response to adverse cellular events such as pathogen attack or tumour development. It is a defence mechanism that allows recognition of foreign or un-desirable molecules. Therefore, we need to understand that these events will occur under precise conditions.

In conclusion, the ultimate aim of this thesis is to set the foundations regarding IFITM1 cellular function and to inspire upcoming projects. We begin to understand a new fundamental role of IFITM1/IFITM3 as is proposed in our model (Figure 7.1). In summary, these data have implications for the function of IFITM1/IFITM3 proteins mediating IFNγ-stimulated MHC class I synthesis in the cancer progression sequence. All this work is been integrated in a model (Figure 7.1) that combines the most pertinent results throughout this thesis.

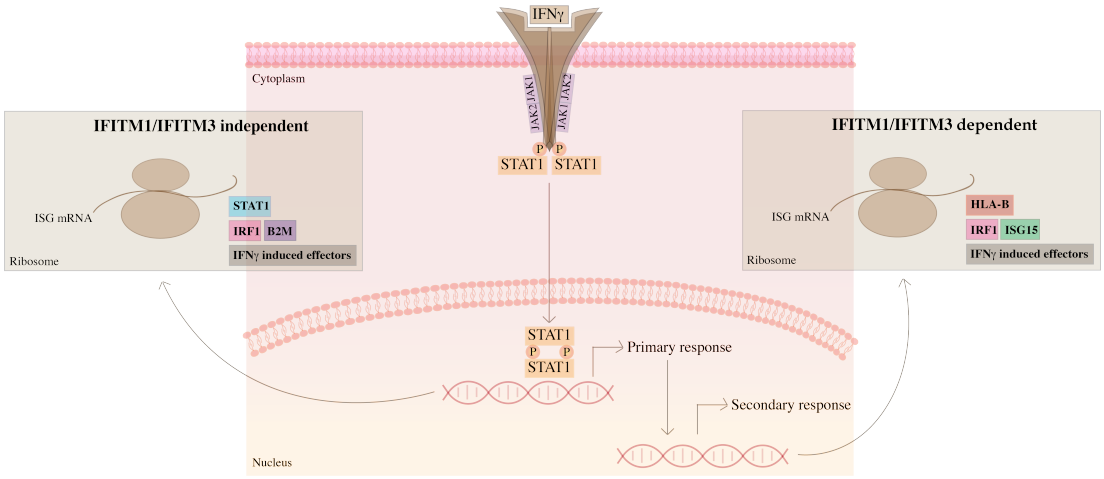

Figure 7.1: The IFITM1 signalling model (Gomez Herranz *et al.*, 2019). IFN stimulation can lead to increase in IFITM1/IFITM3 protein co-association with ribosomal proteins including SRSF1. This association of IFITM1/IFITM3 to ribosomal fractions led us to examine whether there are any IFN-stimulated proteins whose synthesis are IFITM1/IFITM3-dependent. Pulse labelling using SILAC methodologies identifies an IFITM1/IFITM3-dependent synthesis of IRF1 protein early after IFN stimulation. Independent to this event, is an IFITM1/IFITM3-independent synthesis of STAT1 (Figure 5.9) that presumably cooperates with IRF1 protein to transactivate IFN responsive genes; and the dominant proteins synthesized much later after IFN stimulation in an IFITM1/IFITM3-dependent manner are MHC class I molecules and ISG15. Methodologies including immunofluorescence, immunoblotting, and subcellular fractionation confirm that there are defects in HLA-B production and localization in *IFITM1/IFITM3* double null cells (Figure 4.16). The siRNA-mediated depletion of IFITM1 also represented an orthogonal assay that identified reductions in ISG15 and MHC class I molecules (Figure 3.2). STAT1 protein reflects a distinct mechanism of control by IFITM1/IFITM3. Although pulse SILAC revealed that its synthesis is IFITM1/IFITM3-independent (Figure 5.8 and Figure 5.9), the steady state levels of STAT1 protein are reduced after targeted depletion of IFITM1 (Figure 3.2). These data suggest that turnover of STAT1 protein is dependent on IFITM1/IFITM3 but its synthesis is independent of IFITM1/IFITM3. Altogether, these data place IFITM1 as a co-ordinator of synthesis and/or steady state levels of several key players in the IFN response. The notable induction of MHC class I molecules and ISG15, all anti-viral proteins, suggests previously unidentified routes whereby the IFITM1/IFITM3 pathway might suppress viral propagation.

Appendices

Appendix A

Supplementary material to generate isogenic *IFITM1* null cells, *IFITM1/IFITM3* double null cells, and *IFITM3* null cells lines by CRISPR/Cas9 system

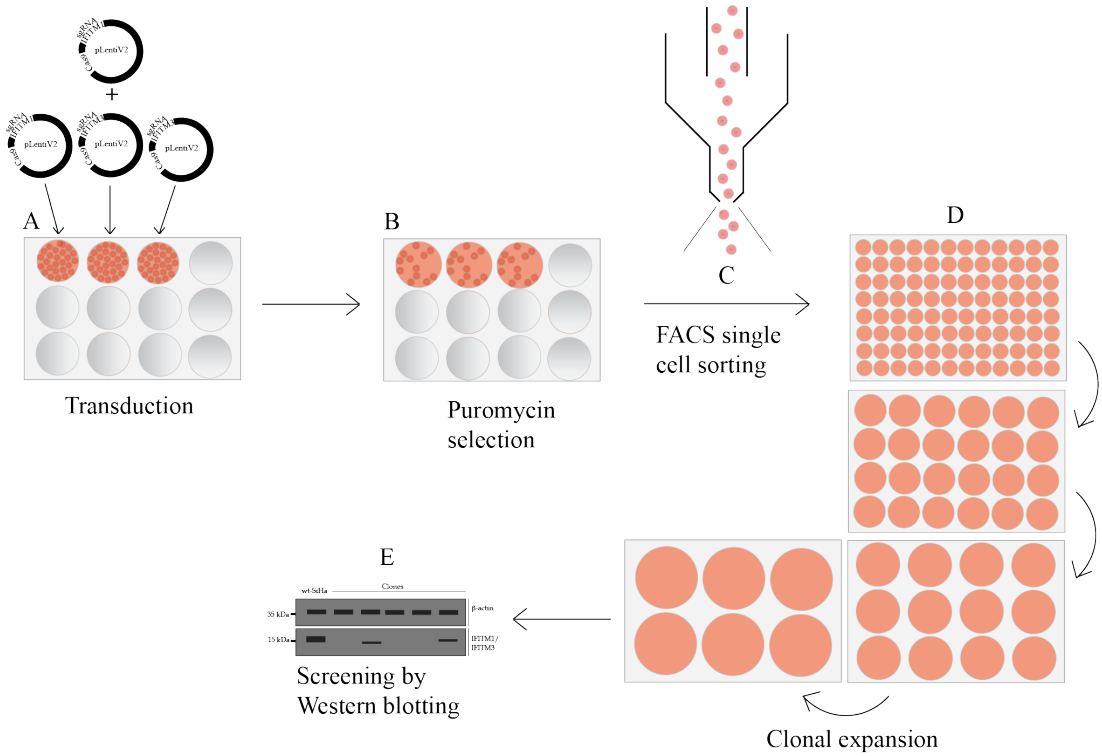

Figure A.1: Workflow for CRISPR/Cas9 gene editing. (A)The wt-SiHa cells were transduced with pLentiV2 plasmid containing the Cas9 cassette and either IFITM1 sgRNA or IFITM3 sgRNA to generate *IFITM1* null cells or *IFITM3* null cells, respectively. The *IFITM1/IFITM3* double null cells were generated by transducing pLentiV2 plasmid containing Cas9 cassette and IFITM3 sgRNA into *IFITM1* null cells. (B) The next day, medium with lentivirus was removed and the cells were resuspended in fresh media containing 10 μg/ml of puromycin. (C) Puromycin selection was continued for about two weeks, after which single cells were sorted by FACS into 96-well plates. (D) These cells were propagated to form colonies originating from a single cell. (E) Finally, cell clones were tested by Western blotting. At the time *IFITM1* null cells were engineered we did not have a specific antibody for IFITM1 suitable for Western blotting. For this reason, *IFITM1* null cells were tested by immunoprecipitation using rabbit anti-IFITM1 (CVY), an antibody that detects the C-terminus of IFITM1. Afterwards, cells were tested by Western blotting using the IFITM1/IFITM3 antibody for detection (Figure A.2 A).

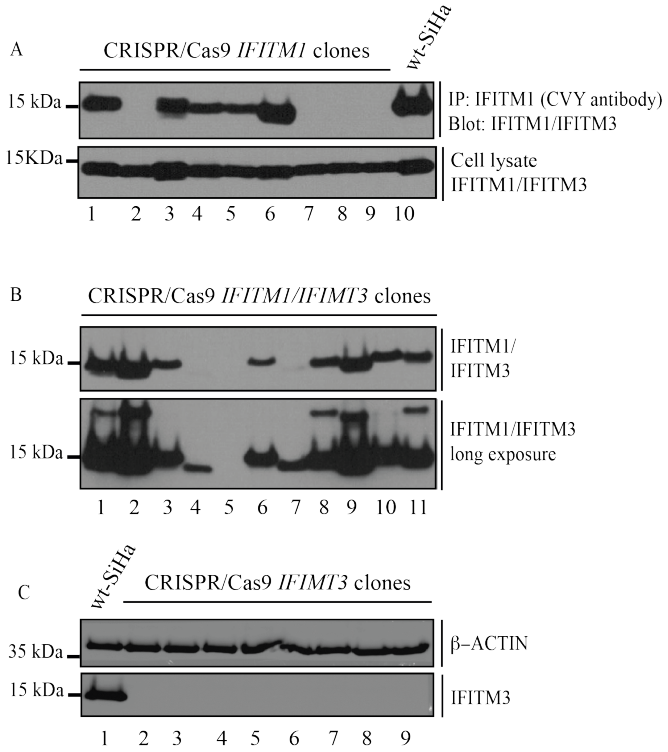

Figure A.2: Individual clone screening for *IFITM1* null, *IFITM1/IFITM3* double null and *IFITM3* null SiHa candidates subjected to CRISPR/Cas9 methodology by immunoblotting. Individual clones were screened for absence of IFITM1 (A) or IFITM1/IFITM3 (B) and IFITM3 (C) protein expression by Western blotting. Representative blot to test the *IFITM1* null clones (A), IFITM1 was immunoprecipitated using rabbit anti-IFITM1 (CVY) antibody (specific antibody against C-terminus of IFITM1 not compatible for Western blotting) as at the time there was no specific commercial antibody against IFITM1. Eluates were tested with IFITM1/IFITM3 antibody (upper panel). CRISPR-clone 4 (lane 2) was used in this thesis. Representative blot to test the *IFITM1/IFITM3* double null clones (B), IFITM1/IFITM3 proteins were detected by Western blotting using IFITM1/IFITM3 antibody. CRISPR-clone 5 (lane 5) was used in this thesis. Representative blot to test the *IFITM3* null clones (C), IFITM3 protein was detected by Western blotting using IFITM3 specific antibody. CRISPR-clone 29 (lane 9) was used in this thesis. Selected clones for *IFITM1* null and *IFITM1/IFITM3* double null and *IFITM3* null-SiHa cells were for further validation by Sanger sequencing and immunofluorescence. This work was performed by Dr. Marta Nekulová, RECAMO, Masaryk Memorial Cancer Institute, Brno.

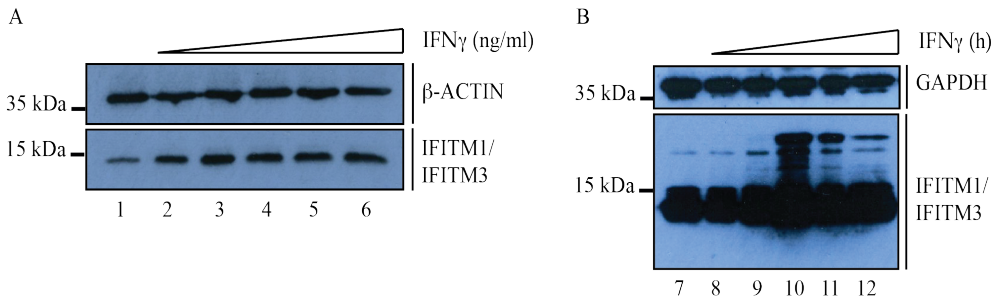

Figure A.3: Determination of IFNγ dosage (A) Dose dependent titration with IFNγ for 24 hours: non-treated (lane 1), 6.25 (lane 2), 12.5 (lane 3), 25 (lane 4), 50 (lane 5), and 100 ng/ml (lane 6). (B) Time course with 100 ng/ml IFNγ: 0 (lane 7), 4 (lane 8), 6 (lane 9), 24 (lane 10), 48 (lane 11), and 72 hours (lane 12).

Appendix B

Supplementary table list

Supplementary Table B.1: Identification of IFITM1-dependent proteins by depleting IFITM1 in wt-SiHa cells using label-free SWATH-MS analysis. Wt-SiHa cells were transfected with IFITM1-targeted-siRNA or scrambled siRNA for 48 hours (columns A to N, in orange) and 72 hours (columns P to AC, in blue). The data acquired from these two biological states were processed in technical triplicates for SWATH-MS analysis. The data are summarized as peak name (columns A and P), gene name (columns B and Q), p-value (columns E and T), and log10 fold change (IFITM1 siRNA/control siRNA) (columns N and AC). The data in this table was used to make Figure 3.2.

Supplementary Table B.2: Identified IFITM1 interacting proteins in wt-SiHa cells by SILAC Orbitrap-MS analysis. Wt-SiHa cells were ectopically transfected under two biological states: with SBP-IFITM1 or SBP-empty vector for 24 hours (column K-P, in orange); or for 48 hours (column Q-V, in blue). Samples were lysed and processed for Orbitrap-MS analysis. These two transfection times were used to cover the variability inherent in transfection of plasmid DNA. The aim was to capture overlapping interacting proteins in both time points, 24 and 48 hours. The data are summarized as peak name (column A), gene name (column B), fold change (SBP-IFITM1/SBP control) (column P and V). The data in this table were used to make Table 4.1.

Supplementary Table B.3: Identified IFITM1 interacting proteins in wt-SiHa cells by label-free SWATH-MS analysis. Wt-SiHa cells were ectopically transfected under two biological states: with SBP-IFITM1 or SBP-empty vectors for 24 hours (columns A-E,in orange); or for 48 hours including IFNγ stimulation for the final 24 hours (columns G-K, in blue). Samples were lysed and processed for SWATH-MS analysis. These two transfection times were used to cover the variability inherent in transfection of plasmid DNA. The data are summarized as peak name (columns A and G), gene name (columns B and H), p-value (columns C and I), fold change (SBP-IFITM1/SBP control) (columns D and J), and log10 fold change (columns E and K). The data in this table were used to make Table 4.2 and Figure 4.13.

Supplementary Table B.4: Ribosomal SWATH-MS analysis after performing a sucrose gradient sedimentation analysis of IFNγ-stimulated wt-SiHa and IFNγ-stimulated *IFITM1/IFITM3* double null cells. The wt-SiHa and *IFITM1/IFITM3* double null cells were IFNγ-stimulated for 24 hours. The lysates were applied to the sucrose gradient for sedimentation; the 40S, 60S, 80S, and polysomal fractions were pooled based on the elution profiles derived from the A254 trace (Figure 5.3 A). The data acquired after SWATH analysis are summarized in four spread sheet tabs named as 40S, 60S, 80S, and polysomes. Key information is shown as peak name (column A), gene name (column B), p-value (column D, highlighted in yellow), and log10 fold change (wt-SiHa cells/*IFITM1/IFITM3* double null cells) (column O, highlighted in yellow). The data derived from these tables were used to make Figure 5.5.

Supplementary Table B.5: Relative quantification values (heavy vs light ratios) in wt-SiHa, *IFITM1* single null, *IFITM1/IFITM3* double null cells non-stimulated or IFNγ-stimulated for 6 and 24 hours and pulse labelled in heavy-SILAC media for 6 and 24 hours. All samples were processed as biological triplicates. Comparisons from heavy vs light SILAC media were performed from pulse-labelled newly-synthetized protein (heavy) vs total protein amount in the cell (light). Each excel spread sheet tab exported from Proteome Discoverer 1.4 shows one condition, from left to right: wt-SiHa cells (6 hours); wt-SiHa cells (6 hours with IFNγ); *IFITM1/IFITM3* dobule null cells (6 hours); *IFITM1/IFITM3* double null cells (6 hours with IFNγ); *IFITM1* null cells (6 hours); *IFITM1* null cells (6 hours with IFNγ); wt-SiHa cells (24 hours); wt-SiHa cells (24 hours with IFNγ); *IFITM1/IFITM3* double null cells (24 hours); *IFITM1/IFITM3* double null cells (24 hours with IFNγ); *IFITM1* null cells (24 hours); *IFITM1* null cells (24 hours with IFNγ). Key information is shown as peak name (column A), gene name (column B), fold change (heavy/light, in three biological triplicate) (columns K, N and Q). The data derived from these tables were used to make Figure 5.8 and Figure 5.9.

Supplementary Table B.6: Transcriptome study of wt-SiHa cells, *IFITM1* null cells, and *IFITM1/IFITM3* double null cells non-stimulated or IFNγ-stimulated for 24 hours. Three biological replicates for wt-SiHa cells, *IFITM1* null cells, and *IFITM1/IFITM3* double null cells non-stimulated or IFNγ-stimulated for 24 hours were combined in equal RNA amounts and processed to study their transcriptome using RNA sequencing. In the RNA-Seq spread sheet tab, key information is shown as gene name (column A), identifier (column D). Gene counts (TPM) for each cell type are represented as wt-SiHa cells (column G), IFNγ-stimulated wt-SiHa cells (column K), *IFITM1* null cells (column O), IFNγ-stimulated *IFITM1* null cells (column S), *IFITM1/IFITM3* double null (column W), and IFNγ-stimulated *IFITM1/IFITM3* double null cells (column AA). The data derived from these tables were used to make Figure 6.7. In the comparison spread sheet tab, key information is shown as gene name (column A), identifier (column D). Gene comparison between to cell conditions are represented as log2 (wt-SiHa cells vs *IFITM1* null cells) (column N), log2 (wt-SiHa cells vs *IFITM1/IFITM3* double null cells) (column O), log2 (IFNγ-stimulated wt-SiHa cells vs IFNγ-stimulated *IFITM1* null cells) (column P), log2 (IFNγ-stimulated wt-SiHa cells vs IFNγ-stimulated *IFITM1/IFITM3* double null cells) (column Q), log2 (wt-SiHa cells vs IFNγ-stimulated wt-SiHa cells) (column R), log2 (*IFITM1* null cells vs IFNγ-stimulated *IFITM1* null cells) (column S), and log2 (*IFITM1/IFITM3* double null cells vs IFNγ-stimulated *IFITM1/IFITM3* double null cells) (column T). The data derived from these tables were used to make Figure 6.6.

Appendix C

The effects of *IFITM1* and *IFITM3* gene deletion on IFNγ-stimulated protein synthesis

Cellular Signalling 60 (2019) 39–56

Contents lists available at ScienceDirect

Cellular Signalling

journal homepage: www.elsevier.com/locate/cellsig

The effects of IFITM1 and IFITM3 gene deletion on IFNγ stimulated protein synthesis

Maria Gómez-Herranz[a], Marta Nekulova[b], Jakub Faktor[b], Lenka Hernychova[b], Sachin Kote[c], Elizabeth H. Sinclair[a], Rudolf Nenutil[b], Borivoj Vojtesek[b,*], Kathryn L. Ball[a,b,*], Ted R. Hupp[a,b,c,*]

[a] University of Edinburgh, Institute of Genetics and Molecular Medicine, Edinburgh EH4 2XR, United Kingdom
[b] Regional Centre for Applied Molecular Oncology, Masaryk Memorial Cancer Institute, 656 53 Brno, Czech Republic
[c] University of Gdansk, International Centre for Cancer Vaccine Science, Department of Chemistry, Gdansk, Poland

ARTICLE INFO

Keywords:
Cervical cancer
IFITM1
Interferon
SILAC mass spectrometry
MHC Class I molecule
CAS9 gene editing

ABSTRACT

Interferon-induced transmembrane proteins IFITM1 and IFITM3 (IFITM1/3) play a role in both RNA viral restriction and in human cancer progression. Using immunohistochemical staining of FFPE tissue, we identified subgroups of cervical cancer patients where IFITM1/3 protein expression is inversely related to metastasis. Guide RNA-CAS9 methods were used to develop an isogenic *IFITM1/IFITM3* double null cervical cancer model in order to define dominant pathways triggered by presence or absence of IFITM1/3 signalling. A pulse SILAC methodology identified IRF1, HLA-B, and ISG15 as the most dominating IFNγ inducible proteins whose synthesis was attenuated in the *IFITM1/IFITM3* double-null cells. Conversely, SWATH-IP mass spectrometry of ectopically expressed SBP-tagged IFITM1 identified ISG15 and HLA-B as dominant co-associated proteins. ISG15ylation was attenuated in IFNγ treated *IFITM1/IFITM3* double-null cells. Proximity ligation assays indicated that HLA-B can interact with IFITM1/3 proteins in parental SiHa cells. Cell surface expression of HLA-B was attenuated in IFNγ treated *IFITM1/IFITM3* double-null cells. SWATH-MS proteomic screens in cells treated with IFITM1-targeted siRNA cells resulted in the attenuation of an interferon regulated protein subpopulation including MHC Class I molecules as well as IFITM3, STAT1, B2M, and ISG15. These data have implications for the function of IFITM1/3 in mediating IFNγ stimulated protein synthesis including ISG15ylation and MHC Class I production in cancer cells. The data together suggest that pro-metastatic growth associated with IFITM1/3 negative cervical cancers relates to attenuated expression of MHC Class I molecules that would support tumor immune escape.

1. Introduction

Interferons (IFNs) are pleiotropic cytokines produced by the innate immune system as a defensive response [1]. Many biological functions have been described for the interferon pathway. Among them, the best characterized are anti-tumor activity, immunomodulatory effects, anti-pathogen, and anti-viral activity [2]. IFN effects rely on three different types of receptors: Type I (IFNα, IFNβ and IFNω), Type II (IFNγ) and Type III (IFNλ) [3,4]. IFNs increase in response to a broad range of factors such as persistent viral infection or DNA damaging agents which activate the JAK kinase-STAT pathway. Ultimately, this signalling cascade will regulate the transcriptional synthesis of interferon stimulated genes (ISGs) [5,6].

Type I IFNs facilitate anti-proliferative and pro-apoptotic pathways in a wide range of cell types and it has been extensively used as anti-tumor therapeutic agent. High doses of IFNs are used for cancer therapy and can activate anti-tumor immunity as well as pro-apoptotic and anti-proliferative programs. By contrast, it has been demonstrated that sustained low level of IFN causes a steady-state expression of the interferon resistance DNA damage signature (IRDS) which is comprised of a subset of interferon-stimulated genes [7]. IRDS proteins promote phenotypes that contribute to the tumor development such as resistance to DNA damage, suppression of T cell toxicity, metastasis, and facilitation of epithelial–mesenchymal transition [8].

Abbreviations: B2M, beta-2-microglobulin; FASP, filter-aided sample preparation; FA, formic acid; HLA, human leucocyte antigen; IFN, interferon; IFITM1/3, interferon-induced transmembrane receptors 1 and 3; ISG15, interferon-stimulated gene 15; IRF1, interferon regulatory factor 1; MHC, major histocompatibility complex; MS, mass spectrometry; NMWCO, nominal molecular weight cut-off; PBS, phosphate-buffered saline; PLA, proximity ligation assay; RT, room temperature; SWATH-IP, SWATH immunoprecipitation; SBP, twin streptavidin binding protein; UPLC, ultra performance liquid chromatography

* Corresponding authors at: University of Edinburgh, Institute of Genetics and Molecular Medicine, Edinburgh EH4 2XR, United Kingdom.
E-mail addresses: vojtesek@mou.cz (B. Vojtesek), kathryn.ball@ed.ac.uk (K.L. Ball), ted.hupp@ed.ac.uk (T.R. Hupp).

https://doi.org/10.1016/j.cellsig.2019.03.024
Received 31 January 2019; Received in revised form 29 March 2019; Accepted 29 March 2019
Available online 02 April 2019
0898-6568/

IFITM1 is a pro-oncogenic receptor which is a component of the IRDS pathway. Basal expression of IFITM proteins is observed in some cells and expression can also be induced by Type I and Type II interferons. IFITM1 is up-regulated during development of radiation resistance, escaping from pro-apoptotic and anti-proliferative effects [9,10]. IFITM1 expression has been extensively reported in many types of cancer; breast, cervix, colon, ovary, brain and oesophagus cancer and its high expression correlates with tumor progression and can lead to a poor outcome [10–16].

IFITM1 was previously known as IFI 17 (interferon induced protein 17), IFI 9–27 (interferon inducible protein 9–27), CD225 (cluster of differentiation) and Leu-13 (leucocyte surface protein). It is a membrane protein that plays a key role in restriction of anti-viral immune response and belongs to the interferon induced transmembrane family (IFITM) [17]. IFITM1 is coded by the *IFITM1* gene located on chromosome 11p15.5 and flanked by *IFITM2* and *IFITM3* genes. The *IFITM* immunity-related protein family are composed of short amino-terminal and carboxy-terminal domains, two transmembrane domains, and a cytoplasmic domain. IFITM1 is slightly different from IFITM2 and IFITM3, with some studies demonstrating that IFITM1 is uniquely expressed at the cell surface [18,19].

IFITM family members are capable of attenuating the entrance of many human and animal viruses. They suppress the entry of viruses such as influenza A virus (IAV), West Nile virus, dengue virus, SARS coronavirus, filoviruses, VSV, and HCV among others [20]. IFITM family proteins inhibit cytosolic entry of viruses by preventing fusion of viral and host membranes. The protein-protein interaction networks by which IFITM proteins inhibit viral propagation are just emerging. One study using yeast two-hybrid methodology has identified an interaction of IFITM3, IFITM2, and IFITM1 with VAPA that in turn mediates an accumulation of cholesterol in multivesicular structures [21]. This reduces the fusion of intraluminal virion-containing vesicles with endosomal membranes and thereby inhibits virus release into the cytosol. In addition, different family members exhibit specific viral preferences. In the case of IFITM1, it is more active in controlling filoviruses, Influenza A, and SARS [17,20,22]. In this report, we focus on applying methodologies in interactomics, gene editing, SWATH-immunoprecipitation mass spectrometry, and pulse-SILAC mass spectrometry to propose an IFNγ responsive biochemical function for the IFITM1/3 proteins.

2. Experimental procedures

2.1. Cell culture

All chemicals and reagents were obtained from *Sigma* unless indicated otherwise. All antibodies from *Thermofisher* unless indicated otherwise. SiHa, *IFITM1* null-SiHa, and *IFITM1/IFITM3* null-SiHa cell lines were grown in RPMI 1640 medium (Invitrogen) supplemented with 10% (*v*/v) fetal bovine serum (Labtech) and 1% penicillin/streptomycin (Invitrogen) and incubated at 37 °C with 5% CO_2.

2.2. Tissue microarray

Cervical cancer samples were obtained at the Masaryk Memorial Cancer Institute where patients gave written consent for tissue use according to local ethical regulations. Tissues were fixed in 4% formaldehyde for approximately 24 h before processing into paraffin wax and sectioned (4 μm). After sections were cut, the antigens were retrieved, and samples were probed with primary antibodies (including those to p16 protein (data not shown), and IFITM1/3 proteins (using the Mab-MHK); Supplementary Fig. 1). Following this stage, the tissue sections were incubated with secondary antibodies conjugated to streptavidin–HRP. Sections were incubated with DAB (Dako), counterstained with haematoxylin and mounted for visualization, as previously described [23].

2.3. Generation of IFITM1 null and IFITM1/IFITM3 double null cell line using CRISPR/CAS9 technology

Guide RNA sequences were designed for *IFITM1* (5′ TCCAAGGTCC ACCGTGATCA 3′) and for *IFITM3* (5′ GTCAACAGTGGCCAGCCCCC 3′). The guide RNA was cloned into the lentiCRISPRv2 expression vector [24]. After transfection, cells were selected with puromycin and sorted in a 96-well plate using FACS. After 3 weeks, individual clones were screened for absence of IFITM1 and/or IFITM3 protein expression by Western Blot using the Mab-MHK (Supplementary Fig. 1). Chromosomal DNA from the positive clones were sequenced for a final validation to define the precise gene edit (as in Figs. 2 and 3).

2.4. DNA extraction and sequence validation of guide RNA edits

Chromosomal DNA was extracted from frozen cell pellets following the instruction manual (Gentra Puregene Cell kit, Qiagen). Validation of the edited DNA sequence was confirmed by cloning the genomic *IFITM1* and *IFITM3* PCR products into a holding vector and by amplifying the entire gene and 500 bp surrounding the guide RNA targeting site followed by Sanger sequencing at Source BioScience Service (Scotland).

2.5. Cloning, transfection and affinity purification of SBP-IFITM1 protein

IFITM1 cDNA was cloned by PCR into pEXPR-IBA105 expression vector containing SBP tag at the N-terminus of the coding region (SBP vector (IBA)). SiHa cells were grown in RPMI as a duplicate. For transfection, cells were grown to approximately 80% confluency and transfected using Attractene (Qiagen). Cells were transfected with SBP-empty vector (control cells) and SBP-IFITM1 for 48 h. 48 h after transfection, cells were treated with carrier or with 100 ng/ml IFNγ (Invitrogen) for 24 h in order to “stabilize” potential interferon-activated SBP-IFITM1 interacting proteins. Cells were washed twice in ice cold PBS and scraped into buffer containing 100 mM KCl, 20 mM HEPES pH 7.5, 1 mM EDTA, 1 mM EGTA, 0.5 mM Na_3VO_4, 10 mM NaF, 10% (*v*/v) glycerol, protease inhibitor mix, and 0.1% triton X-100, then incubated for 30 min on ice and centrifuged at 13,000 rpm for 15 min at 4 °C. Equal amounts of protein were used for performing the affinity capture. Streptavidin Agarose conjugated beads (Millipore) were pre-washed with in PBS. Then cell lysate was added and incubated for 2 h at RT with gentle rotation. Binding proteins were eluted with a buffer containing 20 mM HEPES pH 8, 2 mM DTT, and 8 M Urea.

2.6. Transient transfection of siRNA

Small interfering RNA directed against the human *IFITM1* (Qiagen) and an AllStars negative controls FlexiTube siRNA (Qiagen) were used to transfect SiHa cells for 48 and 72 h. Cells were transfected using HiPerFect (Qiagen) following the manufacturer's instructions.

2.7. SILAC labeling of cells for use in pulse SILAC

For performing “pulse” SILAC, Parental SiHa, *IFITM1/IFITM3* double null cells, and *IFITM1* single null cells were grown as biological triplicate and incubated with SILAC heavy media for 6 and 24 h with or without 100 ng/ml IFNγ before harvesting [25–27]. Cells were isotopically pulse-labeled using SILAC RPMI-heavy media (Dundee Cell Products, UK); L-[$^{13}C6^{14}N4$] arginine (R6) and L-[$^{13}C6^{14}N2$] lysine (K6). Cells were harvested in a buffer containing 8 M Urea, 0.1 M Tris pH 8.5. Total protein extracts were measured by the Bradford assay [28].

2.8. Antibodies

Proteins were detected using the following primary antibodies: mouse monoclonal anti-bodies generated to a peptide that is identical in

IFITM1 and IFITM3 (Mab-MHK) (Moravian Biotechnology, this study is their first description). The antibody we name Mab-MHK can therefore detect co-expression of both IFITM1 and IFITM3 proteins (Supplementary Fig. 1). Other sources include, rabbit monoclonal anti-STAT1 (Cell Signalling), mouse monoclonal anti-IRF1 (BD Transduction Laboratories), rabbit polyclonal anti-HLA-B (Thermo Fisher), rabbit polyclonal antibody anti-ISG15 (Cell Signalling), mouse monoclonal anti-SBP-tag (Sigma), mouse monoclonal anti-β-actin (Sigma), and the mouse monoclonal anti-GAPDH (Abcam).

2.9. Western blotting

Protein from lysed samples was quantified using Protein Assay Dye Reagent (Bio-Rad). Proteins were resolved by SDS-PAGE using 15% gels [29] and transferred onto nitrocellulose membranes (Amersham Protran, GE Healthcare). Immunoblots were processed by enhanced chemiluminescence (ECL).

2.10. Immunofluorescence

Parental SiHa and *IFITM1/IFITM3* double null cells were grown over 16 mm diameter glass coverslips. Stimulated cells were treated with 100 ng/ml IFNγ for 24 h. Cells were fixed with 4% (*v*/v) paraformaldehyde in PBS for 15 min at room temperature and permeabilized using 0.25% triton X-100 in PBS for 10 min. Then, the cells were blocked with 3% BSA in PBS for 30 min. The primary antibody was incubated at a 1:1000 dilution overnight. Alexa Fluor 488 goat anti-rabbit IgG (H + L) (Invitrogen) was incubated as a secondary antibody at 1:2000 dilution for 1 h. The fluorescent signal was detected using a Zeiss Axioplan 2 microscope at 63×. Replicates are described in the Fig. 6 legend. Fluorescence was measured using ImageJ software; cells were selected, and information was extracted on the area, integrated density, and mean gray values by selecting set measurements in the *Analyse* menu. A region with no fluorescence was selected as background for each image. The following formula was applied for each 50 cells analyzed: CTCF = Integrated Density – (Area of selected cell × Mean fluorescence of background readings); *CTCF = corrected total cell fluorescence.

2.11. Proximity ligation assay

Parental SiHa and *IFITM1/IFITM3* double null cells were grown and processed as described in the Immunofluorescence method (above). Primary antibodies from different species were incubated with the fixed and permeabilized cells: MHK mouse MAb with rabbit polyclonal anti-HLA-B, at 1:250 dilution overnight. Duolink® assays (Sigma) were carried out following supplier's instructions. The fluorescent signal was detected using a Zeiss Axioplan 2 microscope at 63×. Fluorescence was measured using ImageJ software, as above reviewed for standard immunofluorescence.

2.12. Mass spectrometric experimental screens

2.12.1. Peptide generation using FASP

Cell lysates, immunoprecipitates, or gradient fractions were processed using filter-aided sample preparation protocol (FASP) [30,31]. Urea buffer (8 M Urea in 0.1 M Tris pH 8.5) was added to a 30 kDa spin filter column (MRCPRT010, Microcon). Protein concentration was determined using the RC-DC method (Bio-rad). Normalized sample was added into the spin filter column and was centrifuged at 14000 *g* for 15 min at 20 °C. Urea buffer was added again with 100 mM Tris (2-carboxyethyl) phosphine hydrochloride (Aldrich) and mixed. The column was left on a thermo-block set at 37 °C shaking at 600 rpm and centrifuged at 12,210 rpm at 20 °C for 15 min. Urea buffer and 300 mM of iodoacetamide (Sigma) were mixed using a thermo-mixer at 600 rpm in the dark for 1 min, then was maintained statically for a further 20 min at room temperature in the dark. The sample was centrifuged at 12,210 rpm at 20 °C for 15 min and the supernatant was discarded. A solution containing 100 mM ammonium bicarbonate were added to the column and then it was centrifuged at 12,210 rpm at 20 °C for 20 min. This step was repeated one more time. The column was placed in a new collecting tube (low binding affinity) and 50 mM ammonium bicarbonate was added along with trypsin diluted in trypsin buffer (Promega) at a 1:100 ratio. The column was incubated at 37 °C overnight. The following day the column was centrifuged at 12,210 rpm at 20 °C for 15 min. Determination of the peptide concentration was performed using the Quantitative Colorimetric Peptide Assay (Pierce, ThermoScientific).

2.13. Desalting peptides using C18 column

Peptides were desalted on micro spin columns C-18 (Harvard Apparatus, USA). C-18 columns were conditioned three times with 100% acetonitrile (AcN) and 0.1% formic acid (FA) and centrifuged at 1200 rpm at room temperature for 2 min. The column was washed with 0.1% FA and centrifuged at 1200 rpm at room temperature for 2 min. The column was hydrated in 0.1% FA for 15 min following centrifugation at 1800 rpm at room temperature for 3 min. The sample was loaded into the column and centrifuged at 2300 rpm for 3 min. After washing the column three times with 0.1% FA, the peptides were eluted in three consecutive centrifugations at 2300 rpm for 3 min using 50%–80% and 100% AcN with 0.1% FA. Subsequently, peptide eluates were evaporated and dissolved in 5% AcN with 0.05% FA.

2.14. LC-MS/MS analyses

There were three distinct mass spectrometric screens used in the manuscript. The rationale for replicates in each distinct approach is as follows; (i) the SWATH-IP (immunoprecipitation) to identify IFITM1-enriched associated proteins (Fig. 8). The immunoprecipitation and immunoblots of SBP-IFITM1 vs SBP control is representative of experiments performed at least three times. The representative enrichment of IFITM1-associated proteins (in Fig. 8 from Supplementary Table 2) was processed by label free (SWATH) mass-spectrometry in technical triplicates. The measured fold-changes and *p*-values for quantified proteins are listed in Supplementary Table 2 and Fig. 8; (ii) the siRNA SWATH-MS (Fig. 9A and B). Targeted siRNA to deplete IFITM1 in SiHa cells was performed in at least three separate experiments. A representative depletion of IFITM1 protein (Fig. 9A) was performed in technical triplicates using two different biological states (48 and 72 h). The statistical rationale for performing two biological states (equivalent plating of cell number and differing by time of interferon exposure) rather than two biological replicates at the same time point, was due to the variable induction and suppression of the interferon cascade over this time frame. Thus, any proteins that are observed in two biological states as a function of time are thought to have higher significance than an analysis performed in duplicates at one time point. The samples in the two biological states were processed in technical triplicate for label-free (SWATH) analysis (Fig. 8; Supplementary Table 2); (iii) Pulse SILAC to measure protein synthesis as a function of genotype. Twelve enzymatically digested samples (four samples of parental SiHa, four samples of *IFITM1* null, and four samples of *IFITM1/IFITM3* double null), each of them as independent biological triplicates, were processed using isotopically labeled amino acids and were separated using LC-MS/MS analysis (Fig. 5; Supplementary Fig. 2; Supplementary Table 1). The statistical rationale for using three biological replicates with one injection per replicate, rather three technical replicates from one biological sample, relates to the dynamics and variability in the interferon dynamics. By using biological triplicates, any common overlaps are deemed to be more significant because of the possible variability in the cell plating and interferon cascade.

2.15. LC-MS/MS analysis of SILAC labeled samples

SILAC samples were separated using UltiMate 3000 RSLCnano chromatograph (Thermo Fisher Scientific, Massachusetts, USA). Peptides were loaded on a pre-column (μ-precolumn, 30 mm i.d., 5 mm length, C18 PepMap 100, 5 μm particle size, 100 Å pore size) and further separated on an Acclaim PepMap RSLC column (75 mm i.d., length 500 mm, C18, particle size 2 mm, pore size 100 Å) with a 300 nl/min flow rate using a linear gradient: 2% B over 4 min, 2–40% B over 64 min, 40–98% B over 2 min, with A = 0.1% aq. formic acid and B = 80% AcN in 0.08% aq. formic acid. Peptides eluting from the column were introduced into an Orbitrap Elite (Thermo Fisher Scientific, Massachusetts, USA) operating in Top20 data dependent acquisition mode. A survey scan of 400–2000 *m/z* was performed in the Orbitrap at 120000 resolution with an AGC target of 1 × 106 and 200 ms injection time followed by twenty data-dependent MS2 scans performed in the LTQ linear ion trap with 1 microscan, 10 ms injection time and 10,000 AGC.

2.16. Database searching and analysis

The data from mass spectrometer were processed either using Proteome Discoverer 1.4 or Proteome Discoverer 2.2 that is employed with imbedded statistical tools (both programs were from Thermo Fisher Scientific, Massachusetts, USA). Proteome Discoverer 1.4 processed the data using Mascot engine with the following search settings: database Swiss-Prot human (April 2016); enzyme trypsin; 2 missed cleavage sites; precursor mass tolerance 10 ppm; fragment mass tolerance 0.6 Da; dynamic modifications: carbamidomethyl [C], oxidation [M], acetyl [protein N-terminus]. The results of the search were further submitted to generate the final report considering 1% FDR on both PSM and peptide group levels. Only unique peptides were used for the protein quantification. SILAC labels of R6 and K6 were chosen for heavy and R0 and K0 for light. The relative quantification value was represented as heavy/light ratio (Supplementary Table 1). In the processing and consensus workflows subsequent nodes were used: the Minora feature detector, the Precursor ion quantifier, and the Feature mapper. The data were processed using Sequest HT engine with the following search settings: database Swiss-Prot 2017-10-25, # sequences 42,252, taxonomy: *Homo sapiens* (updated February 2018); enzyme trypsin; 2 missed cleavage sites; precursor mass tolerance 10 ppm; fragment mass tolerance 0.6 Da; static modification carbamidomethyl [+57.021 Da, (C)], label 13C(6) [+6.020 Da (K, R)]; dynamic modifications oxidation [peptide terminus, +15.995 Da (M)], Met-loss +Acetyl [protein terminus, −89.030 Da (M)]. The results of the search were further submitted to generate the final report with a 1% FDR using Percolator. For the protein quantification and statistical assessment of the biological triplicates, only unique peptides and razor peptides were used. The relative quantification value is represented as the relative peak area of the peptides with the heavy isotope labels with IFNγ treated cells/IFNγ untreated cells ratios (Supplementary Table 3B).

2.17. SWATH-MS

Label free quantitation was performed using FASP-processed tryptic digests with liquid chromatography coupled to tandem mass spectrometry on an Eksigent Ekspert nanoLC 400 (SCIEX, California, USA) online connected to a TripleTOF 5600+ (SCIEX, Toronto, Canada) mass spectrometer. Cells lysates were processed in technical triplicates. Prior to the separation the peptides were concentrated and desalted on a cartridge trap column (300 μm i.d. × 5 mm) packed with a C18 PepMap100 sorbent with a 5 μm particle size (Thermo Fisher Scientific, Waltham, MA, USA). After a 10 washing using 0.05% trifluoroacetic acid in 5% acetonitrile and 95% water, the peptides were eluted using a gradient of acetonitrile/water (300 nl/min) using a capillary emitter column PicoFrit® nanospray columns 75 μm × 210 mm (New Objective, Massachusetts, USA) self-packed with ProntoSIL 120-3-C18 AQ sorbent with 3 μm particles (Bischoff, Leonberg, Germany). Mobile phase A was composed from 0.1% (*v*/v) formic acid in water, and mobile phase B was composed of 0.1% (v/v) formic acid in acetonitrile. Gradient elution started at 5% mobile phase B for the first 30 min and then the proportion of mobile phase B increased linearly up to 40%B for the following 120 min. Output from the separation column was directly coupled to an ion source (nano-electrospray). Nitrogen was used as a drying and nebulizing gas. Temperature and flow of the drying gas was set to 150 °C and 12 psi. Voltage at the capillary was 2.65 kV.

Pooled sample for the spectral library was measured in data-dependent positive mode (IDA). The MS precursor mass range was set from *m/z* 400 up to m/z 1250 and from m/z 200 up to m/z 1600 in MS/MS. Cycle time was 2.3 s and in each cycle 20 most intensive precursor ions were fragmented. Subsequently, their corresponding MS/MS spectra were measured. Precursor exclusion time was set to 12 s. Precursor ions with intensity below 50cps were suspended from the IDA experiment. The extraction of mass spectra from chromatograms, their annotation and deconvolution were performed using Protein Pilot 4.5 (SCIEX, Toronto, Canada). MS and MS/MS data were searched using the Uniprot+swissprot database (02. 2016, 69,987 entries) restricted to *Homo sapiens* taxonomy. Fixed modification – alkylation on cysteine using iodoacetamide and digestion using trypsin was set for all searches. FDR analysis was performed by searching the shotgun data against the decoy search database. The resulting group file was imported into Peakview 1.2.0.3 (SCIEX, Toronto, Canada), where only proteins with FDR below 1% were imported into the spectral library (465 proteins for SBP-IFITM1 pull down SWATH). In SWATH mode, the mass spectrometer operated in high sensitivity positive mode. Precursor range was set from *m/z* 400 up to m/z 1200. It was divided into 67 precursor ion windows with the width of 12 Da and 1 Da overlap. Accumulation time was 50 ms per SWATH window and the duty cycle was 3.0 s, which enabled acquisition of at least 10 data points across a chromatographic peak. Product ions were scanned from m/z 400 up to m/z 1600. Data extraction was performed in Peakview 1.2.0.3 (SCIEX, Toronto, Canada) with the spectral library. The retention time window for extraction was manually set to 4 min for SBP-IFITM1 pull down SWATH and for the siRNA SWATH (Fig. 9). Protein quantification was performed using up to 4 peptides and 6 transitions per protein to define the statistically significant proteins. Scope of peptides used for quantification was narrowed to only those with peptide confidence higher than 99% and without any variable modification. Protein summed peak areas were normalized using total area sums option in MarkerView 1.2.1.1 (SCIEX, Toronto, Canada). Samples were compared pairwise using paired *t*-test. The mass spectrometric data have been deposited to the ProteomeXchange Consortium via the PRIDE partner repository with the dataset identifier PXD007562". For Reviewers, the details include; Username: reviewer17106@ebi.ac.uk and Password: OfTomSm7.

2.18. Flow cytometry for detection of HLA on the cell surface

The parental SiHa and *IFITM1/IFITM3* double null cells were grown in RPMI (supplemented with 10% FBS, pen-strep and pyruvate) to 50% confluence in 6-well plates and treated with 100 ng/ml IFNγ for 24 h. Cells were harvested using Accutase (Sigma-Aldrich, A6964), centrifuged 1000 rpm for 5 min with RPMI and kept on ice in 1% BSA in PBS for 20 min. Primary antibodies (HLA-B: PA5-35345) were diluted in 1% BSA/PBS to 1:100. Cells were centrifuged as before, and cell pellets were resuspended in 100 μl of diluted primary antibodies or in the same amount of 1% BSA/PBS (for control samples) and incubated 45 min a room temperature on a tube rotator. After a triple wash in ice-cold 1% BSA/PBS, cells were incubated with 100 μl of secondary antibody (Abcam, Goat Anti-Rabbit IgG H&L DyLight 488), diluted 1:200, on a tube rotator for 30 min at room temperature. After a triple wash in ice-cold 1% BSA/PBS, cells were resuspended in 500 μl of 1% BSA/PBS and kept on ice before measurement. Samples were measured on

FACSVerse (BD Biosciences) and data were analyzed using FACSuite software (BD Biosciences). A negative control without primary antibody was prepared for each sample. HLA expression on the cell surface was counted as FITC median fluorescence intensity (MFI) divided by the MFI of the negative control. Two independent experiments were performed, each with two independently isolated *IFITM1/IFITM3* double null cells and two different HLA antibodies (HLA-A (data not shown) and HLA-B (Fig. 6)).

3. Results

3.1. Identifying a clinically relevant model to dissect IFITM1 and IFITM3 (IFITM1/3) signalling

IFITM1 and IFITM3 (IFITM1/3) can function as oncogenic factors in several cancer cells [32,33]. Attenuation of IFITM1 protein expression can inhibit growth, invasion, and/or migration of cancer cells [34]. Patient subgroups with clinically relevant expression data are not well-defined. We developed a panel of monoclonal antibodies to a N-terminal peptide with a high homology between IFITM1 and IFITM3 (Supplementary Fig. 1A, B). This would allow the development of monoclonal antibodies that detect the co-expression of both IFITM1 and IFITM3 proteins. We aimed to use such tools to screen a large panel of human cancers for those that express IFITM1/3 proteins. This would identify clinically relevant models for a focus to dissect IFITM1/3-mediated signalling pathways. The monoclonal antibody chosen (named Mab-MHK; Supplementary Fig. 1B) can bind to IFITM1/3 antigens in a range of human cancer cells (Supplementary Fig. 1C). Some cancer cells exhibit no expression of IFITM1/3 such as the lymphoma cell line WHU-NHL (Supplementary Fig. 1C). Further studies confirmed that Mab-MHK can bind to both IFITM1 and IFITM3 proteins, as defined using single *IFITM1* single null and *IFITM1/IFITM3* double null cells (see below).

Mab-MHK was used to screen large panels of archival formalin-fixed human cancer tissues to identify potential clinically relevant models. We could detect differential expression of IFITM1/3 in breast cancer, colon cancer, and oesophagus cancer (data not shown). We could also detect differential expression of IFITM1/3 protein in a cervical cancer array (Fig. 1A–F). Squamous cervical cancer samples expressed either high levels of IFITM1/3 (Fig. 1A), lower levels of IFITM1/3 (Fig. 1B), or undetectable levels of the antigens (Fig. 1C). Cervical adenocarcinoma often exhibited high expression (Fig. 1D). Interestingly, some normal squamous cervical epithelium exhibited high expression in the basal 'stem' cell or pluripotent layer only (Fig. 1E), but not the differentiating cell layers. We can conclude that 64 out of 74 cervical cancer specimens are positive for IFITM1/3 proteins using the Mab-MHK (Fig. 1F, top panel). What is also interesting is that there is a statistically significant inverse association between IFITM1/3 protein expression and the number of lymph node metastases in patients (Fig. 1F, bottom panel). This will be rationalized in the discussion based on data that emerges below.

3.2. Developing an IFITM1 and IFITM3 double null cell line using a CRISPR-guide RNA methodology

IFITM1 is implicated in IFNγ mediated growth control in some cancer cells with an active p53 pathway [35]. IFITM1 is also implicated in a growth stimulatory role in cervical squamous cancers [36] [37]. The HPV16+ and IFITM1/3 positive cervical cancer cell line SiHa [38] [39] exhibit IFNγ inducible STAT1, IRF1, and IFITM1/3 proteins (Fig. 1G). As such, we focused on using this cervical cancer cell line (SiHa) as a model to identify IFITM1/3 dependent signalling pathways.

In order to continue to develop a cervical cancer cell model that reflects the clinical data (IFITM1/3 positive or IFITM1/3 negative cancers; Fig. 1F), we set out to develop a double null *IFITM1* and *IFITM3* cell line model. We first generated an isogenic *IFITM1* null cell panel through gene editing to validate the guide RNA. *IFITM1* knock-out mice are viable [40] so it was likely we would be able to generate *IFITM1* null cells. Guide RNAs targeting exon 1 in the *IFITM1* gene (Figure 2A) were cloned into pLentiV2. Cells were transfected and selected for resistance to puromycin to allow stable integration of the *IFITM1* targeting guide RNA cassette. Cell clones were chosen for sequencing across the guide RNA targeting site (Fig. 2A) using PCR (Fig. 2B). Both *IFITM1* alleles were gene edited in a representative *IFITM1*-null clone that creates two distinct frameshifts (Fig. 2C and D). We examined four representative *IFITM1* null cells in DNA damage response assays and all lines were shown to be either chemosensitive or X-irradiation sensitive (data not shown). Since all single knock-out clones behaved similarly, we chose one representative *IFITM1* null cell line for continued study. The *IFITM3* gene was next targeted using guide RNA methodologies (Fig. 3A) to to create a *IFITM1/IFITM3* double null cell (Fig. 3A–C). *IFITM3* null mice, and mice with the entire *IFITM* chromosomal locus deleted, are also viable [40,41]. This created an isogenic cell model that removed any redundancy of IFITM3 in the IFITM1 interaction landscape, especially as they both are reported to interact with VAPA [21]. Immunoblotting confirmed that IFITM1 and IFITM3 proteins are not detected in the *IFITM1/IFITM3* double null cell, respectively (Fig. 3D; lanes 5 and 6). We chose a representative double-null cell line for subsequent studies.

3.3. Pulse SILAC mass spectrometry methodologies identify IFITM1/3 dependent protein synthesis in response to IFNγ signalling

Given that one established effector of IFITM1 is IFNγ [35], we evaluated IFNγ responsive protein synthesis in IFNγ stimulated parental SiHa, *IFITM1* single null, and *IFITM1/IFITM3* double null cells. The parental SiHa, *IFITM1* single null, and *IFITM1/IFITM3* double null cells were treated with heavy isotopic amino acid labeling media (the SILAC method) for 6 or 24 h, in the absence or presence of IFNγ (Fig. 4). Cell lysates were then processed by FASP [30,31] and then analyzed for IFITM1/3-dependent protein synthesis using mass spectrometry. The SILAC methodology has been subjected to an analysis of random error associated with the multiple steps in this approach including; cell plating in biological replicates, switch to heavy isotopic media, cell recovery from plastic plates, cell lysis, centrifugation, filter assisted trypsinization, and tryptic peptide recovery and processing. This error can be reduced by employing multiple replicates ($n = 3$) as highlighted previously [42]. To highlight the importance of biological replicates and the inherent error in this multiple step process, we plot the data not as an average of three replicates, but as individual points from all three replicates (as in Supplementary Fig. 2 and Fig. 5).

The dominant IFNγ responsive protein to be identified at 6-h post labelling is IRF1 protein (Supplementary Fig. 2B vs 2A) with an attenuation of isotopically labeled IRF1 peptides recovered in the biological triplicates from *IFITM1/IFITM3* double null cells (Supplementary Fig. 2H). This suggests that IRF1 is partially dependent upon IFITM1/3 signalling and this was confirmed using IRF1 transcriptional reporter assays (data not shown). This data provides some degree of confidence that the methodology is able to identify a known IFNγ responsive target (IRF1). There are other proteins whose synthesis was detected at 6 hours post-isotopic labelling including STAT1, EIF1, and B2M (Supplementary Fig. 2I–K). EIF1 is not known to be linked to interferon signalling, but it is known to regulate the accuracy of AUG codon selection by the scanning pre-initiation complexes [43]. EIF1 might prove to be involved in regulating interferon dependent anti-viral mRNA selection. Nevertheless, all three proteins are also IFTM1/3-independent (Supplementary Fig. 2I–K). STAT1 and B2M are also both known IFNγ responsive proteins further validating the methodology used to measure quantitative changes in protein synthesis. That all three proteins (STAT1, EIF1, and B2M) exhibit equivalent protein synthesis rates in the parental and double-null cell model indicates that the double null has retained many key regulatory features of the parental cell. This

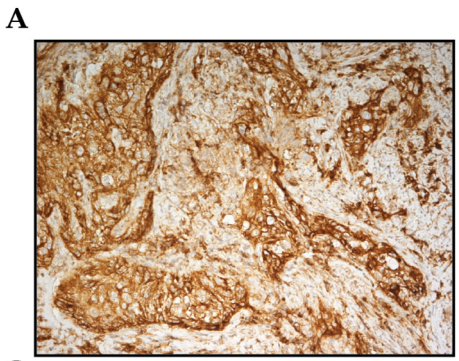

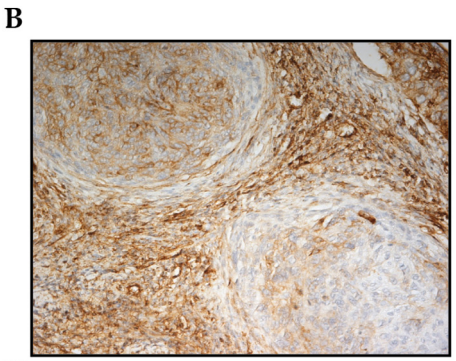

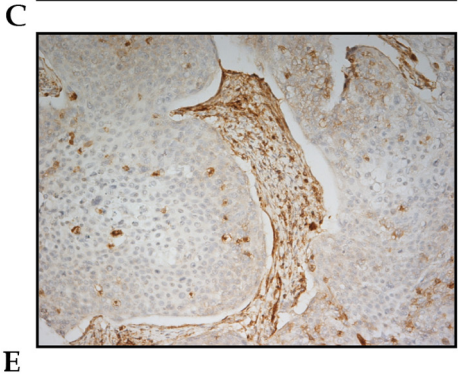

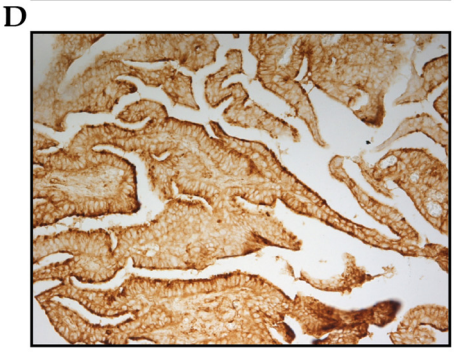

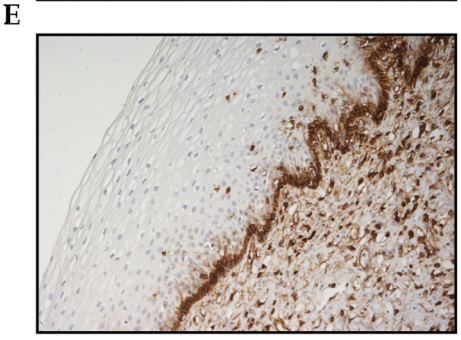

F Quantitation of IFITM1/3 expression in cervical cancer

Expression of IFITM1/3 as a function of histology

	Squamous	Adenocarcinoma	Neuroendocrine
IFITM1/3 -ve	8	1	1
IFITM1/3 focally +ve	23	4	0
IFITM1/3 strongly +ve	29	7	1

Expression of IFITM1/3 as a function of metastasis

	Negative nodes	Positive nodes
IFITM1/3 -ve	4	6
IFITM1/3 focally +	18	9
IFITM1/3 strongly +	29	7

p value=0.042 (chi square)

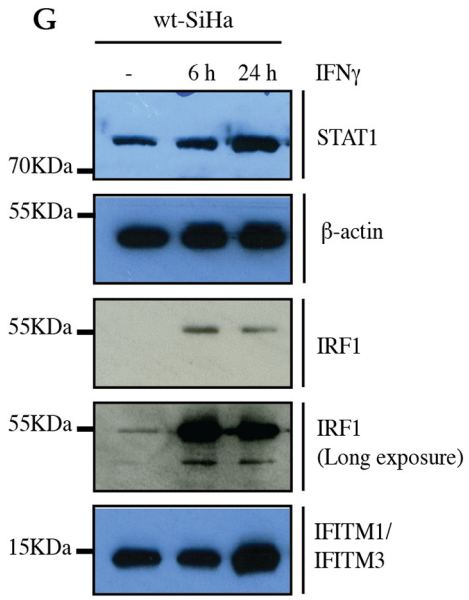

Fig. 1. Immunohistochemical analysis of IFITM1/3 protein expression in cervical cancers using the Mab-MHK. Formalin-fixed, paraffin-embedded cervical carcinoma tissue was processed as stated in the Experimental Procedures using the Mab-MHK that binds to shared epitopes in the N-terminal domains of IFITM1 and IFITM3 (Supplementary Fig. 1A, B). Representative images highlight grades of IFITM1/3 protein expression; (A). high expression in squamous cell carcinoma, (B). medium expression in squamous cell carcinoma, (C). absence of expression in squamous cell carcinoma, (D). high expression in adenocarcinoma, and (E). expression in basal stem cell layer in normal tissue. (F). (Top panel); Quantification of IFITM1/3 protein expression in cervical cancer in relation to histology type and (Bottom panel) IFITM1/3 protein expression in cervical cancer in relation to lymph node metastasis, excluding neuroendocrine. (G). Immunoblotting of protein expression in the parental SiHa cells after IFNγ treatment for the indicated time points. Proteins evaluated include; STAT1; β-actin, IRF1, and IFITM1/3.

suggests that many IFN regulatory features of the double null cell have been retained despite the selection process creating the cell model.

By 24-h post IFNγ treatment of SiHa cells, HLA family members, B2M, and STAT1 proteins were detected (Fig. 5B vs 5A), again indicating that the methodology can detected known IFNγ inducible proteins. By 24-h post IFNγ treatment, isotopically labeled IRF1

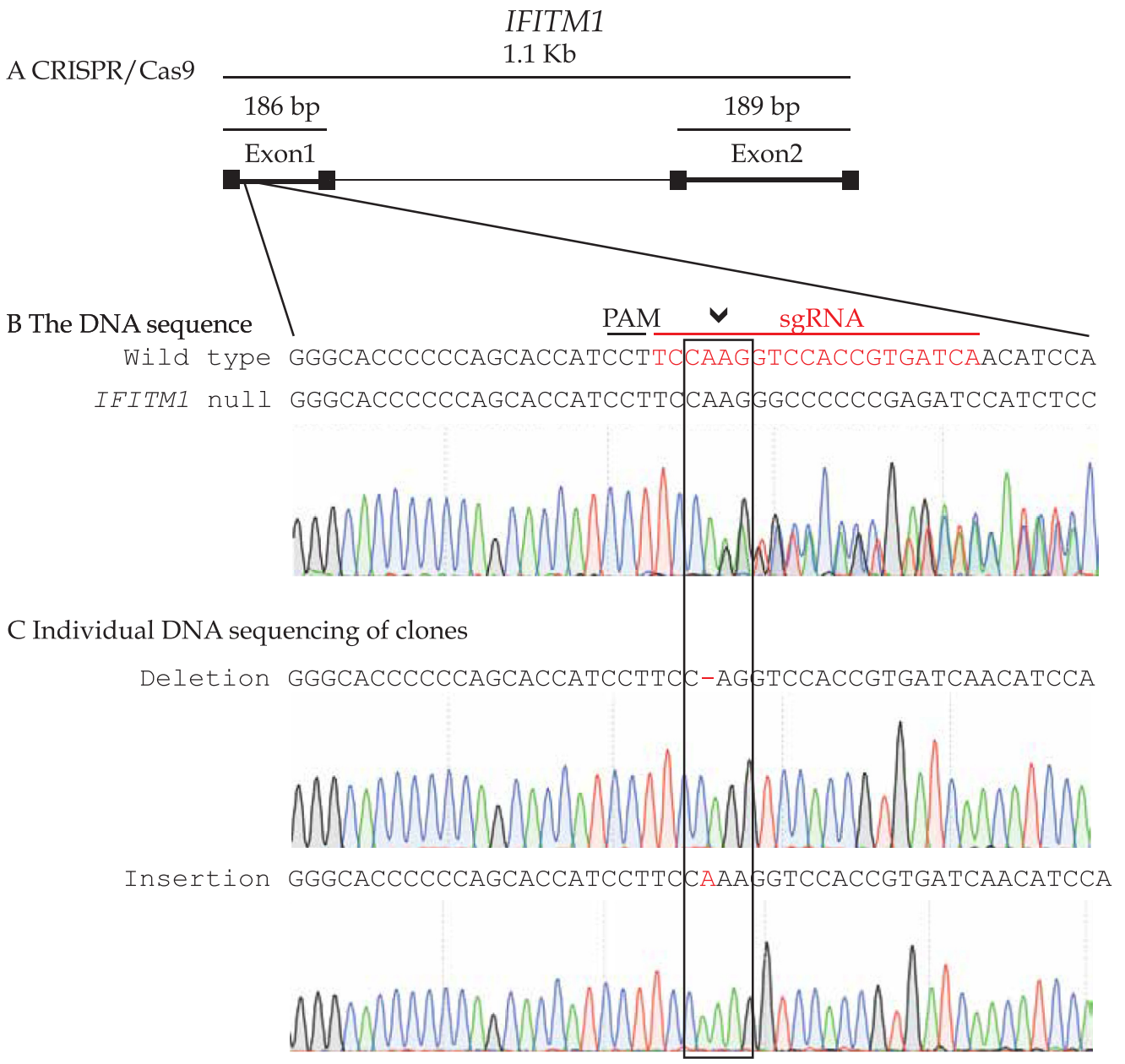

D Predicted translation in *IFITM1* null

```
Wild type    MHKEEHEVAVLGAPPSTILPRSTVINIHSETSVPDHVVWSLFNTLFLNWCCLGFIAF
Deletion     MHKEEHEVAVLGAPPSTILPGPPStop------------------------------
Insertion    MHKEEHEVAVLGAPPSTILPKVHRDQHPQRDLRARPCRLVPVQHPLLELVLSGLHSI

Wild type    AYSVKSRDRKMVGDVTGAQAYASTAKCLNIWALILGILMTIGFILLLVFGSVTVYHI
Deletion     ------------------------------------------------------
Insertion    RLLREGAYGPGGNPGGAGEPGAPPAHMLPGVGTCVSLStop---------------

Wild type    MLQIIQEKRGY
Deletion     ----------
Insertion    ----------
```

(caption on next page)

Fig. 2. Validation of the IFITM1 guide RNA. (A). Gene structure of the *IFITM1* gene highlighting its two coding exons and one intron. The genomic region surrounding the gRNA target site (with PAM site and homology region in red) for *IFITM1* was amplified and subjected to DNA sequencing. The raw DNA sequence reads in the *IFITM1* gene are highlighted in (B). Genomic DNA sequence of the heterozygote *IFITM1* indels after cloning the PCR amplified *IFITM1* region into a vector and then sequencing individual plasmids for the type of gene edit. One allele of *IFITM1* has a one bp insertion and the other a one bp deletion, both resulting in frame-shift stop edits are highlighted in C. Predicted translation of each allele giving rise to premature stop codons are highlighted in D. (For interpretation of the references to colour in this figure legend, the reader is referred to the web version of this article.)

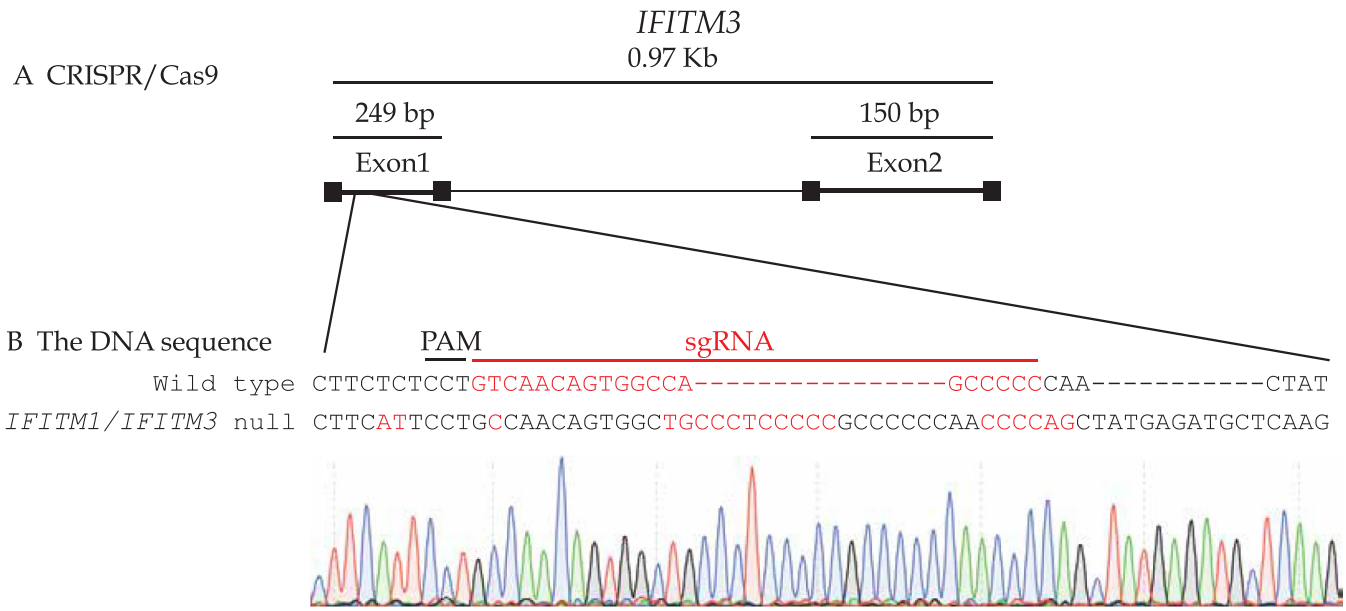

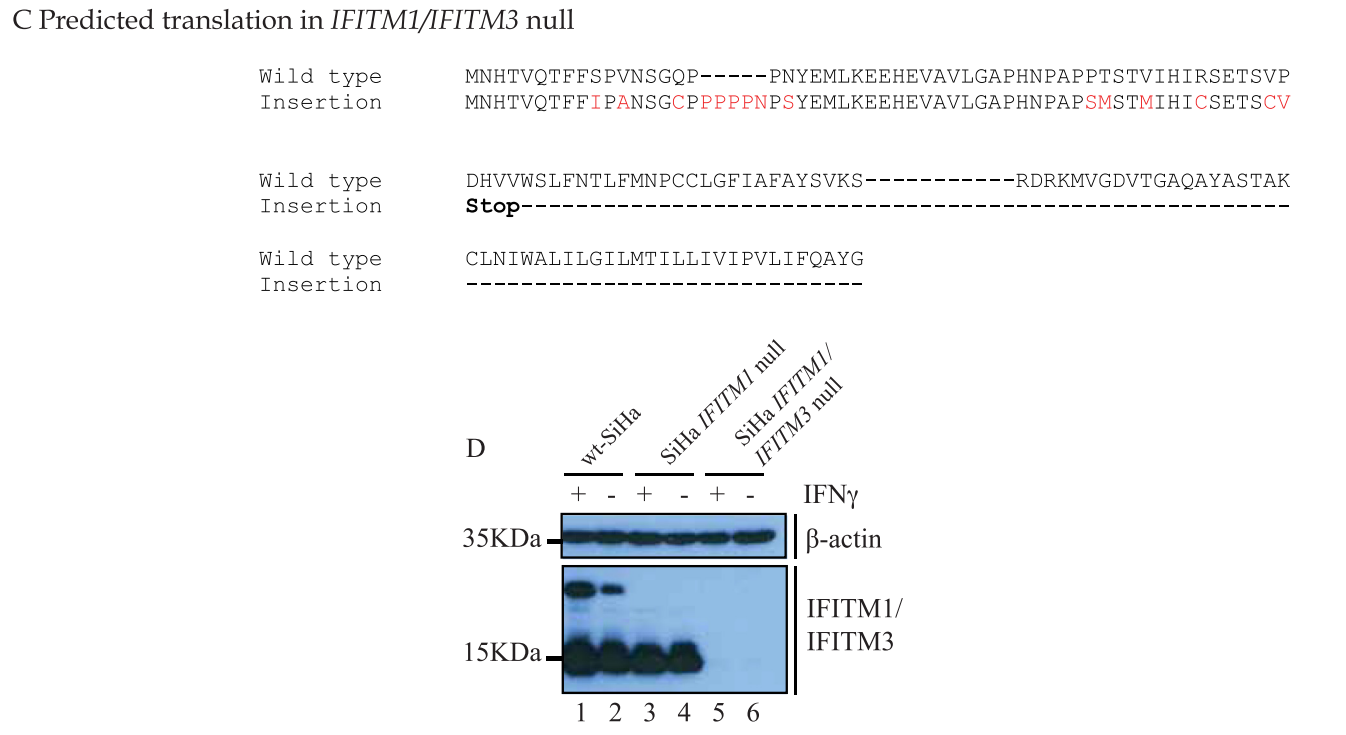

Fig. 3. Validation of the IFITM3 guide RNA. (A). Gene structure of the *IFITM3* gene highlighting its two coding exons and one intron. The genomic region surrounding the gRNA target site (with PAM site and homology region in red) for *IFITM3* was amplified and subjected to DNA sequencing. The raw DNA sequencing reads in the *IFITM3* gene are highlighted in (B). (For interpretation of the references to colour in this figure legend, the reader is referred to the web version of this article.)

The *IFITM3* gene has two insertions that result in a poly-proline frame-shift creating a stop codon (C). (D). Immunoblotting was performed using Mab-MHK with lysates from SiHa cells (lanes 1 and 2); *IFITM1* single null cells (lanes 3 and 4); and *IFITM1/IFITM3* double null cells (lanes 5 and 6). The cells were either untreated or treated with IFNγ (100 ng/ml) for 24 h and processed for immunoblotting with either a β-actin antibody or Mab-MHK.

peptides are attenuated (Fig. 5H), which is consistent with the early and transient induction of IRF1 by IFNγ. The synthesis of MHC Class I molecules was IFITM1/3-dependent (Fig. 5B vs 5F; quantified in biological triplicates in Fig. 5L). All three, major HLA alleles exhibited attenuated synthesis in the double null cell, as defined using the tryptic peptide coverage (Supplementary Fig. 3). Isotopically labeled ISG15 tryptic peptides are also not observed in the early interferon response (Supplementary Fig. 2), and the isotopically labeled ISG15 peptide recovery after 24 h is attenuated in the *IFITM1/IFITM3* double null cells (quantified in biological triplicates in Fig. 5G) suggesting that ISG15 protein synthesis is largely IFITM1/3 dependent. By contrast, STAT1 protein synthesis at 24 h appears largely IFITM1/3-independent (quantified in biological triplicates in Fig. 5I). Providing another internal control, another well-known inducible IFNγ protein, B2M, exhibits equivalent synthesis in the *IFITM1/IFITM3* double null cell (quantified in biological triplicates in Fig. 5K). This indicates that one key regulatory feature of the double null cell, STAT1 production, has remained intact.

3.4. Orthogonal validation of IFITM1/3 dependent induction of HLA-B and ISG15

These data first demonstrate that using the pulse-SILAC methodology, the SiHa cell model reflects the classic IFNγ responsive induction of STAT1, IRF1, B2M, ISG15, and MHC Class I molecules (Fig. 5B vs 5A and Supplementary Fig. 2). Also of note is attenuation of HLA-A, HLA-B, HLA-C, and ISG15 protein synthesis 24 h post-IFNγ treatment in the *IFITM1/IFITM3* double null cells compared to parental SiHa (Fig. 5F vs 5B).

In order to determine if IFITM1 deletion alone impacted on this set of gene products, the parental SiHa and *IFITM1*-null cells were in parallel treated with SILAC heavy-labeling media for 6 or 24 h. As with the double *IFITM1/IFITM3* double null cells, IFNγ dependent induction of IRF1 protein synthesis is attenuated 6 hours post labelling in the *IFITM1*-single null cells (Supplementary Fig. 2D vs 2B). This suggests that IRF1 is dependent upon IFITM1. Elevation of STAT1 protein synthesis are IFITM1-independent based on the equivalent induction of STAT1 in the *IFITM1*-single null cells (Fig. 5I). HLA-B protein synthesis is attenuated 24 hours post-IFNγ treatment in the *IFITM1* single null cells (Fig. 5L). ISG15 synthesis is also attenuated in the *IFITM1* single null cell (Fig. 5G). Together, these data suggest that MHC Class I family members and ISG15 require at least *IFITM1* for maximal IFNγ stimulated protein synthesis.

The software used to identify HLA orthologues in the pulse-SILAC screen (Fig. 4) can discriminate between HLA-A, HLA-B, and HLA-C based on tryptic peptide sequences (Supplementary Fig. 3). We focus here on HLA-B, which shows accurate identification of HLA-B specific peptides and it is also a member of the IRDS pathway [7]. We thus validated HLA-B protein expression in orthogonal assays to determine whether apparent reductions in HLA-B protein synthesis reduction in the *IFITM1/IFITM3* double null cells was reflected in total steady state protein levels and subcellular localization on the plasma membrane.

First, immunofluorescence of HLA-B was defined in parental SiHa and *IFITM1/IFITM3* double null cells. Parental SiHa cells revealed significant induction of HLA-B immunoreactivity 24 h after IFNγ treatment (Fig. 6C vs 6B and quantified in 6G). By contrast, basal HLA-B protein expression was attenuated in the *IFITM1/IFITM3* double null cells after IFNγ treatment (Fig. 6F vs 6E). Quantitation of the total immunofluorescence in the absence and presence of IFNγ, in the parental SiHa and *IFITM1/IFITM3* double null cells, also confirms attenuated HLA-B induction in the null cell panel (Fig. 6H vs 6G). This is consistent with the reduced protein synthesis observed for HLA-B in the pulse SILAC quantitation in the *IFITM1/IFITM3* double null cells.

The dominant subcellular localization of HLA-B is thought to reside on the cell surface as an antigen presentation carrier. We therefore evaluated whether HLA-B expression on the plasma membrane was altered in the *IFITM1/IFITM3* double null cell using FACS analysis with non-permeabilized cells. Two independent *IFITM1/IFITM3* double null cell clones were used as a form of biological replicate in comparison to the parental SiHa cell line. Twenty-four hours post treatment, HLA-B was elevated on the plasma membrane in the parental SiHa cell line (data not shown). Quantitation revealed reduced levels of HLA-B in both independent *IFITM1/IFITM3* double null biological replicates in the absence and presence of IFNγ (Fig. 6I). These data indicate that the

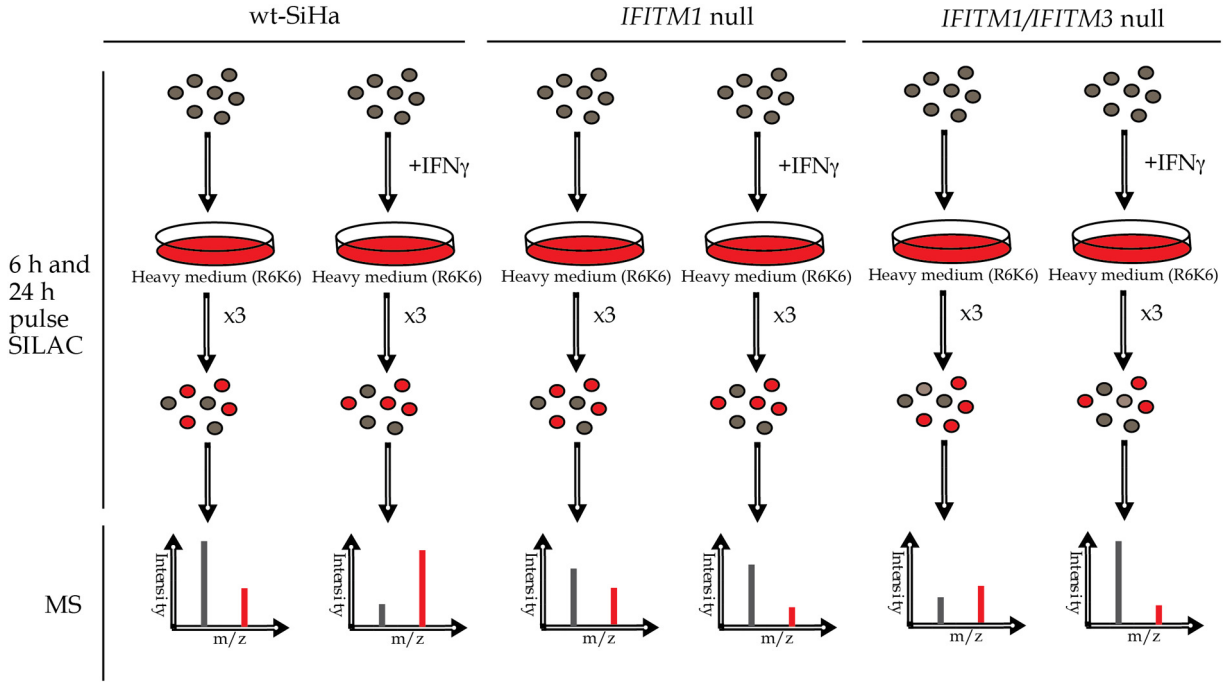

Fig. 4. Methodological approach to identify signalling pathways altered in IFITM1 and IFITM3 double null cells. The indicated cells (parental SiHa, *IFITM1* single null, or *IFITM1/IFITM3* double null) were pre-treated with carrier or IFNγ for 24 h. The media was replaced with R6K6 isotopically labeled media with carrier or IFNγ for 6 or 24 h. Cells were harvested, lysed, and tryptic peptides processed for analysis by mass spectrometry (MS) as indicated in the Experimental Procedures.

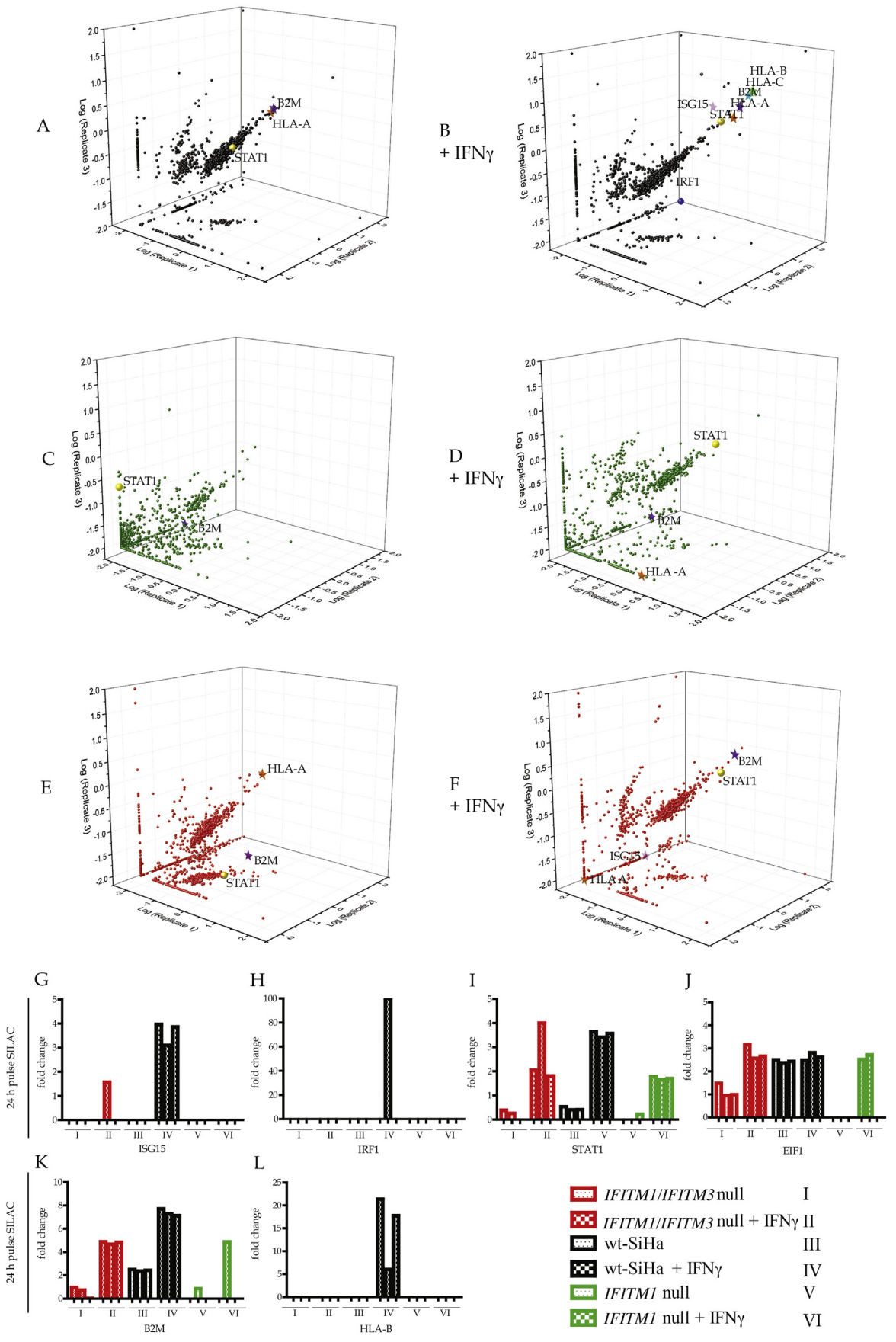

(caption on next page)

Fig. 5. Dominant proteins whose synthesis is attenuated after IFN-γ treatment in *IFITM1* single null cells, and *IFITM1/IFITM3* double null cells. SILAC pulse-labelling for 24 h was performed (A and B) in parental SiHa cells; (C and D) in *IFITM1* single null cells; and (E and F) in *IFITM1/IFITM3* double null cells (Supplementary Table 1). Cells were incubated with IFN-γ for 24 h in B, D and F. Data were plotted as a function of log10 fold change of heavy/light peptide intensities. Triplicates were represented in the x, y, and z-axis. In samples (G-L), representative peptides used for quantification in biological triplicates are highlighted to demonstrate a protein that is induced independent of *IFITM1/IFITM3* (STAT1, I and EIF1, J) and proteins that are IFITM1/3 dependent (ISG15; G, HLA-B, L).

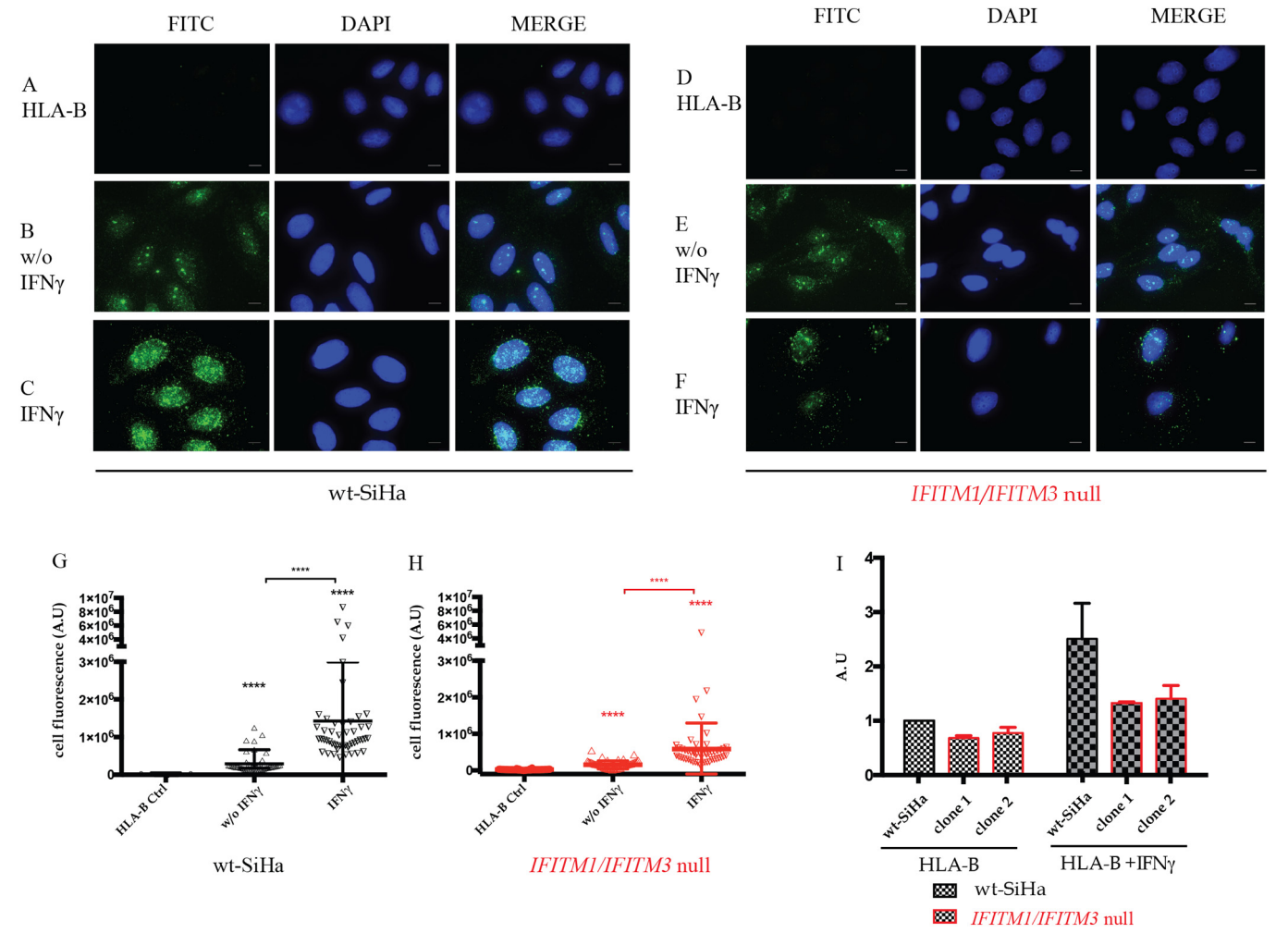

Fig. 6. Quantitation of HLA-B levels in parental SiHa and *IFITM1/IFITM3* double null cells using immunofluorescence. (A–F). The indicated cell panels were fixed without (B and E) or with 24 h of IFNγ treatment (C and F). Samples were fixed, and cells incubated with an HLA-B specific antibody. FITC images identify HLA-B (depicted in green) and DAPI (used for nuclear staining (depicted in blue)). $n = 3$. Scale bar: 10 μm. (G and H) Quantification of HLA-B total fluorescence per cell in presence or absence of IFNγ stimulation in (G) parental SiHa and (H) IFITM1/IFITM3 double null cells. For quantitation, three independent assays were performed, and each assay had two independent biological replicates. For each assay, fluorescence was measured in at least 50 cells per condition. Fluorescence was measured using ImageJ software. Statistical study was performed with 1-way Anova and Bonferroni correction (p-value $< .0001$). (I). FACS analysis was performed to measure the relative amount of HLA-B expressed on the surface of non-permeabilized cells treated with carrier or IFNγ for 24 h. The parental SiHa cell was used as a positive control and the two independently isolated *IFITM1/IFITM3* double null cells were used as biological replicates. Samples were processed in two independent experiments and HLA-B expression was normalized to 1.0 in the parental SiHa cell line. The data are plotted as relative arbitrary units (AU) as a function of the clone, treated with carrier or with IFNγ. (For interpretation of the references to colour in this figure legend, the reader is referred to the web version of this article.)

reduced synthesis of HLA-B in the *IFITM1/IFITM3* double null cell (Fig. 5) has an impact on its subcellular localization at the plasma membrane.

We next also examine whether there is any direct protein-protein interaction between IFITM1 and HLA-B since they are both co-synthesized, have transmembrane localizations on the cell surface, and are both IRDS components. In vivo proximity ligation assays are emerging methodologies that have been shown to demonstrate the "association" of two endogenously expressed proteins in fixed cells without the need for harsh lysis [44]. The method can be considered as an in situ mimic of an "immunoprecipitation assay". Proximity ligation assays can identify a protein-protein interaction/association with a distance of 10–30 nm that is in the upper range of that observed using FRET (5–20 nm) and this methodology can detect authentic endogenous proteins in situ that does not rely on transfected or artificially GFP-tagged protein vectors [45]. We evaluated whether IFITM1/3 and HLA-B co-associate using this methodology using antibodies to HLA-B and Mab-MHK (that can bind to both IFITM1 and IFITM3 proteins; Supplementary Fig. 1). A significant protein-protein interaction was observed in the IFNγ treated cells (representative images; Fig. 7A–D). These foci were absent in the *IFITM1/IFITM3* double null cells (Fig. 7E–H). Together, these data validate the pulse-SILAC data that identified HLA-B as a downstream effector of IFITM1/3.

ISG15 was not easily visualized using immunofluorescence in situ

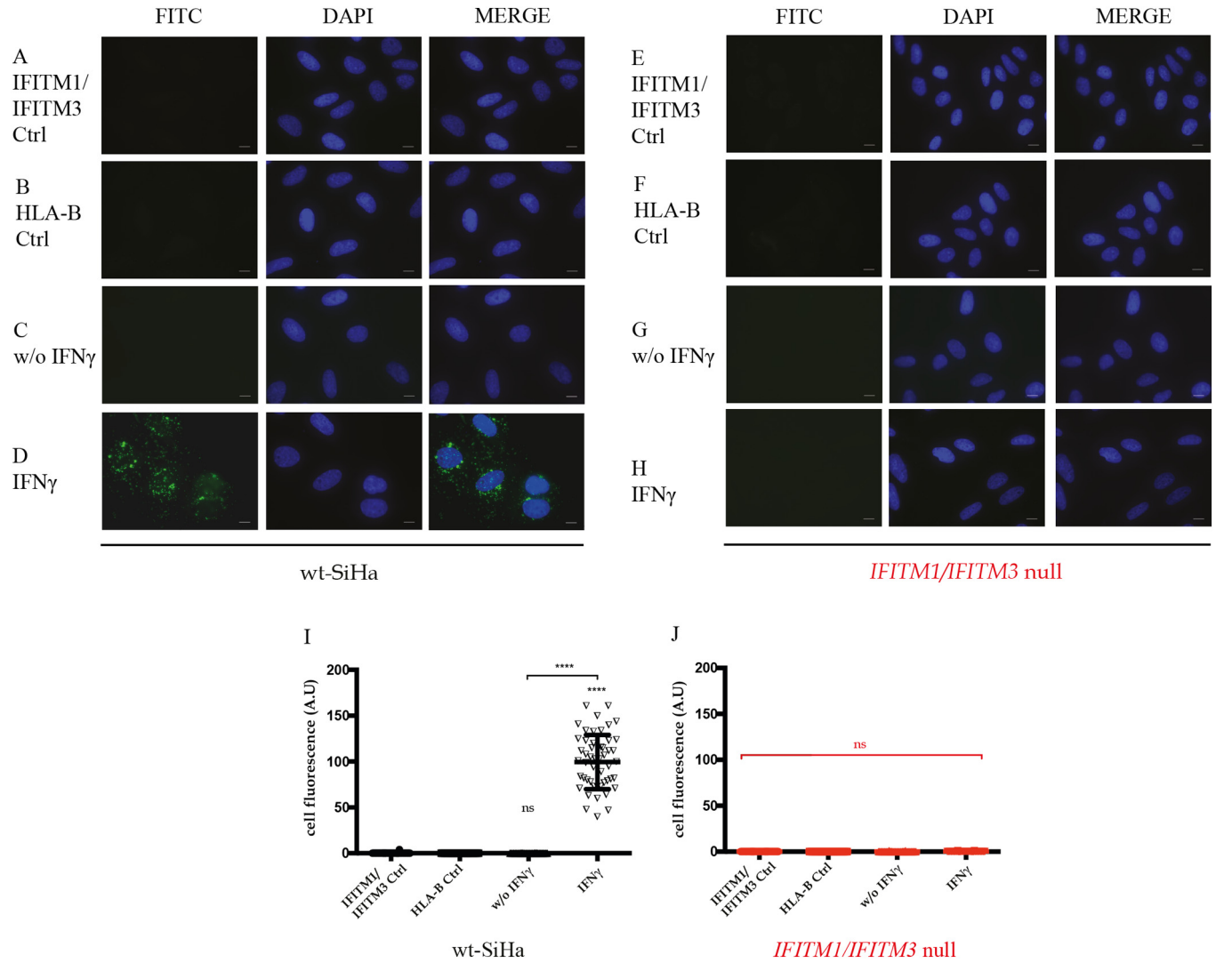

Fig. 7. Evaluation of the IFITM1/IFITM3:HLA-B protein-protein interaction in situ. Proximity ligation assays were used to study the endogenous interaction between HLA-B and IFITM1/3 proteins in parental SiHa (A–D) and *IFITM1/IFITM3* double null cells (*E*–H). Representative FITC images identify the protein-protein association foci (depicted in green) and DAPI was used for nuclear staining (depicted in blue). (A–B and E–F). Cells were incubated as negative controls using IFITM1/3 or HLA-B antibodies only. (C and G). Cells were incubated with both IFITM1/3 and HLA-B antibodies to define protein-protein foci in non-stimulated cells. (D and H) Cells were incubated with both IFITM1/3 and HLA-B antibodies to define protein-protein foci in IFN-γ stimulated cells. $n = 3$. Scale bar: 10 μm. (I and J) Quantification of HLA-B and IFITM1/3 total fluorescence per cell in presence or absence of IFNγ stimulation in (I) parental SiHa and (J) *IFITM1/IFITM3* double null cells. For quantitation, three independent assays were performed, and each assay had two independent biological replicates. For each assay, fluorescence was measured in at least 50 cells per condition. Fluorescence was measured using ImageJ software. Statistical study was performed with 1-way Anova and Bonferroni correction (p-value $<$ .0001). (For interpretation of the references to colour in this figure legend, the reader is referred to the web version of this article.)

(data not shown) nor could we identify a protein-protein association between IFITM1/3 proteins and ISG15 using proximity ligations (data not shown). We thus used an independent assay for orthogonal validation of ISG15 induction. We developed a SBP-tagged IFITM1 expression construct in order to ectopically express the protein in the parental SiHa cells and design methodologies for capturing IFITM1 associated proteins. The transfection of the SBP-IFITM1 expression could be detected as migrating at a higher mass (due to the SBP tag) than endogenous IFITM1/3 proteins in the parental SiHa cells (Fig. 8A, lane 3 vs lane 1) and specifically captured after affinity purification following expression in the *IFITM1/IFITM3* double null cell (Fig. 8A, lane 4 vs 2).

SWATH-MS analysis of the affinity purified material (SBP-IFITM1 vs SBP-only; material Fig. 8A, lane 4 vs lane 2), from untreated vs interferon treated, identified proteins that were enriched without or with IFN-γ treatment of parental SiHa cells, respectively (Fig. 8B; Supplementary Table 2). The data first highlight the detection of peptides belonging to a homologous sequence for IFITM1/2/3 proteins (Fig. 8B, Fig. 8C). Since IFITM1 was our bait protein we presume that it was the detected isoform, serving as an internal positive control (Fig. 8A). Nevertheless, IFITM1 may also be interacting with IFITM2 or IFITM3. The previously identified IFITM1/2/3 interacting protein VAPA was also detected (Fig. 8B and C), Supplementary Table 2. The proteins with the most significant *p*-values were enriched in IFN-γ treated cells, relative to non-treated cells (Fig. 8B and C, Supplementary Table 2). These included several proteins involved in cell-cell or cell matrix interactions including cornifin, galectin-7, desmocolin, JUP, hornerin, and desmoglein (Fig. 8C; Supplementary Table 3). This is suggestive of a pathway interaction of IFITM1 with membrane-dependent cell-cell communications. The enrichment of higher confident targets in IFN-γ treated cells also suggests that IFN-γ treatment may be required to fully 'activate' the IFITM1 protein interaction landscape. Interestingly, proteins related to IFNγ signalling were also detected; ISG15 and HLA-B (Fig. 8B and C). Immunoblotting also confirmed that ISG15ylation was

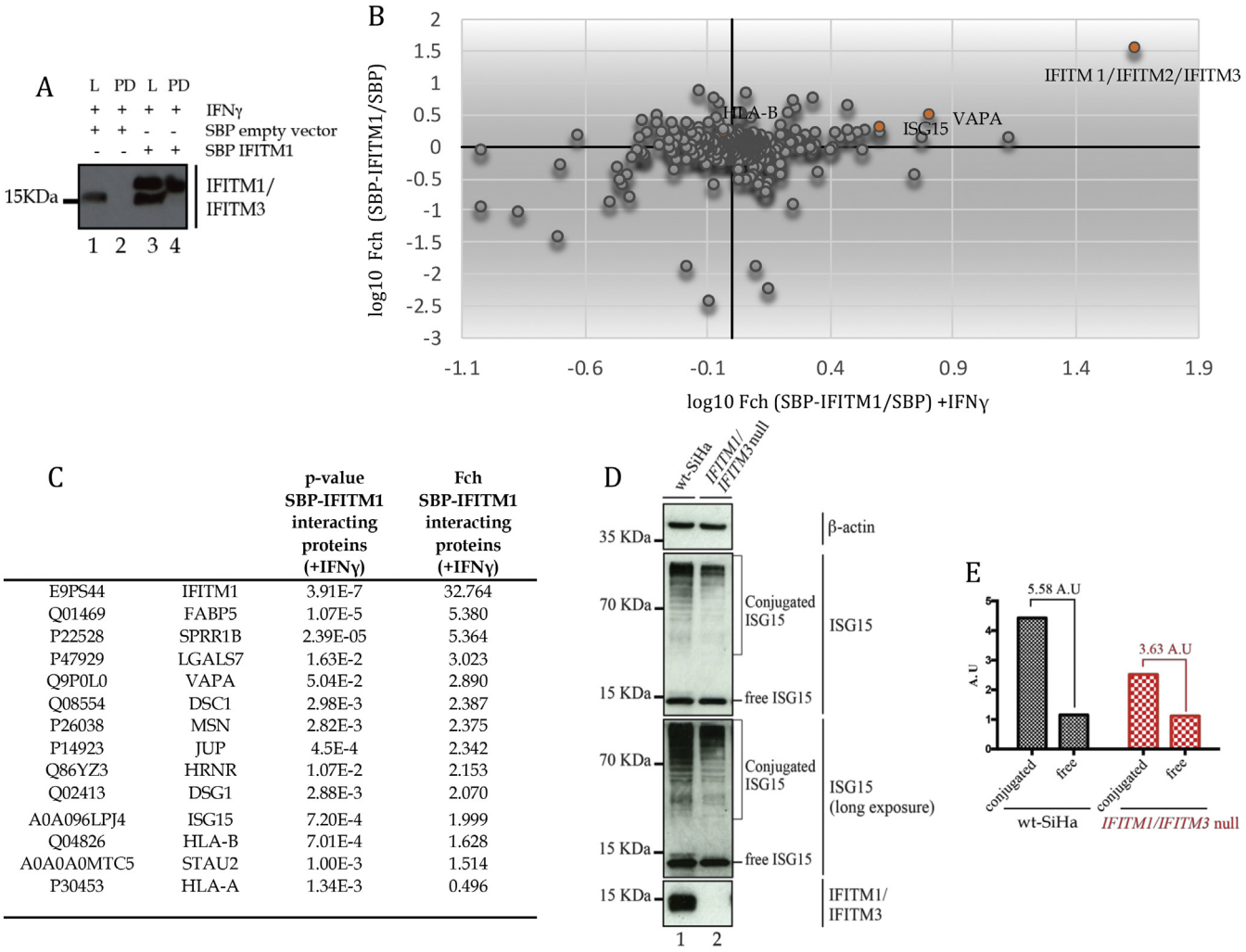

Fig. 8. Identification of IFITM1 interacting proteins in IFNγ treated cells. (A). SBP vector or SBP-tagged IFITM1 were transfected into parental SiHa cells and treated with IFNγ. Cells were lysed (L) and subjected to immunoprecipitation (PD) and evaluated by immunoblotting with Mab-MHK that can detect untagged or SBP-tagged IFITM1. (B). A 4-quadrant plot showing the relative quantification for binding proteins corresponding to fold change of cells transfected with SBP-IFITM1 versus SBP-empty vector and affinity purified with IFN-γ for 24 h (X-axis) or without IFN-γ stimulation (Y-axis). (C). Table with selected binding proteins detected by mass spectrometry for SBP-IFITM1 enrichment without or with IFN-γ stimulation (from Supplementary Table 3). (D). Cells (parental SiHa; lane 1; or *IFITM1/IFITM3* double null (lane 2) were transfected with empty vector (as in 8A) and treated with IFNγ. Samples were processed by immunoblotting with antibodies to ISG15. Free, monomeric ISG15 protein is highlighted, as well as conjugated ISG15. Free ISG15 protein is expressed at similar levels in both cells whilst conjugated ISG15 is attenuated in the IFITM1/IFITM3 double null cell (lane 2 vs 1). This suggests that ISG15ylation protein synthesis is linked to covalent conjugation under these conditions, under conditions where attenuated ISG15 protein synthesis was observed using pulse SILAC (Fig. 5). Antibodies to β-actin and IFITM1/3 proteins were used as loading controls, as indicated. (E). Free and conjugated ISG15 were quantified using ImageJ software. The relative units (in A.U.) define expression as a function of free or conjugated ISG15 in parental and *IFITM1/IFITM3* double null cells. The relative change in ISG15 conjugation over free ISG15 was 5.58 A.U. in parental cells. The relative change in ISG15 conjugation over free ISG15 was 3.63 A.U. in *IFITM1/3* double null cells.

attenuated in *IFITM1/IFITM3* double null cells after IFNγ stimulation (Fig. 8D). By contrast free ISG15 protein remained equivalent in both cells (Fig. 8D), suggesting that the ISG15 synthesis detected using pulse SILAC is directly linked to IFN stimulated protein conjugation. The ratio changes of conjugated to free ISG15 is summarized in Fig. 8E. Together, the orthogonal validation of HLA-B and ISG15 is consistent with the pulse SILAC data; IFITM1/3 proteins are required for maximal induction of HLA-B and ISG15ylation in IFNγ treated cells.

3.5. Orthogonal validation of the IFITM1 signalling protein landscape

We were unable to complement the IFITM1 and IFITM3 gene back into the double-null SiHa cells to stimulate ISG15ylation and HLA-B protein levels in IFN-γ treated cells (data not shown). As such, we took an independent approach to define dominating IFITM1-dependent signalling pathways and whether these overlap with the signalling proteins identified using the pulse-SILAC experimental methods. Although the majority of analyses identified HLA-B and ISG15 protein expression changes using *IFITM1/IFITM3* double null cells, we did create an *IFITM1* single null cell that revealed similar reductions in ISG15 and HLA-B after IFNγ treatment (Fig. 5D, G, and L). As such, we examined IFITM1 dependence in the steady-state proteome levels using IFITM1 targeted siRNA treatment of parental SiHa cells (Fig. 9A, lanes 4 and 2 vs 3 and 1) to determine if attenuation of IFITM1 by this method gave rise to similar proteome changes. However, there is a caveat to this method. Similar to plasmid transfection [46], double stranded RNA can also induce an IRF-1 dependent transcriptional interferon response [47]. Accordingly, we have also found that siRNA transfection methodologies can induce an IRF1 transcriptional response (data not shown). Nevertheless, siRNA is a powerful tool to determine gene dependencies in cell models. When parental SiHa cells, treated from 48 and 72 h with control siRNA or IFITM1-targeted siRNA, there was

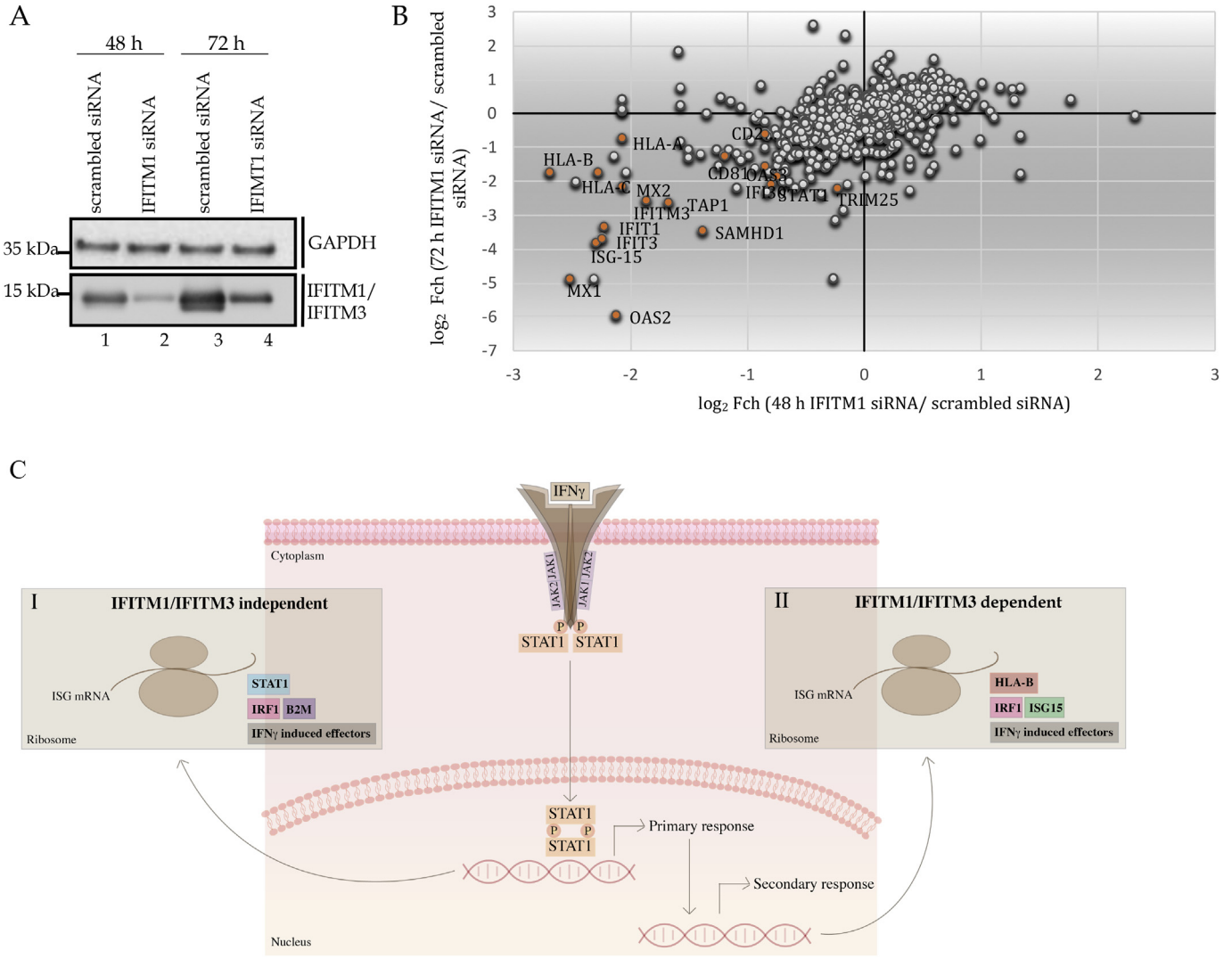

Fig. 9. The impact of IFITM1 targeted siRNA on the steady-state proteome. (A). Immunoblotting to demonstrate that IFITM1-targeted siRNA can attenuate IFITM1/3 protein levels. Cells were treated with the indicated control or targeted siRNA for two time points to capture the overlap in the transient dynamics of the interferon signalling cascade. Lysates were immunoblotted with the Mab-MHK antibody (the MHK monoclonal antibody cross reacts to a common N-terminal epitope in IFITM1 and IFITM3, see Supplementary Fig. 1) to quantify IFITM1/3 protein and the loading control (GAPDH), as highlighted. (B). Evaluation of the total steady-state proteome in response to siRNA targeting of IFITM1 in SiHa cells using SWATH-MS (data from Supplementary Table 3). The impact of IFITM1-targeted siRNA treatment for 48 and 72 h. These time points were a point of focus since the siRNA treatment activates the IRF1 transcriptional response over these two-time frames (data not shown). As such, the screen is conducted under experimental conditions in which we consider that the IRF1 response is activated by RNA treatment. The data from these two biological states are plotted as log2 fold change in protein levels (using SWATH-MS) as a function of either the 48 or 72-hour time point. The key proteins whose steady-state levels were suppressed after IFITM1-targeted siRNA treatment are highlighted in red, in the lower left quadrant. (C) The IFITM1 signalling model. Pulse labelling using SILAC methodologies identified STAT1 as a dominant protein synthesized after IFNγ treatment. This forms an internal positive control and is consistent with the classic JAK-STAT response to IFNγ treatment. (I). STAT1 can produce mRNAs that are translated in response to IFNγ treatment including IRF1 and other interferon effectors such as B2M. (II). By contrast to STAT1 and B2M, some of the IFNγ stimulated factors are *IFITM1* dependent including MHC Class I molecules and ISG15 (Fig. 5G and L). The siRNA-mediated depletion of IFITM1 represents an orthogonal assay that identified reductions in ISG15 and MHC Class I molecules (Fig. 9A). STAT1 protein reflects a distinct mechanism of control by IFITM1/3. Although pulse SILAC revealed that STAT1 synthesis is IFITM1/3-independent (Fig. 5), the steady state levels of STAT1 protein are reduced after targeted depletion of IFITM1 in SiHa cells (Fig. 9A). These data suggest that turnover of STAT1 protein might be dependent on IFITM1/3, but its synthesis is independent of IFITM1/3. However, these methodologies are complicated to compare directly, since the siRNA methodology uses an intrinsic RNA signal (double stranded RNA) that stimulates IRF1 but without exogenously added IFNγ, whilst the pulse SILAC used IFNγ without RNA ligands. Altogether, these data place IFITM1/3 proteins as a coordinator of the synthesis and/or steady state levels of a subset of key players in the IFNγ response. The notable induction of MHC Class I molecules and ISG15 in an IFITM1/3 dependent manner identifies a coordinated signalling pathway with potential clinical relevance (Fig. 1). The recent observation that lowered HLA-A, HLA-B, and HLA-C alleles correlates with poor prognosis and enhanced metastatic growth in cervical cancers [54] is further consistent with the existence of an IFITM1/3:HLA signalling pathway regulating cervical cancer outcomes. (For interpretation of the references to colour in this figure legend, the reader is referred to the web version of this article.)

striking and selective reduction in interferon-responsive proteins using label free quantitative mass spectrometry at both time points (Fig. 9B and Supplementary Table 3). Some of these proteins, including IFITM1 itself, are also components of the interferon-stimulated DNA damage resistant signature of proteins [9,10]. Interestingly, ISG15 and HLA-B are also lowered after the treatment of SiHa cells with IFITM1 targeted siRNA. However, there is one notable difference in the pulse-SILAC (Fig. 5) vs the siRNA methodology (Fig. 9B); STAT1 and B2M are IFITM1/3-independent as defined using pulse SILAC (Fig. 5); whilst STAT1 and B2M are IFITM1-dependent using the siRNA methodology

(Fig. 9B, Supplementary Table 3). This might reflect that fact that the RNA ligand (siRNA) induces additional RNA-activated pathways in the targeted siRNA proteome screen than IFNγ alone.

In conclusion, the pulse SILAC methodology in the IFITM1 single null (Fig. 5) and the siRNA treatment using IFITM1 targeted siRNA in parental SiHa cells (Fig. 9) both gave rise to overlapping proteome changes; mainly ISG15 and HLA-B. These data suggest that IFITM1 might alone function as an effector to these two proteins. However, we cannot rule out a role for IFITM3 in the *IFITM1* single null cell, since IFITM3 is also reduced by IFITM1 targeted siRNA treatment of SiHa cells (Fig. 9B). Thus, IFITM1 and IFITM3 might cooperate to mediate these effects.

4. Discussion

The IFITM protein family was identified in whole genome siRNA screens as RNA virus restriction factors [20]. The molecular functions of the IFITM family in the anti-viral response are just beginning to be defined. Yeast-two hybrid, with IFITM3 as a bait, was used as a methodology to discover new protein-protein interactions within the IFITM family that mediate viral restriction [21]; a protein-protein interaction was identified for IFITM3 and the Vesicle-membrane-protein-associated protein A (VAPA). The VAPA interaction occurred with IFITM1, IFITM2, or IFITM3 and these three were not distinguished from each other in this assay. Nevertheless, the study focused on defining how VAPA interaction with IFITM3 results in reduction of VAPA binding to oxysterol-binding protein (OSBP), disrupting cholesterol homeostasis, and preventing viral maturation. As IFITM1 and IFITM2 are also reported to bind to VAPA, it is not yet clear whether they play minor and/or redundant roles in controlling cholesterol-mediated viral maturation [21]. Interestingly, VAPA was also identified in our SWATH-IP using SBP-tagged IFITM1 (Fig. 8), which is consistent with VAPA being a dominant interactor for the IFITM family. In addition to VAPA, palmitoylation of IFITM1/2/3 family members has been reported to be required for some anti-viral functions [48]. Whether the anti-viral associations with VAPA or palmitoylation by the IFITM family impact on cancer growth control is not yet known.

The IFITM family also have reported roles in oncogenic and/or pro-metastatic cancer cell growth. It is not known if the anti-viral and pro-oncogenic functions of the IFITM family overlap. Within the IFITM1 family, IFTM1 is the most well documented to have pro-metastatic roles and it is the only IFITM family member with a partial residence in the plasma membrane [19]. IFITM1 is also the only IFITM family member that is a component of the Interferon-regulated DNA damage resistance (IRDS) pathway [10]. The IRDS contains a subset of approximately 30 interferon responsive genes that are up-regulated late in the viral response, upregulated during development of radiation resistance, and upregulated as a result of chronic exposure to lower levels of type I or type II interferons. IRDS pathway expression is mediated by 'unphosphorylated' STAT1 [49] and can be stimulated by IRF9 [50]. Interestingly, two IRDS genes (ISG15 and HLA-B) are induced after IFNγ exposure in a 'IFITM1-dependent' manner (Fig. 9C). Our unpublished data also indicate that IFITM1 single null cells are X-ray sensitive or cisplatin-sensitive, consistent with the hypothesis that IFITM1 expression is linked to chemo or irradiation resistance. The mechanisms whereby IFITM1 itself regulates such chemoresistant or pro-metastatic cell signalling events have not been mechanistically defined.

In this report, we begin to set up biochemical assays that could shed light on dominant cancer-associated functions of IFITM1. We first aimed to identify a clinically relevant human cancer model to study IFITM family of proteins. This required us to develop a pan-specific antibody that binds to both IFITM1 and IFITM3 proteins (Supplementary Fig. 1). This resulted in a focus on cervical cancer (Fig. 1) that exhibited high, medium or no expression of IFITM1/3 proteins (Fig. 1F). Of particular interest was the inverse correlation between IFITM1/3 protein expression and lymph node metastasis (Fig. 1F) suggesting that loss of IFITM1/3 protein expression correlates with evasion of the immune system. If IFITM1/3 are 'pro-oncogenic', why would cervical cancer panels reveal an inverse correlation between IFITM1/3 expression and cancer-positive lymph nodes in patients?

It is now becoming apparent that there are two distinct modes of metastatic cell growth. The first is the more classically defined metastasis due to enhanced 'invasion and migration" to secondary tissue niches. The second represents metastasis due to cancer cell escape from immune surveillance [51]. IFITM1/3-positive cancers might indeed be pro-invasive, depending on the microenvironment and tissue type, leading to poor clinical prognosis. The methodologies that highlighted such classic pro-metastatic roles for IFITM1 include over-expression by ectopic transfection of plasmid encoded genes or attenuation of gene expression using targeted siRNA [14]. By such experimental approaches, IFITM1 does indeed promote cancer cell growth and/or 'cell invasion' (i.e. a model of metastatic growth) [16]. Consistent with this, using clinical material IFITM1 protein has often been shown in literature to be over-produced in cancers using immunohistochemistry and this often correlates with poor prognosis [12,52].

However, our data reviewed using cervical cancer (Fig. 1) indicate that there can be two distinct states of cervical cancer with respect to IFITM1/3 expression. IFITM1/3 negative cervical cancers might also be more pro-invasive due to immune escape. This is based on the data indicating that the most dominant proteins whose synthesis depends on IFITM1/3 using the pulse SILAC methodology are in fact HLA family members (Figs. 4 and 5). HLA family members are components of the IRDS, they play a role in anti-viral immunity through the presentation of viral peptides through the MHC Class I system, and HLA expression is linked to immune rejection of cancer cells [53]. This suggests that although IFITM1/3 might be pro-oncogenic under some conditions, IFITM1/3-HLA signalling would presumably function as a 'tumor suppressor' signal via engagement of CD8+ T-cells. Such IFITM1/3 and HLA positive cancers might not metastasize because they produce neoantigen presenting MHC Class I molecules that keep the primary tumor in a local chronic state of equilibrium with the immune system. IFITM1/3-negative cancers by contrast might be expected to produce lower amounts of MHC Class I molecules following IFNγ stimulation (Fig. 9) resulting in lowered neoantigen expression, immune escape, and metastasis. Such hypotheses are consistent with two clinical observations in cervical cancers. First, an inverse correlation exists between IFITM1/3 expression and lymph-node positive cancers (Fig. 1). Second, a recent study has highlighted that lowered MHC Class I expression also predicts poor prognosis in cervical cancers [54]. This data is also consistent with several studies that highlight elevated rates of metastatic cancer cell growth in vivo are inversely correlated to MHC Class I expression including deletion of the MHC Class I locus [53].

Although expression of IFITM1/3 was detected in cancer cells (Fig. 1), it is interesting that IFITM1/3 protein expression was observed and confined to the basal 'stem cell' layer in representative normal tissue controls using immunohistochemistry (Fig. 1 E). Expression was not observed even on one cell layer up from the basal layer. In squamous human skin, this basal layer is reflective of p63 (a squamous stem cell transcription factor) and phosphorylated p53 positive stem cell populations after UV irradiation [55]. Thus, this expression might reflect a role for IFITM1 in squamous stem cell pluripotency. We do not have very many samples reflecting a 'normal' human cervical epithelium, but the few cases we have exhibit very strong staining in the basal layer (data not shown). During the course of these studies *the Human Protein Atlas* has also populated their immunohistochemical library with expression patterns of IFITM1 protein in normal tissues. We can see in this library that IFITM1 protein is also confined to the "basal stem cell" layer in normal squamous oesophagus, cervix, and oral mucosa (Supplementary Fig. 4). Together, these data would suggest that IFITM1 might play a role in squamous stem cell physiology as its expression appears specifically confined to the basal layer and is not expressed in suprabasal normal squamous cells. As the 'normal' squamous cervical

epithelium we have used is from patients undergoing screening for cervical cancer or dysplasia, we cannot rule out a role for HPV in this expression in normal cervical cells. However, as the oesophagus squamous epithelium also exhibits IFITM1 protein expression in the basal cells of normal squamous epithelium (Protein Atlas, Supplementary Fig. 4), and the normal oesophagus is not noted for HPV infection, we would suggest that the expression of IFITM1 protein in basal cells is not related to HPV status. The signalling pathways that might trigger basal IFITM1 protein expression in squamous stem cell populations are not precisely defined. However, at the mRNA level, differential expression patterns of *ifitm1* gene expression were identified in the uteri of mice and there were correlations between the patterns of *ifitm1* gene expression and Wnt/β-catenin expression [56]. These data might suggest a role for Wnt signalling as an upstream regulator of IFITM1 in stem cells.

Our focus on cervical cancer as a model to understand the cancer-associated role of IFITM1/3 is interesting considering IFITM1/IFITM3 are themselves RNA viral restriction factors and HPV infection is a risk factor in cervical cancer progression. There is evidence that IFITM1 and IFITM3 might be a positive cofactor for a DNA virus; HPV16 viral propagation [57]. We do not have any data that defines the HPV status of the cervical cancers we have analyzed (Fig. 1), as the main clinically approved assay for diagnostics is p16 positive cancer cells [58]. There is a close relation between persistent viral infection, development of cancer and failure in immune response. As an example, cervical as well as vulvar intraepithelial neoplasia are pre-cancerous conditions characterized by sustained HPV-16 infection. A clinical study shows favorable prognosis related to an increase in IFNγ-producing CD8+ cytotoxic T following to robust cell response induced by vaccination [59]. Vaccination delivers a high dose of specific antigen against HPV-16 oncoproteins E6 and E7 and mediates MHC-binding peptide complex presentation [60]. A similar outcome was also observed after vaccination of a preclinical mouse model of HPV positive cervical cancer [61]. There is a significant correlation between MHC Class I (not found for MHC Class II) expression on malignant cells and T-cell infiltration (TIL) in human ovarian cancer [62], being a positive prognostic factor. Thus, IFITM1 and IFITM3 might have dual roles in stimulating HPV propagation, but also in suppressing cancer escape from immune surveillance.

One of the key approaches we used to evaluate the role of IFITM1 in IFNγ dependent protein production was the utilization of CRISPR-Cas9 guide RNAs to create isogenic knock-out cells. At the outset, we relied less on the use of siRNA to deplete IFITM1 since this would only give a transient reduction in a target protein but also siRNA itself can induce an interferon response (data not shown; [46]). This would have complicated our analysis of the interferon-responsive nature of any IFITM1 protein interactions we visualize and measure. Nevertheless, siRNA was used as a final orthogonal approach to define IFITM1 signalling events (Fig. 9A, B). By contrast, the limitation of using gene knockout tools to reduce expression of a protein requires that loss of the protein is not a lethal event. In the case of *IFITM1* and *IFITM3* knock-out mice are reported as viable [41], thus it was not unexpected that we were able to generate single *IFITM1* null and double *IFITM1/IFITM3* double null cell panels (Figs. 2 and 3). However, we were unable to generate single *IFITM3* null cells under experiments carried out in parallel to those reported in this manuscript (data not shown).

Using these isogenic cell panels, we were able to determine whether there were defects in IFNγ dependent protein synthesis using pulse SILAC methodologies. We chose to use a pulse-SILAC approach to identify the isotopically labeled tryptic peptides with the most significant fold change after IFNγ treatment and which are altered in the double *IFITM1/IFITM3* or *IFITM1* single null cells. The most significantly suppressed proteins in the double *IFITM1/IFITM3* or *IFITM1* single null cells after IFNγ treatment were MHC Class I orthologues encoded by the HLA-A, HLA-B, and HLA-C genes (Fig. 5). As rationalized above, the data suggested an inverse correlation between IFITM1/3 protein and HLA expression with metastatic growth in cervical cancer.

The interferon-responsive protein ISG15 was also attenuated in the double *IFITM1/IFITM3* null cells or single *IFITM1* single null cells after IFNγ treatment (Fig. 5G). The fact that ISG15 and HLA-B are enriched in the SBP-IFITM1 protein affinity purification after IFNγ treatment (Fig. 8) suggests a co-operative activity exists between the two proteins. Indeed, as HLA-B can interact in situ with IFITM1/3 after IFNγ treatment (Fig. 7), and as ISG15 is a high-confident IFITM1-associated protein using SWATH-IP mass spectrometry (Fig. 8), these data suggest that the two proteins are directly involved in the IFITM1/3 dependent IFNγ response. ISG15 is also a component of an interferon and immune responsive gene cluster that are suppressed by stem cell pluripotent gene product expression [63], suggesting that, like HLA suppression, ISG15 suppression might be co-incident with immune escape. In the case of IFITM1/3 signalling, we do not see defects in 'free' monomeric ISG15 in the double *IFITM1/IFITM3* null cells, but reductions in the conjugation of higher molecular mass ISG15ylated adducts (Fig. 8D). These data suggest that conjugation of proteins to ISG15 during interferon stimulation might play a coordinated role in the IFITM1/3 dependent immune-tumor cell interactions. Overproduction of ISG15 has been reported previously to stabilize IFITM3 [64], consistent with our data that ISG15 is detected in the SBP-IFITM1 complex (Fig. 8). Ubiquitination of IFITM3 might counteract the stimulatory effect of ISG15 on the anti-viral functions of the protein [65]. How ubiquitination and ISG15ylation regulate IFITM1 and/or IFITM3 in a coordinated fashion is not defined.

These data together provide a novel biochemical pathway relevant for cancer associated functions of IFITM1/3 that correlates with the interferon-responsive nature of IFITM1/3 signalling; they can mediate IFNγ dependent protein production of MHC Class I proteins and ISG15 (Fig. 5), whilst the maintenance of STAT1 protein in response to IFNγ involves by a different signalling mechanism that is IFITM1/3-independent (Fig. 9B). Both antigen presentation and ISG15ylation signalling events are important for anti-viral signalling as well as immune regulation of cancer cells at the immune-cancer synapse [66–71]. Further research will shed light on how reductions in HLA and ISG15ylation can impact on both oncogenic signalling and/or anti-viral activity in response to IFITM1/3 expression.

Supplementary data to this article can be found online at https://doi.org/10.1016/j.cellsig.2019.03.024.

Acknowledgements

This work was supported by the Medical Research Scotland (MGH); Ministry of Education Youth and Sports (MEYS) NPS-I – LO1413 and LM2015089, with Czech Science Foundation (GACR) 18-23773Y (MN, JF) and MH CZ - DRO (MMCI, 00209805), the BBSRC (BB/C511599/1; United Kingdom); The International Centre for Cancer Vaccine Science project is carried out within the International Research Agendas programme of the Foundation for Polish Science cofinanced by the European Union under the European Regional Development Fund.

References

[1] A. Takaoka, H. Yanai, Interferon signalling network in innate defence, Cell. Microbiol. 8 (6) (2006) 907–922.
[2] L.C. Platanias, Mechanisms of type-I- and type-II-interferon-mediated signalling, Nat. Rev. Immunol. 5 (5) (2005) 375–386.
[3] J. Bekisz, H. Schmeisser, J. Hernandez, N.D. Goldman, K.C. Zoon, Human interferons alpha, beta and omega, Growth Factors 22 (4) (2004) 243–251.
[4] E.C. Borden, G.C. Sen, G. Uze, R.H. Silverman, R.M. Ransohoff, G.R. Foster, G.R. Stark, Interferons at age 50: past, current and future impact on biomedicine, Nat. Rev. Drug Discov. 6 (12) (2007) 975–990.
[5] J.E. Darnell Jr., I.M. Kerr, G.R. Stark, Jak-STAT pathways and transcriptional activation in response to IFNs and other extracellular signaling proteins, Science 264 (5164) (1994) 1415–1421.
[6] B.R. Williams, Transcriptional regulation of interferon-stimulated genes, Eur. J. Biochem. / FEBS 200 (1) (1991) 1–11.

[7] H. Cheon, E.C. Borden, G.R. Stark, Interferons and their stimulated genes in the tumor microenvironment, Semin. Oncol. 41 (2) (2014) 156–173.
[8] T.A. Wallace, D.N. Martin, S. Ambs, Interactions among genes, tumor biology and the environment in cancer health disparities: examining the evidence on a national and global scale, Carcinogenesis 32 (8) (2011) 1107–1121.
[9] N.N. Khodarev, B. Roizman, R.R. Weichselbaum, Molecular pathways: interferon/stat1 pathway: role in the tumor resistance to genotoxic stress and aggressive growth, Clin. Cancer Res. 18 (11) (2012) 3015–3021 an official journal of the American Association for Cancer Research.
[10] R.R. Weichselbaum, H. Ishwaran, T. Yoon, D.S. Nuyten, S.W. Baker, N. Khodarev, A.W. Su, A.Y. Shaikh, P. Roach, B. Kreike, B. Roizman, J. Bergh, Y. Pawitan, M.J. van de Vijver, A.J. Minn, An interferon-related gene signature for DNA damage resistance is a predictive marker for chemotherapy and radiation for breast cancer, Proc. Natl. Acad. Sci. U. S. A. 105 (47) (2008) 18490–18495.
[11] T.H. Wu, K. Schreiber, A. Arina, N.N. Khodarev, E.V. Efimova, D.A. Rowley, R.R. Weichselbaum, H. Schreiber, Progression of cancer from indolent to aggressive despite antigen retention and increased expression of interferon-gamma inducible genes, Cancer Immun. 11 (2011) 2.
[12] D. Borg, C. Hedner, A. Gaber, B. Nodin, R. Fristedt, K. Jirstrom, J. Eberhard, A. Johnsson, Expression of IFITM1 as a prognostic biomarker in resected gastric and esophageal adenocarcinoma, Biomark Res. 4 (2016) 10.
[13] B. Gyorffy, M. Dietel, T. Fekete, H. Lage, A snapshot of microarray-generated gene expression signatures associated with ovarian carcinoma, Int. J. Gynecol. Cancer 18 (6) (2008) 1215–1233.
[14] I.N. Sari, Y.G. Yang, L.T. Phi, H. Kim, M.J. Baek, D. Jeong, H.Y. Kwon, Interferon-induced transmembrane protein 1 (IFITM1) is required for the progression of colorectal cancer, Oncotarget 7 (52) (2016) 86039–86050.
[15] J. Ogony, H.J. Choi, A. Lui, M. Cristofanilli, J. Lewis-Wambi, Interferon-induced transmembrane protein 1 (IFITM1) overexpression enhances the aggressive phenotype of SUM149 inflammatory breast cancer cells in a signal transducer and activator of transcription 2 (STAT2)-dependent manner, Breast Cancer Res.: BCR 18 (1) (2016) 25.
[16] F. Yu, D. Xie, S.S. Ng, C.T. Lum, M.Y. Cai, W.K. Cheung, H.F. Kung, G. Lin, X. Wang, M.C. Lin, IFITM1 promotes the metastasis of human colorectal cancer via CAV-1, Cancer Lett. 368 (1) (2015) 135–143.
[17] C.C. Bailey, G. Zhong, I.C. Huang, M. Farzan, IFITM-family proteins: the cell's first line of antiviral Defense, Annu. Rev. Virol. 1 (2014) 261–283.
[18] R. Jia, S. Ding, Q. Pan, S.L. Liu, W. Qiao, C. Liang, The C-terminal sequence of IFITM1 regulates its anti-HIV-1 activity, PLoS One 10 (3) (2015) e0118794.
[19] S. Weston, S. Czieso, I.J. White, S.E. Smith, P. Kellam, M. Marsh, A membrane topology model for human interferon inducible transmembrane protein 1, PLoS One 9 (8) (2014) e104341.
[20] A.L. Brass, I.C. Huang, Y. Benita, S.P. John, M.N. Krishnan, E.M. Feeley, B.J. Ryan, J.L. Weyer, L. van der Weyden, E. Fikrig, D.J. Adams, R.J. Xavier, M. Farzan, S.J. Elledge, The IFITM proteins mediate cellular resistance to influenza A H1N1 virus, West Nile virus, and dengue virus, Cell 139 (7) (2009) 1243–1254.
[21] S. Amini-Bavil-Olyaee, Y.J. Choi, J.H. Lee, M. Shi, I.C. Huang, M. Farzan, J.U. Jung, The antiviral effector IFITM3 disrupts intracellular cholesterol homeostasis to block viral entry, Cell Host Microbe 13 (4) (2013) 452–464.
[22] I.C. Huang, C.C. Bailey, J.L. Weyer, S.R. Radoshitzky, M.M. Becker, J.J. Chiang, A.L. Brass, A.A. Ahmed, X. Chi, L. Dong, L.E. Longobardi, D. Boltz, J.H. Kuhn, S.J. Elledge, S. Bavari, M.R. Denison, H. Choe, M. Farzan, Distinct patterns of IFITM-mediated restriction of filoviruses, SARS coronavirus, and influenza A virus, PLoS Pathog. 7 (1) (2011) e1001258.
[23] R. Nenutil, J. Smardova, S. Pavlova, Z. Hanzelkova, P. Muller, P. Fabian, R. Hrstka, P. Janotova, M. Radina, D.P. Lane, P.J. Coates, B. Vojtesek, Discriminating functional and non-functional p53 in human tumours by p53 and MDM2 immunohistochemistry, J. Pathol. 207 (3) (2005) 251–259.
[24] N.E. Sanjana, O. Shalem, F. Zhang, Improved vectors and genome-wide libraries for CRISPR screening, Nat. Methods 11 (8) (2014) 783–784.
[25] M.K. Doherty, R.J. Beynon, Protein turnover on the scale of the proteome, Expert Rev. Proteomics 3 (1) (2006) 97–110.
[26] M.K. Doherty, D.E. Hammond, M.J. Clague, S.J. Gaskell, R.J. Beynon, Turnover of the human proteome: determination of protein intracellular stability by dynamic SILAC, J. Proteome Res. 8 (1) (2009) 104–112.
[27] X. Wang, Y. Liang, L. Liu, J. Shi, H.J. Zhu, Targeted absolute quantitative proteomics with SILAC internal standards and unlabeled full-length protein calibrators (TAQSI), Rapid Commun. Mass Spectrom. 30 (5) (2016) 553–561.
[28] N.J. Kruger, The Bradford method for protein quantitation, Methods Mol. Biol. 32 (1994) 9–15.
[29] U.K. Laemmli, Cleavage of structural proteins during the assembly of the head of bacteriophage T4, Nature 227 (5259) (1970) 680–685.
[30] L.L. Manza, S.L. Stamer, A.J. Ham, S.G. Codreanu, D.C. Liebler, Sample preparation and digestion for proteomic analyses using spin filters, Proteomics 5 (7) (2005) 1742–1745.
[31] J.R. Wisniewski, A. Zougman, N. Nagaraj, M. Mann, Universal sample preparation method for proteome analysis, Nat. Methods 6 (5) (2009) 359–362.
[32] D. Li, Z. Peng, H. Tang, P. Wei, X. Kong, D. Yan, F. Huang, Q. Li, X. Le, Q. Li, K. Xie, KLF4-mediated negative regulation of IFITM3 expression plays a critical role in colon cancer pathogenesis, Clin. Cancer Res. 17 (11) (2011) 3558–3568 an official journal of the American Association for Cancer Research.
[33] N.T. Seyfried, L.C. Huysentruyt, J.A. Atwood 3rd, Q. Xia, T.N. Seyfried, R. Orlando, Up-regulation of NG2 proteoglycan and interferon-induced transmembrane proteins 1 and 3 in mouse astrocytoma: a membrane proteomics approach, Cancer Lett. 263 (2) (2008) 243–252.
[34] F. Yu, S.S. Ng, B.K. Chow, J. Sze, G. Lu, W.S. Poon, H.F. Kung, M.C. Lin, Knockdown of interferon-induced transmembrane protein 1 (IFITM1) inhibits proliferation, migration, and invasion of glioma cells, J. Neuro-Oncol. 103 (2) (2011) 187–195.
[35] G. Yang, Y. Xu, X. Chen, G. Hu, IFITM1 plays an essential role in the anti-proliferative action of interferon-gamma, Oncogene 26 (4) (2007) 594–603.
[36] Z. Pan, S. Chen, X. Pan, Z. Wang, H. Han, W. Zheng, X. Wang, F. Li, S. Qu, R. Shao, Differential gene expression identified in Uigur women cervical squamous cell carcinoma by suppression subtractive hybridization, Neoplasma 57 (2) (2010) 123–128.
[37] W. Zheng, Z. Zhao, X. Yi, Q. Zuo, H. Li, X. Guo, D. Li, H. He, Z. Pan, P. Fan, F. Li, Y. Liao, R. Shao, Down-regulation of IFITM1 and its growth inhibitory role in cervical squamous cell carcinoma, Cancer Cell Int. 17 (2017) 88.
[38] C.C. Baker, W.C. Phelps, V. Lindgren, M.J. Braun, M.A. Gonda, P.M. Howley, Structural and transcriptional analysis of human papillomavirus type 16 sequences in cervical carcinoma cell lines, J. Virol. 61 (4) (1987) 962–971.
[39] W.C. Phelps, P.M. Howley, Transcriptional trans-activation by the human papillomavirus type 16 E2 gene product, J. Virol. 61 (5) (1987) 1630–1638.
[40] C.C. Bailey, I.C. Huang, C. Kam, M. Farzan, Ifitm3 limits the severity of acute influenza in mice, PLoS Pathog. 8 (9) (2012) e1002909.
[41] A.R. Everitt, S. Clare, J.U. McDonald, L. Kane, K. Harcourt, M. Ahras, A. Lall, C. Hale, A. Rodgers, D.B. Young, A. Haque, O. Billker, J.S. Tregoning, G. Dougan, P. Kellam, Defining the range of pathogens susceptible to Ifitm3 restriction using a knockout mouse model, PLoS One 8 (11) (2013) e80723.
[42] G. Zhang, D. Fenyo, T.A. Neubert, Evaluation of the variation in sample preparation for comparative proteomics using stable isotope labeling by amino acids in cell culture, J. Proteome Res. 8 (3) (2009) 1285–1292.
[43] A. Thakur, A.G. Hinnebusch, eIF1 loop 2 interactions with met-tRNAi control the accuracy of start codon selection by the scanning preinitiation complex, Proc. Natl. Acad. Sci. U. S. A. 115 (18) (2018) E4159–E4168.
[44] I. Weibrecht, K.J. Leuchowius, C.M. Clausson, T. Conze, M. Jarvius, W.M. Howell, M. Kamali-Moghaddam, O. Soderberg, Proximity ligation assays: a recent addition to the proteomics toolbox, Expert Rev. Proteomics 7 (3) (2010) 401–409.
[45] D. Raykova, B. Koos, A. Asplund, M. Gelleri, Y. Ivarsson, U.H. Danielson, O. Soderberg, Let there be light!, Proteomes 4 (4) (2016).
[46] S. Huerfano, B. Ryabchenko, J. Forstova, Nucleofection of expression vectors induces a robust interferon response and inhibition of cell proliferation, DNA Cell Biol. 32 (8) (2013) 467–479.
[47] X.Q. Li, X.N. Li, J.J. Liang, X.B. Cai, Q. Tao, Y.X. Li, Q. Qin, S.P. Xu, T.R. Luo, IRF1 up-regulates isg15 gene expression in dsRNA stimulation or CSFV infection by targeting nucleotides −487 to −325 in the 5′ flanking region, Mol. Immunol. 94 (2018) 153–165.
[48] S.K. Narayana, K.J. Helbig, E.M. McCartney, N.S. Eyre, R.A. Bull, A. Eltahla, A.R. Lloyd, M.R. Beard, The interferon-induced transmembrane proteins, IFITM1, IFITM2, and IFITM3 inhibit hepatitis C virus entry, J. Biol. Chem. 290 (43) (2015) 25946–25959.
[49] H. Cheon, G.R. Stark, Unphosphorylated STAT1 prolongs the expression of interferon-induced immune regulatory genes, Proc. Natl. Acad. Sci. U. S. A. 106 (23) (2009) 9373–9378.
[50] J. Nan, Y. Wang, J. Yang, G.R. Stark, IRF9 and unphosphorylated STAT2 cooperate with NF-kappaB to drive IL6 expression, Proc. Natl. Acad. Sci. U. S. A. 115 (15) (2018) 3906–3911.
[51] D. Hanahan, R.A. Weinberg, Hallmarks of cancer: the next generation, Cell 144 (5) (2011) 646–674.
[52] J. Lee, S.H. Goh, N. Song, J.A. Hwang, S. Nam, I.J. Choi, A. Shin, I.H. Kim, M.H. Ju, J.S. Jeong, Y.S. Lee, Overexpression of IFITM1 has clinicopathologic effects on gastric cancer and is regulated by an epigenetic mechanism, Am. J. Pathol. 181 (1) (2012) 43–52.
[53] N. McGranahan, R. Rosenthal, C.T. Hiley, A.J. Rowan, T.B.K. Watkins, G.A. Wilson, N.J. Birkbak, S. Veeriah, P. Van Loo, J. Herrero, C. Swanton, T.R. Consortium, Allele-specific HLA loss and immune escape in lung cancer evolution, Cell 171 (6) (2017) (1259–1271 e11).
[54] D.M. Ferns, A.M. Heeren, S. Samuels, M.C.G. Bleeker, T.D. de Gruijl, G.G. Kenter, E.S. Jordanova, Classical and non-classical HLA class I aberrations in primary cervical squamous- and adenocarcinomas and paired lymph node metastases, J. Immunother. Cancer 4 (2016) 78.
[55] L.E. Finlan, R. Nenutil, S.H. Ibbotson, B. Vojtesek, T.R. Hupp, CK2-site phosphorylation of p53 is induced in DeltaNp63 expressing basal stem cells in UVB irradiated human skin, Cell Cycle 5 (21) (2006) 2489–2494.
[56] H.J. Park, I.S. Kuk, J.H. Kim, J.H. Kim, S.J. Song, B.C. Choi, B. Kim, N.H. Kim, H. Song, Characterisation of mouse interferon-induced transmembrane protein-1 gene expression in the mouse uterus during the oestrous cycle and pregnancy, Reprod. Fertil. Dev. 23 (6) (2011) 798–808.
[57] C.J. Warren, L.M. Griffin, A.S. Little, I.C. Huang, M. Farzan, D. Pyeon, The antiviral restriction factors IFITM1, 2 and 3 do not inhibit infection of human papillomavirus, cytomegalovirus and adenovirus, PLoS One 9 (5) (2014) e96579.
[58] H.R. Wang, Y.C. Li, H.Q. Guo, L.L. Yu, Z. Wu, J. Yin, G.D. Liao, Y.M. Qu, Y. Jiang, D. Wang, W. Chen, A cocktail of p16(INK4a) and Ki-67, p16(INK4a) and mini-chromosome maintenance protein 2 as triage tests for human papillomavirus primary cervical cancer screening, Oncotarget 8 (48) (2017) 83890–83899.
[59] G.G. Kenter, M.J. Welters, A.R. Valentijn, M.J. Lowik, D.M. Berends-van der Meer, A.P. Vloon, F. Essahsah, L.M. Fathers, R. Offringa, J.W. Drijfhout, A.R. Wafelman, J. Oostendorp, G.J. Fleuren, S.H. van der Burg, C.J. Melief, Vaccination against HPV-16 oncoproteins for vulvar intraepithelial neoplasia, N. Engl. J. Med. 361 (19) (2009) 1838–1847.
[60] C.J. Melief, S.H. van der Burg, Immunotherapy of established (pre)malignant disease by synthetic long peptide vaccines, Nat. Rev. Cancer 8 (5) (2008) 351–360.
[61] S. Zwaveling, S.C. Ferreira Mota, J. Nouta, M. Johnson, G.B. Lipford, R. Offringa,

S.H. van der Burg, C.J. Melief, Established human papillomavirus type 16-expressing tumors are effectively eradicated following vaccination with long peptides, J. Immunol. 169 (1) (2002) 350–358.
[62] S. Kooi, H.Z. Zhang, R. Patenia, C.L. Edwards, C.D. Platsoucas, R.S. Freedman, HLA class I expression on human ovarian carcinoma cells correlates with T-cell infiltration in vivo and T-cell expansion in vitro in low concentrations of recombinant interleukin-2, Cell. Immunol. 174 (2) (1996) 116–128.
[63] M. Farshchian, M.M. Matin, O. Armant, D. Geerts, M. Dastpak, S. Nakhaei-Rad, M. Tajeran, A. Jebelli, M. Shahriyari, M. Bahrami, A. Fallah, V. Yaghoobi, M. Mirahmadi, M.R. Abbaszadegan, A.R. Bahrami, Suppression of dsRNA response genes and innate immunity following Oct4, Stella, and Nanos2 overexpression in mouse embryonic fibroblasts, Cytokine 106 (2018) 1–11.
[64] N.M. Chesarino, T.M. McMichael, J.S. Yount, E3 ubiquitin ligase NEDD4 promotes influenza virus infection by decreasing levels of the antiviral protein IFITM3, PLoS Pathog. 11 (8) (2015) e1005095.
[65] J.S. Yount, R.A. Karssemeijer, H.C. Hang, S-palmitoylation and ubiquitination differentially regulate interferon-induced transmembrane protein 3 (IFITM3)-mediated resistance to influenza virus, J. Biol. Chem. 287 (23) (2012) 19631–19641.
[66] M. Bassani-Sternberg, E. Braunlein, R. Klar, T. Engleitner, P. Sinitcyn, S. Audehm, M. Straub, J. Weber, J. Slotta-Huspenina, K. Specht, M.E. Martignoni, A. Werner, R. Hein, D. H Busch, C. Peschel, R. Rad, J. Cox, M. Mann, A.M. Krackhardt, Direct identification of clinically relevant neoepitopes presented on native human melanoma tissue by mass spectrometry, Nat. Commun. 7 (2016) 13404.
[67] J. Burks, R.E. Reed, S.D. Desai, Free ISG15 triggers an antitumor immune response against breast cancer: a new perspective, Oncotarget 6 (9) (2015) 7221–7231.
[68] P.F. Dos Santos, D.S. Mansur, Beyond ISGlylation: functions of free intracellular and extracellular ISG15, J. Interf. Cytokine Res. 37 (6) (2017) 246–253.
[69] A. Okumura, G. Lu, I. Pitha-Rowe, P.M. Pitha, Innate antiviral response targets HIV-1 release by the induction of ubiquitin-like protein ISG15, Proc. Natl. Acad. Sci. U. S. A. 103 (5) (2006) 1440–1445.
[70] N. van Montfoort, E. van der Aa, A.M. Woltman, Understanding MHC class I presentation of viral antigens by human dendritic cells as a basis for rational design of therapeutic vaccines, Front. Immunol. 5 (2014) 182.
[71] A. Wahl, F. Schafer, W. Bardet, R. Buchli, G.M. Air, W.H. Hildebrand, HLA class I molecules consistently present internal influenza epitopes, Proc. Natl. Acad. Sci. U. S. A. 106 (2) (2009) 540–545.
[72] E.G. Worrall, B. Wawrzynow, L. Worrall, M. Walkinshaw, K.L. Ball, T.R. Hupp, Regulation of the E3 ubiquitin ligase activity of MDM2 by an N-terminal pseudo-substrate motif, J. Chem. Biol. 2 (3) (2009) 113–129.

Bibliography

Ackrill, A. M., Reid, L. E., Gilbert, C. S., Gewert, D. R., Porter, A. C., Lewin, A. R., Stark, G. R. & Kerr, I. M. (1991). Differential response of the human 6-16 and 9-27 genes to alpha and gamma interferons. *Nucleic acids research*, 19 (3), pp. 591–8.

Adiko, A. C., Babdor, J., Gutiérrez-Martínez, E., Guermonprez, P. & Saveanu, L. (2015). Intracellular transport routes for MHC I and their relevance for antigen cross-presentation. *Frontiers in Immunology*, 6 (JUL), pp. 1–11. DOI: 10.3389/fimmu.2015.00335.

AgilentTechnologies (2011). *Time-of-Flight Mass Spectrometry- Technical Overview*. Tech. rep., pp. 1–16.

Akyerli, C. B., Beksac, M., Holko, M., Frevel, M., Dalva, K., Özbek, U., Soydan, E., Özcan, M., Özet, G., Ilhan, O., Gürman, G., Akan, H., Williams, B. R. G. & Özçelik, T. (2005). Expression of IFITM1 in chronic myeloid leukemia patients. *Leukemia Research*, 29 (3), pp. 283–286. DOI: 10.1016/j.leukres.2004.07.007.

Algarra, I., Collado, A. & Garrido, F. (1997). Altered MHC class I antigens in tumors. *International Journal of Clinical and Laboratory Research*, 27 (2), pp. 95–102. DOI: 10.1007/BF02912442.

Allavena, P., Sica, A., Solinas, G., Porta, C. & Mantovani, A. (2008). The inflammatory microenvironment in tumor progression: The role of tumor-associated macrophages. *Critical Reviews in Oncology/Hematology*, 66 (1), pp. 1–9. DOI: 10.1016/j.critrevonc.2007.07.004.

Amini-Bavil-Olyaee, S., Choi, Y. J., Lee, J. H., Shi, M., Huang, I. C., Farzan, M. & Jung, J. U. (2013). The antiviral effector IFITM3 disrupts intracellular cholesterol homeostasis to block viral entry. *Cell Host and Microbe*, 13 (4), pp. 452–464. DOI: 10.1016/j.chom.2013.03.006. arXiv: NIHMS150003.

Andersen, J. B., Aaboe, M., Borden, E. C., Goloubeva, O. G., Hassel, B. A. & Ørntoft, T. F. (2006). Stage-associated overexpression of the ubiquitin-like protein, ISG15, in bladder cancer. *British Journal of Cancer*, 94 (10), pp. 1465–1471. DOI: 10.1038/sj.bjc.6603099.

Andreu, P., Colnot, S., Godard, C., Laurent-Puig, P., Lamarque, D., Kahn, A., Perret, C. & Romagnolo, B. (2006). Identification of the IFITM family as a new molecular marker in human colorectal tumors. *Cancer Research*, 66 (4), pp. 1949–1955. DOI: 10.1158/0008-5472.CAN-05-2731.

Bach, E. A., Aguet, M. & Schreiber, R. D. (1997). THE IFNγ RECEPTOR:A Paradigm for Cytokine Receptor Signaling. *Annual Review of Immunology*, 15 (1), pp. 563–591. DOI: 10.1146/annurev.immunol.15.1.563.

Bailey, C. C., Huang, I. C., Kam, C. & Farzan, M. (2012). Ifitm3 Limits the Severity of Acute Influenza in Mice. *PLoS Pathogens*, 8 (9). DOI: 10.1371/journal.ppat.1002909.

Bailey, C. C., Zhong, G., Huang, I. C. & Farzan, M. (n.d.). IFITM-Family Proteins: The Cell's First Line of Antiviral Defense. (). DOI: 10.1146/annurev-virology-031413-085537.

Balkwill F., M. A. (2001). Inflammation and cancer: back to Virchow? *Lancet*, 357 (9255), pp. 539–45. DOI: 10.1016/S0140-6736(00)04046-0.

Bani, M. R., Nicoletti, M. I., Alkharouf, N. W., Ghilardi, C., Petersen, D., Erba, E., Sausville, E. A., Liu, E. T. & Giavazzi, R. (2004). Gene expression correlating with response to paclitaxel in ovarian carcinoma xenografts. *Molecular cancer therapeutics*, 3 (2), pp. 111–21. DOI: 10.1016/s0955-0674(98)80095-1.

Bass, B. L., Weintraub, H., Catttaneo, R. & Billeter, M. A. (1989). Biased Hypermutation of Viral RNA Genomes Could Be Due to Unwinding/Modification of Double-Stranded RNA. *Cell*, 56, p. 331. DOI: 10.1016/0143-4004(89)90024-6.

Bassani-Sternberg, M., Bräunlein, E., Klar, R., Engleitner, T., Sinitcyn, P., Audehm, S., Straub, M., Weber, J., Slotta-Huspenina, J., Specht, K., Martignoni, M. E., Werner, A., Hein, R., H. Busch, D., Peschel, C., Rad, R., Cox, J., Mann, M. & Krackhardt, A. M. (2016). Direct identification of clinically relevant neoepitopes presented on native human melanoma tissue by mass spectrometry. *Nature Communications*, 7 (May), p. 13404. DOI: 10.1038/ncomms13404.

Bedard, K. M., Daijogo, S. & Semler, B. L. (2007). A nucleo-cytoplasmic SR protein functions in viral IRES-mediated translation initiation. *The EMBO journal*, 26 (2), pp. 459–67. DOI: 10.1038/sj.emboj.7601494.

Bekisz, J., Schmeisser, H., Hernandez, J., Goldman, N. D. & Zoon, K. C. (2004). Mini ReviewHuman Interferons Alpha, Beta and Omega. *Growth Factors*, 22 (4), pp. 243–251. DOI: 10.1080/08977190400000833.

Bernabei, P., Coccia, E. M., Rigamonti, L., Bosticardo, M., Forni, G., Pestka, S., Krause, C. D., Battistini, A. & Novelli, F. (2001). Interferon-γ receptor 2 expression as the deciding factor in human T, B, and myeloid cell proliferation or death. *Journal of Leukocyte Biology*, 70 (6), pp. 950–960.

Blighe, K. (2019). EnhancedVolcano: Publication-ready volcano plots with enhanced colouring and labelling. R package version 1.0.1. URL: https://github.com/kevinblighe/EnhancedVolcano.

Blomstrom, D. C., Fahey, D., Kutny, R., Korant, B. D. & Knight, E. (1986). Molecular Characterization of the Interferon-induced 15-kDa Protein. 261 (19), pp. 8811–8816.

Bluyssen, H. A., Muzaffar, R., Vlieststra, R. J., Made, A. C. van der, Leung, S., Stark, G. R., Kerr, I. M., Trapman, J. & Levy, D. E. (1995). Combinatorial association and abundance of

components of interferon-stimulated gene factor 3 dictate the selectivity of interferon responses. *Proceedings of the National Academy of Sciences*, 92 (12), pp. 5645–5649. DOI: 10.1073/pnas.92.12.5645.

Boasso, A., Shearer, G. M. & Chougnet, C. (2009). Immune dysregulation in human immunodeficiency virus infection: know it, fix it, prevent it? *Journal Intern Medicine*, 265, pp. 78–96.

Boehm, U., Klamp, T., Groot, M. & Howard, J. C. (1997). Cellular responses to interferon-g., 15:749–95.

Boes, B., Hengel, H., Ruppert, T., Multhaup, G., Koszinowski, U. H. & Kloetzel, P. M. (1994). Interferon g stimulation modulates the proteolytic activity and cleavage site preference of 20S mouse proteasomes. 179 (March).

Bonifacino, J. S. & Traub, L. M. (2003). Signals for Sorting of Transmembrane Proteins to Endosomes and Lysosomes. *Annual Review of Biochemistry*, 72 (1), pp. 395–447. DOI: 10.1146/annurev.biochem.72.121801.161800.

Borden, E. C., Sen, G. C., Uze, G., Silverman, R. H., Ransohoff, R. M., Foster, G. R. & Stark, G. R. (2007). Interferons at age 50: past, current and future impact on biomedicine. *Nature Reviews: Drug Discovery*, 6, pp. 975–990. DOI: 10.1038/nrd2422.

Borg, D., Hedner, C., Gaber, A., Nodin, B., Fristedt, R., Jirström, K., Eberhard, J. & Johnsson, A. (2016). Expression of IFITM1 as a prognostic biomarker in resected gastric and esophageal adenocarcinoma. *Biomarker research*, 4, p. 10. DOI: 10.1186/s40364-016-0064-5.

Bouchal, P., Roumeliotis, T., Hrstka, R., Nenutil, R., Vojtesek, B. & Garbis, S. D. (2009). Biomarker Discovery in Low-Grade Breast Cancer Using Isobaric Stable Isotope Tags and Two-Dimensional Liquid Chromatography-Tandem Mass Spectrometry (iTRAQ-2DLC-MS/MS) Based Quantitative Proteomic Analysis. *Journal of Proteome Research*, 8 (1), pp. 362–373. DOI: 10.1021/pr800622b.

Bradbury, L. E., Kansas, G. S., Levy, S., Evans, R. L. & Tedder, T. F. (1992). The CD19 / CD21 signal transducing complex of human B lymphocytes includes the target of antiproliferative antibody-1 and Leu-13 • Rapid Reviews ! 30 days * from submission to initial decision Information about subscribing to The Journal of Immunology is. *J Immunol*, 149, pp. 2841–50.

Brandhorst, B. P. (2004). Isolating DNA, RNA, polysomes, and protein. *Methods in cell biology*, 74, pp. 579–599. DOI: 10.1016/S0091-679X(04)74023-6.

Brass, A. L., Huang, I. C., Benita, Y., John, S. P., Krishnan, M. N., Feeley, E. M., Ryan, B., Weyer, J. L., Van Der Weyden, L., Fikrig, E., Adams, D. J., Xavier, R. J., Farzan, M. & Elledge, S. J. (2009). IFITM Proteins Mediate the Innate Immune Response to Influenza A H1N1 Virus, West Nile Virus and Dengue Virus. 139 (7), pp. 1243–1254.

Brem, R., Oroszlan-Szovik, K., Foser, S., Bohrmann, B. & Certa, U. (2003). Inhibition of proliferation by 1-8U in interferon-α-responsive and non-responsive cell lines. *Cellular*

and Molecular Life Sciences, 60 (6), pp. 1235–1248. DOI: 10.1007/s00018-003-3016-9.

Briesemeister, D., Sommermeyer, D., Loddenkemper, C., Loew, R., Uckert, W., Blankenstein, T. & Kammertoens, T. (2011). Tumor rejection by local interferon gamma induction in established tumors is associated with blood vessel destruction and necrosis. *International Journal of Cancer*, 128 (2), pp. 371–378. DOI: 10.1002/ijc.25350.

El-Brolosy, M.A., Kontarakis, Z., Rossi1, A., Kuenne, C., Günther, S., Fukuda, N., Kikhi, K., Boezio1, G. L. M., Takacs, C. M., Lai1, S., Fukuda1, R., Gerri, C., Giraldez, A. J. & Stainier, D. Y. R. (2019). Genetic compensation triggered by mutant mRNA degradation. *Nature*, 568, pp. 193–197.

Buchman, A. R. & Berg, P. (1988). Comparison of intron-dependent and intron-independent gene expression. *Molecular and Cellular Biology*, 8 (10), pp. 4395–4405. DOI: 10.1128/MCB.8.10.4395.

Buermans, H.P.J. & Dunnen, J.T. den (2014). Next generation sequencing technology: Advances and applications. *Biochemistry and Biophysics Acta*, 10, pp. 1932–1941.

Burd, E (2003). Human papillomavirus and cervical cancer. *Clin Microbiol Rev*, 16 (1), pp. 1–17. DOI: 10.1128/CMR.16.1.1.

Burks, J., Reed, R. E. & Desai, S. D. (2015). Free ISG15 triggers an antitumor immune response against breast cancer: a new perspective. *Oncotarget*, 6 (9), pp. 7221–7231. DOI: 10.18632/oncotarget.3372.

Burnet, M. (1955). Cancer- A biological approach. *British Medical Journal*, pp. 841–47.

C. Schindler, J. E. D. Jr. (1995). Transcriptional responses to polypeptide ligands: The JAK-STAT Pathway. *Annual review of biochemistry*, 64:621–51.

Cabrera, T., Fernandez, M. A., Sierra, A., Garrido, A., Herruzo, A., Escobedo, A., Fabra, A. & Garrido, F. (1996). High Frequency of Altered HLA Class I Phenotypes in Invasive Breast Carcinomas. *Immunology*, 8859 (96).

Cáceres, J. F., Screaton, G. R. & Krainer, A. R. (1998). A specific subset of SR proteins shuttles continuously between the nucleus and the cytoplasm. *Genes & development*, 12 (1), pp. 55–66.

Cáceres, Javier F, Misteli, Tom, Screaton, Gavin R, Spector, David L & Krainer, Adrian R (1997). Role of the modular domains of SR proteins in subnuclear localization and alternative splicing specificity. *Journal of Cell Biology*, 138 (2), pp. 225–238. DOI: 10.1083/jcb.138.2.225.

Callahan, T. L. & Caughey, A. B. (2013). *Blueprints Obstetrics & Gynecology*. 6th Ed. Lippincott Williiams & Wilkins, p.298.

Chang, C. H., Hammer, J., Loh, J. E., Fodor, W. L. & Flavell, R. A. (1992). The activation of major histocompatibility complex class I genes by interferon regulatory factor-1 (IRF-1)., pp. 378–384.

Chang, Y.E. & Laimonis, L.A. (2000). Microarray Analysis Identifies Interferon Inducible-Genes and Stat-1 as Major Transcriptional Targets of Human Papillomavirus Type 31. *Journal of Virology*, 60, pp. 4174–4182.

Chattopadhyay, I., Phukan, R., Singh, A., Vasudevan, M., Purkayastha, J., Hewitt, S., Kataki, A., Mahanta, J., Kapur, S. & Saxena, S. (2009). Molecular profiling to identify molecular mechanism in esophageal cancer with familial clustering. *Oncology reports*, 21, pp. 1135–46. DOI: 10.3892/or. arXiv: NIHMS150003.

Chen, Y. X., Welte, K., Gebhard, D. H. & Evans, R. L. (1984). Induction of T cell aggregation by antibody to a 16kd human leukocyte surface antigen. *Journal of immunology (Baltimore, Md. : 1950)*, 133 (5), pp. 2496–501.

Cheon, H., Borden, E. C. & Stark, G. R. (2014). Interferons and their stimulated genes in the tumor microenvironment. *Seminars in oncology*. DOI: 10.1053/j.seminoncol.2014.02.002.

Cheon, H., Holvey-Bates, E. G., Schoggins, J. W., Forster, S., Hertzog, P., Imanaka, N., Rice, C. M., Jackson, M. W., Junk, D. J. & Stark, G. R. (2013). IFNβ-dependent increases in STAT1, STAT2, and IRF9 mediate resistance to viruses and DNA damage. *EMBO Journal*, 32 (20), pp. 2751–2763. DOI: 10.1038/emboj.2013.203. arXiv: NIHMS150003.

Cheon, H. & Stark, G. R. (2009). Unphosphorylated STAT1 prolongs the expression of interferon-induced immune regulatory genes. *Proceedings of the National Academy of Sciences*, 106 (23), pp. 9373–9378. DOI: 10.1073/pnas.0903487106.

Cheon, H., Yang, J. & Stark, G. R. (2011). The Functions of Signal Transducers and Activators of Transcriptions 1 and 3 as Cytokine-Inducible Proteins. *Journal of Interferon & Cytokine Research*, 31 (1), pp. 33–40. DOI: 10.1089/jir.2010.0100.

Chernushevich, I. V., Loboda, A. V. & Thomson, B. A. (2001). An introduction to quadrupole-time-of-flight mass spectrometry. *Journal of Mass Spectrometry*, 36 (8), pp. 849–865. DOI: 10.1002/jms.207.

Cheung, Y. N., Maag, D., Mitchell, S. F., Fekete, C. A., Algire, M. A., Takacs, J. E., Shriokikh, N., Pestova, T., Lorsch, J. R. & Hinnebusch, A. G. (2007). Dissociation of eIF1 from the 40S ribosomal subunit is a key step in start codon selection in vivo. *Genes & Development*, 21, pp. 1217–1230. DOI: 10.1101/gad.1528307.of.

Chorev, M. & Carmel, L. (2012). The funtion of introns. *Frontiers in Genetics*, 3, pp. 1–15.

Chung, S. & Perry, R. P. (1989). Importance of intron for expression of mouse ribosomal protein gene rpL32. *Molecular and Cellular Biology*, 9 (5), pp. 2075–2082.

Ciampricotti, M., Vrijland, K., Hau, C. S., Pemovska, T., Doornebal, C. W., Speksnijder, E. N., Wartha, K., Jonkers, J. & De Visser, K. E. (2011). Development of metastatic HER2+ breast cancer is independent of the adaptive immune system. *Journal of Pathology*, 224 (1), pp. 56–66. DOI: 10.1002/path.2837.

Ciehanover, A., Hod, Y. & Rershkol, A. (1978). A HEAT-STABLE POLYPEPTIDE COMPONENT OF AN ATP-DEPENDENT PROTEOLYTIC SYSTEM FROM RETICDLOCYTES. *Biochemical and Biophysical Research Communications*, 81 (4), pp. 1100–1105.

Clementz, M. A., Chen, Z., Banach, B. S., Wang, Y., Sun, L., Ratia, K., Baez-Santos, Y. M., Wang, J., Takayama, J., Ghosh, A. K., Li, K., Mesecar, A. D. & Baker, S. C. (2010). Deubiquitinating and Interferon Antagonism Activities of Coronavirus Papain-Like Proteases. *Journal of Virology*, 84 (9), pp. 4619–4629. DOI: 10.1128/JVI.02406-09.

Coley, W. B. (1893). The treatment of malignant tumors by repeated innoculations of erysipelas: with a report of ten original cases. *American Journal of the Medical Sciences*, 105:5, pp. 488–511.

Comai, L. & Katz, J. E. (2017). *Proteomics. Methods and Protocols*. Ed. by L. Comai, J. E. Katz & P. Mallick. Springer Nature, pp. 1–375. ISBN: 9781493967452.

Cong, L., Ran, F. A., Cox, D., Lin, S., Barrtto, R., Habib, N., Hsu, P. D., Wu, X., Jiang, W., Marraffini, L. A. & Zhang, F. (2013). Multiplex Genome Engineering Using CRISPR/Cas Systems. *Science*, 339 (February), pp. 819–824.

Connor, M. E. & Stern, P. L. (1990). Loss of MHC class-I expression in cervical carcinomas. *International Journal of Cancer*, 46 (6), pp. 1029–1034. DOI: 10.1002/ijc.2910460614.

Costa-Pereira, A. P., Williams, T. M., Strobl, B., Watling, D., Briscoe, J. & Kerr, I. M. (2002). The antiviral response to gamma interferon. *Journal of virology*, 76 (18), pp. 9060–8. DOI: 10.1128/JVI.76.18.9060-9068.2002.

Cramer, P., Caceres, J. F., Cazalla, D., Kadener, S., Muro, A. F., Baralle, F. E. & Kornblihtt, A. R. (1999). Coupling of transcription with alternative splicing: RNA pol II promoters modulate SF2/ASF and 9G8 effects on an exonic splicing enhancer. *Mol Cell*, 4 (2), pp. 251–258.

Croitoru-Lamoury, J., Lamoury, F. M. J., Caristo, M., Suzuki, K., Walker, D., Takikawa, O., Taylor, R. & Brew, B. J. (2011). Interferon-γ Regulates the Proliferation and Differentiation of Mesenchymal Stem Cells via Activation of Indoleamine 2,3 Dioxygenase (IDO). *PLoS ONE*, 6 (2), e14698. DOI: 10.1371/journal.pone.0014698.

Cromme, F. V., Bommel, P. F. J. van, Walboomers, J. M. M., Gallee, M. P. W., Stern, P. L., Kenemans, P., Helmerhorst, Th. J. M., Stukart, M. J. & Meijer, C. J. L. M. (1994). Differences in MHC and TAP-1 expression in cervical cancer lymph node metastases as compared with the primary tumours. *British Journal of Cancer*, 69 (6), pp. 1176–1181. ISSN: 15321827. DOI: 10.1038/bjc.1994.231.

Cromme, F. V., Meijer, C. J. L. M., Snijders, P. J., Uyterlinde, A., Kenemans, P., Helmerhorst, T., Stern, P. L., Brule, A. J. C. van den & Walboomers, J. M. M. (1993). Analysis of MHC class I and II expression in relation to presence of HPV genotypes in premalignant and malignant cervical lesions. *British Journal of Cancer*, 67 (6), pp. 1372–1380. DOI: 10.1038/bjc.1993.254.

Cunha, J. D., Knight, E., Haast, A. L., Truitt, R. L. & Borden, E. C. (1996). Immunoregulatory properties of ISG15, an interferon-induced cytokine. *Immunology*, 93 (January), pp. 211–215. DOI: 10.1073/pnas.93.1.211.

Dalton, D., Pitts-Meek, S., Keshav, S., Figari, I., Bradley, A. & Stewart, T. (1993). Multiple defects of immune cell function in mice with disrupted interferon-gamma genes. *Science*, 259 (5102), pp. 1739–1742. DOI: 10.1126/science.8456300.

Darb-Esfahani, S., Sinn, B. V., Rudl, M., Sehouli, J., Braicu, I., Dietel, M. & Denkert, C. (2014). Interferon-stimulated Gene, 15 kDa (ISG15) in Ovarian High-grade Serous Carcinoma: Prognostic Impact and Link to NF-κB Pathway. *International Journal of Gynecological Pathology*, 33 (1), pp. 16–22. DOI: 10.1097/PGP.0b013e31827b25a2.

Darnell, J. E., Kerr, I. M. & Stark, G. R. (1994). Jak-STAT pathways and transcriptional activation in response. *Science*, 264 (5164), pp. 1415–1421. DOI: 10.1126/science.8197455.

Das, S. & Krainer, A. R. (2014). Emerging functions of SRSF1, splicing factor and oncoprotein, in RNA metabolism and cancer. *Molecular cancer research : MCR*, 12 (9), pp. 1195–204. DOI: 10.1158/1541-7786.MCR-14-0131.

Dastur, A., Beaudenon, S., Kelley, M., Krug, R. M. & Huibregtse, J. M. (2006). Herc5, an interferon-induced HECT E3 enzyme, is required for conjugation of ISG15 in human cells. *Journal of Biological Chemistry*, 281 (7), pp. 4334–4338. DOI: 10.1074/jbc.M512830200.

Deblandre, G. A., Marinx, O. P., Evans, S. S., Majjaj, S., Leo, O., Caput, D., Huez, G. A. & Wathelet, M. G. (1995). Expression cloning of an interferon-inducible 17-kDa membrane protein implicated in the control of cell growth*. *The Journal of biological chemistry*, 270 (40), pp. 23860–23866.

Del Prete, M. J., Vernal, R., Dolznig, H., Müllner, E. W. & Garcia-Sanz, J. A. (2007). Isolation of polysome-bound mRNA from solid tissues amenable for RT-PCR and profiling experiments. *RNA*, 13 (3), pp. 414–421. DOI: 10.1261/rna.79407.

Deligdisch, L., Jacobs, A. J. & Cohen, C. J. (1982). Histologic correlates of virulence in ovarian adenocarcinoma. II. Morphologic correlates of host response. *American Journal of Obstetrics and Gynecology*, 144 (8), pp. 885–889. DOI: 10.1016/0002-9378(82)90178-8.

Deltcheva, E., Chylinski, K., Sharma, C. M., Gonzales, K., Chao, Y., Pirzada, Z. A., Eckert, M. R., Vogel, J. & Charpentier, E. (2011). CRISPR RNA maturation by trans-encoded small RNA and host factor RNase III. *Nature*, 471 (7340), pp. 602–607. DOI: 10.1038/nature09886.

Dendrou, C. A., Petersen, J., Rossjohn, J. & Fugger, L. (2018). HLA variation and disease. *Nature Reviews Immunology*, 18 (5), pp. 325–339. DOI: 10.1038/nri.2017.143.

Der, S. D., Zhou, A., Williams, B. R. G. & Silverman, R. H. (1998). Identification of genes differentially regulated by interferon alpha, beta, or gamma using oligonucleotide arrays. *Proceedings of the National Academy of Sciences*, 95 (26), pp. 15623–15628. DOI: 10.1073/pnas.95.26.15623.

Desai, S. D., Haas, A. L., Wood, L. M., Tsai, Y. C., Pestka, S., Rubin, E. H., Saleem, A., Nur-E-Kamal, A. & Liu, L. F. (2006). Elevated expression of ISG15 in tumor cells interferes

with the ubiquitin/26S proteasome pathway. *Cancer Research*, 66 (2), pp. 921–928. DOI: 10.1158/0008-5472.CAN-05-1123.

Desai, S. D., Reed, R. E., Burks, J., Wood, L. M., Pullikuth, A. K., Haas, A. L., Liu, L. F., Breslin, J. W., Meiners, S. & Sankar, S. (2012). ISG15 disrupts cytoskeletal architecture and promotes motility in human breast cancer cells. *Experimental Biology and Medicine*, 237 (1), pp. 38–49. DOI: 10.1258/ebm.2011.011236.

Dighe, A. S., Richards, E., Old, L. J. & Schreiber, R. D (1994). Enhanced In Vivo Growth and Resistance to Rejection of Tumor Cells Expressing Dominant Negative IFNy Receptors. 1, pp. 447–456.

Dijk, E.L. van, Auger, H., Jaszczyszyn, Y. & Thermes, C. (2014). Ten years of next-generation sequencing technology. *Cell Press*, 9, pp. 418–426.

Ding, J. H., Zhong, X. Y., Hagopian, J. C., Cruz, M. M., Ghosh, G., Feramisco, J., Adams, J. A. & Fu, X. D. (2006). Regulated cellular partitioning of SR protein-specific kinases in mammalian cells. *Molecular biology of the cell*, 17 (2), pp. 876–85. DOI: 10.1091/mbc.E05-10-0963.

Doherty, M. K. & Beynon, R. J. (2006). Protein turnover on the scale of the proteome. *Expert review of proteomics*, 3 (1), pp. 97–110. DOI: 10.1586/14789450.3.1.97.

Doherty, M. K., Hammond, D. E., Clague, M. J., Gaskell, S. J. & Beynon, R. J. (2009). Turnover of the Human Proteome : Determination of Protein Intracellular Stability by Dynamic SILAC. *Journal of Proteome Research*, pp. 104–112. DOI: 10.1021/pr800641v.

Duarte, C. W., Willey, C. D., Zhi, D., Cui, X., Harris, J. J., Vaughan, L. K., Mehta, T., McCubrey, R. O., Khodarev, N. N., Weichselbaum, R. R. & Gillespie, G. Y. (2012). Expression signature of IFN/STAT1 signaling genes predicts poor survival outcome in glioblastoma multiforme in a subtype-specific manner. *PLoS ONE*, 7 (1), pp. 1–8. DOI: 10.1371/journal.pone.0029653.

Dunn, G. P., Bruce, A. T., Ikeda, H., Old, L. J. & Schreiber, R. D. (2002). Cancer immunoediting: from immunosurveillance to tumor escape. *Nature Immunology*, 3 (11), pp. 991–998. DOI: 10.1038/ni1102-991.

Dunn, Gavin P., Koebel, Catherine M. & Schreiber, Robert D. (2006). Interferons, immunity and cancer immunoediting. *Nature Reviews Immunology*, 6 (11), pp. 836–848. DOI: 10.1038/nri1961. arXiv: arXiv:1011.1669v3.

Durbin, J. E., Hackenmiller, R., Simon, M. C. & Levy, D. E. (2016). Targeted Disruption of the Mouse Stat1 Gene Results in Compromised Innate Immunity to Viral Disease. *Cell*, 84 (3), pp. 443–450. DOI: 10.1016/S0092-8674(00)81289-1.

Durfee, L. A. & Huibregtse, J. M. (2012). The ISG15 conjugation system. *Methods in molecular biology (Clifton, N.J.)*, 832, pp. 141–9. DOI: 10.1007/978-1-61779-474-2_9.

Durfee, L. A., Lyon, N., Seo, K. & Huibregtse, J. M. (2010). The ISG15 Conjugation System Broadly Targets Newly Synthesized Proteins: Implications for the Antiviral Function of ISG15. *Molecular Cell*, 38 (5), pp. 722–732. DOI: 10.1016/j.molcel.2010.05.002. arXiv: NIHMS150003.

Dvorak, H. F. (2016). Tumors : Wounds that do not heal–Redux. 3 (1), pp. 1–11. DOI: 10.1158/2326-6066.CIR-14-0209.Tumors.

Eddy, S.R (2001). Non-coding RNA genes and the modern RNA world. *Nature Reviews Genetics*, 2, pp. 919–929.

Ehrlich, P. (1909). Ueber den jetzigen Stand der Karzinomforshung. *Nederlandsch Tijdschrift voor Geneeskunde*, pp. 273–90.

Einav, U., Tabach, Y., Getz, G., Yitzhaky, A., Ozbek, U., Amariglio, N., Izraeli, S., Rechavi, G. & Domany, E. (2005). Gene expression analysis reveals a strong signature of an interferon-induced pathway in childhood lymphoblastic leukemia as well as in breast and ovarian cancer. *Oncogene*, 24 (42), pp. 6367–6375. DOI: 10.1038/sj.onc.1208797.

Epperson, D. E., Arnold, D., Spies, T., Cresswell, P., Pober, J. S. & Johnson, D. R. (2018). Cytokines increase transporter in antigen processing-1 expression more rapidly than HLA class I expression in endothelial cells.

Epstein, N. A. & Fatti, L. P. (1976). Prostatic Carcinoma: some morphological features affecting prognosis. *Cancer*, 37, pp. 2455–2465. DOI: 10.1056/NEJM197904123001504.

Erdal, E., Haider, S., Rehwinkel, J., Harris, A. L. & McHugh, P. J. (2017). A prosurvival DNA damage-induced cytoplasmic interferon response is mediated by end resection factors and is limited by Trex1. *Genes and Development*, 31 (4), pp. 353–369. DOI: 10.1101/gad.289769.116.

Evans, S. S., Collea, R. P., Leasure, J. A. & Lee, D. B. (1993). IFN-alpha induces homotypic adhesion and Leu-13 expression in human B lymphoid cells. *J Immunol*, 150 (3), pp. 736–747.

Evans, S. S., Lee, D. B., Han, T., Tomasi, T. B. & Evans, R. L. (1990). Monoclonal antibody to the interferon-inducible protein Leu-13 triggers aggregation and inhibits proliferation of leukemic B cells. *Blood*, 76, pp. 2583–2593.

Everitt, A. R., Clare, S., Pertel, T., John, S. P., Wash, R. S., Smith, S. E., Chin, C. R., Feeley, E. M., Sims, J. S., Adams, D. J., Wise, H. M., Kane, L., Goulding, D., Digard, P., Anttila, V., Baillie, J. K., Walsh, T. S., Hume, D. A., Palotie, A., Xue, Y., Colonna, V., Tyler-Smith, C., Dunning, J., Gordon, S. B., Smyth, R. L., Openshaw, P. J., Dougan, G., Brass, A. L. & Kellam, P. (2012). IFITM3 restricts the morbidity and mortality associated with influenza. *Nature*, 484 (7395), pp. 519–523. DOI: 10.1038/nature10921.

Ewing, B. & Green, P. (2000). Analysis of expressed sequence tags indicates 35,000 human genes. *Nature Genetics letter*, 25, pp. 232–234.

Farrel, P. J., Broeze, R. & Lengyel, P. (1979). Accomulation of an mRNA and protein in interferon-treated Ehrlich ascites tumour cells. *Nature*, 279, pp. 523–25.

Feeley, E. M., Sims, J. S., John, S. P., Chin, C. R., Pertel, T., Chen, L. M., Gaiha, G. D., Ryan, B. J., Donis, R. O., Elledge, S. J. & Brass, A. L. (2011). IFITM3 inhibits influenza A virus infection by preventing cytosolic entry. *PLoS pathogens*. DOI: 10.1371/journal.ppat.1002337.

Feng, J., Cao, Z., Wang, L., Wan, Y., Peng, N., Wang, Q., Chen, X., Zhou, Y. & Zhu, Y. (2017). Inducible GBP5 Mediates the Antiviral Response via Interferon-Related Pathways during Influenza A Virus Infection. *Journal of Innate Immunity*, 9, pp. 419–435.

Fensterl, V. & Sen, G. C. (2011). The ISG56/IFIT1 Gene Family. *Journal of Interferon & Cytokine Research*, 31 (1), pp. 71–78. DOI: 10.1089/jir.2010.0101.

Ferns, D. M., Heeren, A. M., Samuels, S., Bleeker, M. C. G., de Gruijl, T. D., Kenter, G. G. & Jordanova, E. S. (2016). Classical and non-classical HLA class I aberrations in primary cervical squamous- and adenocarcinomas and paired lymph node metastases. *Journal for ImmunoTherapy of Cancer*, 4 (1), pp. 1–11. DOI: 10.1186/s40425-016-0184-3.

Ferrara, T. A., Hodge, J. W. & Gulley, J. L. (2009). Combining radiation and immunotherapy for synergistic antitumor therapy. *Curr Opin Mol Ther*, 11 (1), pp. 37–42. DOI: 10.1038/ki.2009.479.Commonly. arXiv: NIHMS150003.

Friedman, R. L., Manly, S. P., McMahon, M., Kerr, I. M. & Stark, G. R. (1984). Transcriptional and posttranscriptional regulation of interferon-induced gene expression in human cells. *Cell*, 38 (3), pp. 745–755.

Früh, K. & Yang, Y. (1999). Antigen presentation by MHC class I and its regulation by interferon γ. *Current Opinion in Immunology*, 11 (1), pp. 76–81. DOI: 10.1016/S0952-7915(99)80014-4.

Fumoto, S., Shimokuni, T., Tanimoto, K., Hiyama, K., Otani, K., Ohtaki, M., Hihara, J., Yoshida, K., Hiyama, E., Noguchi, T. & Nishiyama, M. (2008). Selection of a novel drug-response predictor in esophageal cancer: A novel screening method using microarray and identification of IFITM1 as a potent marker gene of CDDP response. *International Journal of Oncology*, 32 (2), pp. 413–423.

Gaj, T., Gersbach, C. A. & Barbas, C. F. (2013). ZFN, TALEN and CRISPR/Cas-based methods for genome engineering. *Trends Biotechnology*, 31 (7), pp. 397–405. DOI: 10.1016/j.tibtech.2013.04.004.

Garbe, C., Krasagakis, K., Zouboulis, C. C., Shröder, K., Krüger, S., Stadler, R. & Orfanos, C. E. (1990). Antitumor activities of interferon Alpha, Beta, and Gamma and their Combinatoin of Human Melanoma Cells in Vitro: Changes of Proliferation, Melanin Synthesis and Immunophenotype. *The Society for Investigative Dermatology*.

Garneau, N.L., Wilusz, J. & Wilusz, J. (2007). The highways and byways of mRNA decay. *Nature Reviews Molecular Cell Biology*, 8, pp. 113–126.

Garnett, C. T., Palena, C., Chakarborty, M., Tsang, K. Y., Schlom, J. & Hodge, J. W. (2004). Sublethal irradiation of human tumor cells modulates phenotype resulting in enhanced killing by cytotoxic T lymphocytes. *Cancer Research*, 64 (21), pp. 7985–7994. DOI: 10.1158/0008-5472.CAN-04-1525.

Garrido, F., Aptsiauri, N., Doorduijn, E. M., Garcia Lora, A. M. & van Hall, T. (2016). The urgent need to recover MHC class I in cancers for effective immunotherapy. *Current Opinion in Immunology*, 39, pp. 44–51. DOI: 10.1016/j.coi.2015.12.007.

Garrido, F., Cabrera, T. & Aptsiauri, N. (2010). "Hard" and "soft" lesions underlying the HLA class I alterations in cancer cells: Implications for immunotherapy. *International Journal of Cancer*, 127 (2), pp. 249–256. DOI: 10.1002/ijc.25270.

Garrido, F., Cabrera, T., Concha, A., Glew, S., Ruiz-Cabello, F. & Stern, P. L. (1993). Natural history of HLA expression during tumour development. *Immunology Today*, 14 (10), pp. 491–499. DOI: 10.1016/0167-5699(93)90264-L.

Garrido, F., Perea, F., Bernal, M., Sánchez-Palencia, A., Aptsiauri, N. & Ruiz-Cabello, F. (2017). The Escape of Cancer from T Cell-Mediated Immune Surveillance: HLA Class I Loss and Tumor Tissue Architecture. *Vaccines*, 5 (1), p. 7. DOI: 10.3390/vaccines5010007.

Garrido, F., Ruiz-Cabello, F., Cabrera, T., Pérez-Villar, J. J., López-Botet, M., Duggan-Keen, M. & Stern, P. L. (1997). Implications for immunosurveillance of altered HLA class I phenotypes in human tumours. *Immunology Today*, 18 (2), pp. 89–95. DOI: 10.1016/S0167-5699(96)10075-X.

Gentile, M., Latonen, L. & Laiho, M. (2003). Cell cycle arrest and apoptosis provoked by UV radiation-induced DNA damage are transcriptionally highly divergent responses. *Nucleic Acids Research*, 31 (16), pp. 4779–4790. DOI: 10.1093/nar/gkg675.

Gerber, S. A., Sedlacek, A. L., Cron, K. R., Murphy, S. P., Frelinger, J. G. & Lord, E. M. (2013). IFN-γ Mediates the Antitumor Effects of Radiation Therapy in a Murine Colon Tumor. *The American Journal of Pathology*, 182 (6), pp. 2345–2354. DOI: 10.1016/j.ajpath.2013.02.041.

Giannakopoulos, N. V., Luo, J. K., Papov, V., Zou, W., Lenschow, D. J., Jacobs, B. S., Borden, E. C., Li, J., Virgin, H. W. & Zhang, D. E. (2005). Proteomic identification of proteins conjugated to ISG15 in mouse and human cells. *Biochem. Biophys. Res. Commun.*, 336, pp. 496–506.

Giannopoulos, A., Constantinides, C., Fokaeas, E., Stravadimos, C., Giannopoulou, M., Kyroudi, A. & Gounaris, A. (2003). The Immunomodulating Effect of Interferon- γ Intravesical Instillations in Preventing Bladder Cancer Recurrence. *Clinical Cancer Research*, 9, pp. 5550–5558.

Gibson, U.E.M., Heid, C.A. & Williams, P.M. (1996). A Novel Method for Real Time Quantitative RT-PCR. *Genome Research*, 6, pp. 995–1001.

Gillet, L. C., Navarro, P., Tate, S., Röst, H., Selevsek, N., Reiter, L., Bonner, R. & Aebersold, R. (2012). Targeted Data Extraction of the MS/MS Spectra Generated by Data-independent Acquisition: A New Concept for Consistent and Accurate Proteome Analysis. *Molecular & Cellular Proteomics*, 11 (6), O111.016717.1–O111.016717.17. DOI: 10.1074/mcp.O111.016717.

Gleave, M. E., Elhilali, M., Fradet, Y., Davis, I., Venner, P., Saad, F., Klotz, L. H., Moore, M. J., Paton, V., Bajamonde, A., Bell, D., Ernst, S., Ramsey, E., Chin, J., Morales, A., Martins, H. & Sanders, C. (1998). Interferon Gamma-1b Compared with Placebo in Metastatic

Renal-Cell Carcinoma. *New England Journal of Medicine*, 338 (18), pp. 1265–1271. DOI: 10.1056/NEJM199804303381804.

Gomez Herranz, M., Nekulova, M., Faktor, J., Hernychova, L., Kote, S., Sinclair, E. H., Nenutil, R., Vojtesek, B., Ball, K. L. & Hupp, T. R. (2019). The efects of IFITM1 and IFITM3 gene deletion on IFNγ stimulated protein synthesis. *Cellular Signalling*, 74, pp. 39–56.

Gorbacheva, V. Y., Lindner, D., Sen, G. C. & Vestal, D. J. (2002). The interferon (IFN)-induced GTPase, mGBP-2. *Journal of Biological Chemistry*, 277 (8), pp. 6080–6087. DOI: 10.1074/jbc.M110542200.

Gough, D. J., Messina, N. L., Hii, L., Gould, J. A., Sabapathy, K., Robertson, A. P. S., Trapani, J. A., Levy, D. E., Hertzog, P. J., Clarke, C. J. P. & Johnstone, R. W. (2010). Functional crosstalk between type I and II interferon through the regulated expression of STAT1. *PLoS Biology*, 8 (4). DOI: 10.1371/journal.pbio.1000361.

Greenlund, A. C., Schreiber, R. D., Goeddel, D. V. & Pennica, D. (1993). Interferon-gamma induces receptor dimerization in solution and on cells. *Journal of Biological Chemistry*, 268 (24), pp. 18103–18110.

Groettrup, M., Soza, A., Eggers, M., Kuehn, L., Dick, T. P., Schids, H., Rammensees, H. G., Koszinowski, U. & Kloetzel, P. M. (1996). A role for the proteasome regulator PA28a in anigen presentation. *Nature*, 381:166–68.

Gross, L. (1943). Intradermal Immunization of C3H Mice against a Sarcoma That Originated in an Animal of the Same Line. *Cancer Research*, 3 (5), pp. 326–333.

Guan, S. & Marshall, A. G. (1993). Stored Waveform Inverse Fourier Transform (SWIFT) Axial Excitation/Ejection for Quadrupole Ion Trap Mass Spectrometry. *Analytical Chemistry*, 65 (16), pp. 1288–1294.

Guo, C., Manjili, M. H., Subjeck, J. R., Sarkar, D., Fisher, P. B. & Wang, X. Y. (2013). Therapeutic Cancer Vaccines: Past, Present and Future. *Accounts of Chemical Research*, 45 (119), pp. 421–475. DOI: 10.1038/jid.2014.371. arXiv: NIHMS150003.

Györffy, B., Dietel, M., Fekete, T. & Lage, H. (2008). A snapshot of microarray-generated gene expression signatures associated with ovarian carcinoma. *International Journal of Gynecological Cancer*, 18 (6), pp. 1215–1233. DOI: 10.1111/j.1525-1438.2007.01169.x.

Ha, M. H., Wei, L., Rao, H. Y., Liu, F. & Wang, X. Y (2008). Effect of interferon-gamma on hepatic stellate cells stimulated by acetaldehyde. *Hepatogastroenterology*, (55), pp. 1059–65.

Haas, A. L., Ahrens, P., Bright, P. M. & Ankel, H. (1987). Interferon induced a 15-kilodalton protein exhibiting marked homology to ubiquitin. *Journal of Biological Chemistry*, 262 (23), pp. 11315–11323.

Hach, J. C., McMichael, T., Chesarino, N. M. & Yount, J. S. (2013). Palmitoylation on Conserved and Nonconserved Cysteines of Murine IFITM1 Regulates Its Stability and Anti-Influenza A Virus Activity. 87 (17), pp. 9923–9927. DOI: 10.1128/JVI.00621-13.

Halle, S., Halle, O. & Förster, R. (2017). Mechanisms and Dynamics of T Cell-Mediated Cytotoxicity In Vivo. *Trends in Immunology*, 38 (6), pp. 432–443. DOI: 10.1016/j.it.2017.04.002.

Haller, O. & Kochs, G. (2002). Interferon-induced Mx proteins: Dynamin-like GTPases with antiviral activity. *Traffic*, 3 (10), pp. 710–717. DOI: 10.1034/j.1600-0854.2002.31003.x.

Hamanishi, J., Mandai, M., Iwasaki, M., Okazaki, T., Tanaka, Y. & Yamaguchi, K. (2007). Programmed cell death 1 ligand 1 and tumor-infiltrating CD8+ T lymphocytes are prognostic factors of human ovarian cancer. *PNAS*, 104 (9), pp. 3360–3365.

Hamilton, J. A., Whitty, G. A., Kola, I. & Hertzog, P. J. (1996). Endogenouse IFN-alpha beta suppresses colony-stimulating factor (CSF)-1-stimulated macrophage DNA synthesis and mediates inhibitory effects of lipopolysaccharide and TNF-alpha. *The Journal of Immunology*, 156, pp. 2553–57. DOI: 10.4049/jimmunol.168.12.6199.

Hanahan, D. & Weinberg, R. A. (2000). The Hallmarks of Cancer. *Cell*, 100, pp. 57–70.

— (2011). Hallmarks of Cancer: The Next Generation. *Cell*, 144, pp. 646–674. DOI: 10.1016/j.cell.2011.02.013.

Harada, H., Takahashi, E., Itoh, S., Harada, K., Hori, T. A. & Taniguchi, T. (1994). Structure and regulation of the human interferon regulatory factor 1 (IRF-1) and IRF-2 genes: implications for a gene network in the interferon system. *Molecular and cellular biology*, 14 (2), pp. 1500–1509. DOI: 10.1128/MCB.14.2.1500.

Hatano, H., Kudo, Y., Ogawa, I., Tsunematsu, T., Kikuchi, A., Abiko, Y. & Takata, T. (2008). IFN-Induced Transmembrane Protein 1 Promotes Invasion at Early Stage of Head and Neck Cancer Progression. *Clinical Cancer Research*, 14 (19), pp. 6097–6105. DOI: 10.1158/1078-0432.CCR-07-4761.

Hausen, H. Z. U. R. (1991). Viruses in Human Cancers. *Science*, 254 (1990), pp. 1167–73.

Hernandez-Valladares, M., Aasebø, E., Mjaavatten, O., Vaudel, M., Bruserud, Ø., Berven, F. & Selheim, F. (2016). Reliable FASP-based procedures for optimal quantitative proteomic and phosphoproteomic analysis on samples from acute myeloid leukemia patients. *Biological Procedures Online*, 18 (1), pp. 1–10. DOI: 10.1186/s12575-016-0043-0.

Hershko, A., Ciechanover, A., Heller, H., Haas, A. L. & Rose, I. A. (1980). Proposed role of ATP in protein breakdown: conjugation of protein with multiple chains of the polypeptide of ATP-dependent proteolysis. *Proceedings of the National Academy of Sciences*, 77 (4), pp. 1783–1786. DOI: 10.1073/pnas.77.4.1783.

Hicks, M. J., Yang, C. R., Kotlajich, M. V. & Hertel, K. J. (2006). Linking splicing to Pol II transcription stabilizes pre-mRNAs and influences splicing patterns. *PLoS Biology*, 4 (6), pp. 0943–0951. DOI: 10.1371/journal.pbio.0040147.

Hilders, C. G. J. M., Morgado, I., Nooyen, Y. & Jan Fleuren, G. (1995). Altered HLA Expression by Metastatic Cervical Carcinoma Cells as a Factor in Impaired Immune Surveillance. *Gynecologic oncology*, 57, pp. 366–375.

Honma, S., Tsukada, S., Honda, S., Nakamura, M., Takakuwa, K., Maruhashi, T., Kodama, S., Kanazawa, K., Takahashi, T. & Tanaka, K. (1994). Biological-Clinical Significance of Selective loss of HLA-Class-I allelic product expression in Squamos-Cell carcinoma of the uterine cervix. 655, pp. 650–655.

Hovavessian, A. G. (1993). Interferon-induced dsRNA-activated protein kinase (PKR)*: antiproliferative, antiviral and antitumoral functions. *virology*, 4, pp. 237–45.

Hsiang, T. Y., Zhao, C. & Krug, R. M. (2009). Interferon-Induced ISG15 Conjugation Inhibits Influenza A Virus Gene Expression and Replication in Human Cells. *Journal of Virology*, 83 (12), pp. 5971–5977. DOI: 10.1128/JVI.01667-08.

Huang, I. C., Bailey, C. C., Weyer, J. L., Radoshitzky, S. R., Becker, M. M., Chiang, J. J., Brass, A. L., Ahmed, A. A., Chi, X., Dong, L., Longobardi, L. E., Boltz, D., Kuhn, J. H., Elledge, S. J., Bavari, S., Denison, M. R., Choe, H., Farzan, M. & Baric, R. S. (2011). Distinct Patterns of IFITM-Mediated Restriction of Filoviruses, SARS Coronavirus, and Influenza A Virus. *PLoS Pathog*, 7 (1). DOI: 10.1371/journal.ppat.1001258.

Huang, M., Qian, F., Hu, Y., Ang, C., Li, Z. & Wen, Z. (2002). Chromatin-remodelling factor BRG1 selectively activates a subset of interferon-α-inducible genes. *Nature Cell Biology*, 4 (10), pp. 774–781. DOI: 10.1038/ncb855.

Huang, S., Hendriks, W., Althage, A., Hemmi, S., Bluethmann, H., Kamijo, R., Vilcek, J., Zinkernagel, R. M. & Aguet, M. (1993). Immune response in mice that lack the interferon-gamma receptor [see comments]. *Science*, 259 (5102), pp. 1742–1745.

Huang, T., Wang, J., Yu, W. & He, Z. (2012). Protein inference: A review. *Briefings in Bioinformatics*, 13 (5), pp. 586–614. DOI: 10.1093/bib/bbs004.

Huang, Y., Yario, T. A. & Steitz, J. A. (2004). A molecular link between SR protein dephosphorylation and mRNA export. *Proceedings of the National Academy of Sciences of the United States of America*, 101 (26), pp. 9666–70. DOI: 10.1073/pnas.0403533101.

Huerfano, S., Ryabchenko, B. & Forstová, J. (2013). Nucleofection of expression vectors induces a robust interferon response and inhibition of cell proliferation. *DNA and cell biology*, 32 (8), pp. 467–79. DOI: 10.1089/dna.2012.1950.

Hughes, E. A., Hammond, C. & Cresswell, P. (1997). Misfolded major histocompatibility complex class I heavy chains are translocated into the cytoplasm and degraded by the proteasome. *Proceedings of the National Academy of Sciences*, 94 (5), pp. 1896–1901. DOI: 10.1073/pnas.94.5.1896.

Ikeda, H., Old, L. J. & Schreiber, R. D. (2002). The roles of IFNy in protection against tumor development and cancer immunoediting. *Cytokine and Growth Factor Reviews*, 13 (2), pp. 95–109. DOI: 10.1016/S1359-6101(01)00038-7.

Ishino, Y., Shinagawa, H., Makino, K., Amemura, M. & Nakata, A. (1987). Nucleotide sequence of the iap gene, responsible for alkaline phosphatase isozyme conversion in Escherichia coli, and identification of the gene product. *Journal of Bacteriology*, 169 (12), pp. 5429–5433. DOI: 10.1128/jb.169.12.5429-5433.1987. arXiv: NIHMS150003.

Jackson, R.J., Hellen, C.U.T. & Pestova, T.V. (2010). The mechanism of eukaryotic translation initiation and principles of its regulation. *Nature Reviews Molecular Cell Biology*, 11:2, pp. 113–127. DOI: 10.1038/nrm2838.

Jansen, R., Embden, J., Gaastra, W. & Schouls, L. (2002). Identification of genes that are associated with DNA repeats in prokaryotes. *Molecular microbiology*, 43 (6), pp. 1565–1575.

Jass, J. R. (1986). Lymphocytic infiltration and survival in rectal cancer. *Journal of Clinical Pathology*, 39 (6), pp. 585–589. DOI: 10.1136/jcp.39.6.585.

Jeon, Y. J., Jo, M. G., Yoo, H. M., Hong, S. H., Park, J. M., Ka, S. H., Oh, K. H., Seol, J. H., Jung, Y. K. & Chung, C. H. (2012). Chemosensitivity is controlled by p63 modification with ubiquitin-like protein ISG15. *The Journal of Clinical Investigation*, 19 (7), pp. 2623–36. DOI: 10.1172/JCI61762DS1.

Jeong, H., Mason, S. P., Barabási, A. L. & Oltvai, Z. N. (2001). Lethality and centrality in protein networks. *Nature*, 411 (6833), pp. 41–42. DOI: 10.1038/35075138. arXiv: 0105306.

Jett, J. R., Maksymiuk, A. W., Su, J. Q., Mailliard, J. A., Krook, J. E., Tschetter, L. K., Kardinal, C. G., Twito, D. I., Levitt, R. & Gerstner, J. B. (1994). Phase III trial of recombinant interferon gamma in complete responders with small-cell lung cancer. *Journal of clinical oncology*, 12 (11), pp. 2321–2326. DOI: 10.1200/JCO.1994.12.11.2321.

Jia, R., Ding, S., Pan, Q., Liu, S., Qiao, W. & Liang, C. (2015). The C-Terminal Sequence of IFITM1 Regulates Its Anti-HIV-1 Activity. *PLOS ONE*, pp. 1–17. DOI: 10.1371/journal.pone.0118794.

Jia, R., Pan, Q., Ding, S., Rong, L., Liu, S. L., Geng, Y., Qiao, W. & Liang, C. (2012). The N-Terminal Region of IFITM3 Modulates Its Antiviral Activity by Regulating IFITM3 Cellular Localization. *Journal of Virology*, 86 (24), pp. 13697–13707. DOI: 10.1128/JVI.01828-12.

Jia, R., Xu, F., Qian, J., Yao, Y., Miao, C., Zheng, Y. M., Liu, S. L., Guo, F., Geng, Y., Qiao, W. & Liang, C. (2014). Identification of an endocytic signal essential for the antiviral action of IFITM3. *Cellular microbiology*, 16 (7), pp. 1080–93. DOI: 10.1111/cmi.12262.

Jiang, D., Weidner, J. M., Qing, M., Pan, X.-B., Guo, H., Xu, C., Zhang, X., Birk, A., Chang, J., Shi, P.-Y., Block, T. M. & Guo, J.-T. (2010). Identification of Five Interferon-Induced Cellular Proteins That Inhibit West Nile Virus and Dengue Virus Infections. *Journal of Virology*, 84 (16), pp. 8332–8341. DOI: 10.1128/JVI.02199-09.

Jinek, M., Chylinski, K., Fonfara, I., Hauer, M., Doudna, J. A. & Charpentier, E. (2012). *A Programmable Dual-RNA – Guided DNA Endonuclease in Adaptive Bacterial Immunity*. DOI: 10.1126/science.1225829. arXiv: 38.

Jinek, M., East, A., Cheng, A., Lin, S., Ma, E. & Doudna, J. (2013). RNA-programmed genome editing in human cells. *eLife*, 2013 (2), pp. 1–9. DOI: 10.7554/eLife.00471.

John, S. P., Chin, C. R., Perreira, J. M., Feeley, E. M., Aker, A. M., Savidis, G., Smith, S. E., Elia, A. E. H., Everitt, A. R., Vora, M., Pertel, T., Elledge, S. J., Kellam, P. & Brass, A. L.

(2013). The CD225 Domain of IFITM3 Is Required for both IFITM Protein Association and Inhibition of Influenza A Virus and Dengue Virus Replication. *Journal of Virology*, 87 (14), pp. 7837–7852. DOI: 10.1128/JVI.00481-13.

Jordan, M. A. & Wilson, L. (1998). Microtubles and actin filaments: dynamic targets for cancer chemotherapy. *Curr. Opinion Cell Bio.*, 10, pp. 123–130.

Jouanguy, E., Lamhamedi-Cherradi, S., Altare, F., Fondanèche, M. C., Tuerlinckx, D., Blanche, S., Emile, J. F., Gaillard, J. L., Schreiber, R., Levin, M., Fischer, A., Hivroz, C. & Casanova, J. L. (1997). Partial interferon-γ receptor 1 deficiency in a child with tuberculoid bacillus Calmette-Guerin infection and a sibling with clinical tuberculosis. *Journal of Clinical Investigation*, 100 (11), pp. 2658–2664. DOI: 10.1172/JCI119810.

Kaplan, D. H., Shankaran, V., Dighe, A. S., Stockert, E., Aguet, M., Old, L. J. & Schreiber, R. D. (1998). Demonstration of an interferon g-dependent tumor surveillance system in immunocompetent mice. 95, pp. 7556–7561.

Kelly, J. M., Gilbert, C. S., Stark, G. R. & Kerr, I. M. (1985). Differential regulation of interferon-induced mRNAs and c-myc mRNA by α- and γ-interferons. *European Journal of Biochemistry*, 153 (2), pp. 367–371. DOI: 10.1111/j.1432-1033.1985.tb09312.x.

Kenter, G. G., Welters, M. J. P., Valentijn, A. R. P. M., Lowik, M. J. G., Berends-van der Meer, D. M. A., Vloon, A. P. G., Essahsah, F., Fathers, L. M., Offringa, R., Drijfhout, J. W., Wafelman, A. R., Oostendorp, J., Fleuren, G. J., van der Burg, S. H. & Melief, C. J. M. (2009). Vaccination against HPV-16 Oncoproteins for Vulvar Intraepithelial Neoplasia. *New England Journal of Medicine*, 361 (19), pp. 1838–1847. DOI: 10.1056/NEJMoa0810097.

Khodarev, N. N., Beckett, M., Labay, E., Darga, T., Roizman, B. & Weichselbaum, R. R. (2004). *Proceedings of the National Academy of Sciences*, 101 (6), pp. 1714–1719. DOI: 10.1073/pnas.0308102100.

Khodarev, N. N., Minn, A. J., Efimova, E. V., Darga, T. E., Labay, E., Beckett, M., Mauceri, H. J., Roizman, B. & Weichselbaum, R. R. (2007). Signal transducer and activator of transcription 1 regulates both cytotoxic and prosurvival functions in tumor cells. *Cancer Research*, 67 (19), pp. 9214–9220. DOI: 10.1158/0008-5472.CAN-07-1019.

Khodarev, N. N., Roach, P., Pitroda, S. P., Golden, D. W., Bhayani, M., Shao, M. Y., Darga, T. E., Beveridge, M. G., Sood, R. F., Sutton, H. G., Beckett, M. A., Mauceri, H. J., Posner, M. C. & Weichselbaum, R. R. (2009). STAT1 pathway mediates amplification of metastatic potential and resistance to therapy. *PLoS ONE*, 4 (6), pp. 1–14. DOI: 10.1371/journal.pone.0005821.

Khodarev, N. N., Roizman, B. & Weichselbaum, R. R. (2012). Molecular pathways: Interferon/Stat1 pathway: Role in the tumor resistance to genotoxic stress and aggressive growth. *Clinical Cancer Research*, 18 (11), pp. 3015–3021. DOI: 10.1158/1078-0432.CCR-11-3225.

Khong, H. T. & Restifo, N. P. (2002). Natural selection of tumor variants in the generation of "tumor escape" phenotypes. *Nature Immunology*, 3 (11), pp. 999–1005. DOI: 10.1038/ni1102-999. arXiv: NIHMS150003.

Kiessling, A., Hogrefe, C., Erb, S., Bobach, C., Fuessel, S., Wessjohann, L. & Seliger, B. (2009). Expression, regulation and function of the ISGylation system in prostate cancer. *Oncogene*, 28 (28), pp. 2606–2620. DOI: 10.1038/onc.2009.115.

Kim, K. Y., Blatt, L. & Taylor, M. W. (2000). The effects of interferon on the expression of human papillomavirus oncogenes. *Journal of General Virology*, 81 (3), pp. 695–700. DOI: 10.1099/0022-1317-81-3-695.

Kim, T. J., Choi, J. J., Kim, W. Y., Choi, C. H., Lee, J. W., Bae, D. S., Son, D. S., Kim, J., Park, B. K., Ahn, G., Cho, E. Y. & Kim, B. G. (2007). Gene expression profiling for the prediction of lymph node metastasis in patients with cervical cancer. *Cancer Science*, 0 (0), 071106234520002–??? DOI: 10.1111/j.1349-7006.2007.00652.x.

Kingdom, K. H. (1923). A METHOD FOR THE NEUTRALIZATION OF ELECTRON SPACE CHARGE BY POSITIVE IONIZATION AT VERY LOW GAS PRESSURES. *Physical Review Journal*, 21, pp. 408–18.

Kita, K., Sugaya, S., Zhai, L., Wu, Y. P., Wano, C., Chigira, S., Nomura, J., Takahashi, S., Ichinose, M. & Suzuki, N. (2003). Involvement of LEU13 in Interferon-Induced Refractoriness of Human RSa Cells to Cell Killing by X Rays. *Radiation Research*, 160 (3), pp. 302–308. DOI: 10.1667/RR3039.

Klein, G. (1966). Tumor antigens. *annu. Rev. Microbiol.*, 20, pp. 223–52.

Klein, G. & Klein, E. (1956). Genetic studies of the relationship of tumour-host cells. *Nature*, 178, pp. 79–81. DOI: 10.1038/1781020a0.

Knigth, E., Fahey, D., Cordova, B., Hillman, M., Kutny, R., Reich, N. & Blomstrom, D. (1988). A 15-kDa interferon-induced protein is derived by COOH-terminal processing of a 17-kDa precursor. *Journal of Biological Chemistry*, 263 (10), pp. 4520–4522.

Kooi, S., Zhang, H. Z., Patenia, R., Edwards, C. L., Platsoucas, C. D. & Freedman, R. S. (1996). HLA class I expression on human ovarian carcinoma cells correlates with T-cell infiltration in vivo and T-cell expansion in vitro in low concentrations of recombinant interleukin-2. *Cellular immunology*, 174 (2), pp. 116–28. DOI: 10.1006/cimm.1996.0301.

Koopman, L. A., Corver, W. E., Van Der Slik, A. R., Giphart, M. J. & Fleuren, G. J. (2000). Multiple Genetic Alterations Cause Frequent and Heterogeneous Human Histocompatibility Leukocyte Antigen Class I Loss in Cervical Cancer. *J. Exp. Med*, 191 (6), pp. 961–975. DOI: 10.1084/jem.191.6.961.

Koopmann, J. O., Albring, J., Hüter, E., Bulbuc, N., Spee, P., Neefjes, J., Hämmerling, G. J. & Momburg, F. (2000). Export of antigenic peptides from the endoplasmic reticulum intersects with retrograde protein translocation through the Sec61p channel. *Immunity*, 13 (1), pp. 117–127. DOI: 10.1016/S1074-7613(00)00013-3.

Koos, B., Andersson, L., Clausson, C. M., Grannas, K., Klaesson, A., Cane, G. & Söderberg, O. (2014). *"Analysis of Protein Interactions in situ by Proximity Ligation Assays" current topics in Microbiology and Immunology- High-Dimensional Single Cell Analysis*. Ed. by Harris G. Fienberg. USA: Springer, 377, 111–126 (.

Korants, B. D., Blomstrom, D. C., Jonak, G. J. & Knight, E. (1984). Interferon-induced Proteins. PURIFICATION AND CHARACTERIZATION OF A 15,000-DALTON PROTEIN FROM HUMAN AND BOVINE CELLS INDUCED BY INTERFERON. 259 (23), pp. 14835–14839.

Lau, S. L. Y., Yuen, M. L., Kou, C. Y. C., Au, K. W., Zhou, J. & Tsui, S. K. W. (2012). Interferons induce the expression of IFITM1 and IFITM3 and suppress the proliferation of rat neonatal cardiomyocytes. *Journal of Cellular Biochemistry*, 113 (3), pp. 841–847. DOI: 10.1002/jcb.23412.

Lee, W. Y. J., Fu, R. M., Liang, C. & Sloan, R. D. (2018). IFITM proteins inhibit HIV-1 protein synthesis. *Scientific Reports*, 8 (1), pp. 1–15. DOI: 10.1038/s41598-018-32785-5.

Lee, W. Y. J., Liang, C. & Sloan, R. D. (2017). IFITMs inhibit HIV-1 protein synthesis. *bioRxiv*, pp. 1–39.

Lenschow, D. J., Giannakopoulos, N. V., Lacey, J., Johnston, C., Guin, A. K. O., Robert, E., Levine, B., Iv, H. W. V., Gunn, L. J. & Schmidt, R. E. (2005). Identification of Interferon-Stimulated Gene 15 as an Antiviral Molecule during Sindbis Virus Infection In Vivo. *Journal of Virology*, 79 (22), pp. 13974–13983. DOI: 10.1128/JVI.79.22.13974.

Lenschow, D. J., Lai, C., Frias-Staheli, N., Giannakopoulos, N. V., Lutz, A., Wolff, T., Osiak, A., Levine, B., Schmidt, R. E., Garcia-Sastre, A., Leib, D. A., Pekosz, A., Knobeloch, K.-P., Horak, I. & Virgin, H. W. (2007). IFN-stimulated gene 15 functions as a critical antiviral molecule against influenza, herpes, and Sindbis viruses. *Proceedings of the National Academy of Sciences*, 104 (4), pp. 1371–1376. DOI: 10.1073/pnas.0607038104.

Lewin, A. R., Reid, L. E., McMahon, M., Stark, G. R. & Kerr, I. M. (1991). Molecular analysis of a human interferon-inducible gene family. *European journal of biochemistry / FEBS*, 199 (2), pp. 417–23. DOI: 10.1111/j.1432-1033.1991.tb16139.x.

Li, K., Jia, R., Li, M., Zheng, Y. M., Miao, C., Yao, Y., Ji, H. L., Geng, Y., Qiao, W., Albritton, L. M., Liang, C. & Liu, S. L. (2015). A sorting signal suppresses IFITM1 restriction of viral entry. *Journal of Biological Chemistry*, 290 (7), pp. 4248–4259. DOI: 10.1074/jbc.M114.630780.

Li, K., Markosyan, R. M., Zheng, Y. M., Golfetto, O., Bungart, B., Li, M., Ding, S., He, Y., Liang, C., Lee, J. C., Gratton, E., Cohen, F. S. & Liu, S. L. (2013). IFITM Proteins Restrict Viral Membrane Hemifusion. *PLoS Pathogens*, 9 (1). DOI: 10.1371/journal.ppat.1003124.

Liao, J. B. (2006). Viruses and Human Cancer. *The Yale Journal of bBology and Medicine*, 79, pp. 115–122. DOI: 10.1007/978-1-4939-0870-7.

Lindner, H. A., Lytvyn, V., Qi, H., Lachance, P., Ziomek, E. & Ménard, R. (2007). Selectivity in ISG15 and ubiquitin recognition by the SARS coronavirus papain-like protease.

Archives of Biochemistry and Biophysics, 466 (1), pp. 8–14. DOI: 10.1016/j.abb.2007.07.006.

Lipponen, P. K., Eskelinen, M. J., Jauhiainen, K., Harju, E. & Terho, R. (1992). Tumour infiltrating lymphocytes as an independent prognostic factor in transitional cell bladder cancer. *European journal of cancer (Oxford, England : 1990)*, 29A (1), pp. 69–75.

Liu, M., Hummer, B. T., Li, X. & Hassel, B. A. (2004). Camptothecin Induces the Ubiquitin-like Protein, ISG15, and Enhances ISG15 Conjugation in Response to Interferon. *JOURNAL OF INTERFERON & CYTOKINE RESEARCH*, 654, pp. 647–654.

Liu, X., Wang, Q., Chen, W. & Wang, C. (2013). Cytokine & Growth Factor Reviews Dynamic regulation of innate immunity by ubiquitin and ubiquitin-like proteins. *Cytokine and Growth Factor Reviews*, 24 (6), pp. 559–570. DOI: 10.1016/j.cytogfr.2013.07.002.

Liu, Y. H., Lin, J., Guo, J., Wang, Z. G., Zhong, D., Yang, X. L., Zhang, Z. S., Xiao, B. & Guo, W. Y. (2008). Detection of interferon-induced transmembrane-1 gene expression for clinical diagnosis of colorectal cancer. *J. South Med. Univ.*, 28 (11), pp. 1950–3.

Loeb, K. R. & Haas, A. L. (1992). The interferon-inducible 15-kDa ubiquitin homolog conjugates to intracellular proteins. *Journal of Biological Chemistry*, 267 (11), pp. 7806–7813.

— (1994). Conjugates of ubiquitin cross-reactive protein distribute in a cytoskeletal pattern. *Molecular and cellular biology*, 14 (12), pp. 8408–19. DOI: 10.1128/MCB.14.12.8408.Updated.

Long, J. C. & Caceres, J. F. (2009). The SR protein family of splicing factors: master regulators of gene expression. *The Biochemical journal*, 417 (1), pp. 15–27. DOI: 10.1042/BJ20081501.

Lu, J., Pan, Q., Rong, L., Liu, S. L. & Liang, C. (2011). The IFITM Proteins Inhibit HIV-1 Infection. *Journal of Virology*, 85 (5), pp. 2126–2137. DOI: 10.1128/JVI.01531-10.

Lunn, R. M., Jahnke, G. D. & Rabkin, C. S. (2017). Tumour virus epidemiology. *Philosophical Transactions of the Royal Society B: Biological Sciences*, 372 (1732). DOI: 10.1098/rstb.2016.0266.

Ma, W., Tummers, B., Esch, E. M. G. van, Goedemans, R., Melief, C. J. M., Meyers, C., Boer, J. M. & Burg, S. H. van der (2016). Human Papillomavirus Downregulates the Expression of IFITM1 and RIPK3 to Escape from IFNγ- and TNFα-Mediated Antiproliferative Effects and Necroptosis. *Frontiers in Immunology*, 496, pp. 1–15.

Mach, B., Steimle, V. & Martinez-Soria, E. (1996). REGULATION OF MHC CLASS II GENES : Lessons from a Disease.

Maier, J. A. M., Morelli, D. & Balsaris, A. (1995). The differential response to interferon g by normal and transformed endothelial cells. *Biochemical and biophysical research communications*, 214:582–88.

Makarov, A. (2000). Electrostatic Axially Harmonic Orbital Trapping: A High-Performance Technique of Mass Analysis. 72 (6), pp. 1156–1162.

Malakhov, M. P., Malakhova, O. A., Il Kim, K., Ritchie, K. J. & Zhang, D. E. (2002). UBP43 (USP18) specifically removes ISG15 from conjugated proteins. *Journal of Biological Chemistry*, 277 (12), pp. 9976–9981. DOI: 10.1074/jbc.M109078200.

Malakhova, O. A., Yan, M., Malakhov, M. P., Yuan, Y., Ritchie, K. J., Kim, K. I., Peterson, L. F., Shuai, K. & Zhang, D. E. (2003). Protein ISGylation modulates the JAK-STAT signaling pathway. *Genes and Development*, 17 (4), pp. 455–460. DOI: 10.1101/gad.1056303.

Malakhova, O. A. & Zhang, D. E. (2008). ISG15 inhibits Nedd4 ubiquitin E3 activity and enhances the innate antiviral response. *Journal of Biological Chemistry*, 283 (14), pp. 8783–8787. DOI: 10.1074/jbc.C800030200.

Manguso, R. T., Pope, H. W., Zimmer, M. D., Brown, F. D., Yates, K. B., Miller, B. C., Collins, N. B., Bi, K., LaFleur, M. W., Juneja, V. R., Weiss, S. A., Lo, J., Fisher, D. E., Miao, D., Van Allen, E., Root, D. E., Sharpe, A. H., Doench, J. G. & Haining, N. (2018). In vivo CRISPR screening identifies Ptpn2 as a cancer immunotherapy target. *Nature*, 547 (4), pp. 413–418. DOI: 10.1017/S1092852915000371.Neuroimaging.

Mann, M. (2006). Functional and quantitative proteomics using SILAC. *Nature*, 7 (December), pp. 952–958.

Manza, L. L., Stamer, S. L., Ham, A. J. L., Codreanu, S. G. & Liebler, D. C. (2005). Sample preparation and digestion for proteomic analyses using spin filters. *Proteomics*, 5 (7), pp. 1742–1745. DOI: 10.1002/pmic.200401063.

Marc, E. & Moulin, F. (2003). DISSEMINATED MYCOBACTERIUM PEREGRINUM INFECTION IN A CHILD WITH COMPLETE INTERFERON-GAMMA RECEPTOR-1 DEFICIENCY. 22 (4), pp. 378–380.

Marie, I., Durbin, J. E. & Levy, D. E. (1998). Differential viral induction of distinct interferon-alpha genes by positive feedback through interferon regulatory factor-7. *The EMBO Journal*, 17 (22), pp. 6660–6669. DOI: 10.1093/emboj/17.22.6660.

Marth, C., Fiegl, H., Zeimet, A. G., Müller-Holzner, E., Deibl, M., Doppler, W. & Daxenbichler, G. (2004). Interferon-γ expression is an independent prognostic factor in ovarian cancer. *American Journal of Obstetrics and Gynecology*, 191 (5), pp. 1598–1605. DOI: 10.1016/j.ajog.2004.05.007.

Matsumoto, A. K., Martin, D. R., Carter, R. H., Klickstein, L. B., Ahearn, S. J. M. & Fearon, D. T. (1993). Functional Dissection of the CD21/CD19/TAPA-1/Leu-13 Complex of B Lymphocytes. *Journal of Experimental Medicine*, 178 (October), pp. 1407–17.

McCarthy, E. F. (2006). The toxins of William B. Coley and the treatment of bone and soft-tissue sarcomas. *The Iowa Orthopaedic Journal*, 26, pp. 154–58.

Melief, C. J. M. & Van Der Burg, S. H. (2008). Immunotherapy of established (pre)malignant disease by synthetic long peptide vaccines. *Nature Reviews Cancer*, 8 (5), pp. 351–360. DOI: 10.1038/nrc2373.

Mellor, A. L. & Munn, D. H. (2008). Creating immune privilege: Active local suppression that benefits friends, but protects foes. *Nature Reviews Immunology*, 8 (1), pp. 74–80. DOI: 10.1038/nri2233.

Meyer, B., Papasotiriou, D. G. & Karas, M. (2011). 100% protein sequence coverage: A modern form of surrealism in proteomics. *Amino Acids*, 41 (2), pp. 291–310. DOI: 10.1007/s00726-010-0680-6.

Meyskens, F. L., Kopecky, K., Samson, M., Hersh, E., Macdonald, J., Jaffe, H., Crowley, J. & Coltman, C. (1990). Recombinant human interferon gamma: adverse effects in high-risk stage I and II cutaneous malignant melanoma. *Journal of the National Cancer Institute*, 82 (12), p. 1071.

Minn, Andy J. (2015). Interferons and the Immunogenic Effects of Cancer Therapy. *Trends in Immunology*, 36 (11), pp. 725–737. DOI: 10.1016/j.it.2015.09.007. arXiv: 15334406.

Miyauchi, K., Kim, Y., Latinovic, O., Morozov, V. & Melikyan, G. B. (2009). HIV Enters Cells via Endocytosis and Dynamin-Dependent Fusion with Endosomes. *Cell*, 137 (3), pp. 433–444. DOI: 10.1016/j.cell.2009.02.046.

Moffatt, P., Gaumond, M. H., Salois, P., Sellin, K., Bessette, M. C., Godin, É., De Oliveira, P. T., Atkins, G. J., Nanci, A. & Thomas, G. (2008). Bril: A novel bone-specific modulator of mineralization. *Journal of Bone and Mineral Research*, 23 (9), pp. 1497–1508. DOI: 10.1359/jbmr.080412.

Monaco, E. L., Tremante, E., C., Cristina, Melucci, E., Sibilio, L., Zingoni, A., Nicotra, M. R., Natali, P. G. & Giacomini, P. (2011). Human Leukocyte Antigen E Contributes to Protect Tumor Cells from Lysis by Natural Killer Cells. *Neoplasia*, 13 (9), 822–IN14. DOI: 10.1593/neo.101684.

Mortaz, E., Tabarsi, P., Mansouri, D., Khosravi, A., Garssen, J., Velayati, A. & Adcock, M. (2016). Cancers related to Immunodeficiencies: Update and Perspectives. *Frontiers in Immunology*, 7, pp. 1–13.

Mortillaro, M. J., Blencowe, B. J., Wei, X., Nakayasu, H., Du, L., Warren, S. L., Sharp, P. A. & Berezney, R. (1996). A hyperphosphorylated form of the large subunit of RNA polymerase II is associated with splicing complexes and the nuclear matrix. *Proceedings of the National Academy of Sciences*, 93 (16), pp. 8253–8257. DOI: 10.1073/pnas.93.16.8253.

Mosmann, T. R. & Coffman, R. L. (1989). Th1 and Th2 cells: different patterns of lymphokine secretion lead to different functional properties. *Annu. Rev. Immunol*, 7, pp. 145–73. DOI: 10.15713/ins.mmj.3.

Mossman, K. L., Macgregor, P. F., Rozmus, J. J., Goryachev, A. B., Edwards, A. M. & Smiley, J. R. (2001). Herpes simplex virus triggers and then disarms a host antiviral response. *Journal of virology*, 75 (2), pp. 750–8. DOI: 10.1128/JVI.75.2.750-758.2001.

Mou, H., Smith, J. L., Peng, L., Yin, H., Moore, J., Zhang, X. O., Song, C. Q., Sheel, A., Wu, Q., Ozata, D. M., Li, Y., Anderson, D. G., Emerson, C. P., Sontheimer, E. J., Moore, M. J., Weng, Z. & Xue, W. (2017). CRISPR/Cas9-mediated genome editing induces exon skipping by alternative splicing or exon deletion. *Genome Biology*, 18 (1), pp. 4–11. DOI: 10.1186/s13059-017-1237-8.

Muller, M., Laxton, C., Briscoe, J., Schindler, C., Darnell, J. E., Stark, G. R. & Kerr, I. M. (1993). Complementation of a mutantcelline:central role of the 91 kDa polypeptide of ISGF3 in the interferon-a and -y signal transduction pathways. 1 (1), pp. 4221–4228.

Muñoz, M. J., Santangelo, M. S. P., Paronetto, M. P., de la Mata, M., Pelisch, F., Boireau, S., Glover-Cutter, K., Ben-Dov, C., Blaustein, M., Lozano, J. J., Bird, G., Bentley, D., Bertrand, E. & Kornblihtt, A. R. (2009). DNA Damage Regulates Alternative Splicing through Inhibition of RNA Polymerase II Elongation. *Cell*, 137 (4), pp. 708–720. DOI: 10.1016/j.cell.2009.03.010.

Murphy, D., Detjen, K. M., Welzel, M., Wiedenmann, B. & Rosewicz, S. (2001). Interferon-α delays S-phase progression in human hepatocellular carcinoma cells via inhibition of specific cyclin-dependent kinases. *Hepatology*, 33 (2), pp. 346–356. DOI: 10.1053/jhep.2001.21749.

Nacopoulou, L., Azaris, P., Papacharalmpous, N. & Davaris, P. (1981). Prognostic significance of histologic host response in cancer of the large bowel. *Cancer*, 47, pp. 930–36. DOI: 10.1002/1097-0142(19810301)47.

Naito, Y., Saito, K., Shiiba, K., Ohuchi, A., Saigenji, K., Nagura, H. & Ohtani, H. (1998). CD8+ T cells infiltrated within cancer cell nests as a prognostic factor in human colorectal cancer. *Cancer Research*, 58 (16), pp. 3491–3494. DOI: 10.1002/(SICI)1096-9896(199707)182:3<318::AID-PATH862>3.0.CO;2-6.

Narayana, S. K., Helbig, K. J., McCartney, E. M., Eyre, N. S., Bull, R. A., Eltahla, A., Lloyd, A. R. & Beard, M. R. (2015). The interferon-induced transmembrane proteins, IFITM1, IFITM2, and IFITM3 inhibit hepatitis C virus entry. *Journal of Biological Chemistry*, 290 (43), pp. 25946–25959. DOI: 10.1074/jbc.M115.657346.

Naro, C., Bielli, P., Pagliarini, V. & Sette, C. (2015). The interplay between DNA damage response and RNA processing: the unexpected role of splicing factors as gatekeepers of genome stability. *Frontiers in Genetics*, 6, pp. 1–10.

Neefjes, J. J. & Ploegh, H. L. (1988). Allele and locus-specific differences in cell surface expression and the association of HLA class I heavy chain with β2-microglobulin: differential effects of inhibition of glycosylation on class I subunit association. *European Journal of Immunology*, 18 (5), pp. 801–810. DOI: 10.1002/eji.1830180522.

Neefjes, J. J., Smit, L., Gehrmann, M. & Ploegh, H. L. (1992). The fate of the three subunits of major histocompatibility complex class I molecules. *European Journal of Immunology*, 22 (6), pp. 1609–1614. DOI: 10.1002/eji.1830220639.

Neefjes, J., Jongsma, M. L. M., Paul, P. & Bakke, O. (2011). Towards a systems understanding of MHC class i and MHC class II antigen presentation. *Nature Reviews Immunology*, 11 (12), pp. 823–836. DOI: 10.1038/nri3084. arXiv: arXiv:1011.1669v3.

Negrini, S., Gorgoulis, V. G. & Halazonetis, T. D. (2010). Genomic instability an evolving hallmark of cancer. *Nature Reviews Molecular Cell Biology*, 11 (3), pp. 220–228. DOI: 10.1038/nrm2858.

Neumann, F., Hemmerich, P., Mikecz, A. von, Peter, H.H. & Krawinkel, U. (1995). Human ribosomal protein L7 inhibits cell-free translation in reticulocyte lysates and affects the expression of nuclear proteins upon stable transfection into Jurkat T-lymphoma cells. *Nucleic Acids Reasearch*, 23, pp. 195–202.

Neumann, F. & Krawinkel, U. (1997). Constitutive Expression of Human Ribosomal Protein L7 Arrests the Cell Cycle in G1 and Induces Apoptosis in Jurkat T-Lymphoma Cells. *Experimental Cell Research*, 230, pp. 252–261.

Newport, M., Huxley, C., Huston, S., Hawrylowicz, C., Oostra, B., Williamson, R. & Levin, M. (2017). A mutation in the interferon- γ-receptor gene and susceptibility to mycobacterial infection. *The New England Journal of Medicine*, 335 (26), pp. 1941–1949.

Nicholl, M. J., Robinson, L. H. & Preston, C. M. (2000). Activation of cellular interferon-responsive genes after infection of human cells with herpes simplex virus type 1. *The Journal of general virology*, 81 (Pt 9), pp. 2215–8. DOI: 10.1099/0022-1317-81-9-2215.

Niessen, W. M. A. (1999). *MS–MS and MSn, In Encyclopedia of Spectroscopy and Spectrometry*. Ed. by J. C. Lindon. 2nd. Vol. 2. Academic Press, pp. 936–941. ISBN: 9780124095472.

Nolan, T., Hands, R.E. & Bustin, S. A. (2006). Quantification of mRNA using real-time RT-PCR. *Nature Protocols*, 1, pp. 1559–1582.

Novita Sari, I., Yang, Y. G., Hanh Phi, L. T., Kim, H., Jun Baek, M., Jeong, D. & Young Kwon, H. (2016). Interferon-induced transmembrane protein 1 (IFITM1) is required for the progression of colorectal cancer. *Oncotarget*, 7 (52), pp. 86039–86050. DOI: 10.18632/oncotarget.13325.

Ogony, J., Choi, H. J., Lui, A., Cristofanilli, M. & Lewis-Wambi, J. (2016). Interferon-induced transmembrane protein 1 (IFITM1) overexpression enhances the aggressive phenotype of SUM149 inflammatory breast cancer cells in a signal transducer and activator of transcription 2 (STAT2)-dependent manner. *Breast cancer research : BCR*, 18 (1), p. 25. DOI: 10.1186/s13058-016-0683-7.

Okumura, A., Lu, G., Pitha-Rowe, I. & Pitha, P. M. (2006). Innate antiviral response targets HIV-1 release by the induction of ubiquitin-like protein ISG15. *Proc Natl Acad Sci U S A*, 103 (5), pp. 1440–1445. DOI: 10.1073/pnas.0510518103.

Old, L. J. & Boyse, E. A. (1964). Immunology of experimental tumors. *Annu. Rev. Medicine*, 15 (c), pp. 167–86.

Ong, S. E., Blagoev, B., Kratchmarova, I., Kristensen, D. B., Steen, H., Pandey, A. & Mann, M. (2002). Stable Isotope Labeling by Amino Acids in Cell Culture, SILAC, as a Simple and Accurate Approach to Expression Proteomics. *Molecular & Cellular Proteomics*, 1 (5), pp. 376–386. DOI: 10.1074/mcp.M200025-MCP200. arXiv: NIHMS150003.

Ong, S. E. & Mann, M. (2005). Mass Spectrometry–Based Proteomics Turns Quantitative. *Nature Chemical Biology*, 1 (5), pp. 252–262. DOI: 10.1038/nchembio736. arXiv: NIHMS150003.

Palangat, M., Anastasakis, D.G., Fei, D.F., Lindblad, K.E., Bradley, R., Hourigan, C.S., Hafner, M. & Larson, D.R. (2019). The splicing factor U2AF1 contributes to cancer progression through a noncanonical role in translation regulation. *Genes and Development*, 33, pp. 1–16.

Palma, L., Di Lorenzo, N. & Guidetti, B. (1978). Lymphocytic infiltrates in primary glioblastomas and recidi- vous gliomas. Incidence, fate, and relevance to prognosis in 228 operated cases. *J Neurosurg*, 49, pp. 854–861.

Pan, Z., Chen, S., Pan, X., Wang, Z., Han, H., Zheng, W., Wang, X., Li, F., Qu, S. & Shao, R. (2010). Differential gene expression identified in Uigur women cervical squamous cell carcinoma by suppression subtractive hybridization., pp. 2–7. DOI: 10.4149/neo.

Park, J. H., Yang, S. W., Park, J. M., Ka, S. H., Kim, J. H., Kong, Y. Y., Jeon, Y. J., Seol, J. H. & Chung, C. H. (2016). Positive feedback regulation of p53 transactivity by DNA damage-induced ISG15 modification. *Nature Communications*, 7, pp. 1–13. DOI: 10.1038/ncomms12513.

Park, J. M., Yang, S. W., Yu, K. R., Ka, S. H., Lee, S. W., Seol, J. H., Jeon, Y. J. & Chung, C. H. (2014). Modification of PCNA by ISG15 Plays a Crucial Role in Termination of Error-Prone Translesion DNA Synthesis. *Molecular Cell*, 54 (4), pp. 626–638. DOI: 10.1016/j.molcel.2014.03.031.

Parkin, D. M., Wabinga, H., Nambooze, S. & Wabwire-Mangen, F. (1999). AIDS-related cancers in Africa: Maturation of the epidemic in Uganda. *Aids*, 13 (18), pp. 2563–2570. DOI: 10.1097/00002030-199912240-00010.

Passmore, L. A., Schmeing, T. M., Maag, D., Applefield, D. J., Acker, M. G., Algire, M. A. A., Lorsch, J. R. & Ramakrishnan, V. (2007). The Eukaryotic Translation Initiation Factors eIF1 and eIF1A Induce an Open Conformation of the 40S Ribosome. *Molecular Cell*, 26 (1), pp. 41–50. DOI: 10.1016/j.molcel.2007.03.018.

Peh, C. A., Burrows, S. R., Barnden, M., Khanna, R., Cresswell, P., Moss, D. J. & McCluskey, J. (1998). HLA-B27-restricted antigen presentation in the absence of tapasin reveals polymorphism in mechanisms of HLA class I peptide loading. *Immunity*, 8 (5), pp. 531–542. DOI: 10.1016/S1074-7613(00)80558-0.

Penn, I. (1978). Tumors Arising in Organ Transplant Recipients. *Advances in Cancer Research*, 28 (C), pp. 31–61. DOI: 10.1016/S0065-230X(08)60645-4.

Perry, Richard H., Cooks, Graham R. & Noll, Robert J. (2008). Orbitrap Mass Spectrometry: instrumentation, ion motion and applications. *Mass Spectrometry Reviews*, 27, pp. 661–99. DOI: 10.1002/mas. arXiv: NIHMS150003.

Perussia, B. (1991). Lymphokine-activated killer cells, natural killer cells and cytokines. *Curr Opin Immunol*, 3 (1), pp. 49–55.

Pestova, T. V., Kolupaeva, V. G., Lomakin, I. B., Pilipenko, E. V., Shatsky, I. N., Agol, V. I. & Hellen, C. U. T. (2001). Molecular mechanisms of translation initiation in eukaryotes. *Proceedings of the National Academy of Sciences*, 98 (13), pp. 7029–7036. DOI: 10.1073/pnas.111145798.

Pettit, S. J., Seymour, K., O'Flaherty, E. & Kirby, J. A. (2000). Immune selection in neoplasia: towards a microevolutionary model of cancer development. *British Journal of Cancer*, 82 (12), pp. 1900–1906. DOI: 10.1054/bjoc.2000.1206.

Platanias, L. C. (2005). Mechanisms of type-I- and type-II-interferon-mediated signalling. *Nature Reviews Immunology*, 5 (5), pp. 375–386. DOI: 10.1038/nri1604. arXiv: arXiv:1011.1669v3.

Pochel, F., Toomes, C., Bransfield, K., Leong, F.T., Douglas, S.H., Field, S.L., Bell, S.M., Combaret, V., Puisieux, A., Mighell, A.J., Robinson, P.A., Inglehearn, C.F., Isaacs, J.D. & Markham, A.F. (2003). Real-time PCR based on SYBR-Green I fluorescence: An alternative to the TaqMan assay for a relative quantification of gene rearrangements, gene amplifications and micro gene deletions. *BMC Biotechnology*, 3, pp. 1–13.

Popp, M. W. & Maquat, L.E. (2016). Leveraging Rules of Nonsense-Mediated mRNA Decay for Genome Engineering and Personalized Medicine. *Cell*, 165, pp. 1319–1322. DOI: 10.1016/j.cell.2016.05.053.

Price, G. E., Gaszewska-Mastarlarz, A. & Moskophidis, D. (2000). The role of alpha/beta and gamma interferons in development of immunity to influenza A virus in mice. *Journal of virology*, 74 (9), pp. 3996–4003. DOI: 10.1128/JVI.74.9.3996-4003.2000.

Princiotta, M. F., Finzi, D., Qian, S. B., Gibbs, J., Schuchmann, S., Buttgereit, F., Bennink, J. R. & Yewdell, J. W. (2003). Quantitating protein synthesis, degradation, and endogenous antigen processing. *Immunity*, 18 (3), pp. 343–354. DOI: 10.1016/S1074-7613(03)00051-7.

Propper, D. J., Chao, D., Braybrooke, J. P., Bahl, P., Thavasu, P., Balkwill, F., Turley, H., Dobbs, N., Gatter, K., Talbot, D. C., Harris, A. L. & Ganesan, T. S. (2003). Low-dose IFN-gamma induces tumor MHC expression in metastatic malignant melanoma. *Clinical Cancer Research*, 9 (1), pp. 84–92.

Radtke, F. & Clevers, H. (2005). Self-renewal and cancer of the gut: Two sides of a coin. *Science*, 307 (5717), pp. 1904–1909. DOI: 10.1126/science.1104815. arXiv: NIHMS150003.

Ramana, Chilakamarti V, Gil, M Pilar, Schreiber, Robert D & Stark, George R (2002). Stat1-dependent and -independent pathways in IFN-gamma-dependent signaling. *Trends in immunology*, 23 (2), pp. 96–101. DOI: 10.1016/S1471-4906(01)02118-4.

Rammensee, H. G., Falk, K. & Rötzschke, O. (1993). Peptides naturally presented by MHC class I molecules. *Annu. Rev. Immunol*, 11, pp. 213–44.

Ran, F. A., Hsu, P. D., Wright, J., Agarwala, V., Scott, D. A. & Zhang, F. (2013). Genome engineering using the CRISPR-Cas9 system. *Nature Protocols*, 8 (11), pp. 2281–2308. DOI: 10.1038/nprot.2013.143. arXiv: NIHMS150003.

Recht, M., Borden, E. C., Knight, E., Borden, E. C. & Knight, E. (2018). A human 15-kDa IFN-induced protein induces the secretion of IFN-gamma. *Journal of Immunology*, 147, pp. 2617–23.

Reid, L. E., Brasnett, A. H., Gilbert, C. S., Porter, A. C., Gewert, D. R., Stark, G. R. & Kerr, I. M. (1989). A single DNA response element can confer inducibility by both alpha- and gamma-interferons. *Proceedings of the National Academy of Sciences of the United States of America*, 86 (3), pp. 840–4. DOI: 10.1073/pnas.86.3.840.

Reis, L. F. L., Harada, H., Wolchok, J. D. & Taniguchi, T. (1992). Critical role of a common transcription factor , IRF-1 , in the regulation of IFN-3 and IFN-inducible genes. 1 (1), pp. 185–193.

Reits, E. A. J., Vos, J. C., Grammé, M. & Neefjes, J. (2000). The major substrates for TAP in vivo are derived from newly synthesized proteins. *Nature*, 404 (6779), pp. 774–778. DOI: 10.1038/35008103.

Reits, E. A., Hodge, J. W., Herberts, C. A., Groothuis, T. A., Chakraborty, M., Wansley, E., Camphausen, K., Luiten, R. M., de Ru, A. H., Neijssen, J., Griekspoor, A., Mesman, E., Verreck, F. A., Spits, H., Schlom, J., van Veelen, P. & Neefjes, J. J. (2006). Radiation modulates the peptide repertoire, enhances MHC class I expression, and induces successful antitumor immunotherapy. *The Journal of Experimental Medicine*, 203 (5), pp. 1259–1271. DOI: 10.1084/jem.20052494.

Restifo, N. P., Antony, P. A., Finkelstein, S. E., Leitner, W. W., Surman, D. R., Theoret, M. R. & Touloukian, C. E. (2002). Assumptions of the tumor 'escape' hypothesis. *Seminars in Cancer Biology*, 12 (1), pp. 81–86. DOI: 10.1006/scbi.2001.0399.

Rilke, F., Colnaghi, M. I., Cascinelli, N., Andreola, S., Baldini, M. T., Bufalino, R., Della Porta, G., Ménard, S., Pierotti, M. A. & Testori, A. (1991). Prognostic significance of HER-2/neu expression in breast cancer and its relationship to other prognostic factors. *Int. J. Cancer*, 49, pp. 44–49.

Robledo, S., Idol, R.A., Crimmins, D.L, Ladenson, J.H., Mason, P.J & Bessler, M. (2008). The role of human ribosomal proteins in the maturation of rRNA and ribosome production. *RNA*, 14, pp. 1918–1929.

Roelse, J., Grommé, M., Momburg, F., Hämmerling, G. & Neefjes, J. (1994). Trimming of TAP-translocated peptides in the endoplasmic reticulum and in the cytosol during recycling. *The Journal of experimental medicine*, 180 (5), pp. 1591–7. DOI: DOI10.1084/jem.180.5.1591.

Rosa, F. M. & Fellous, M. (1988). Regulation of HLA-DR gene by IFN-gamma . Transcriptional and post-transcriptional control. *The Journal of Immunology*, 140, pp. 1660–1664.

Rowinky, E. K. & Donehower, R. C. (1995). Paclitaxel (Taxol). *The New England Journal of Medicine*, 34 (4), pp. 1004–1014. DOI: 10.1515/ling.1996.34.4.841M4-Citavi. arXiv: arXiv:1011.1669v3.

Russell, J. H. & Ley, T. J. (2002). Lymphocyte-mediated cytotoxicity. *Annual Review of Immunology*, 20 (1), pp. 323–370. DOI: 10.1146/annurev.immunol.20.100201.131730.

Rygaard, J. & Povlsen, C. O. (1974). The mouse mutant nude does not develop spontaneus tumours. *Acta Pathologica Microbiologica Scandinavica Section B*, 82, pp. 99–106. DOI: 10.1111/j.1699-0463.1974.tb02299.x.

Salas, S., Jézéquel, P., Campion, L., Deville, J. L., Chibon, F., Bartoli, C., Gentet, J. C., Charbonnel, C., Gouraud, W., Voutsinos-Porche, B., Brouchet, A., Duffaud, F., Figarella-Branger, D. & Bouvier, C. (2009). Molecular characterization of the response to chemotherapy in conventional osteosarcomas: Predictive value of HSD17B10 and IFITM2. *International Journal of Cancer*, 125 (4), pp. 851–860. DOI: 10.1002/ijc.24457.

Sanford, J. R., Gray, N. K., Beckmann, K. & Cáceres, J. F. (2004). A novel role for shuttling SR proteins in mRNA translation A novel role for shuttling SR proteins in mRNA translation. *Genes & Development*, pp. 755–768. DOI: 10.1101/gad.286404.

Sangfelt, O., Erickson, S., Castro, J., Heiden, T., Gustafsson, A., Einhorn, S. & Grandér, D. (1999). Molecular mechanisms underlying interferon-α-induced G0/G1 arrest: CKI-mediated regulation of G1 Cdk-complexes and activation of pocket proteins. *Oncogene*, 18 (18), pp. 2798–2810. DOI: 10.1038/sj.onc.1202609.

Sanjana, N. E., Shalem, O. & Zhang, F. (2014). Improved vectors and genome-wide libraries for CRISPR screening. *Nature Methods*, 11 (8), pp. 783–784. DOI: 10.1038/nmeth.3047. arXiv: 15334406.

Santos, P. F. dos & Mansur, D. S. (2017). Beyond ISGlylation: Functions of Free Intracellular and Extracellular ISG15. *Journal of Interferon & Cytokine Research*, 37 (6), pp. 246–253. DOI: 10.1089/jir.2016.0103.

Schoggins, J. W., Wilson, S. J., Panis, M., Murphy, M. Y., Jones, C. T., Bieniasz, P. & Rice, C. M. (2011). A diverse range of gene products are effectors of the type I interferon antiviral response. *Nature*, 472 (7344), pp. 481–485. DOI: 10.1038/nature09907.

Schroder, K., Hertzog, P. J., Ravasi, T. & Hume, D. A. (2004). Interferon gamma orchestrates : an overview of signals, mechanisms and functions. *Journal of leukocyte Biology*, 75 (February), pp. 163–189. DOI: 10.1189/jlb.0603252.Journal.

Schroeder, A., Mueller, O., Stocker, S., Salowsky, R., Leiber, M., Gassmann, M., Lightfoot, S., Menzel, W., Granzow, M. & Ragg, T. (2006). The RIN: an RNA integrity number for assigning integrity values to RNA measurements. *BCM Molecular Biology*, 7, pp. 1–14.

Sciabica, K. S., Dai, Q. J. & Sandri-Goldin, R. M. (2003). ICP27 interacts with SRPK1 to mediate HSV splicing inhibition by altering SR protein phosphorylation. *EMBO Journal*, 22 (7), pp. 1608–1619. DOI: 10.1093/emboj/cdg166.

Seliger, B., Cabrera, T., Garrido, F. & Ferrone, S. (2002). HLA class I antigen abnormalities and immune escape by malignant cells. *Seminars in Cancer Biology*, 12 (1), pp. 3–13. DOI: 10.1006/scbi.2001.0404.

Seyfried, N. T., Huysentruyt, L. C., Atwood, J. A., Xia, Q., Seyfried, T. N. & Orlando, R. (2008a). Up-regulation of NG2 proteoglycan and interferon induced transmembrane proteins

1 and 3 in mouse astrocytoma: A membrane proteomics approach. *Cancer*, 263 (2), pp. 243–252. DOI: 10.1016/j.canlet.2008.01.007.Up-regulation.

Seyfried, N. T., Huysentruyt, L. C., Atwood, J. A., Xia, Q., Seyfried, T. N. & Orlando, R. (2008b). Up-regulation of NG2 proteoglycan and interferon-induced transmembrane proteins 1 and 3 in mouse astrocytoma: A membrane proteomics approach. *Cancer Letters*, 263 (2), pp. 243–252. DOI: 10.1016/j.canlet.2008.01.007.

Shin, K. H., Kim, R. H., Kang, M. K., Kim, R., Kim, S., Lim, P. K., Yochim, J. M., Baluda, M. A. & Park, N. H. (2007). p53 promotes the fidelity of DNA end-joining activity by, in part, enhancing the expression of heterogeneous nuclear ribonucleoprotein G. *DNA repair*, 129 (6), pp. 830–840. DOI: 10.1021/ja064902x.Brilliant. arXiv: NIHMS150003.

Shukla, S. A., Rooney, M. S., Rajasagi, M., Tiao, G., Dixon, P. M., Lawrence, M. S., Stevens, J., Lane, W. J., Dellagatta, J. L., Steelman, S., Sougnez, C., Cibulskis, K., Kiezun, A., Hacohen, N., Brusic, V., Wu, C. J. & Getz, G. (2015). Comprehensive analysis of cancer-associated somatic mutations in class i HLA genes. *Nature Biotechnology*, 33 (11), pp. 1152–1158. DOI: 10.1038/nbt.3344. arXiv: 15334406.

Siegrist, F., Ebeling, M. & Certa, U. (2011). The Small Interferon-Induced Transmembrane Genes and Proteins. *Journal of Interferon & Cytokine Research*, 31 (1), pp. 183–197. DOI: 10.1089/jir.2010.0112.

Smyth, M. J., Thia, K. Y. T., Street, S. E. A., Cretney, E., Trapani, J. A., Taniguchi, M., Kawano, T., Pelikan, S. B., Crowe, N. Y. & Godfrey, D. I. (2000). Differential Tumor Surveillance by Natural Killer (Nk) and Nkt Cells. *The Journal of Experimental Medicine*, 191 (4), pp. 661–668. DOI: 10.1084/jem.191.4.661.

Soejima, K. & Rollins, B.J. (2001). A Functional IFN-γ-Inducible Protein-10/CXCL10-Specific Receptor Expressed by Epithelial and Endothelial Cells That Is Neither CXCR3 Nor Glycosaminoglycan. *The American Association of Immunologists*, 167, pp. 6576–6582.

Soong, T. W. & Hui, K. M. (1992). Locus-specific transcriptional control of HLA genes. *J Immunol*, 149 (6), pp. 2008–2020. DOI: 10.1038/ijo.2011.270.

Sreekumar, A., Nyati, M. K., Varambally, S., Barrette, T. R., Ghosh, D., Lawrence, T. S. & Chinnaiyan, A. M. (2001). Profiling of cancer cells using protein microarrays: discovery of novel radiation-regulated proteins. *Cancer Res*, 61, pp. 7585–7593.

Staeheli, P. (1990). Interferon-Induced Proteins and the Antiviral State. *Advances in Virus Research*, 38 (C), pp. 147–200. DOI: 10.1016/S0065-3527(08)60862-3.

Stark, G. R., Kerr, I. M., Williams, B. R., Silverman, R. H. & Schreiber, R. D. (1998). How cells respond to interferons. *Annual review of biochemistry*, 67, pp. 227–64. DOI: 10.1146/annurev.biochem.67.1.227.

Stavropoulos, N. E., Ioachim, E., Pavlidis, N., Pappa, L., Kalomiris, P. & Agnantis, N. J. (1998). Local immune response after intravesical interferon gamma in superficial bladder cancer. *British journal of urology*, 81 (6), pp. 875–9.

Stawowczyk, M., Van Scoy, S., Kumar, K. P. & Reich, N. C. (2011). The interferon stimulated gene 54 promotes apoptosis. *Journal of Biological Chemistry*, 286 (9), pp. 7257–7266. DOI: 10.1074/jbc.M110.207068.

Stetson, D. B. & Medzhitov, R. (2006). Type I Interferons in Host Defense. *Immunity*, 25 (3), pp. 373–381. DOI: 10.1016/j.immuni.2006.08.007.

Strandem, A. M., Staeheli, P. & Pavlovic, J. (1993). Function of the Mouse Mx1 proteins is inhibited by overexpression of the PB2 protein of influenza virus. *Virology*, 197, pp. 642–651.

Street, D., Kaufmann, A. M., Vaughan, A., Fisher, S. G., Hunter, M., Schreckenberger, C., Potkul, R. K., Gissmann, L. & Qiao, L. (1997). Interferon-gamma enhances susceptibility of cervical cancer cells to lysis by tumor-specific cytotoxic T cells. *Gynecologic oncology*, 65 (2), pp. 265–72. DOI: 10.1006/gyno.1997.4667.

Stutman, O. (1979a). Chemical carcinogenesis in nude mice: Comparison between nude mice from homozygous matings and heterozygous matings and effect of age and carcinogen dose. *Journal of the National Cancer Institute*, 62 (2), pp. 353–358. DOI: 10.1093/jnci/62.2.353.

— (1979b). Immunodepression and malignancy. *Advances in Cancer Research*, 22, pp. 261–422.

Subash Sad, R. M. & Tim, F. M. (1995). Cytokine-Induced Differentiation of Precursor Mouse CD8+ T Cells into Cytotoxic CD8+ T Cells Secreting Thl or Th2 Cytokines. *Immunity, Vol.*, 2, pp. 271–279.

Sun, T., Yang, Y., Luo, X., Cheng, Y., Zhang, M., Wang, K. & Ge, C. (2014). Inhibition of Tumor Angiogenesis by Interferon-γ by Suppression of Tumor-Associated Macrophage Differentiation. *Oncology Research Featuring Preclinical and Clinical Cancer Therapeutics*, 21 (5), pp. 227–235. DOI: 10.3727/096504014X13890370410285.

Takahashi, S., Doss, C., Levy, S. & Levy, R. (1990). TAPA-1, the Target of an Antiproliferative Antibody, Defines a New Family of Transmembrane Proteins. *Molecular and Cellular Biology*, 10 (8), pp. 4007–4015.

Takaoka, A., Mitani, Y., Suemori, H., Sato, M., Yokochi, T., Noguchi, S., Tanaka, N. & Taniguchi, T. (2000). Cross Talk Between Interferon-gamma and -alpha /beta Signaling Components in Caveolar Membrane Domains. *Science*, 288 (5475), pp. 2357–2360. DOI: 10.1126/science.288.5475.2357.

Takaoka, A. & Yanai, H. (2006). Interferon signalling network in innate defence. *Cellular Microbiology*, 8 (6), pp. 907–922. DOI: 10.1111/j.1462-5822.2006.00716.x.

Takeuchi, O. & Akira, S. (2010). Pattern Recognition Receptors and Inflammation. *Cell*, 140 (6), pp. 805–820. DOI: 10.1016/j.cell.2010.01.022. arXiv: NIHMS150003.

Takeuchi, T., Inoue, S. & Yokosawa, H. (2006). Identification and Herc5-mediated ISGylation of novel target proteins. *Biochemical and Biophysical Research Communications*, 348 (2), pp. 473–477. DOI: 10.1016/j.bbrc.2006.07.076.

Tamura, T., Yanai, H., Savitsky, D. & Taniguchi, T. (2008). The IRF Family Transcription Factors in Immunity and Oncogenesis. *Annual Review of Immunology*, 26 (1), pp. 535–584. DOI: 10.1146/annurev.immunol.26.021607.090400.

Taniguchi, K., Petersson, M., Höglund, P., Kiessling, R., Klein, G. & Kärre, K. (1987). Interferon gamma induces lung colonization by intravenously inoculated B16 melanoma cells in parallel with enhanced expression of class I major histocompatibility complex antigens. *Proceedings of the National Academy of Sciences of the United States of America*, 84 (10), pp. 3405–9. DOI: 10.1073/pnas.84.10.3405.

Tecalco-Cruz, A. C. & Cruz-Ramos, E. (2018). Protein ISGylation and free ISG15 levels are increased by interferon gamma in breast cancer cells. *Biochemical and Biophysical Research Communications*, 499 (4), pp. 973–978. DOI: 10.1016/j.bbrc.2018.04.030.

Terenzi, F., Saikia, P. & Sen, G. C. (2008). Interferon-inducible protein, P56, inhibits HPV DNA replication by binding to the viral protein E1. *EMBO Journal*, 27 (24), pp. 3311–3321. DOI: 10.1038/emboj.2008.241.

Thigpen, T., DuBois, A., McAlpine, J., DiSaia, P., Fujiwara, K., Hoskins, W., Kristensen, G., Mannel, R., Markman, M., Pfisterer, J., Quinn, M., Reed, N., MarieSwart, A., Berek, J., Colombo, N., Freyer, G., Gallardo, D., Plante, M., Poveda, A., Rubinstein, L., Bacon, M., Kitchener, H. & Stuart, G. C. E. (2011). First-line therapy in ovarian cancer trials. *International Journal of Gynecological Cancer*, 21 (4), pp. 756–762. DOI: 10.1097/IGC.0b013e31821ce75d.

Thomas, L. (1959). *Discussion of Cellular and Humoral Aspects of Hypersensitivity States*, pp. 529–532.

Tirosh, B., Daniel-Carmi, V., Carmon, L., Paz, A., Lugassy, G., Vadai, E., Machlenkin, A., Bar-Haim, E., Do, M. S., Ahn, I. S., Fridkin, M., Tzehoval, E. & Eisenbach, L. (2007). '1-8 Interferon inducible gene family': Putative colon carcinoma-associated antigens. *British Journal of Cancer*, 97 (12), pp. 1655–1663. DOI: 10.1038/sj.bjc.6604061.

Tomaic, V. (2016). Functional Roles of E6 and E7 Oncoproteins in HPV-Induced Malignancies at Diverse Anatomical Sites. *Cancers*, 8, pp. 1–22.

Torres, L. M., Cabrera, T., Concha, A., Oliva, M. R., Ruiz-Cabello, F. & Garrido, F. (1993). HLA class I expression and HPV-16 sequences in premalignant and malignant lesions of the cervix. *Tissue Antigens*, 41 (2), pp. 65–71. DOI: 10.1111/j.1399-0039.1993.tb01981.x.

Trowsdale, J. (2005). HLA genomics in the third millennium. *Current Opinion in Immunology*, 17 (5), pp. 498–504. DOI: 10.1016/j.coi.2005.07.015.

Trowsdale, J., Handson, I., Mockridge, I., Beck, S., Townsend, A. & Kelly, A. (1990). Sequences encoded in the class II region of the MHC related to the "ABC" superfamily of transporters. *Nature*, 348:741–44.

Tsai, M. H., Cook, J. A., Chandramouli, G. V. R., DeGraff, W., Yan, H., Zhao, S., Coleman, C. N., Mitchell, J. B. & Chuang, E. Y. (2007). Gene Expression Profiling of Breast, Prostate,

and Glioma Cells following Single versus Fractionated Doses of Radiation. *Cancer Research*, 67 (8), pp. 3845–52. DOI: 10.1158/0008-5472.can-06-4250.

Van den Broek, M. F., Kägi, D., Ossendorp, F., Toes, R., Vamvakas, S., Lutz, W. .K, Melieffl, C. J. M., Zinkernagel, R. M. & Hengartner, H. (1996). Decreased tumor surveillance in perforin-deficient mice. *J. Exp. Med.*, 184, pp. 1781–90.

van Montfoort, N., van der Aa, E. & Woltman, A. M. (2014). Understanding MHC class I presentation of viral antigens by human dendritic cells as a basis for rational design of therapeutic vaccines. *Frontiers in Immunology*, 5 (APR), pp. 1–14. DOI: 10.3389/fimmu.2014.00182.

Van Overbeek, M., Capurso, D., Carter, M. M., Hoffman, G. R., Fuller, C. K., May, A. P., Thompson, M. S., Frias, E., Russ, C., Reece-Hoyes, J. S., Nye, C., Gradia, S., Vidal, B. & Zheng, J. (2016). DNA Repair Profiling Reveals Nonrandom Outcomes at Cas9-Mediated Breaks Article. *Molecular Cell*, 63, pp. 1–14. DOI: 10.1016/j.molcel.2016.06.037.

Vannucchi, S., Chiantore, M. V., Fiorucci, G., Percario, Z. A., Leone, S., Affabris, E. & Romeo, G. (2005). TRAIL is a key target in S-phase slowing-dependent apoptosis induced by interferon-β in cervical carcinoma cells. *Oncogene*, 24 (15), pp. 2536–2546. DOI: 10.1038/sj.onc.1208403.

Vasil, V., Clancy, M., Ferl, R.J., Vasil, I.K. & L., Curtis Hannah (1989). Increased Gene Expression by the First Intron of Maize Shrunken-1 Locus in Grass Species. *Plant Physiology*, 91, pp. 1575–1579.

Verhelst, J., Parthoens, E., Schepens, B., Fiers, W. & Saelens, X. (2012). Interferon-Inducible Protein Mx1 Inhibits Influenza Virus by Interfering with Functional Viral Ribonucleoprotein Complex Assembly. *Journal of Virology*, 86 (24), pp. 13445–13455. DOI: 10.1128/JVI.01682-12.

Vermeulen, C. F. W., Jordanova, E. S., Zomerdijk-Nooijen, Y. A., Ter Haar, N. T., Peters, A. A. W. & Fleuren, G. J. (2005). Frequent HLA class I loss is an early event in cervical carcinogenesis. *Human Immunology*, 66 (11), pp. 1167–1173. DOI: 10.1016/j.humimm.2005.10.011.

Vincent-Chong, V. K., Ismail, S. M., Rahman, Z. A.A., Sharifah, N. A., Anwar, A., Pradeep, P. J., Ramanathan, A., Karen-Ng, L. P., Kallarakkal, T. G., Mustafa, W. M.W., Abraham, M. T., Tay, K. K. & Zain, R. B. (2012). Genome-wide analysis of oral squamous cell carcinomas revealed over expression of ISG15, Nestin and WNT11. *Oral Diseases*, 18 (5), pp. 469–476. DOI: 10.1111/j.1601-0825.2011.01894.x.

Vogel, S. N. & Fertsch, D. (1984). Endogenous interferon production by endotoxin-responsive macrophages provides an autostimulatory differentiation signal. *Infection and Immunity*, 45 (2), pp. 417–423.

Vyas, J. M., Van Der Veen, A. G. & Ploegh, H. L. (2008). The known unknowns of antigen processing and presentation. *Nature Reviews Immunology*, 8 (8), pp. 607–618. DOI: 10.1038/nri2368. arXiv: NIHMS150003.

Wacher, C., Muller, M., Hofer, M. J., Getts, D. R., Zabaras, R., Ousman, S. S., Terenzi, F., Sen, G. C., King, N. J. C. & Campbell, I. L. (2007). Coordinated Regulation and Widespread Cellular Expression of Interferon-Stimulated Genes (ISG) ISG-49, ISG-54, and ISG-56 in the Central Nervous System after Infection with Distinct Viruses. *Journal of Virology*, 81 (2), pp. 860–871. DOI: 10.1128/JVI.01167-06.

Wahl, A., Schafer, F., Bardet, W., Buchli, R., Air, G. M. & Hildebrand, W. H. (2009). HLA class I molecules consistently present internal influenza epitopes. *Proc Natl Acad Sci U S A*, 106 (2), pp. 540–5. DOI: 10.1073/pnas.0811271106.

Walboomers, J. M. M., Jacobs, M. V., Manos, M. M., Bosch, F. X., Kummer, J. A., Shah, K. V., Snijders, P. J. F., Peto, J., Meijer, C. J. L. M. & Muñoz, N. (1999). Human Papillomavirus Is a Necessary Cause of invasive cervical cancer worldwide. *Journal of Pathology*, 19 (May), pp. 12–19.

Wall, L., Burke, F., Barton, C., Smyth, J. & Balkwill, F. (2003). IFN-gamma induces apoptosis in ovarian cancer cells in vivo and in vitro. *Clinical cancer research : an official journal of the American Association for Cancer Research*, 9 (7), pp. 2487–2496.

Wallace, T. A., Martin, D. N. & Ambs, S. (2011). Interactions among genes, tumor biology and the environment in cancer health disparities: Examining the evidence on a national and global scale. *Carcinogenesis*, 32 (8), pp. 1107–1121. DOI: 10.1093/carcin/bgr066.

Walsh, D. & Mohr, I. (2013). Coupling 40S ribosome recruitment to modification of a cap-binding initiation factor by eIF3 subunint e. *Genes and Development*, 28, pp. 835–840.

Wang, C., Pflugheber, J., Sumpter, R., Sodora, D. L., Hui, D., Sen, G. C. & Gale, M. (2003). Alpha interferon induces distinct translational control programs to suppress hepatitis C virus RNA replication. *Society*, 77 (7), pp. 3898–3912. DOI: 10.1128/JVI.77.7.3898.

Wang, S., Patsis, C. & Koromilas, A.E. (2015). Stat1 stimulates cap-independent mRNA translation to inhibit cell proliferation and promote survival in response to antitumor drugs. *PNAS*, E2149–E2155.

Wang, Z., Cao, R., Taylor, K. & Caldwell C. Cheng, J. (2013). The Properties of Genome Conformation and Spatial Interaction and Regulation Network of Normal and Malignant Human Cell Types. *PLOS ONE*, 8, pp. 1–13.

Warren, C. J., Griffin, L. M., Little, A. S., Huang, I. C., Farzan, M. & Pyeon, D. (2014). The Antiviral Restriction Factors IFITM1, 2 and 3 Do Not Inhibit Infection of Human Papillomavirus, Cytomegalovirus and Adenovirus. *Plos One*, 9, e96579.

Wei-Cheng, W., Houng-Wen, L. & Alan, L. (2007). Human ribosomal protein L7 displays an ER binding property and is involved in ribosome-ER association. *Federation of European Biochemical Societies*, 581, pp. 651–657.

Weichselbaum, R. R., Ishwaran, H., Yoon, T., Nuyten, D. S. A., Baker, S. W., Khodarev, N., Su, A. W., Shaikh, A. Y., Roach, P., Kreike, B., Roizman, B., Bergh, J., Pawitan, Y., Van De Vijver, M. J. & Minn, A. J. (2008a). An interferon-related gene signature for DNA

damage resistance is a predictive marker for chemotherapy and radiation for breast cancer. *PNAS*, 105 (47), pp. 18490–95.

Weichselbaum, R. R., Ishwaran, H., Yoon, T., Nuyten, D. S. A., Baker, S. W., Khodarev, N., Su, A. W., Shaikh, A. Y., Roach, P., Kreike, B., Roizman, B., Bergh, J., Pawitan, Y., Vijver, M. J. van de & Minn, A. J. (2008b). An interferon-related gene signature for DNA damage resistance is a predictive marker for chemotherapy and radiation for breast cancer. *Proceedings of the National Academy of Sciences*, 105 (47), pp. 18490–18495. DOI: 10.1073/pnas.0809242105. arXiv: arXiv:1408.1149.

Weiss, R. A. & Vogt, P. K. (2011). 100 years of Rous sarcoma virus. *The Journal of Experimental Medicine*, 208 (12), pp. 2351–2355. DOI: 10.1084/jem.20112160.

Weston, S., Czieso, S., White, I. J., Smith, S. E., Kellam, P. & Marsh, M. (2014). A Membrane Topology Model for Human Interferon Inducible Transmembrane Protein 1. *PLoS ONE*. DOI: 10.1371/journal.pone.0104341.

Whiteside, M. A., Chen, D. T., Desmond, R. A., Abdulkadir, S. A. & Johanning, G. L. (2004). A novel time-course cDNA microarray analysis method identifies genes associated with the development of cisplatin resistance. *Oncogene*, 23 (3), pp. 744–752. DOI: 10.1038/sj.onc.1207164.

Wickramasinghe, V. O. & Venkitaraman, A. R. (2016). RNA Processing and Genome Stability : Cause and Consequence. *Molecular Cell*, 61 (4), pp. 496–505. DOI: 10.1016/j.molcel.2016.02.001.

Wiedenheft, B., Sternberg, S. H. & Doudna, J. A. (2012). RNA-guided genetic silencing systems in bacteria and archaea. *Nature*, 482 (7385), pp. 331–338. DOI: 10.1038/nature10886. arXiv: 37.

Wiesenfeld, M., O'Connell, M. J., Wieand, H. S., Gonchoroff, N. J., Donohue, J. H., Fitzgibbons Jr, R. J., Krook, J. E., Mailliard, J. A., Gerstner, J. B. & Pazdur, R. (1995). Controlled clinical trial of interferon-gamma as postoperative surgical adjuvant therapy for colon cancer. *Journal of clinical oncology*, 13 (9), pp. 2324–2329. DOI: 10.1200/JCO.1995.13.9.2324.

Wilkins, C., Woodward, J., Lau, D. T. Y., Barnes, A., Joyce, M., McFarlane, N., McKeating, J. A., Tyrrell, D. L. & Gale, M. (2013). IFITM1 is a tight junction protein that inhibits hepatitis C virus entry. *Hepatology (Baltimore, Md.)*, 57 (2), pp. 461–9. DOI: 10.1002/hep.26066.

Williams, B. R. G. (1991). Transcriptional regulation of interferon-stimulated genes. *Eur. J. Biochem*, 200, pp. 1–11.

Wilson, D. N. & Doundna Cate, J. H. (2012). Structure and function of the eukaryotic ribosome. *Cold Spring Harbor Laboratory Press*, 4, a011536. DOI: 10.1101/cshperspect.a011536.

Windbichler, G. H., Hausmaninger, H., Stummvoll, W., Graf, A. H., Kainz, C., Lahodny, J., Denison, U., Muller-Holzner, E. & Marth, C. (2000). Interferon-gamma in the first-line

therapy of ovarian cancer: a randomized phase III trial. *Br J Cancer*, 82 (6), pp. 1138–1144. DOI: S0007092099910534[pii]\r10.1054/bjoc.1999.1053.

Wiśniewski, J. R., Zougman, A., Nagaraj, N., Mann, M., Wisniewski, J. R., Zougman, A., Nagaraj, N., Mann, M., Wiśniewski, J. R., Zougman, A., Nagaraj, N. & Mann, M. (2009). Universal sample preparation method for proteome analysis. Supplemental. *Nature methods*, 6 (5), pp. 359–363. DOI: 10.1038/nmeth.1322. arXiv: 0402594v3 [arXiv:cond-mat].

Wood, L. M., Pan, Z. K., Seavey, M. M., Muthukumaran, G. & Paterson, Y. (2012). The ubiquitin-like protein, ISG15, is a novel tumor-associated antigen for cancer immunotherapy. *Cancer Immunology, Immunotherapy*, 61 (5), pp. 689–700. DOI: 10.1007/s00262-011-1129-9.

Woods, M. W., Kelly, J. N., Hattlmann, C. J., Tong, J. G. K., Xu, L. S., Coleman, M. D., Quest, G. R., Smiley, J. R. & Barr, S. D. (2011). Human HERC5 restricts an early stage of HIV-1 assembly by a mechanism correlating with the ISGylation of Gag. *Retrovirology*, 8 (November), p. 95. DOI: 10.1186/1742-4690-8-95.

Yang, G., Xu, Y., Chen, X. & Hu, G. (2007). IFITM1 plays an essential role in the antiproliferative action of interferon-gamma. *Oncogene*, 26 (4), pp. 594–603. DOI: 10.1038/sj.onc.1209807.

Yang, Y., Lee, J. H., Kim, K. Y., Song, H. K., Kim, J. K., Yoon, S. R., Cho, D., Song, K. S., Lee, Y. H. & Choi, I. (2005). The interferon-inducible 9-27 gene modulates the susceptibility to natural killer cells and the invasiveness of gastric cancer cells. *Cancer Letters*, 221 (2), pp. 191–200. DOI: 10.1016/j.canlet.2004.08.022.

Yewdell, J. W. (2001). Not such a dismal science: The economics of protein synthesis, folding, degradation and antigen processing. *Trends in Cell Biology*, 11 (7), pp. 294–297. DOI: 10.1016/S0962-8924(01)02030-X.

Yewdell, J. W., Reits, E. & Neefjes, J. (2003). Making sense of mass destruction: Quantitating MHC class I antigen presentation. *Nature Reviews Immunology*, 3 (12), pp. 952–961. DOI: 10.1038/nri1250.

Yount, J. S., Moltedo, B., Yang, Y. Y., Charron, G., Moran, T. M., López, C. B. & Hang, H. C. (2010). Palmitoylome profiling reveals S-palmitoylation–dependent antiviral activity of IFITM3. *Nature Chemical Biology*, 6, pp. 610–14. DOI: 10.1038/nchembio.405.

Yu, F., Ng, S., Chow, B., Sze, J., Lu, G., Poon, W., Kung, H. F. & Lin, M. C. (2011). Knockdown of interferon-induced transmembrane protein 1 (IFITM1) inhibits proliferation, migration, and invasion of glioma cells. *Journal of Neuro-Oncology*, 103 (2), pp. 187–195. DOI: 10.1007/s11060-010-0377-4.

Yu, F., Xie, D., Ng, S. S., Lum, C. T., Cai, M. Y., Cheung, W. K., Kung, H. F., Lin, G., Wang, X. & Lin, M. C. (2015). IFITM1 promotes the metastasis of human colorectal cancer via CAV-1. *Cancer Letters*, 368 (1), pp. 135–143. DOI: 10.1016/j.canlet.2015.07.034.

Yuan, W. & Krug, R. M. (2001). Influenza B virus NS1 protein inhibits conjugation of the interferon (IFN) -induced ubiquitin-like ISG15 protein. *EMBO Journal*, 20 (3), pp. 362–371.

Zhang, D. & Zhang, D. E. (2011). Interferon-stimulated gene 15 and the protein ISGylation system. *Journal of interferon & cytokine research : the official journal of the International Society for Interferon and Cytokine Research*, 31 (1), pp. 119–30. DOI: 10.1089/jir.2010.0110.

Zhang, W., Xie, M., Shu, M.D., Steitz, J.A. & Dimaio, D. (2016). A proximity-dependent assay for specific RNA-protein interactions in intact cells. *RNA*, 22, pp. 1785–1792.

Zhang, Z., Liu, J., Li, M., Yang, H. & Zhang, C. (2012). Evolutionary Dynamics of the Interferon-Induced Transmembrane Gene Family in Vertebrates. *PLoS ONE*, 7 (11), pp. 1–13. DOI: 10.1371/journal.pone.0049265.

Zhao, B., Wang, H., Zong, G. & Li, P. (2013). The role of IFITM3 in the growth and migration of human glioma cells. *BMC Neurology*, 13. DOI: 10.1186/1471-2377-13-210.

Zhao, C., Beaudenon, S. L., Kelley, M. L., Waddell, M. B., Yuan, W., Schulman, B. A., Huibregtse, J. M. & Krug, R. M. (2004). The UbcH8 ubiquitin E2 enzyme is also the E2 enzyme for ISG15, an IFN- / -induced ubiquitin-like protein. *Proceedings of the National Academy of Sciences*, 101 (20), pp. 7578–7582. DOI: 10.1073/pnas.0402528101.

Zhao, C., Denison, C., Huibregtse, J. M., Gygi, S. & Krug, R. M. (2005). Human ISG15 conjugation targets both IFN-induced and constitutively expressed proteins functioning in diverse cellular pathways. *Proceedings of the National Academy of Sciences*, 102 (29), pp. 10200–10205. DOI: 10.1073/pnas.0504754102.

Zheng, W., Zhao, Z., Yi, X., Zuo, Q., Li, H., Guo, X., Li, D., He, H., Pan, Z., Fan, P., Li, F., Liao, Y. & Shao, R. (2017). Down-regulation of IFITM1 and its growth inhibitory role in cervical squamous cell carcinoma. *Cancer Cell International*, 17 (1), pp. 1–12. DOI: 10.1186/s12935-017-0456-0.

Zwaveling, S., Mota, S. C. F., Nouta, J., Johnson, M., Lipford, G. B., Offringa, R., Burg, S. H. van der & Melief, C. J. M. (2002). Established Human Papillomavirus Type 16-Expressing Tumors Are Effectively Eradicated Following Vaccination with Long Peptides. *The Journal of Immunology*, 169 (1), pp. 350–358. DOI: 10.4049/jimmunol.169.1.350.